

TALLINN UNIVERSITY OF TECHNOLOGY
DOCTORAL THESIS
6/2019

Anion Recognition and the Templated Solid-State Synthesis of Hemicucurbiturils

SANDRA KAABEL



TALLINN UNIVERSITY OF TECHNOLOGY

School of Science

Department of Chemistry and Biotechnology

This dissertation was accepted for the defense of the degree 12/12/2018

Supervisor: Assoc. Prof. Riina Aav
Department of Chemistry and Biotechnology
Tallinn University of Technology
Tallinn, Estonia

Co-supervisor: Prof. Kari Rissanen
Department of Chemistry
University of Jyväskylä
Jyväskylä, Finland

Opponents: Prof. Michael Hardie
School of Chemistry
Head of Inorganic Chemistry
University of Leeds
Leeds, United Kingdom

Prof. Risto Laitinen
Laboratory of Inorganic Chemistry
Environmental and Chemical Engineering
University of Oulu
Oulu, Finland

Defense of the thesis: 25/01/2019, Tallinn

Declaration:

Hereby I declare that this doctoral thesis, my original investigation and achievement, submitted for the doctoral degree at Tallinn University of Technology has not been submitted for doctoral or equivalent academic degree.

Sandra Kaabel

signature



Copyright: Sandra Kaabel, 2019

ISSN 2585-6898 (publication)

ISBN 978-9949-83-377-1 (publication)

ISSN 2585-6901 (PDF)

ISBN 978-9949-83-378-8 (PDF)

TALLINNA TEHNIKAÜLIKOOL
DOKTORITÖÖ
6/2019

**Hemikukurbituriilid kui anioonide
retseptorid ning nende mehhanokeemiline
süntees tahkes faasis**

SANDRA KAABEL

Contents

LIST OF PUBLICATIONS.....	7
OTHER PUBLICATIONS BY THE AUTHOR (NOT DISCUSSED IN THIS THESIS).....	8
INTRODUCTION.....	9
ABBREVIATIONS.....	11
1 LITERATURE OVERVIEW.....	13
1.1 Supramolecular chemistry.....	13
1.2 Anion-binding host-guest chemistry.....	14
1.2.1 Challenges of anion binding.....	15
1.2.2 Host design strategies for anion sensing applications.....	16
1.2.3 Host design strategies for the transport of anions.....	17
1.2.4 Host design strategies for anion extraction applications.....	19
1.2.5 Host design for anion-induced supramolecular organocatalysis.....	20
1.2.6 Material design based on supramolecular anion binding hosts.....	21
1.3 Cucurbiturils and hemicucurbiturils.....	22
1.3.1 Properties of hemicucurbiturils.....	23
1.3.2 Dynamic covalent chemistry in the synthesis of cucurbituril-type hosts.....	24
1.3.3 Role of the anionic templates in hemicucurbituril synthesis.....	25
1.4 Solid-state organic synthesis.....	26
1.4.1 Mechanochemistry.....	27
1.4.2 Solvent-free imine condensation reactions.....	28
1.4.3 Equilibrium of reversible mechanochemical covalent reactions.....	29
1.4.4 Synthesis of macrocyclic molecules by mechanochemistry.....	30
2 MOTIVATION AND AIMS FOR THE WORK.....	34
3 DETAILS OF USED METHODS.....	35
3.1 Calculation of the anion volumes.....	35
4 RESULTS AND DISCUSSION.....	36
4.1 Synthesis and structure of (<i>all-R</i>)-cyclohexanohemicucurbit[8]uril (Publication I) ..	36
4.1.1 Template-controlled synthesis conditions.....	36
4.1.2 Single crystal X-ray diffraction analysis.....	37
4.2 Complexation properties of (<i>all-R</i>)-cyclohexanohemicucurbit[8]uril (Publication II) ..	38
4.2.1 Solid-state studies of the anion inclusion complexes with cycHC[8].....	39
4.2.2 Solution studies on the anion complexation properties of cycHC[8].....	42
4.2.3 The pathway and kinetics of anion complexation with cycHC[8].....	45
4.3 Solid-state study of hemicucurbituril hosts (Publication III).....	47
4.3.1 Anion and guest binding motifs in the crystal structures of hemicucurbiturils.....	47
4.3.2 Guest influence on the shape of the hemicucurbiturils.....	49
4.4 Solid-state synthesis of cycHC[<i>n</i>] (Publication IV).....	51
4.4.1 Mechanochemical synthesis of cycHC[6] by ball milling.....	51
4.4.2 Combining ball milling with aging for the synthesis of cycHC[6].....	52
4.4.3 Adapting the developed approach to the solid state synthesis of cycHC[8].....	55
4.4.4 Aging step followed <i>in situ</i> by solid-state NMR.....	56
4.4.5 Aging followed <i>ex situ</i> by PXRD and SEM.....	58
5 CONCLUSIONS.....	60
REFERENCES.....	62

ACKNOWLEDGEMENTS	68
ABSTRACT.....	69
LÜHIKOKKUVÕTE.....	70
APPENDIX 1	71
APPENDIX 2	119
APPENDIX 3	121
AUTHOR'S CONFERENCE PRESENTATIONS	126
CURRICULUM VITAE.....	127
ELULOOKIRJELDUS	129

LIST OF PUBLICATIONS

This thesis is based on the following publications, which are referred to in the text by the Roman numerals:

- I E. Prigorchenko, M. Öeren, **S. Kaabel**, M. Fomitšenko, I. Reile, I. Järving, T. Tamm, F. Topić, K. Rissanen, R. Aav, 'Template-controlled synthesis of chiral cyclohexylhemicucurbit[8]uril,' *Chem. Commun.* **2015**, *51*, 10921–10924.
- II **S. Kaabel**, J. Adamson, F. Topić, A. Kiesilä, E. Kalenius, M. Öeren, M. Reimund, E. Prigorchenko, A. Lõokene, H. J. Reich, K. Rissanen, R. Aav, 'Chiral hemicucurbit[8]uril as an anion receptor: selectivity to size, shape and charge distribution,' *Chem. Sci.* **2017**, *8*, 2184–2190.
- III **S. Kaabel**, R. Aav, 'Templating effects in the dynamic chemistry of cucurbiturils and hemicucurbiturils,' *Isr. J. Chem.* **2018**, *58*, 296–313.
- IV **S. Kaabel**, R. S. Stein, M. Fomitšenko, I. Järving, T. Friščić, R. Aav, 'Size-control by anion templating in mechanochemical synthesis of hemicucurbiturils in the solid state,' 2018, *submitted to a peer-reviewed journal, manuscript available from ChemRxiv doi: 10.26434/chemrxiv.7376489.v1.*

AUTHOR'S CONTRIBUTION

Author's contribution to **Publications I – IV**:

- I The author was responsible for conducting and presenting the crystallographic analysis of the novel cyclohexano-hemicucurbit[8]uril macrocycle and participated in the preparation of the manuscript.
- II The author was involved in planning the experiments, conducted, interpreted, and presented the crystallographic analysis of the anion inclusion complexes with cyclohexano-hemicucurbit[8]uril. The author was also responsible for a considerable portion of the solution binding studies, namely nuclear magnetic resonance (NMR) titrations and Job plots. The author wrote the manuscript, with contributions from the co-authors, and compiled the supporting information.
- III The author analyzed the anion binding motifs and the geometries of all hemicucurbituril hosts in the respective crystal structures, as published in the Cambridge Structural Database. The author wrote the corresponding section (Hemicucurbiturils in the Solid State) of the manuscript and participated in the preparation of the remainder of the manuscript. The author designed, together with Prof. Riina Aav and Ms. Dina Mid, the cover graphic for the *Isr. J. Chem.* special issue titled 'Cucurbiturils and Related Cavitands,' in which this paper was published.
- IV The author was responsible for planning and conducting all the experiments, except for the electrospray ionization mass spectrometry (ESI-MS, conducted by Dr. Maria Fomitšenko) and the solid-state NMR measurements (performed by Dr. Robin S. Stein). The author wrote the manuscript, with contributions from the co-authors, and compiled the supporting information.

OTHER PUBLICATIONS BY THE AUTHOR (NOT DISCUSSED IN THIS THESIS)

Book chapter: R. Aav, **S. Kaabel**, M. Fomitšenko, Cucurbiturils: Synthesis, Structures, Formation Mechanisms, and Nomenclature. In *Comprehensive Supramolecular Chemistry II* (Ed. J. L. Atwood), Elsevier, Oxford, **2017**, Volume 3 (Ed. K. Rissanen), p. 203–220.

1. A. Peterson, **S. Kaabel**, I. Kahn, T. Pehk, R. Aav, J. Adamson, 'Unsubstituted Oxacalix[n]arenes ($n=4$ and 8): A Conformational Study in Solution and Solid State and Interaction Studies with Aromatic Guests,' *ChemistrySelect* **2018**, *3*, 9091–9095.
2. D. Trubitsõn, S. Žari, **S. Kaabel**, M. Kudrjashova, K. Kriis, I. Järving, T. Pehk, T. Kanger, 'Asymmetric Organocatalytic Cascade Synthesis of Tetrahydro-furanyl Spirooxindoles.' *Synthesis*, **2018**, *50*, 314–322.
3. M. Kaasik, **S. Kaabel**, K. Kriis, I. Järving, R. Aav, K. Rissanen, T. Kanger, 'Synthesis and characterization of chiral triazole-based halogen bond donors: halogen bonds in solid state and in solution.' *Chem. Eur. J.*, **2017**, *23*, 7337–7344.
4. Y. A. Konik, G. Z. Elek, **S. Kaabel**, I. Järving, M. Lopp, D. Kananovich, 'Synthesis of γ -keto sulfones by copper-catalyzed oxidative sulfonylation of tertiary cyclopropanols.' *Org. Biomol. Chem.*, **2017**, *15*, 8334–8340.
5. G. Pregel, E. Silm, **S. Kaabel**, I. Järving, K. Rissanen, M. Lopp, 'Asymmetric Organocatalytic Michael Addition–Cyclization Cascade of Cyclopentane-1,2-dione with Substituted α,β -Unsaturated Aldehydes.' *Synthesis*, **2017**, *49*, 3118–3125.
6. Y. A. Konik, M. Kudrjashova, N. Konrad, **S. Kaabel**, I. Järving, M. Lopp, D. Kananovich, 'Two-step Conversion of Carboxylic Esters into Distally Fluorinated Ketones via Ring Cleavage of Cyclopropanol Intermediates: Application of Sulfinatate Salts as Fluoroalkylating Reagents.' *Org. Biomol. Chem.*, **2017**, *15*, 4635–4643.
7. M. Fomitšenko, A. Peterson, I. Reile, H. Cong, **S. Kaabel**, E. Prigorchenko, I. Järving R. Aav, 'A quantitative method for analysis of mixtures of homologues and stereoisomers of hemicucurbiturils that allows us to follow their formation and stability.' *New J. Chem.*, **2017**, *41*, 2490–2497.
8. K. Kriis, T. Melnik, K. Lips, I. Juhanson, **S. Kaabel**, I. Järving, T. Kanger, 'Asymmetric Synthesis of 2,3,4-Trisubstituted Piperidines.' *Synthesis*, **2017**, *49*, 604–614
9. M. Ošek, M. Kimm, **S. Kaabel**, I. Järving, K. Rissanen, T. Kanger, 'Asymmetric Organocatalytic Wittig [2,3]-Rearrangement of Oxindoles.' *Org. Lett.*, **2016**, *18*, 1358–1361
10. K. Lippur, **S. Kaabel**, I. Järving, K. Rissanen, T. Kanger, 'CaCl₂, Bisoxazoline, and Malonate: A Protocol for an Asymmetric Michael Reaction.' *J. Org. Chem.*, **2015**, *80*, 6336–6341
11. S. Žari, A. Metsala, M. Kudrjashova, **S. Kaabel**, I. Järving, T. Kanger, 'Asymmetric Organocatalytic Aza-Michael Reactions of Isatin Derivatives.' *Synthesis*, **2015**, *47*, 875–886.

INTRODUCTION

Supramolecular chemistry takes advantage of the directional non-covalent interactions between small and relatively simple building blocks to construct nanoscale systems capable of performing various tasks. Advances in this interdisciplinary field have led, for example, to methods for controlled drug delivery in therapeutics^[1] and chemosensors for disease diagnostics.^[2] However, supramolecular chemistry can also offer inventive solutions to other modern challenges, such as higher density data storage,^[3] higher capacity^[4] and/or longer lifetime^[5] energy storage, capture of CO₂,^[6] and methods to improve recycling nuclear waste.^[7]

Anions are involved in the regulation of many biological processes, and are therefore important targets for the development of supramolecular hosts. This may lead to improved diagnosis and therapy of diseases related to anion mis-regulation, such as cystic fibrosis.^[8] Given the larger size of anions, and, consequently, the lower charge density than cations, the developed complementary hosts must be large and possess a more intricate binding site design, as the individual host-guest interactions are weaker.

Macrocyclic hosts can offer high selectivity and strong host-guest association, due to the preorganization of a complementary binding site for the target guest. Moreover, macrocyclic molecules are often constructed from common, simple, modifiable building blocks, often in one-pot synthesis, allowing for easy access to a wide landscape of supramolecular hosts.

These two concepts are elegantly combined in the recently discovered hemicucurbituril macrocycles, which are the novel anion-binding analogues of the well-known cucurbiturils. By varying the substituents on the monomeric ethyleneurea unit, diverse geometries of macrocycles have been achieved,^[9] with useful guest-binding behavior for anion sensing,^[10,11] chirality sensing,^[12,13] selective transmembrane anion transport,^[14–16] catalysis,^[17–19] and photoinduced electron transfer.^[20] Whereas most of the known examples of hemicucurbiturils are six-membered macrocycles, which contain a cavity size-matched for halide anions, development of novel, larger homologues could offer alternative guest selectivity, and thus, new avenues of application.

One of the key advantages of hemicucurbiturils is the robust high-yielding anion-templated synthesis, in contrast to the non-selective and inefficient high-dilution synthesis frequently used in the construction of macrocyclic compounds. Moreover, the success of hemicucurbituril synthesis at high concentrations suggests that it could be adapted for mechanochemical synthesis. Mechanochemistry is a rapidly advancing environmentally-friendly synthetic technique, which utilizes mechanical agitation to achieve chemical transformations and material synthesis in the solid state; thus, virtually eliminating the solvent-waste from chemical reactions.^[21] The construction of nanoscale materials, such as metal-organic frameworks, conventionally synthesized by crystallization from solution,^[22] have especially benefited from the cleaner and faster mechanochemical reactions.^[23] However, only a few examples of mechanochemical synthesis of macrocycles have been published, while molecular templating in covalent mechanochemical reactions has not yet been reported. Therefore, the anion-templated synthesis of hemicucurbiturils provides both a powerful method for the discovery of new supramolecular hosts and an excellent model for studying thermodynamically-driven templated reactions in a solid state.

This dissertation first outlines the main objectives for developing anion receptors, supplying key examples of successful receptor design strategies based on the current

literature. This is followed by an introduction to hemicucurbiturils, the fast-growing class of anion-binding supramolecular hosts, synthesized through anion-templated dynamic covalent chemistry. The literature overview provides a concise introduction to the field of mechanochemistry and solid-state synthesis, together with a comprehensive overview of mechanochemical covalent synthesis of macrocyclic compounds.

The results presented in this thesis include the templated solution-based synthesis and the crystal structure of a novel cyclohexanohemicucurbit[8]uril macrocyclic host (**Publication I**) and its properties as an anion receptor (**Publication II**). Single crystal X-ray diffraction analysis was employed to determine the anion-binding sites of the cyclohexanohemicucurbit[8]uril in the solid state. Mass spectrometry, NMR spectroscopy, isothermal titration calorimetry (ITC), and computational methods revealed the anion binding behavior of this new host molecule in gas phase and solution. This was followed by a study of the anion binding motifs in the host-guest complexes of all hemicucurbiturils (**Publication III**), based on the crystallographic data published in the Cambridge Structural Database. **Publication IV** described the development of a mechanochemical solid-state approach for the synthesis of the six- and eight-membered cyclohexanohemicucurbit[*n*]uril hosts.

In addition to these publications, the results of this thesis have been presented at several international conferences, in Estonia, Latvia, Croatia (2), Germany, Czech Republic, the United Kingdom, the Republic of Korea, South-Africa, the United States, and Canada (2).

ABBREVIATIONS

ADP	Adenosine diphosphate
aq.	Aqueous
ATP	Adenosine triphosphate
BU[<i>n</i>]	Bambus[<i>n</i>]uril
CB[<i>n</i>]	Cucurbit[<i>n</i>]uril
CCDC	Cambridge Crystallographic Data Centre
CD	Cyclodextrin
CP-MAS	Cross-polarization magic angle spinning
CPK	Corey, Pauling, Koltun molecular model
CSD	Cambridge Structural Database
cycHC[<i>n</i>]	Cyclohexanohemicucurbit[<i>n</i>]uril
DCL	Dynamic covalent library
DFT	Density functional theory
DMSO	Dimethylsulfoxide
ESI-MS	Electrospray ionization mass spectrometry
HC[<i>n</i>]	Hemicucurbit[<i>n</i>]uril
HPLC	High-performance liquid chromatography
ITC	Isothermal titration calorimetry
LAG	Liquid-assisted grinding
LC	Liquid chromatography
LMWG	Low molecular weight gelator
MOF	Metal-organic framework
NMR	Nuclear magnetic resonance (spectroscopy)
PC	Packing coefficient
PFA	Paraformaldehyde
PTFE	Polytetrafluoroethylene
PXRD	Powder X-ray diffraction
RH	Relative humidity
<i>s.o.f.</i>	Site occupancy factor
SEM	Scanning electron microscopy
TBA	Tetrabutylammonium
TBP	Tetrabutylphosphonium
TEA	Triethylamine
UV	Ultraviolet
vdW	Van der Waals (radius)
VT-NMR	Variable-temperature nuclear magnetic resonance (spectroscopy)
η (eta)	Liquid-to-solid ratio ($\mu\text{l mg}^{-1}$) in a LAG experiment

1 LITERATURE OVERVIEW

1.1 Supramolecular chemistry

Supramolecular chemistry, as a research field, was introduced and strongly influenced by the synthesis and systematic study of crown ethers in the late 1960s. Charles J. Pedersen described the formation of stable complexes of the cyclic polyethers with alkali and alkaline earth metals,^[24] and, followed by Jean-Marie Lehn and Donald J. Cram, went on to investigate the chemical basis of molecular recognition. The importance of selective complexation processes in biological systems was highlighted and new classes of organic compounds with improved complexation properties were developed, for which Pedersen, Lehn and Cram were jointly awarded the 1987 Nobel Prize in Chemistry.^[25–27] The term *host-guest chemistry* was specified by D. J. Cram and J. M. Cram, who defined the *host*, as the larger molecule in the binding pair, which recognizes the smaller *guest* molecule by its steric features and specific interaction sites.^[28] The term *receptor* was used interchangeably with *host* by the authors in the field. Typically, the host-guest pair is held together by a collection of non-covalent bonds, which individually are significantly weaker than covalent bonds (Table 1), but in co-operation can stabilize the formation of host-guest complexes. The intermolecular forces include electrostatic interactions, hydrogen and halogen bonds, π - π interactions, van der Waals forces, and solvophobic interactions. These forces can vary in strength from 2 kJ mol⁻¹ for the weak dispersion interactions to 300 kJ mol⁻¹ for strong ion-ion interactions.^[29] The region of the host or guest involved in the non-covalent interactions is defined as the binding site.

Table 1. Strength of supramolecular interactions compared to covalent interactions^[29–31]

Interaction	Sub-Type	Strength (kJ mol ⁻¹)
Electrostatic	Ion-ion	200 – 300
	Ion-dipole	50 – 200
	Dipole-dipole	5 – 50
Hydrogen bonding		4 – 120
Halogen bonding		10 – 150
π - π interactions		0 – 50
Cation- π		5 – 80
Van der Waals		< 5 ^[a]
Solvophobic		0 – 100 ^[b]
Covalent		150 – 450

[a] Dependent on the surface area of the molecules.

[b] Dependent on the solvent-solvent interactions, host geometry / size of the binding pocket, and the nature of the functional groups lining the host's binding site.

Usually, the host-guest binding affinity for a target guest molecule is enhanced by maximizing the number of simultaneous weak interactions to the guest by host design. Preorganization of the interacting groups of the host into a convergent binding site results in higher host-guest affinity, compared to complexes where the binding pocket is formed only upon guest binding.^[32,33] Therefore, many supramolecular chemists have focused on the development of macrocyclic host molecules. The smaller solvent-accessible surface area of macrocyclic hosts, as compared to the acyclic analogues, results in a smaller energetic penalty from de-solvating the binding site. Macrocyclic molecules are

generally conformationally more rigid than acyclic hosts, and thus, fewer degrees of freedom are lost upon complex formation, as the entropic penalty from host reorganization is not paid during guest complexation.^[34]

Following the example of the cation-binding crown ether hosts, many types of organic macrocyclic compounds have been developed for binding various guest molecules. Even though the discovery of the host molecules, for example cyclodextrins,^[35] calixarenes,^[36] and cucurbiturils,^[37] predates the advent of supramolecular chemistry, the useful binding properties have only recently been recognized and applied. Among the applications of supramolecular chemistry to real-world technologies are sensors for blood glucose or blood ion monitoring, compounds for biological imaging and drug delivery, and ligands for metal extraction from ores and radioactive waste.^[38] Ground-breaking technologies improving, for example, cancer therapy,^[39] relieving environmental pollution,^[40] and energy- and electron-transfer systems^[41] have also been developed based on supramolecular chemistry.

Introduced by Jean-Marie Lehn, the term *supramolecular chemistry* encompasses, in its contemporary meaning, host-guest chemistry, molecular devices and machines, as well as the concepts of self-assembly, self-organization, and nanotechnology.^[34] The scientific endeavors in supramolecular chemistry are often interdisciplinary, and call for collaborations across the fields of chemistry, physics, biochemistry, and biology. The studies described in this thesis, both within the literature overview and in the author's publications, clearly highlight how establishing an understanding of a supramolecular system is a collaborative effort between synthetic organic chemists, analytical and computational chemists, crystallographers, and solid-state chemists. The serendipitous nature of the early discoveries in the field and the continued design of new functional structures used in cutting-edge technologies have attracted many researchers who have made supramolecular chemistry into the highly vital field it is today.

1.2 Anion-binding host-guest chemistry

Although the first anion-binding macrobicyclic hosts, called *katapinands*, were reported concurrently with crown ethers in 1968 by C. H. Park and H. E. Simmons,^[42] the development of cation-binding chemistry far outpaced the advancement of anion-binding hosts. The main reason for this lies in the properties of anions, discussed in the following section, which make complexation challenging. Only in the late 1980s was there a renaissance in the field of anion binding, rooted in the growing understanding of the features that govern molecular recognition, which quickly resulted in a highly diverse pool of cleverly designed host architectures.^[34,43,44]

Due to the relatively recent blossoming of the field of anion complexation, it is no surprise that established real-world applications of anion receptors are still scarce. However, the topics of anion sensing and extraction, transport of anions in living organisms, anion-driven organocatalysis, and anion-driven self-assembly of supramolecular architectures have gathered significant interest.^[45] Until recently, the focus of anion-complexation chemistry had mainly been on the synthesis and characterization of new anion receptors, whereas in recent years, the focus has shifted to developing specific applications.^[46]

Sensing or controlling anion transport is a promising target for medicinal chemistry, as anions are essential to the regulation of many biochemical processes. For instance, chloride anions are responsible for the maintenance of osmotic balance in cells and phosphate anions (i.e. ATP or ADP) are the fuel or cofactor in most enzymatic

processes.^[34,43] Extraction of anions by supramolecular systems could alleviate the harm to the environment caused by nitrate- and phosphate-containing fertilizers, or from specific pollutants generated through energy production.^[34] The anion-controlled self-assembly of supramolecular systems is already within the repertoire of engineers, who aim to create novel nanoscale architectures or molecular devices.^[29]

1.2.1 Challenges of anion binding

Compared to the small and predominantly spherical cations, which are targeted size-selectively by devoted receptors, anions possess intrinsic properties that complicate the design of efficient hosts.

First, anions are large and come in different shapes. The lower charge density compared to cations requires a more careful design of the binding site, reflecting the geometry of the guest to yield strong host-guest interactions. Anionic guests range from the smallest spherical halides (F^- , Cl^- , Br^- , I^-), with F^- (1.33 Å) comparable in ionic radius to K^+ (1.38 Å), through linear (CN^- , N_3^-), planar (NO_3^- , $PtCl_4^{2-}$), tetrahedral (PO_4^{3-} , SO_4^{2-} , BF_4^-), and octahedral anions (PF_6^- , $Fe(CN)_6^-$), to various carboxylates, mono- and polyphosphate organic anions also present in the structure of proteins and nucleic acids.^[43]

Any host for anions (or cations) must compete with the surrounding medium, due to the relatively high free energy of ion solvation, caused by the electrostatic ion-dipole interactions between the ion and the solvent.^[47] The host's strength in binding anions depends largely on the nature of the solvent, and thus the host design must take into account the intended operating medium.^[43]

Furthermore, as the energy of solvation varies for different anions in a given solvent, the binding *selectivity* of the host is also dependent on the medium.^[48] The anion selectivity in polar solvents generally follows the *Hofmeister series*, established by Franz Hofmeister in 1888 when studying the 'salting out' effect of ions on hen egg white globulin protein (Figure 1).^[49,50] 'Soft' anions at the polarizable end of the series were observed by Hofmeister to increase the solubility of globulin. In contrast, 'hard' anions at the opposite end of the scale were observed to induce the aggregation of the protein, resulting in its precipitation. The molecular level explanation of the Hofmeister effect is still debated and is being continuously investigated. Hofmeister's originally proposed explanation relating the precipitation of macromolecules to the higher solvent absorbance of the salting-out anions^[50,51] has proven to be too simplistic.^[52,53] According to current understanding, ion-specific and salt-specific interactions on the surface of the proteins and the influence of immediately adjacent solvation shells play a key role.^[53-55] Polarizable 'soft' anions preferably interact with hydrophobic and 'hard' anions with hydrophilic surfaces.^[55]

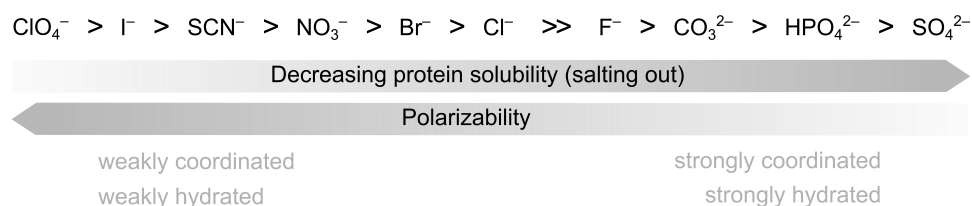


Figure 1. Anions arranged in the Hofmeister Series.^[34,43,52]

The following section aims to provide insight into the purpose of anion receptor development through selected examples of hosts. The examples were chosen to illustrate the interplay of non-covalent interactions and to highlight the key motifs in successful host design for different types of target applications in the relevant operating environments.

1.2.2 Host design strategies for anion sensing applications

Anion sensors are molecular receptors that produce a measurable response upon anion complexation, such as a change in the spectroscopic or electrochemical properties of the receptor / analyte or changes in the mechanical properties of the system (e.g. sol-gel transitions).^[45] The practical nature of the applications, including environmental monitoring and medical diagnostics, has fueled the development of anion sensors.^[56] Many of the intended applications call for the receptors to operate in an aqueous environment, in which anions are strongly hydrated. Strategies to overcome the strong anion-water interactions often include combinations of non-covalent interactions from the supramolecular toolbox (Table 1).

Sindelar and co-workers applied the strong association between bambusuril-based receptors **1** and **2** (Figure 2A) and anions to quantify a mixture of ¹H NMR-silent inorganic anions in an aqueous environment using ¹H NMR spectroscopy.^[11] As the rate of host-guest association was observed to be slow on the NMR timescale, the chemical shifts in the macrocycle hydrogen atoms in the respective anion inclusion complexes were used as a fingerprint to identify and even quantify mixtures of up to nine anions (Figure 2B). The remarkably high binding affinity of anions for the water-soluble host **2** (up to $K_a = 10^7$ in D₂O) was attributed to the combination of the chaotropic effect and multiple weak C–H⋯anion hydrogen bonds (Figure 2C).^[10,57] Notably, the methine protons (Figure 2A, colored blue), directed towards the cavity and involved in the formed hydrogen bonds, also exhibited the most pronounced changes in the chemical shift upon anion complexation. The alternate orientation of the glycoluril monomers resulted in the localization of the partial positive charge in the interior of the bambusuril cavity (Figure 2D), fortifying the host-guest complex by weak electrostatic attraction.^[58]

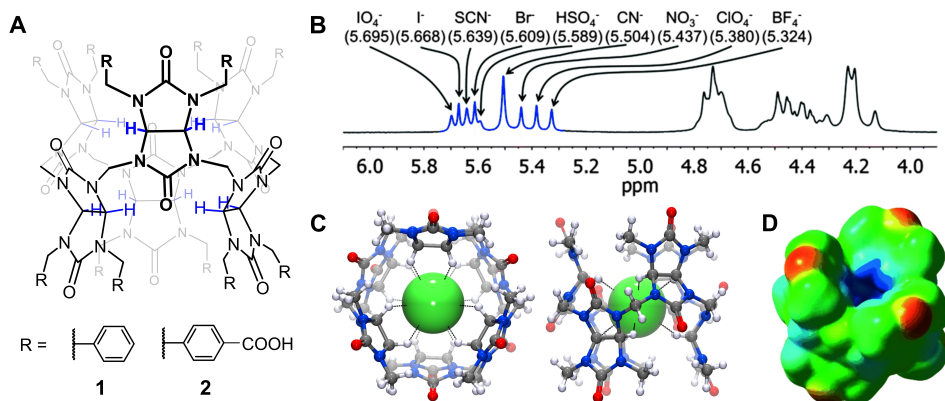


Figure 2. (A) Bambusurils by Sindelar and co-workers. (B) ¹H NMR spectra of **1** with a mixture of anions (in 5% D₂O–DMSO-*d*₆), showing the fingerprint chemical shifts of the methine protons of **1** in the respective anion inclusion complexes (blue). (C) The crystal structure of Cl⁻ within a bambusuril host^[58] with the C–H⋯anion interactions shown as dashed black lines. (D) Map of electrostatic potential of a bambusuril (red to blue: –31 to +36 kcal mol⁻¹). Figures B and D are reprinted, with permission from Royal Society of Chemistry and John Wiley and Sons, ref. [11] and [58], respectively.

C_3 -symmetrical tripodal receptors for sensing the planar trigonal nitrate anion were developed by Singh and Sun (Figure 3A).^[59] Sensing of NO_3^- was targeted, as it is an industrial and agricultural waste contaminant producing harmful environmental effects in the form of acid rain and eutrophication of rivers and lakes. The branched receptors **3a**, **3b**, and **3c** assumed a conical shape in an acidic solution owing to the protonation of the central N-atom and the consequently formed hydrogen bonds to the oxygen atoms in the three branches. The conical, positively charged forms of these hosts were capable of NO_3^- synergistic binding through electrostatic and directional amide $\text{N-H}\cdots\text{anion}$ hydrogen bonding interactions (Figure 3B). The protonated receptors **3a** and **3c** (in the form of a ClO_4^- salt) were found to bind NO_3^- with K_a up to 10^3 M^{-1} in an acetone- d_6 solution. As determined by NMR titration studies, no significant selectivity over HSO_4^- , Cl^- , and Br^- was observed. Receptor **4** was found to assume a conical zwitterionic form in neutral dimethylsulfoxide (DMSO) and could signal the binding of anions by quenched fluorescence response of the incorporated 1-amino-5-naphthalenesulfonic acid groups. Moreover, **4** proved to be more selective towards NO_3^- than the other tested anions in DMSO and in 10-20% water-DMSO solutions ($K_a(\text{NO}_3^-)/K_a(\text{HSO}_4^-) \approx 4 - 5$ determined by fluorescence titration).

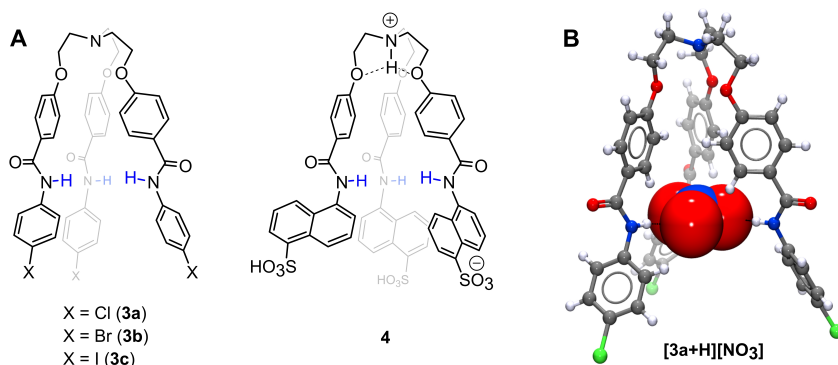


Figure 3. (A) Tripodal receptors by Singh and Sun^[59] constructing a trigonal binding pocket for NO_3^- from amide hydrogen bond donors. (B) Crystal structure of the nitrate complex of **3a**, with the amide $\text{N-H}\cdots\text{NO}_3^-$ hydrogen bonds shown as dashed black lines. The proton on the central tertiary amine is not refined in the published crystal structures of the nitrate complexes of **3a-3c**.

1.2.3 Host design strategies for the transport of anions

The development of synthetic anion transporters is largely driven by potential application in therapeutics; e.g. as artificial anion channels or molecular transporters through lipid bilayer membranes. Malfunctioning anion channel proteins and the resulting disruption of ionic balance in cellular compartments have been linked to several diseases, including the widespread genetic disorder cystic fibrosis.^[60]

Steroid-based anion receptors, cholapods, developed by Davis and co-workers, have been shown to act as effective chloride transmembrane carriers.^[61,62] Owing to a lipophilic core, these receptors are entirely partitioned into the membranes of vesicles in an aqueous solution. High affinity chloride binding in apolar media (up to $K_a 10^{11} \text{ M}^{-1}$ in CHCl_3) was achieved by constructing a preorganized binding pocket of hydrogen bond donor groups onto the rigid steroid scaffold **5** (Figure 4).^[62,63] By varying the substituents at positions 3, 7, and 12, an extremely efficient chloride transporter **6** was found, which promoted the transmembrane flux of chloride at transporter/lipid loading in the vesicle membrane as low as 1:250000.^[64] Interestingly, while **6** was a more effective transporter

than **5**, its affinity to chloride in chloroform was lower (K_a 10^9 M^{-1}), demonstrating that other factors (e.g. anion binding kinetics and mobility of the complex within the membrane) could determine the activity of the transporter.^[64]

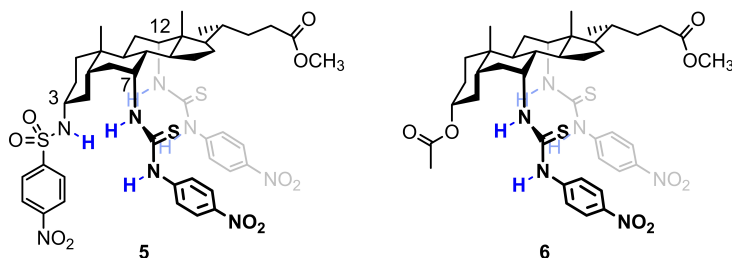


Figure 4. Cholapod anion carriers developed by Davis and co-workers for the transport of chloride through lipid bilayers.^[62,64] The hydrogen atoms involved in anion binding are colored blue.

Pittelkow and co-workers, in collaboration with Davis, found that by exchanging the anion binding motif from conventional hydrogen bonds for the weaker C–H⋯anion interactions, effective chloride transporters could be prepared.^[14] The binding pocket in biotin[6]juril **7** arranged 12 C–H hydrogen bond donor groups around a cavity compatible in size to the halide anions (Figure 5A).^[65] Enhancing the hydrophobicity of **7** through esterification to methyl-, ethyl- and butylhexaesters **8–10** (Figure 5B) ensured partitioning of the transporter to the membrane. All three transporters were observed to bind Cl^- with high affinity in acetonitrile ($K_a = 10^4$), compared to NO_3^- ($K_a = 10^2$), HCO_3^- ($K_a = 10^2$), and SO_4^{2-} (no interaction). The transporters also promoted chloride flux through a vesicle membrane by a Cl^-/NO_3^- antiport mechanism.^[14] HCO_3^- or SO_4^{2-} were not transported through the membrane, demonstrating the selectivity of transporters **8–10**. The rate of chloride transport increased with the higher lipophilicity of the host. Biotin[6]juril **10** was found to be the most active transporter among the hexaesters, achieving Cl^- flux with $t_{1/2} = 180$ seconds at a 1:2500 transporter/lipid molar ratio in the membrane. In comparison, at the same transporter/lipid ratio, the cholapod transporter **6** promoted Cl^- influx at $t_{1/2} = 3$ seconds.^[64]

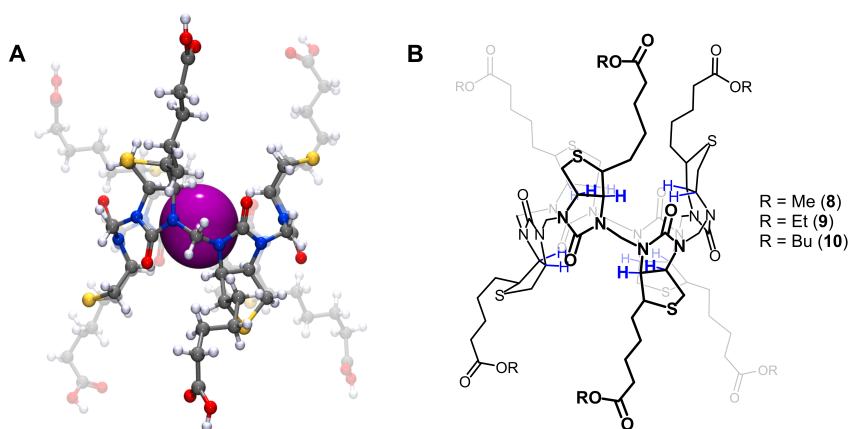


Figure 5. Biotin[6]jurils developed by Pittelkow and co-workers. (A) Crystal structure of the iodide complex of **7**.^[65] (B) Hexaester transmembrane anion carriers **8–10**,^[14] with the hydrogen atoms involved in anion-binding colored blue.

1.2.4 Host design strategies for anion extraction applications

Transmembrane anion carriers are designed to bind anions on the membrane-water interfaces, to migrate through the membrane, and to release the cargo on the other side, preferably with fast association kinetics. The hosts intended for anion extraction should however tightly bind the target anion and remove it from the environment, either by phase transfer to another immiscible liquid or to a solid.

A number of acyclic and macrocyclic hosts for extraction of pertechnetate from aqueous nuclear waste have been developed.^[66] Highly water-soluble TcO_4^- is one of the most hazardous radioactive pollutants in nuclear waste, due to its long half-life ($t_{1/2} = 2.13 \times 10^5$ years), environmental mobility within the earth's crust, and uptake by plants and aquatic organisms.^[66] Commercially available ion exchange resins generally rely only on electrostatic interactions and therefore have low selectivity to TcO_4^- . However, as TcO_4^- has a polarizable electron cloud and low charge density, hosts that include a hydrophobic binding pocket could improve the selectivity by relying on the Hofmeister bias (Figure 1).

Jurisson and co-workers reported a charged cyclotrimeratrylene-based host **11** (Figure 6A), which was used to extract TcO_4^- and the similarly sized ReO_4^- with over 90% efficiency from water into a nitromethane solution. This was accomplished even in the presence of excess competitive anions NO_3^- , SO_4^{2-} , PO_4^{3-} , and ClO_4^- , due to the favorable electrostatic interaction and size-matching deep hydrophobic cavity.^[67] Holman *et al.* demonstrated, by single crystal X-ray diffraction analysis, the inclusion of a weakly coordinating anion PF_6^- within the cavity of **11** (Figure 6B).^[68] Back-extraction of the oxoanions from the organic phase, however, was severely hampered by the irreversible association to the host, with only 3% of the traced ReO_4^- released to a saline solution.^[67] Regeneration of the extracting agent through the triggered release of the anion is an important property of a commercially viable solution for anion extraction.

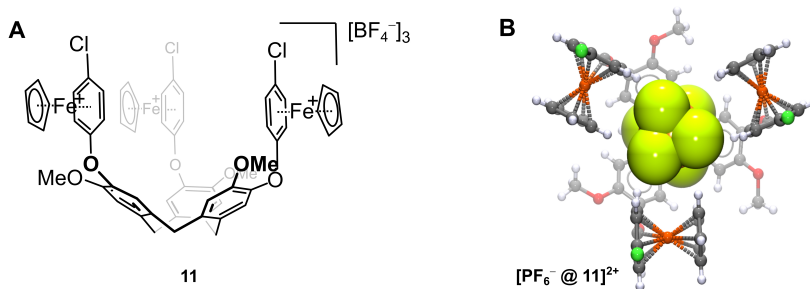


Figure 6. (A) Cyclotrimeratrylene-based host **11** for the extraction of TcO_4^- and (B) the crystal structure of the PF_6^- complex of **11** showing the inclusion of the anion deep within the cavity.^[67,68]

Liquid-liquid extraction of TcO_4^- with macrocyclic polyaza-cryptands (Figure 7) demonstrated that the phase transfer of TcO_4^- was dependent on the protonation state, size-matching with the cavity, and the lipophilicity of the host.^[69,70] The aza-cage **12** with a small cavity displayed the highest efficiency (80%) in extracting ReO_4^- and TcO_4^- from aqueous media at neutral pH into an organic solution.^[69] Back-extraction of the anion was efficiently achieved by lowering the pH of the aqueous phase. Added protonation sites, such as in host **13**, intended to aid anion binding through further hydrogen bonding sites, proved to bind the oxoanions only in a hexaprotonated state at low pH, and no extraction of TcO_4^- was observed at neutral pH.^[70] This was ascribed by Wichmann and co-workers to the higher hydrophilicity of receptor **13**, which prevented its partitioning

into the organic phase. The extraction efficiency and selectivity could be modified by tailoring the lipophilicity of the aza-cages through methylation.^[70] Although the methylated hosts, such as **14**, were indeed more soluble in organic solvents, the extracting efficiency was only slightly improved (20%) and the selectivity towards TcO_4^- over ReO_4^- was lost.

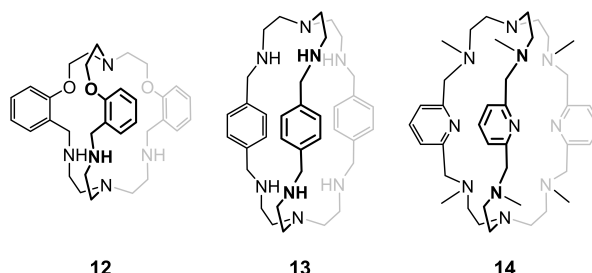


Figure 7. Aza-cages studied for the extraction of TcO_4^- by Vögtle and co-workers^[69] (**12**) and Wichmann and co-workers^[70] (**13** and **14**).

1.2.5 Host design for anion-induced supramolecular organocatalysis

Development of supramolecular catalysts has mainly focused on metal-organic compounds, which offer reaction rate acceleration and high selectivity by virtue of the confined catalytic sites around metal centers.^[71] However, considering the sustainability and environmental impact of chemical processes, organocatalytic alternatives for supramolecular catalysis are actively developed.^[45]

A decade ago, a new perspective emerged on the mode of action of conventional dual-hydrogen bond catalysts, such as thioureas, which showed that in appropriate reaction conditions the anion-catalyst complex acted as the reactive species.^[72] A seminal example of organocatalysis through halide binding to the chiral thiourea **15** was shown by Taylor and Jacobsen in the Pictet-Spengler cyclization providing *N*-acetyl tetrahydro- β -carboline (Figure 8A).^[73]

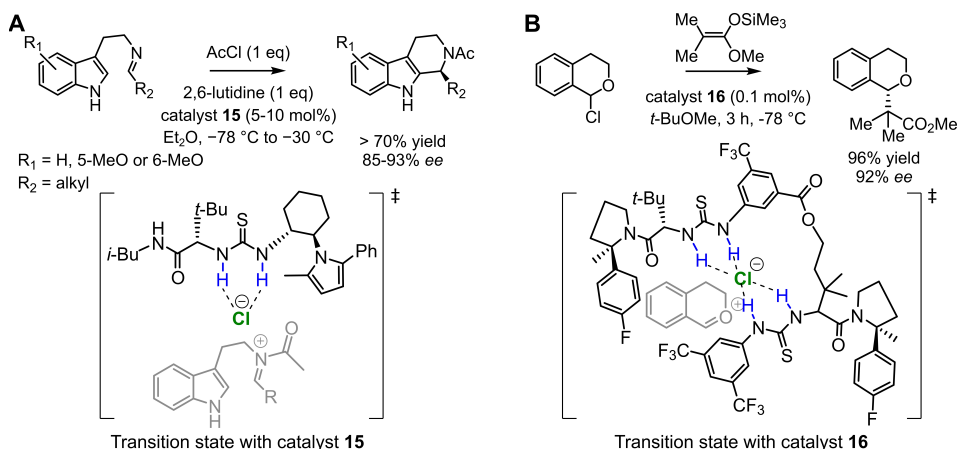


Figure 8. Supramolecular catalysts **15** and **16** by Jacobsen and co-workers in the respective chloride complexes with (A) *N*-acetyl iminium in a Pictet-Spengler cyclization^[73,74] and (B) oxocarbenium formed during an α -chloroisochroman alkylation reaction^[75].

In the initial report, little explanation was offered for the mechanism of these asymmetric transformations ($ee > 90\%$). Further investigations revealed that the enantioselective cyclization proceeded through an S_N1 -type abstraction of the chloride and activation of the acyl-iminium intermediate in a complex with the chiral chloride-bound catalyst (Figure 8A).^[74] Strategic design of bis-thiourea catalysts, such as **16**, to limit the effects of catalyst self-association and enhance the chloride binding efficiency, allowed the catalyst loading to be lowered significantly (from 10% to 0.01%). It also afforded higher reaction rates for the enantioselective alkylation of α -chloroisochroman through Cl^- abstraction (Figure 8B).^[75]

1.2.6 Material design based on supramolecular anion binding hosts

Supramolecular self-assembly provides a convenient and efficient method for the design and preparation of materials with specific physical properties. The properties of the bulk material, such as thermal or electrical conductance, color, luminescence, solubility, fluidity, and plasticity are encoded, and therefore can be tuned by the chemical structure of the components. For example, organic white light-emitting diodes (white OLEDs) based on a modular hydrogen-bonded assembly of red, green, and blue emissive compounds were created by Meijer, Schenning and co-workers.^[76] In contrast to the labor-intensive synthesis of new emissive materials, the supramolecular approach demonstrated easy tunability of the emission color by simple mixing of different ratios of the red-green-blue chromophore modules.

Few examples of supramolecular hosts that alter the physical properties of a material through anion binding have been reported. Recognizing the polarization of C–H bonds in cyanostilbenes, Flood and co-workers designed the potent pentameric macrocyclic host **17** by arranging the C–H hydrogen bond donors around a central cavity (Figure 9A).^[77] The neutral host **17**, named *cyanostar*, was shown to self-assemble into 2:1 sandwich complexes with BF_4^- , ClO_4^- , and PF_6^- . The high-affinity binding to large charge-diffuse anions (2:1 complex $\theta_{anion} = 10^{12} M^{-2}$ in $CH_3OH:CH_2Cl_2$ 40:60) was attributed to the formation of a hydrophobic, partially electropositive cavity from the two π -stacked molecules of **17**. In a recent remarkable follow-up, Johnson, Flood and co-workers demonstrated the potential of **17** for the regulation of Li^+ conductivity in the electrolyte solution of lithium ion batteries (LIB).^[78] Common LIB electrolytes consist of PF_6^- , ClO_4^- or BF_4^- salts in an organic solvent. Owing to the supramolecular 2:1 encapsulation of the anion within **17** in tetrahydrofuran (THF), the conductivity of Li^+ was significantly increased, due to enhanced dissociation of the ion pair (Figure 9B).

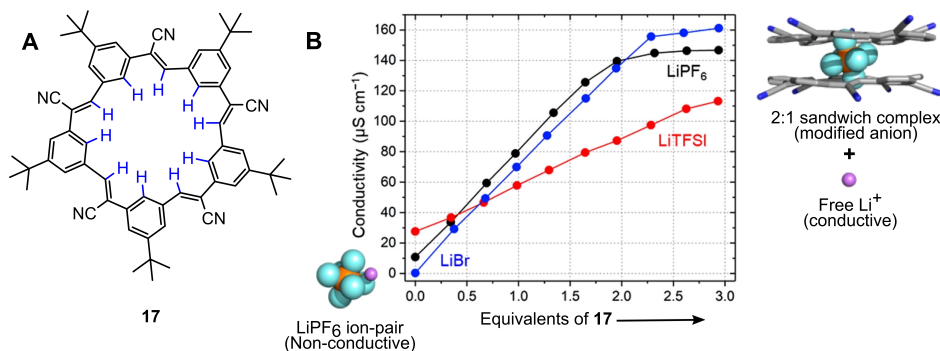


Figure 9. (A) *Cyanostar* **17** by Flood and co-workers.^[77] (B) Conductivity enhancement of LiBr, LiPF₆, and LiTFSI (lithium bis(trifluoromethane)sulfonimide) in THF with an increasing number of equivalents of **17**. Figure B is adapted from ref. [78], copyright 2018 American Chemical Society.

Self-assembly and gelation of low-molecular-weight gelators (LMWGs) rely on the formation of fibers based on 1D or 2D intermolecular non-covalent interactions, such as hydrogen bonds and hydrophobic effects. As the supramolecular anion hosts frequently rely on similar non-covalent forces in the binding of anions, gels formed by LMWGs can exhibit useful anion-responsive properties.^[79] Yamanaka and co-workers prepared the tris-urea gelator **18** (Figure 10), which formed an exceptionally stable gel from acetone (critical gelation concentration of 1.4 wt%), with no precipitation or melting of the gel observed when stored for several months at room temperature. Complete gel-sol transition was observed upon addition of F⁻, Cl⁻, Br⁻, I⁻, or AcO⁻ (in 1-3 equivalents to the gelator), due to the disruption of the hydrogen bonds that interconnect the LMWGs in the gel by the formation of an anion complex with **18**. Re-gelation was achieved by the addition of ZnBr₂, which bound the anions stronger than **18**.

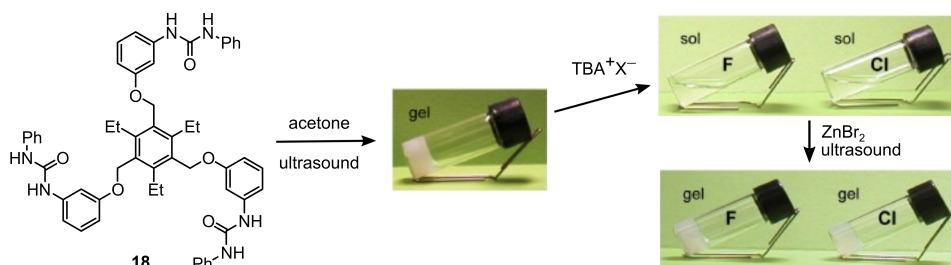


Figure 10. A low-molecular-weight gelator **18** by Yamanaka and co-workers^[80] also acted as a supramolecular host for anions, therefore the gelation of **18** could be controlled by the addition of F⁻, Cl⁻, Br⁻, I⁻, or AcO⁻. The gel-sol transition was reversed by the addition of ZnBr₂. Images of the gels are reprinted, with permission from Elsevier, from ref. [80].

1.3 Cucurbiturils and hemicucurbiturils

The remarkably strong association and compartmentalization of cationic or hydrophobic guests with cucurbit[*n*]urils (CB[*n*]) has impacted many areas of scientific research. These supramolecular hosts have been applied, for example, in nanoparticle-based sensors,^[81] as supramolecular reaction vessels in photocatalytic dimerization,^[82] and as potential drug delivery agents.^[83] The condensation reaction of glycoluril and formaldehyde in acidic conditions was first reported by Behrend, Meyer, and Rusche in 1905.^[37] The chemical structure of the condensation product remained unknown until 1981, when Freeman, Mock, and Shih revealed the macrocyclic structure of CB[6] by single crystal X-ray diffraction analysis.^[84] The authors also presented evidence for the strong and selective binding of alkylammonium guests, which underlies majority of the CB[*n*] applications today^[85–87] and has fueled wide-spread interest in these supramolecular hosts. The field of cucurbiturils (Figure 11) has grown not only in the number of homologues (CB[5]–CB[8] and CB[10]) and substituted derivatives, but has also inspired the advent of acyclic CB analogues^[88] and the anion-binding hemicucurbiturils HC[*n*].^[9] Bambusuril (BU[*n*]) and biotinuril hosts, highlighted earlier as the anion sensor **2** and transmembrane molecular transporters **8–10**, respectively, together with the cyclohexanohemicucurbiturils (cycHC[*n*]) studied in this work, belong to the branch of hemicucurbiturils.

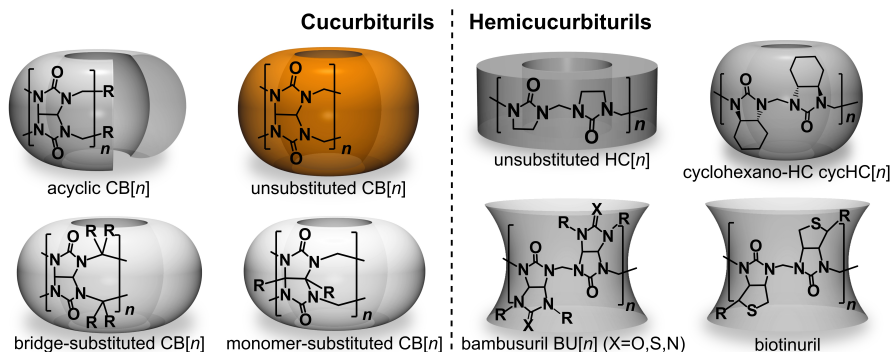


Figure 11. Cucurbiturils (CB[n]) and related anion-binding analogues, hemicucurbiturils (HC[n]), illustrating the approximate shape of the host types.

1.3.1 Properties of hemicucurbiturils

The first hemicucurbiturils were synthesized by Miyahara and co-workers through the condensation of ethyleneurea and 37% formalin in 4 M HCl, which resulted in the precipitation of crystals within 30 minutes.^[89] Single crystal X-ray diffraction analysis revealed that the product was an HCl adduct of HC[6], in which the Cl⁻ template was positioned at the center of the HC[6] cavity (Figure 12A). The authors expected a cone-shaped cucurbituril analogue capable of binding alkali cations, but HC[6] presented a completely new host scaffold for binding anions.

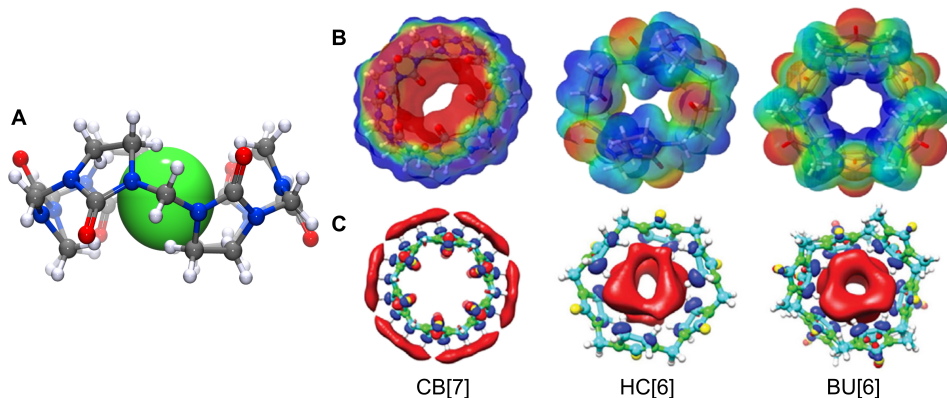


Figure 12. (A) Crystal structure of the chloride complex of HC[6] prepared by Miyahara and co-workers showing the position of the chloride template within the center of the cavity.^[89] The hydronium counter-cation and water molecules (located outside the HC[6]) are omitted for clarity. (B) Map of the electrostatic potential of CB[7], HC[6], and BU[6], with red signifying the negative and blue the positive regions, reprinted from ref. [90] with permission from Elsevier. (C) Lowest unoccupied molecular orbitals of CB[7], HC[6], and BU[6], reprinted from ref. [91] with permission from the Royal Society of Chemistry.

As a consequence of having only single methylene bridges, the monomers in HC[6] adopted an alternate orientation, which transformed the electronic structure of the host, as compared to the parent CB[6]. Computational studies on the frontier molecular orbitals and electrostatic potential of HC[n]s revealed that the anions were attracted by the concentration of positive electrostatic potential (Figure 12B) and the lowest unoccupied molecular orbital (Figure 12C) to the center of the HC[n] cavity.^[91] This effect

was consistent in substituted HCs.^[90–92] In addition, the hydrogen atoms directed into the cavity of HC[n]s created a hydrophobic binding pocket, allowing for the formation of several C–H⋯anion hydrogen bonds simultaneously. This was proposed *in silico*^[91,92] and demonstrated in solution by ¹H NMR and in the solid state by single crystal X-ray diffraction analysis. Non-covalent interactions governing the association of hemicucurbiturils with anions are discussed in detail as a part of the results of this thesis.

1.3.2 Dynamic covalent chemistry in the synthesis of cucurbituril-type hosts

All the cucurbituril-type macrocyclic molecular hosts were synthesized via the condensation of a urea-containing monomer with formaldehyde (Figure 13). In such the acid-catalyzed attack of the urea nitrogen on the electrophilic carbon of the formaldehyde and the subsequent water elimination leads to the formation of an iminium intermediate.^[93] The high-energy iminium intermediate then reacts quickly with available nucleophiles in the reaction media, such as a nitrogen atom of another monomer, resulting after a deprotonation step in the acylaminal linkage - the methylene bridge between monomers. Yoo and Kang proposed that a hydrogen-bonded water molecule on the carbonyl group of the monomer mediates both the nucleophilic attack and the deprotonation of the resulting ammonium intermediate.^[94] By accepting a hydrogen bond from the NH group in close proximity to the carbonyl group, the water molecule forms a six-membered hydrogen-bonded cycle, which exposes the nitrogen's lone electron pair and activates it as the nucleophile. The transfer of the proton to the water molecule deprotonates the ammonium intermediate formed in the nucleophilic attack.

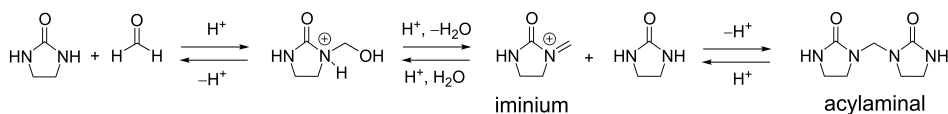


Figure 13. Reversible acid-catalyzed formation of the acylaminal linkage, illustrated on ethyleneurea monomers.

Continuous formation of the acylaminal linkages produces oligomers. However, as the acylaminal linkages are concurrently hydrolyzed back to the iminium species in acidic conditions through protonation on the neighboring nitrogen or the oxygen of the acyl group, these oligomerization reactions are reversible. The acylaminal linkages are less susceptible to hydrolysis than alkyl-aminals, as the electrons on the nitrogen are delocalized over the acyl group, decreasing the basicity of the aminal nitrogen and rendering the acylaminals stable at neutral pH.^[93]

Reversibility of the acylaminal linkages in acidic media allows for the formation of a dynamic covalent library (DCL) of oligomerization products. The product composition of the CB[n] and HC[n] synthesis could be determined by kinetic or thermodynamic effects and have resulted efficiently and selectively in a high yield single product.^[93] Error correction, by virtue of the reversible covalent linkages, is critical for reaching thermodynamic equilibrium in a DCL. Reversible covalent bonds such as imines,^[95] hydrazones,^[96,97] disulfides,^[98] boronates,^[99] aminals,^[100] and hemiaminals^[101] are also frequently used in dynamic covalent chemistry.

The equilibrium of the cucurbituril DCL (Figure 14) relies on the simultaneous and reversible processes of oligomer chain growth (Figure 14A), oligomer-to-macrocyclic cyclization (Figure 14B), and product stabilization (Figure 14C). The equilibrium can be

influenced by acid type and concentration, reagent concentration, temperature, and/or addition of templates.^[93]

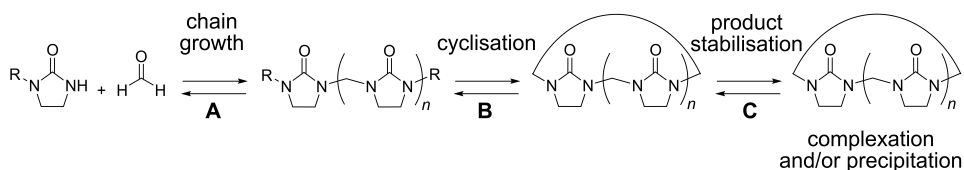


Figure 14. The simultaneous reversible processes within the cucurbituril DCL-s, illustrated on HC[n].

The condensation reaction forming CB[n] or HC[n] oligomers proceeds quickly in acidic conditions and the length of the resulting oligomers is determined by chain-growth equilibrium. The occurrence of a mixture of oligomeric precursors was confirmed by Day and co-workers following the condensation of glycoluril by ¹³C NMR, and by the groups of Pittelkow^[65] and Aav^[102,103] following single-bridged HC[n] synthesis by LC-MS. Notably, in studying the synthesis of cyclohexanohemicucurbit[n]urils (cycHC[n]), Aav and coworkers demonstrated the stark disproportionality of the UV absorbance between the linear oligomeric and macrocyclic species of cycHC[n].^[103] A 10-fold lower UV absorbance at 210 nm was observed for the linear hexamer compared to the corresponding cyclic cycHC[6], and no correlation between the number of monomers and UV absorbance was evident.

For the reaction to lead to macrocycles, chain-cycle equilibrium must favor the accumulation of cyclic product(s). Strong evidence of anion-templating has been observed in the case of HC[n]s, as their synthesis is very sensitive to the type of acid, and in appropriate conditions a single product is obtained in high yield.^[12,58,65,89,104–107] The synthesis of regular CB[n], appears to be less susceptible to templating, as evidenced in studies on the effects of cationic alkali metal templates. Because CB[n] synthesis generally yields a mixture of homologues, it is likely to be more influenced by kinetic effects. Resubmission experiments by Day and co-workers support the hypothesis that the smaller CB[5–7] macrocycles act as kinetic traps.^[108] When CB[8] was boiled in concentrated HCl (100 °C) a mixture of CB[5–8] was obtained, while no interconversion was detected for the smaller CB[5], CB[6], and CB[7] when individually subjected to the same conditions. Day and co-workers established that the degree of CB[n] selectivity was achieved by adjusting the acid concentration and type, temperature, and reactant concentration, but no absolute selectivity could be achieved.^[108]

1.3.3 Role of the anionic templates in hemicucurbituril synthesis

In Pedersen's first publication describing the synthesis of crown ethers, sodium ions were hypothesized to be involved in orienting the reactants through ion-dipole interactions to a conformation preferring the cyclization reaction.^[24] What Pedersen described is in fact the kinetic effect of templates, where the association of the template with a linear oligomer promotes the rate of cyclization of a specific macrocycle. In hemicucurbituril synthesis, a single product is obtained from the DCL owing to the thermodynamic templating effect of anions.^[93] The final product obtained from the reversible transformations between oligomers and macrocycles in DCL corresponds to the macrocycle that forms the thermodynamically most stable complex with the anionic template.

Chloride templating was first demonstrated by Miyahara *et al.* in the synthesis of HC[6] in 4 M HCl.^[89] In the same paper, the synthesis of HC[12] was achieved and it was

suggested that in template-deprived conditions (1 M HCl), longer oligomers could form, as the chain growth process was not terminated by the formation of HC[6]. Halide templating was also used for the synthesis of achiral^[104] and chiral^[12] cycHC[6], BU[6],^[10,58,109,110] semithio-BU[6],^[105] biotinurils,^[65] and norborna-HC[6]^[107] (Figure 15). Sindelar and co-workers noticed that in the absence of suitable templates, the condensation of 2,4-dibenzylglycoluril with paraformaldehyde produced a four-membered bambusuril with a 57% yield.^[109] Similarly, Reany and co-workers obtained semithio-BU[4] in the absence of halide templates.^[105] No accumulation of macrocyclic products was observed in the synthesis of cycHC[n] in the absence of suitable templates.^[102] However, Aav and co-workers found that larger anions, such as CF_3CO_2^- , HCO_2^- , and PF_6^- , promoted the formation of an eight-membered cycHC[8]. The synthesis and properties of cycHC[8] will be discussed in further detail in the results section, as one of the main topics of this thesis. The anion binding motifs of the HC[n], together with a study of the guest influence on the size and shape of the host will also be further discussed, based on the analysis of all the published crystal structures of HC[n].^[93]

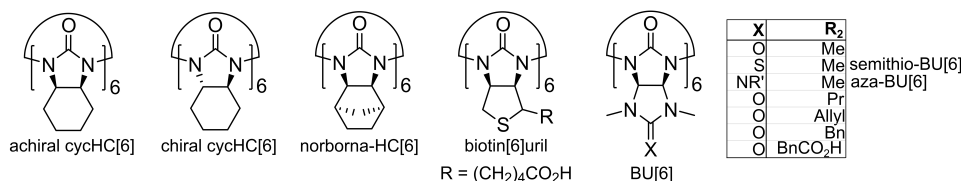


Figure 15. The chemical structures of the substituted six-membered hemicucurbiturils.

1.4 Solid-state organic synthesis

A critical aspect of developing practical applications for supramolecular systems is the simple and efficient chemical synthesis of the employed hosts. Strategies for the synthesis of macrocyclic molecules often include high-dilution experiments to suppress the rate of the intermolecular polymerisation reactions and promote intramolecular cyclization.^[111] Such processes are inefficient, costly, and generate significant solvent waste, which is incompatible with the movement towards more sustainable chemical synthesis.^[112] However, the syntheses of a number of supramolecular hosts do not require high dilution conditions, and a few examples even report solvent-free macrocyclization reactions (Section 1.4.4). Solvent-free covalent reactions occur in the solid state, in the melt, or at the solid-gas interface, and can be initiated, for example, by thermal or mechanochemical treatment,^[113] by microwave,^[114] or by UV radiation.^[115] In the context of this thesis, *solvent-free reactions* refer to processes where no bulk solvent was added. Avoiding bulk solvents has many advantages:^[21,116,117]

- Solvent-free or solid-state reactions can proceed faster due to the high concentrations of the reactants.
- Reducing the amount of solvents leads to sustainable low-waste chemical syntheses, while also lowering the cost of chemical processes.
- Solvent-free reactions can provide access to products that cannot be synthesized by conventional solution-based methods.
- Solid-state reactions expand the range of available reactants to insoluble starting materials.
- Reaction auxiliaries may have a stronger effect on the outcome of the reaction, as supramolecular interactions are not disrupted by the solvent.

1.4.1 Mechanochemistry

Mechanochemistry, in an ever-widening range of chemical processes, has become central to the development of solid-state synthetic procedures. Common to inorganic chemistry and alloying, mechanochemistry has also become an attractive method for organic, organometallic, and supramolecular chemists, with the promise of operationally simple, fast, and efficient reaction protocols.^[113,117–119]

Historically, mechanochemical reactions were conducted exclusively using a mortar and pestle (Figure 16A). However, some of the parameters influencing the chemical reaction during manual grinding have been difficult to define, namely the strength and grinding regime of the experimenter. Automated milling devices have therefore replaced most of the manual grinding in research laboratories, ensuring the reproducibility of experiments.^[120] In a shaker mill (Figure 16D), the sample is enclosed within a cylindrical milling jar (Figure 16C) with ball bearing(s), and shaken at a constant frequency (Figure 16B).

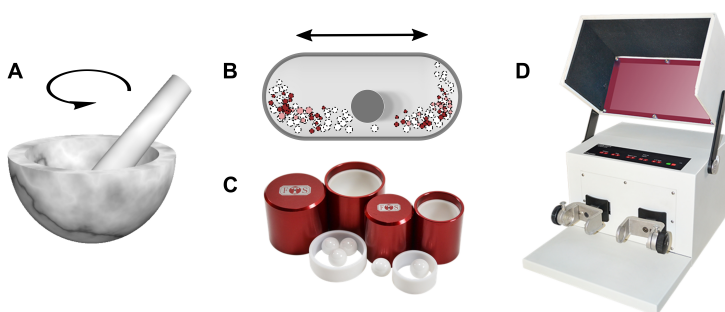


Figure 16. Mechanical agitation (A) by mortar and pestle and (B) in a jar of a shaker mill. (C) Zirconium oxide milling jars with ball bearings and (D) a shaker mill. Photos C and D are reproduced with the permission of Form-Tech Scientific, Inc.

Mechanochemical synthesis can be carried out with neat solid reactants, or by adding a sub-stoichiometric amount of liquid to the reactants in a liquid-assisted grinding (LAG) experiment. The ratio of the liquid to the weight of the reactant mixture (η) is within the range of $0 < \eta < 1 \mu\text{l mg}^{-1}$.^[118] The catalytic amount of liquid can activate the surfaces of the solid particles and promote diffusion of the reactants, and has been shown to accelerate mechanochemical reactions. Varying the type and quantity of the added liquid in LAG has, for example, been used to control the polymorphism of crystalline compounds and co-crystals,^[121–123] the reaction rate and/or stereochemistry of covalent syntheses,^[124,125] and the topology of metal-organic frameworks (MOF).^[126]

Mechanochemistry can be complemented or substituted by the milder, low-energy input solid-state approach of *aging*. Inspired by the natural chemical weathering and biomineralization processes, aging was demonstrated in the synthesis of MOFs from static mixtures of metal oxides with organic ligands.^[127–129] Exposing the reaction mixtures to elevated temperature or solvent vapors was shown to accelerate the aging reactions.

A wide variety of organic reactions have been adapted to solvent-free conditions. The examples described in this overview are limited to the concepts relevant to the development of solid-state synthesis of cycHC[n] (**Publication IV**). Examples include the solid-state aldehyde-amine condensation, achieving thermodynamic or supramolecular control in mechanochemical reactions and the covalent synthesis of macrocyclic

molecules using mechanochemistry. For further examples, the reader is directed to reviews by Toda^[130,131] and Kaupp^[132] on the solvent-free thermal reactions and photoreactions, and to the reviews by the groups of Bolm,^[133,134] Friščić,^[21,118] and Browne^[117] on various mechanochemical organic transformations.

1.4.2 Solvent-free imine condensation reactions

Pioneering work by Toda, Kaupp and co-workers established a solid-state method for the quantitative preparation of azomethines **21** by grinding solid anilines **19** with aromatic aldehydes **20** (Figure 17).^[135] Grinding (by mortar and pestle) was used to reduce the particle size of the crystalline starting materials and expose fresh surfaces for contact, followed by aging for 2–120 hours for quantitative conversion at room temperature. Only the condensation of **19b** and **20c** required 24 hours of aging at 50 °C for full conversion. When a stoichiometric amount of pure **19** and **20** was used, no work-up, other than the evaporation of the formed water, was necessary for the purification of azomethines **21**.

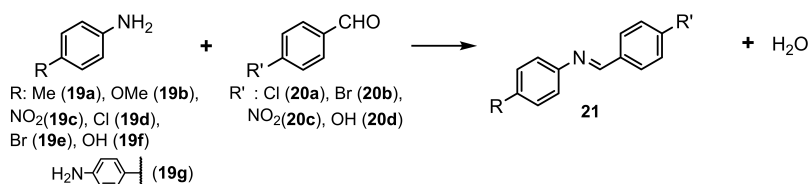


Figure 17. The solvent-free synthesis of azomethines **21**.^[135]

Importantly, Kaupp and co-workers demonstrated a scaled-up mechanochemical imine condensation reaction.^[136] 200 g batches of *p*-aminobenzoic acid and **20d** were reacted in a stoichiometric ratio using a water-cooled 2 L horizontal ball mill (Simoloyer®) loaded with 2 kg of 5 mm diameter steel ball bearings. Pure azomethine derivative was obtained by high-frequency milling at 900 rpm for 15 minutes and no aging was required.

Cinčić and co-workers noticed that the solid-state condensation of the Schiff bases **24a-c** was accelerated by 98% relative humidity (RH) when aging the lightly ground mixtures (10 min, mortar and pestle) of 2-hydroxy-1-napthaldehyde **22** with **23a-c** (Figure 18).^[137] Recognizing the catalytic effect of solvent vapors, the reaction rates for the synthesis of **25** and **26** were significantly improved by fine-tuning the solvent atmosphere in the respective aging reactions. The RH and solvent atmosphere were introduced by sealing a vial containing the solid reactants within a closed system alongside a reservoir of the solvent, with no direct contact between the solids and the liquid. Product **25** was obtained quantitatively by aging 5-aminosalicylic acid with *o*-vanillin for 28 days at 95% RH or, surprisingly, after only one hour in EtOH vapors. Aging 5-aminosalicylic acid with **22** yielded **26** within one day in a vapor mixture of EtOH and an organic base of triethylamine (5% v/v of TEA). **25** and **26** could also be obtained quantitatively by LAG, if milled in the presence of the solvents used for the acceleration of the aging reactions.

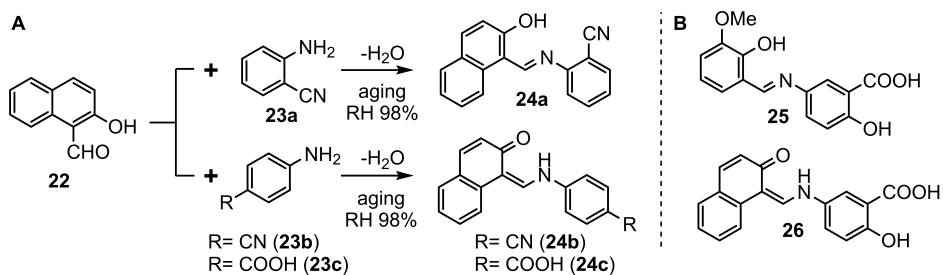


Figure 18. (A) Reaction scheme for the preparation of Schiff bases **24a-c** and (B) the chemical structures of products **25** and **26**.^[137]

1.4.3 Equilibrium of reversible mechanochemical covalent reactions

While the reversibility of covalent bonds under mechanochemical conditions underlines many of the developed solid-state organic transformations, very few studies address the thermodynamic factors that control the reaction outcome. Based on exploring the metathesis of homodimeric disulfides, Belenguer and co-workers demonstrated that the reversible exchange of the groups forming disulfide covalent bonds reached an equilibrium composition under mechanochemical conditions (Figure 19).^[138] Ball milling of homodimers **27** and **28** with a base catalyst led selectively to the formation of a heterodimer **29**, contrasting the statistical distribution 1:1:2 (**27**:**28**:**29**) obtained from the solution reaction. Alternatively, the metathesis of **28** and **30** resulted in a mixture preferring homodimers (80%) over the heterodimer **31** (20%), regardless of whether the starting point was an equimolar mixture of the homodimers or the purified heterodimer **31**. The lattice energy differences between the polymorphs were proposed to be the major factor determining the thermodynamic equilibrium in these systems. The total crystal lattice energies of the homodisulfides and formed heterodisulfides were calculated based on the sum of intermolecular interaction energies and the conformational energy of the disulfides in the crystal lattice.

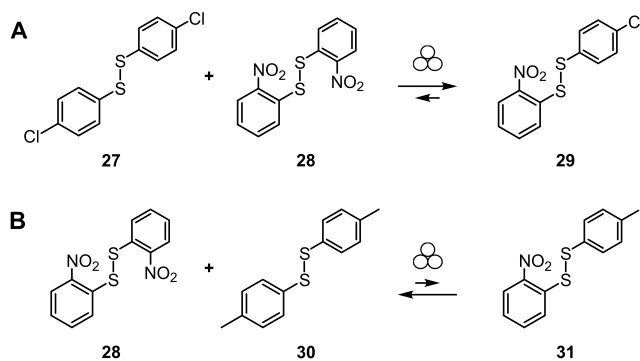


Figure 19. Equilibrium in the reversible disulfide metathesis under mechanochemical conditions.^[138]

In a follow-up study, Belenguer and co-workers further investigated the disulfide **27** and **28** (Figure 19A) metathesis by neat grinding and LAG (acetonitrile).^[139] Two stable polymorphic forms of the heterodimer were obtained by either of the mechanochemical reaction conditions. The different polymorph stability orders in LAG conditions as compared to those in the neat grinding reaction were ascribed to the crystallite surface solvation free energy difference. This could also be one of the determining factors of the thermodynamic equilibrium of LAG reactions. The interconversion between the

polymorphic forms of the heterodimer, if carried out in the presence of the base catalyst, was also found to proceed through the formation of homodimeric intermediates.

Ravnsbæk and Swager reported that a steady degree of polymerization (≈ 40 kDa) of a poly(phenylene vinylene) **33** was reached by solid-state ball milling in either Gilch polymerization of the monomer **32** or by degradation of the higher molecular weight polymers (150 kDa).^[140] The steady state was ascribed to an equilibrium between the competing mechanochemical polymerization and chain scission processes.

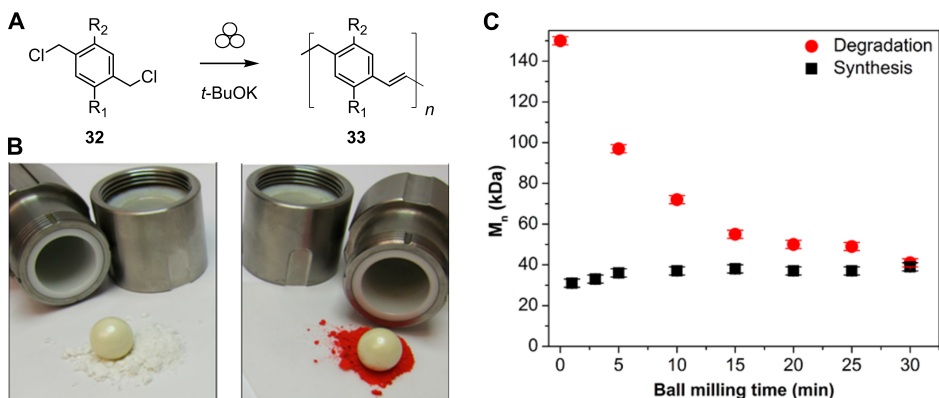


Figure 20. (A) Gilch polymerization in the solid state demonstrated by Ravnsbæk and Swager.^[140] (B) The starting material **32** is a white powder (left), while the polymerization product is bright red (right). (C) Number average molecular weight (M_n) of the polymers as a function of milling time, starting either from the monomer **32** (black squares) or from solution-prepared higher molecular weight (150 kDa) polymers (red circles). Figures B and C are reprinted from ref. [140], copyright 2018 American Chemical Society.

1.4.4 Synthesis of macrocyclic molecules by mechanochemistry

To date, only a few examples of the covalent synthesis of macrocyclic molecules by mechanochemistry have been published. The first report came from Atwood and co-workers,^[141] who used ball milling to improve the access to *p*-benzylcalix[5]arenes, known to encapsulate C_{60} .^[142] A base-catalyzed solution-based condensation of *p*-benzylphenol and formaldehyde yielded a mixture of *p*-benzylcalix[*n*]arenes ($n = 5, 6, 8$). From this the purified even-numbered calixarenes were partially converted to a mixture of *p*-benzylcalix[*n*]arenes ($n = 5, 7, 10$) by ball milling with paraformaldehyde, KOH, and molecular sieves under an argon atmosphere for 4-16 hours (Figure 21A). Thus, the reversibility of the methylene linkages of the macrocycle under mechanochemical conditions was demonstrated. A mechanochemical condensation reaction starting from *p*-benzylphenol, however, resulted only in traces of the calixarenes.

While the base-catalyzed condensation of *p*-alkylphenols can result in macrocycles of various sizes, the acid-catalyzed condensation of resorcinol has been shown to invariably produce tetrameric macrocycles.^[143] Efficient solvent-free synthesis of resorcin[4]arenes **34-38** was established by Roberts and co-workers^[144] through manual grinding of the aldehyde and resorcinol in the presence of a catalytic amount of solid *p*-toluenesulfonic acid (Figure 21B). Upon grinding, the reaction mixtures were observed to first liquify and then stiffen within minutes, affording 80-96% conversion to macrocyclic products. This is in stark contrast to the conventional solution-based synthesis where an aldehyde and resorcinol are refluxed in a mixture of mineral acid and alcohol from several hours up to a few days. Bridge-substituted resorcin[4]arenes, such as **34-38**, can cyclize in four

diastereomeric isomers of which the *cis-cis-cis* (*rccc*) in the crown conformation and the *cis-trans-trans* (*rctt*) in the chair conformation are most frequently obtained.^[143] Roberts *et al.* observed that while the compounds **34-36** were obtained as a 1:2 mixture of the *rccc* and *rctt* stereoisomers, **37** exclusively afforded the *rccc* conformation and the reaction mixture of **38**, containing initially both stereoisomers when left to age converged wholly to the *rctt* isomer.

Solvent-free stereoselective condensation of isovaleraldehyde and pyrogallol by grinding with a catalytic amount of *p*-toluenesulfonic acid was demonstrated by Atwood and co-workers.^[145] The crown isomer of isobutylcalix[4]pyrogallolarene **39**, obtained as a brittle white solid within two minutes from the start of the reaction, self-assembled upon further grinding into hydrogen-bonded nano-capsules comprising six **39** units each (Figure 21C). The nano-capsule enclosed a 1300 Å³ cavity containing water molecules from the condensation reaction and traces of unreacted starting materials, determined by diffusion NMR studies of the reaction products.

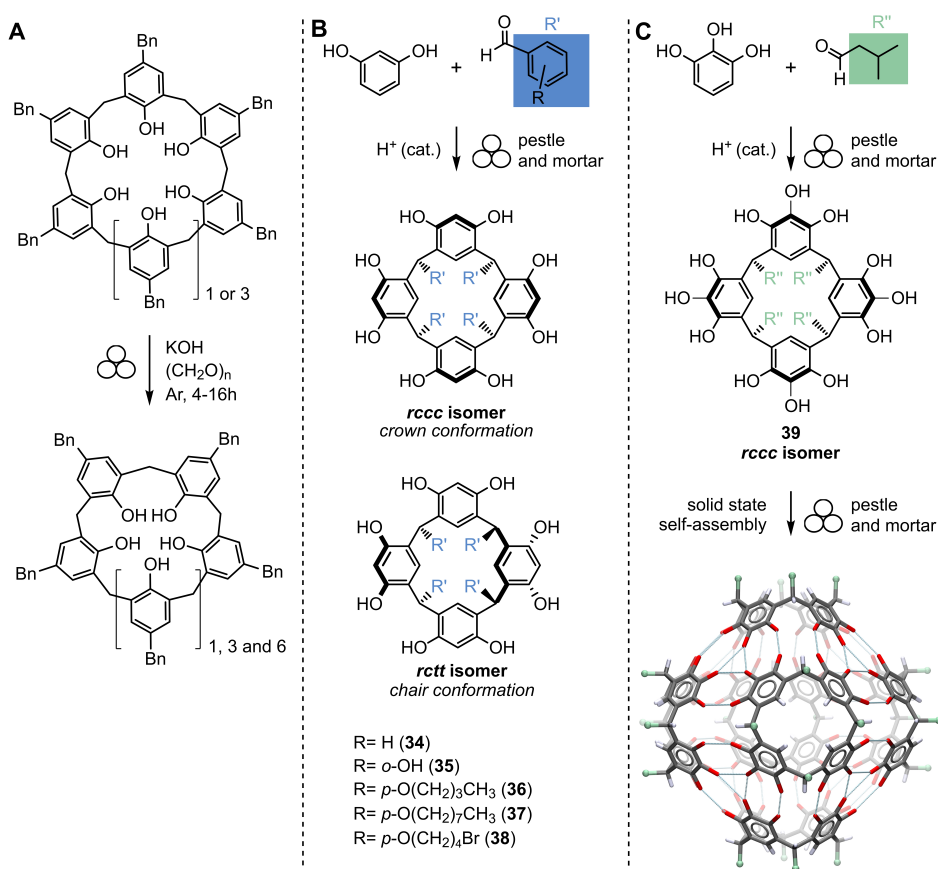


Figure 21. Reaction schemes for (A) the conversion of six- and eight-membered *p*-benzylcalixarenes to five-, seven-, and ten-membered *p*-benzylcalixarenes, (B) formation of resorcin[4]arenes **34-38**, and (C) formation of isobutylcalix[4]pyrogallolarene **39** and its self-assembly into a nano-capsule.

An elegant example of a mechanochemical multicomponent polycondensation of macrobicyclic cage structures was described by Severin and co-workers.^[146] The cages **44** and **45** were obtained by forming simultaneous imine and boronic ester linkages between

1,3,5-*tris*(aminomethyl)-2,4,5-triethylbenzene **40**, pentaerythritol **41**, and either of the rigid linkers, 4-formylphenylboronic acid **42** or 4-(4-formylphenyl)-phenylboronic acid **43** (Figure 22A). The respective one-pot [6+3+2] condensation reactions by ball milling (one hour at 20 Hz) afforded 94% of **44** or 71% of **45**; far superior to the solution-based methods, which provided up to 56% yield of **44** and no isolable amount of the larger cage **45**.

In an extension of this work, the same group later described the similar multi-component polycondensation of borasiloxane-imine macrocycles **46** and **47** (Figure 22B), yielding respectively 85% or 65% isolated product by ball milling for 1.5 hours at 30 Hz.^[147] Imine linkages with boronic ester or borasiloxane motifs were chosen in these two studies as dynamic covalent bonds that can be used in tandem, allowing for the high selectivity of the product by error correction during synthesis.

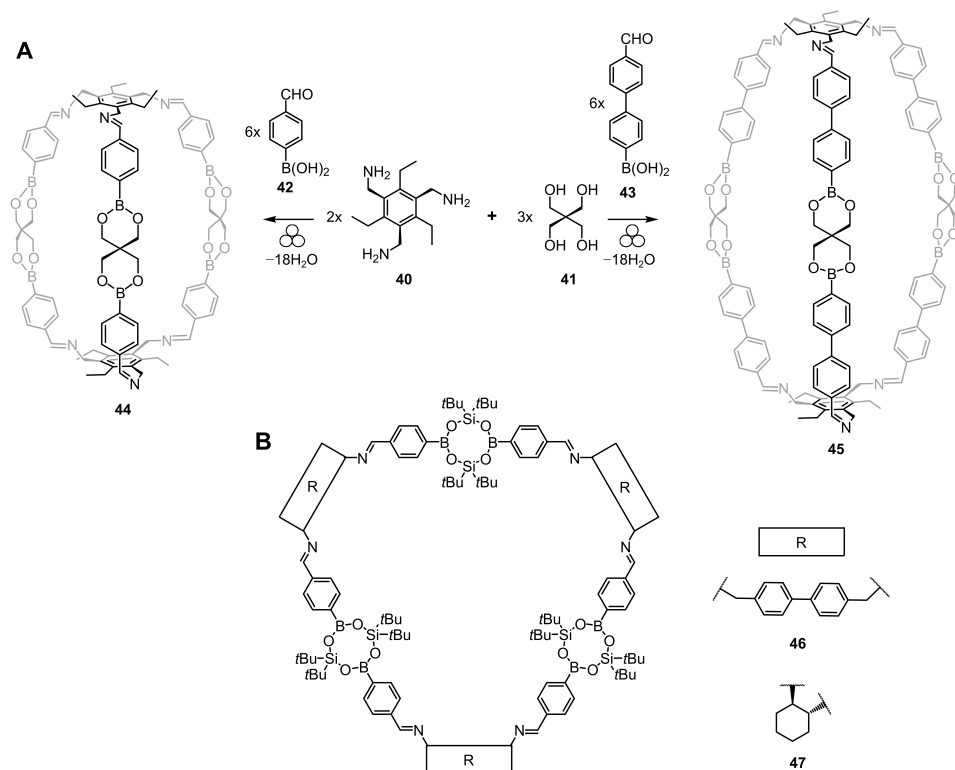


Figure 22. (A) Reaction scheme for the polycondensation of boronate ester-imine macrocyclic cages **44** and **45** by Severin and co-workers.^[146] (B) Borasiloxane-imine macrocycles **46** and **47** from the Severin group.^[147]

A recent contribution by Garcia and co-workers described the selective and versatile mechanochemical synthesis of macrocyclic cyclophosphazane-based structures.^[148] Nucleophilic substitution on the dichlorocyclodiphosphazane **48** with a series of bifunctional organic acids **49a-d** by milling in the presence of Et₃N resulted selectively in dimeric cyclic products **50a-d** (Figure 23). This beautifully demonstrated the potential of solvent-free ball milling for air- and moisture-sensitive synthesis, which would require the use of strictly dried solvents if conducted in solution. More importantly, by using

solvent-free conditions, the scope of the nucleophiles was broadened to those insoluble in toluene or THF generally used in cyclodiphosphazane syntheses.

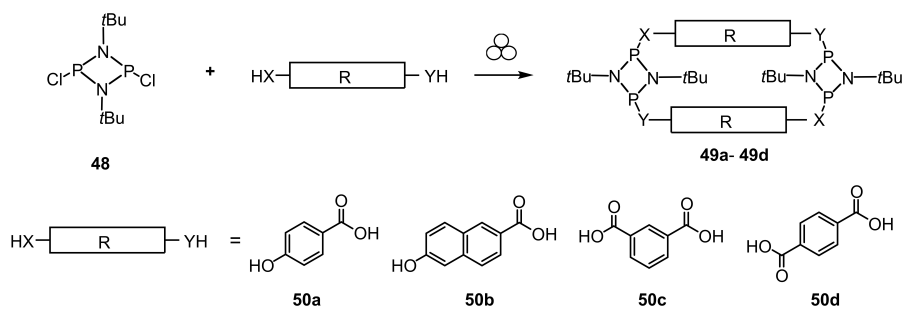


Figure 23. Reaction scheme for the formation of cyclophosphazane-based dimeric macrocycles **49** developed by Garcia and co-workers.^[148]

2 MOTIVATION AND AIMS FOR THE WORK

Hemicucurbiturils have emerged as a new anion-binding scaffold, offering a host design platform that relies on alternative non-covalent interactions; i.e. not the conventional hydrogen bonds and electrostatic interactions commonly employed in the anion receptors. The exact nature of these more exotic non-covalent interactions and phenomena, such as C–H⋯anion interactions, solvophobicity, and the chaotropic effect, is not well understood. Further studies addressing the anion-binding properties of hemicucurbiturils have the unique potential of advancing the fundamental understanding of these types of supramolecular interactions.

Regardless of the short history of hemicucurbiturils, the selectivity of these hosts for size-compatible polarizable halide anions has been recognized and applied in anion sensing and transmembrane transport. An important advantage of hemicucurbiturils, providing a solid foundation to all present and future applications, is their ease of synthesis. Halide anion templating affords high yields of the six-membered hemicucurbiturils in a single step. Developing an anion-templated synthesis protocol for larger hosts has two main objectives: to establish the role of templates in the dynamic covalent chemistry of hemicucurbiturils and to extend the range of available host molecules. Larger hosts are expected to be selective towards different guests, as compared to the currently known six-membered hemicucurbiturils, which could lead to new applications for these supramolecular hosts.

The anion templated hemicucurbit[*n*]uril syntheses provide a valuable opportunity to investigate templated covalent syntheses of macrocycles in the solid state. To date, none of the examples of solvent-free synthesis of macrocycles involve the use of templates. Supramolecular interactions involved in anion templating could even be pronounced in the solid state, due to the lack of competition from solvent molecules.

The specific aims of this thesis were to:

- Crystallize and characterize the structure of the novel chiral eight-membered hemicucurbituril host, (all-*R*)-cyclohexanohemicucurbit[8]uril (cycHC[8]), by single crystal X-ray diffraction analysis.
- Establish the anion complexation properties of cycHC[8] in solution by nuclear magnetic resonance spectroscopic techniques and in the solid state by single crystal X-ray diffraction.
- Investigate the effect of guest molecules (including known templates) on the shape of hemicucurbituril hosts, based on the crystal structures published in the CSD and characterize the anion interaction sites in the crystal structures of the hemicucurbiturils.
- Develop a solid-state approach for the anion-templated synthesis of cycHC[*n*].

3 DETAILS OF USED METHODS

The following section provides a brief description of the method used for anion volume calculation in this thesis. Other detailed experimental protocols can be found in the supporting information of the corresponding publications.

3.1 Calculation of the anion volumes

The anion volumes in this study were calculated using the triangulated sphere model included in the Olex2 program package,^[149] in which all atoms are approximated to isotropic spheres defined by the default CSD van der Waals (vdW) radii. The geometry of the anions was optimized (BP86-D/def2-TZVPD) prior to the volume calculation.¹ The bond lengths for the geometry optimization were restricted to the mean values based on the crystallographic data published in the CSD (Table 2). The coordinates of the optimized anion geometries are included in Appendix 2.

Table 2. Calculated mean bond lengths in the studied anions, based on CSD entries up to May 2016.

Anion	Number of CSD entries ^[a]	Bond	Mean bond length (Å)	V_{anion} (Å ³) ^[b]	Comments
SbF ₆ ⁻	1625	Sb–F	1.846	81.8 ^[c]	
PF ₆ ⁻	16272	P–F	1.568	70.6	
ReO ₄ ⁻	313	Re–O	1.706	64.8	
IO ₄ ⁻	28	I–O	1.746	64.3	3 outliers rejected
ClO ₄ ⁻	20831	Cl–O	1.405	54.7	
BF ₄ ⁻	11361	B–F	1.361	51.6 ^[c]	
CF ₃ SO ₃ ⁻	7898	C–F	1.326	82.3	
		C–S	1.428		
		S–O	1.795		
CF ₃ CO ₂ ⁻	743	C–F	1.318	68.7	
		C–C	1.526		
		C–O	1.232		
HCO ₂ ⁻	204	C–H	0.964	35.1 ^[d]	
		C–O	1.245		
SO ₄ ²⁻	1534	S–O	1.472	54.9 ^[d]	
		S=O	1.466		
CH ₃ CO ₂ ⁻	557	C–H	0.973	49.7 ^[d]	2 outliers rejected
		C–C	1.502		
		C–O	1.256		
		C=O	1.250		

[a] Only entries with defined 3D coordinates were analyzed. [b] Van der Waals radii used by the CSD, from refs. ^[150] and ^[151]: H 1.09 Å, C 1.7 Å, O 1.52 Å, F 1.47 Å, S 1.8 Å, Cl 1.75 Å, I 1.98 Å, P 1.8 Å, B 2 Å, Sb 2 Å, Re 2 Å. [c] According to a recent study by S. Batsanov,^[152] which suggests vdW radii of 2.2 Å for Sb and 1.8 Å for B, these volumes may be slightly under- and overestimated, respectively. However, as these atoms are at the center of the respective anions, SbF₆⁻ and BF₄⁻, the contribution to the overall anion volume is small and the differences in the calculated anion volume are within 5%. [d] Entries up to August 2018 were analyzed.

¹ Geometry optimization performed by Dr. Mario Öeren

4 RESULTS AND DISCUSSION

The results in this dissertation are based on four publications. The following discussion first covers the template-controlled synthesis and structural characterization of the novel cyclohexanohemicucurbit[8]uril (cycHC[8]) macrocyclic host (**Publication I**). The second section focuses on the supramolecular properties of cycHC[8], describing the strength, selectivity, and mechanism of anion encapsulation by this host (**Publication II**). The third section provides an overview of the supramolecular properties of different types of hemicucurbiturils in the solid state based on the published crystal structures (**Publication III**). The final section describes the development of a novel solid state approach for the templated synthesis of cycHC[6] and cycHC[8] (**Publication IV**).

4.1 Synthesis and structure of (*all-R*)-cyclohexanohemicucurbit[8]uril (**Publication I**)

4.1.1 Template-controlled synthesis conditions

The formation of (*all-R*)-cycHC[8], together with small amounts of the seven-, nine-, and 10-membered homologues, was first noticed by careful HPLC-MS analysis of the by-products in the synthesis of (*all-R*)-cycHC[6] from (*R,R*)-hexahydro-2-benzimidazolinone and paraformaldehyde in a 4 M HCl solution.^[153] Alongside the favored cycHC[6] product, 11% of the eight-membered macrocyclic product was isolated. Discovering that the amount of cycHC[8] slowly increased in the HPLC samples containing formic acid led to the optimization of reaction conditions. Thus, the selective formation of cycHC[8] was facilitated by applying acids that dissociate to larger anionic templates, such as formic acid and trifluoroacetic acid. An isolated yield of 71% was obtained starting from the monomer or by interconversion from the cycHC[6] (Figure 24). Again, a careful HRMS analysis indicated the occurrence of cycHC[6-10] together with various linear oligomers during these reactions, which indicated that to the reaction pathway involved a dynamic covalent library (DCL).

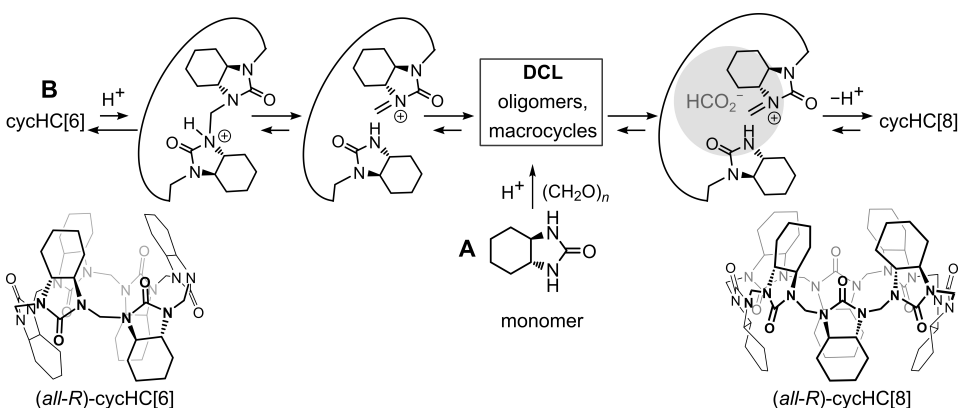


Figure 24. The proposed reaction mechanism for the synthesis of (*all-R*)-cycHC[8] from either (A) the monomer (*R,R*)-hexahydro-2-benzimidazolinone or (B) from the (*all-R*)-cycHC[6], both proceeding through the dynamic covalent library and templated by either HCO_2^- (illustrated), CF_3CO_2^- , or PF_6^- anions.

According to the DFT calculations, the thermodynamic equilibrium in the acid-induced DCL was directed towards cycHC[8] by the formation of a low-energy inclusion complex

with a suitably sized anionic template. This agreed well with the experimental observations, as the reactions catalyzed with the non-templating acetic acid yielded only a mixture of oligomers. This clearly illustrated that the cycHC[*n*] macrocycles were not thermodynamically favored over linear oligomeric products in the absence of suitable templates. To further prove the determining role of the anionic templates, corresponding salts were added to the reactions in the non-templating acetic acid. CycHC[6] was then efficiently transformed into cycHC[8] in the presence of NaPF₆ (90% isolated yield), and cycHC[8] was partially converted back to cycHC[6] in the presence of NaCl (21% isolated yield). The reaction rate was observed to depend on the strength of the acid, which was likely due to the faster acid-promoted transformations between the DCL members.

4.1.2 Single crystal X-ray diffraction analysis

Slow evaporation of a concentrated solution of (all-*R*)-cycHC[8] in methanol afforded transparent needle-like single crystals. Removal of the crystals from the mother liquor resulted in fast crystal deterioration at room temperature. The crystal used for single crystal X-ray diffraction analysis was therefore covered in protective oil and quickly transferred to the liquid nitrogen cooling stream maintaining the temperature at 200 K, effectively preventing deterioration.

The obtained structure revealed that cycHC[8] crystallized with two symmetry-independent molecules in the asymmetric unit, and was surrounded by hydrogen-bonded solvent molecules. The crystal structure of cycHC[8] (Figure 25) confirmed the computationally predicted *C*₄-symmetric barrel-shaped geometry of this host.^[153] The methylene-linked belt of the macrocycle assumed a square shape (Figure 25B), encircling the cavity of cycHC[8]. No solvent molecules could be resolved within the cavity of cycHC[8] in the crystal structure, indicating that the encapsulated solvent had no preferred orientation. The SQUEEZE^[154] procedure of PLATON^[155] revealed that the electron density within the isolated void of the cycHC[8] cavity accounted for a single methanol molecule. The cavity volume of cycHC[8] (123 Å³), calculated using a probe the size of a single hydrogen atom (probe radius 1.2 Å, grid step 0.2 Å), was comparable to the cavity of the regular cucurbit[6]uril (119 ± 21 Å³)^[156] and was 3.5 times larger than that of cycHC[6] (35 Å³).^[12]

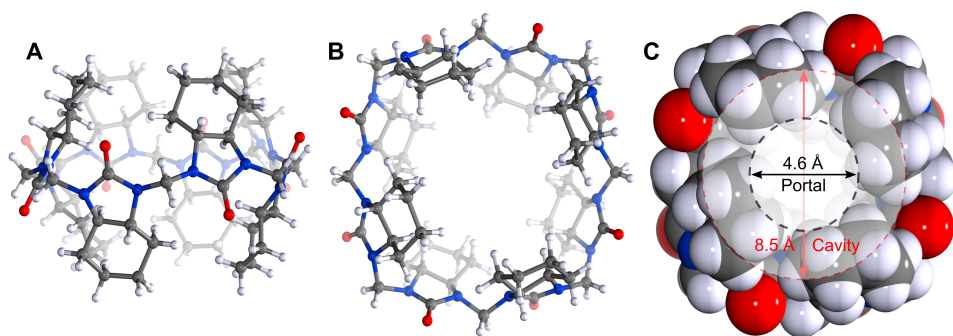


Figure 25. Crystal structure of (all-*R*)-cycHC[8], showing (A) the side and (B) the top view in the ball and stick representation. (C) Illustrates the dimensions of the portal and the cavity of the macrocycle on the CPK model of cycHC[8]. The dimensions shown account for the van der Waals radii of the atoms.

The solvent molecules in the crystal structure were positioned between the stacked cycHC[8], in continuous channels along the crystallographic *b*-axis (Figure 26B and 26C). This suggests that the rapid deterioration of the crystals in air or oil was due to the loss of the co-crystallized solvent at room temperature. At the temperature of the measurement, the solvent molecules hydrogen-bonded to the cycHC[8] carbonyl groups or to each other were located from the Fourier difference map. Nine methanol and one water molecule were modelled in the asymmetric unit (Figure 26A). The contribution of the heavily disordered solvent molecules in the channels that could not be modelled was calculated using the SQUEEZE procedure and subsequently included in the refinement.

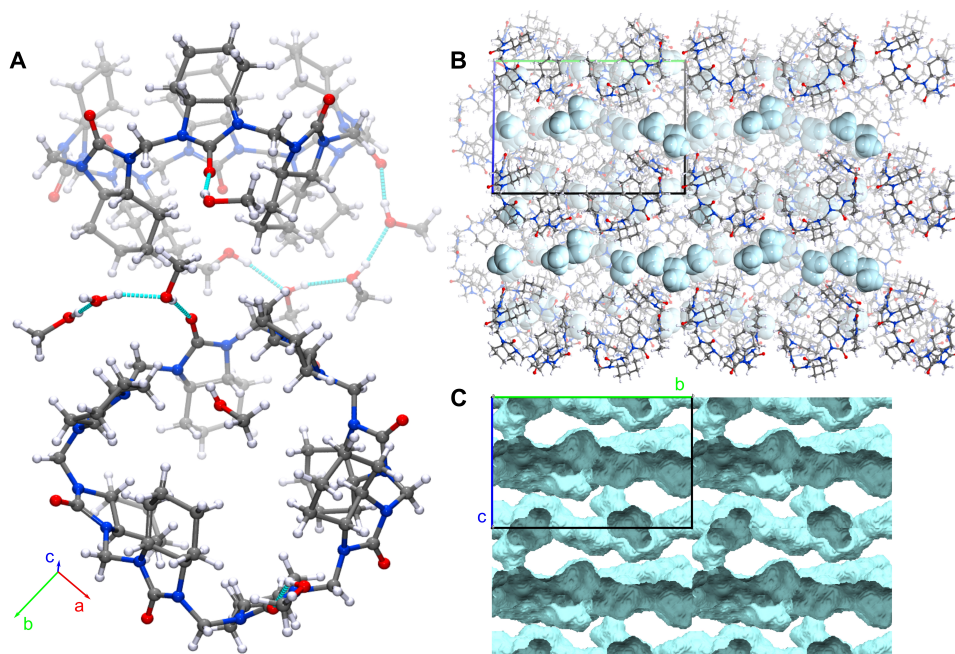


Figure 26. (A) Hydrogen bonds between cycHC[8] and solvent molecules within the asymmetric unit of the crystal structure. The hydrogen bonds are shown as blue dashed lines. (B) Packing of the structure viewed along the crystallographic *a*-axis, showing the arrangement of the solvent molecules into channels along the direction of the *b*-axis (green). The continuity of the channels is more evident in scheme (C) which was generated by removing all the refined solvent molecules and visualizing the resulting voids using the program Mercury^[157] (probe radius 1.2 Å, grid step 0.2 Å). The voids shown (light blue) represent both the channels and the cycHC[8] cavities, and account for 28% of the unit cell volume.

4.2 Complexation properties of (*all-R*)-cyclohexanohemicucurbit[8]uril (Publication II)

The templates established for the synthesis of cycHC[8] in **Publication I** suggested that this host binds larger anions, in contrast with the six-membered hemicucurbiturils, which preferably bind halides. According to the cavity volume (123 Å³) obtained from the crystal structure and a Rebek's ratio of 55% for optimal host-guest packing efficiency,^[158] cycHC[8] can certainly accommodate the used template anions PF₆⁻ (70 Å³), CF₃CO₂⁻ (68 Å³), and HCO₂⁻ (35 Å³). The observation that similarly sized anions CH₃CO₂⁻ (50 Å³) and SO₄²⁻ (55 Å³) were ineffective in templating cycHC[8] suggested that, besides the size of

the anion, there was an additional factor determining the selectivity of cycHC[8]. Anion-binding properties of cycHC[8] were therefore studied by a range of analytical techniques, including mass spectrometry, NMR spectroscopy and ITC, single crystal X-ray diffraction analysis, and computational chemistry.

Gas-phase ESI-MS three-component competition experiments between two anions towards cycHC[8], revealed that the host formed 1:1 complexes with the following anions, listed by relative affinity: $\text{SbF}_6^- = \text{PF}_6^- > \text{ReO}_4^- > \text{ClO}_4^- > \text{SCN}^- > \text{BF}_4^- > \text{HSO}_4^- > \text{CF}_3\text{SO}_3^-$. Halide anions (preferably bound by the six-membered hemicucurbiturils) and the more strongly solvated H_2PO_4^- , CH_3CO_2^- , and NO_3^- formed significantly weaker complexes with cycHC[8]. This was the first evidence that cycHC[8] preferably binds charge-diffuse size-compatible anions.

4.2.1 Solid-state studies of the anion inclusion complexes with cycHC[8]

Single crystal X-ray diffraction analysis offers ultimate proof of molecular or supramolecular structures, by revealing the precise spatial arrangement of atoms in a crystal. In addition, crystallographic data allows for the analysis of supramolecular interactions, steric compatibility, thermal motion, and potential disorder of the components within a supramolecular system providing invaluable information on the characteristics of host-guest complexes.

The host-guest complexes with cycHC[8] were crystallized from a methanol solution in the presence of 1-2 molar equivalents of the anionic guest, introduced as a tetrabutylammonium (TBA) or tetrabutylphosphonium (TBP) salt. The crystal structures unambiguously demonstrated the formation of 1:1 inclusion complexes with SbF_6^- , PF_6^- , ReO_4^- , IO_4^- , ClO_4^- , BF_4^- , and CF_3SO_3^- ; the guest anions completely desolvated and isolated inside the cycHC[8] (Figure 27). Comparing the size of the bulky guests with the narrow dimensions of the cycHC[8] portals suggested that the guest encapsulation and release were accompanied by the conformational changes of the host, which opened and closed the portals, resembling a molecular Pac-Man. While the smaller tetrahedral anions ReO_4^- , IO_4^- , ClO_4^- , and BF_4^- (size range 50–65 Å³) appeared as disordered within the cycHC[8] cavity, larger anions SbF_6^- (82 Å³) and PF_6^- (70 Å³) adopted a fixed orientation, reflecting the compatibility of the size and shape to the cavity of cycHC[8]. Four fluorine atoms of the C_4 -symmetric SbF_6^- and PF_6^- lie in the equatorial plane of the macrocycle, with the corresponding Sb–F or P–F bonds pointing to the four corners of its square-shaped belt (Figure 27A,B). The two remaining Sb–F or P–F bonds point to the opposite portals. CF_3SO_3^- (82 Å³) also adopted a preferred orientation within the cavity. With two oxygen and two fluorine atoms lying close to the equatorial plane and the remaining oxygen and fluorine atom pointing to the direction of the opposite portals, its orientation closely resembled that of the octahedral anions (Figure 27C). The disorder models of the tetrahedral anions alternatively illustrated how the smaller anions had more space, and thus, considerable freedom to move within the cycHC[8] cavity (Figure 27D–G). It also revealed that the cavity of cycHC[8] is relatively rigid, as it did not adapt to the smaller size of the guest, which could be the reason for the selectivity of this host observed by the ESI-MS competition experiments.

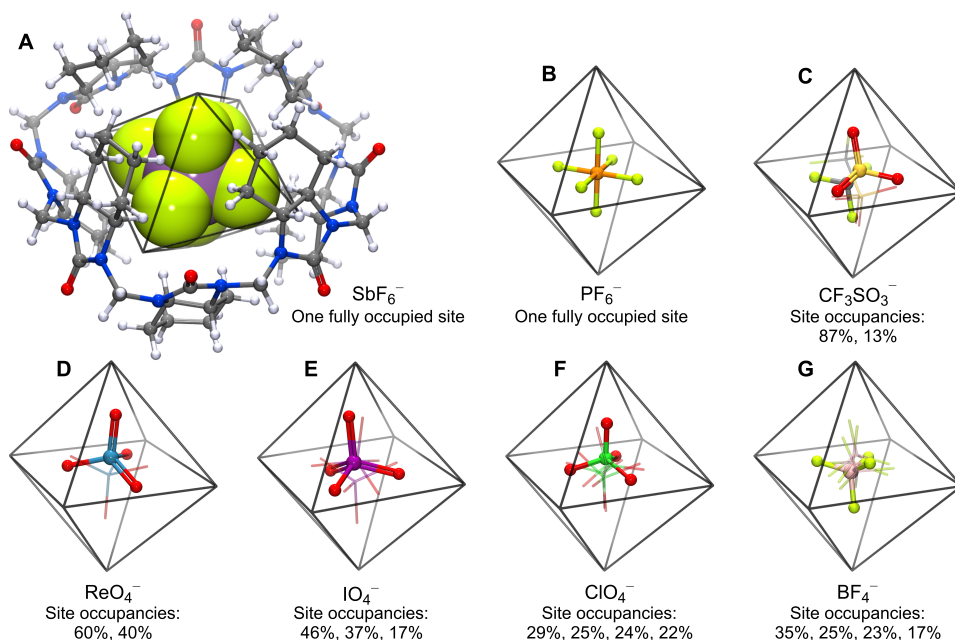


Figure 27. The position of anions in the crystal structures of the 1:1 host-guest complexes of a range of anions with cycHC[8]. In (B-G), the host is depicted by an octahedron, which represents the cavity of cycHC[8]. Minor anion disorder components in (C-G) are shown in the wireframe model, and the freely refined site occupancy factors of the disorder components are listed.

Notably, mass spectrometric collision-induced dissociation (CID) experiments in nitrogen gas revealed that the kinetic stability of the anion inclusion complexes with smaller tetrahedral anions was higher compared to complexes with larger anions. The dissociation of a complex was followed by varying the collision energy (CE) from 5 to 55 V. Higher kinetic stability of the complexes $\text{ReO}_4^-@cycHC[8]$ ($\text{CE}^{50\%}$ 36.1), $\text{ClO}_4^-@cycHC[8]$ ($\text{CE}^{50\%}$ 35.9), and $\text{BF}_4^-@cycHC[8]$ ($\text{CE}^{50\%}$ 35.2) suggested that the remaining space within the cavity of cycHC[8] in complexes with smaller anions provided relaxation through vibration. $\text{CE}^{50\%}$ values represent the collision energy (V) necessary for a complex to dissociate to half its original abundance. The gradual decrease of available space due to the tighter fit of the guest led to the lower kinetic stability of $\text{PF}_6^-@cycHC[8]$ ($\text{CE}^{50\%}$ 26.8), $\text{CF}_3\text{SO}_3^-@cycHC[8]$ ($\text{CE}^{50\%}$ 23.1), and $\text{SbF}_6^-@cycHC[8]$ ($\text{CE}^{50\%}$ 20.9).

The Hirshfeld surfaces were generated for SbF_6^- , IO_4^- , and CF_3SO_3^- to visualize the intermolecular close contacts between cycHC[8] and the differently shaped encapsulated guests (Figure 28). The Hirshfeld surface encircles the space occupied by the anion where its electron density exceeds that of the neighboring molecules, based on the crystal structure.^[159] The color code mapped on the surface indicates where the intermolecular distances are shorter (red), equal (white), or longer (blue) than the sum of the van der Waals radii of the atoms in close contact.^[160] As attractive intermolecular forces cause overlaps of the electron clouds of the atoms involved, then the established close contacts, denoted by red spots, pinpoint the supramolecular interactions in the host-guest complexes.

Overall, the Hirshfeld surfaces indicated that cycHC[8] interacted with the bound anions through weak C–H⋯anion hydrogen bonds. Closer inspection of the intermolecular distances revealed that the octahedral anions and CF_3SO_3^- preferably

interacted with the axial $2ax$ hydrogens in the corners of the cavity (H labelling scheme is shown in Figure 30). Shortest $d(\text{C}-\text{H}\cdots\text{anion})$ distances were seen in the case of SbF_6^- and CF_3SO_3^- , which also formed the highest number of simultaneous interactions with cycHC[8]. Symmetric hydrogen bonds, as seen on the Hirshfeld surface of SbF_6^- (Figure 28a), are presumed to have fixed the orientation of the octahedral guests within cycHC[8]. The tetrahedral anions, due to the shape and size mismatch with the cavity, formed a limited number of simultaneous host-guest interactions in a given orientation. The observed disorder patterns of anions therefore reflected the multitude of available $2ax$ and $6ax$ hydrogen bonding sites within the cavity of cycHC[8], which led to several relatively equally populated orientations of the tetrahedral anions.

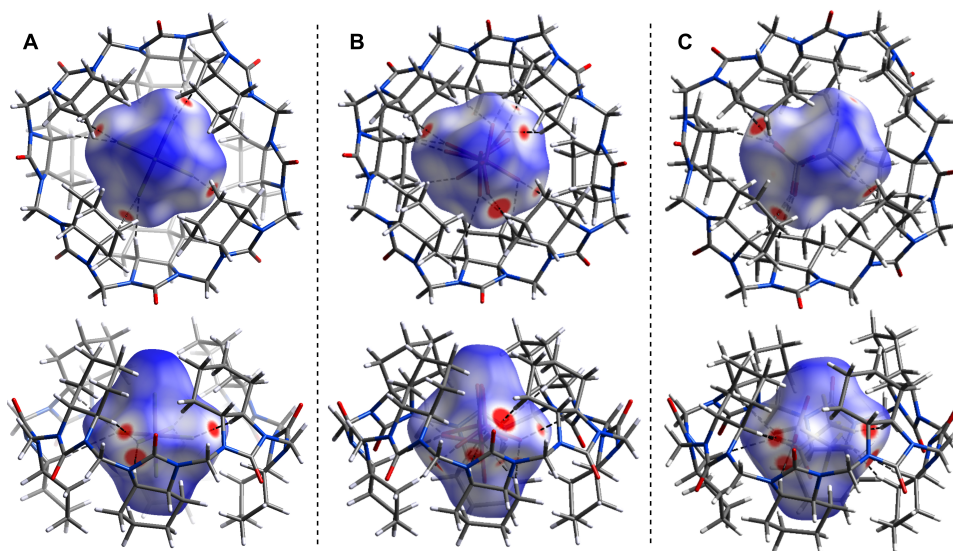


Figure 28. Hirshfeld surfaces for the encapsulated anions (A) SbF_6^- , (B) IO_4^- , and (C) CF_3SO_3^- , mapped with the normalized contact distance, d_{norm} , in the range of -0.1 (red) to 1 (blue). Red spots, together with black dashed lines, show the direction of host-guest interactions, where $d(\text{D}-\text{H}\cdots\text{A})$ is shorter than $\Sigma(r(\text{vdW})[\text{H}, \text{A}])$. For IO_4^- and CF_3SO_3^- , the Hirshfeld surface was generated for all disorder components simultaneously.

The obtained structures were isostructural, indicating that the anion did not change the shape of the host to the extent that would prompt a change in the crystal packing. The counter cations, TBA or TBP, together with solvent molecules filled the space between the host-guest complexes. Changing the cation from TBA to TBP, however, prompted a shift of the crystal lattice. Structures containing TBA crystallized in an orthorhombic space group $P2_12_12_1$, while those containing TBP crystallized as a pseudo-merohedral twin in the monoclinic space group $P2_1$. This occurred in spite of the nearly equal unit cell dimensions and isostructural arrangement of all the molecules (Figure 29). The twin operator, a two-fold rotation around the crystallographic c -axis $[-100\ 0\ -10\ 001]$, mimicked the orthorhombic mmm symmetry, which initially confused the correct space group assignment and hindered the structure solution. Re-processing the data in the monoclinic space group $P2_1$ enabled the structure solution. The minor twin component scale factor refined to $0.2056(6)$ in the case of $\text{TBP}(\text{SbF}_6^-@cyc\text{HC}[8])$ and to $0.3226(6)$ in the case of $\text{TBP}(\text{IO}_4^-@cyc\text{HC}[8])$.

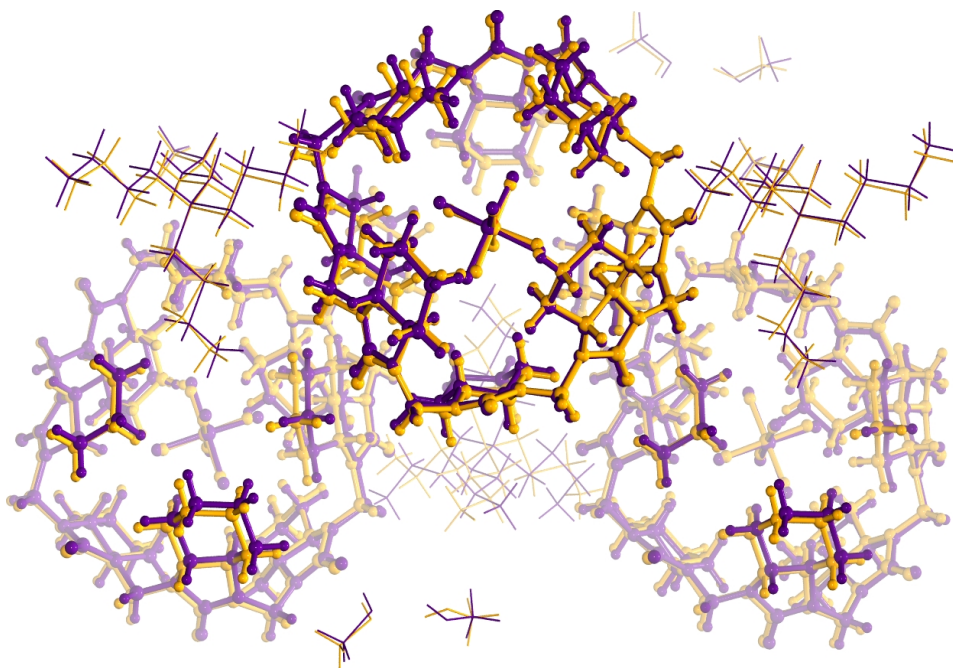


Figure 29. Overlay of the structures of TBA(PF₆⁻@cycHC[8]) in orange and TBP(SbF₆⁻@cycHC[8]) in purple. The TBA and TBP cations and methanol molecules are shown in a wireframe model, and cycHC[8] is shown in a ball and stick model.

Crystals of anion inclusion complexes with cycHC[8] were also obtained when PF₆⁻ or SbF₆⁻ were introduced to the methanol solution as potassium or sodium salts, respectively (Appendix 3). These structures revealed that the anion was isolated within cycHC[8] in the presence of cations capable of forming stronger ion pairs. The cations in both structures appeared disordered between the equal coordination sites close to the cycHC[8] carbonyl groups, sharing the positions with disordered solvent molecules. After several failed attempts, no adequate model for the positional disorder of the solvent and cations could be reached.

No anion inclusion complexes were obtained with the TBA salts of NO₃⁻, SCN⁻, AuBr₄⁻, HSO₄⁻, CH₃CO₂⁻, SiO₆⁻, and benzoate. This strongly suggested that the crystallization event started with the formation of the anion inclusion complex; therefore, anions that did not bind with cycHC[8] yielded no crystals.

4.2.2 Solution studies on the anion complexation properties of cycHC[8]

The strength and stoichiometry of the anion association with cycHC[8] in solution were first characterized by ¹H NMR spectroscopy using titration studies and Job's method. The studies were mainly performed in d₄-methanol, in which cycHC[8] is reasonably soluble (up to 6 mM). CycHC[8] proved to be insoluble in pure water, but somewhat soluble in a 1:1 mixture of D₂O/CD₃OD, which was used to evaluate the association of anions with cycHC[8] in aqueous conditions. The solvents used in the solution studies represented polar environments, in which the host-guest interactions are strongly affected by solvent competition. Thus, anion encapsulation involved the energetically costly disruption of its solvation shell.

Stepwise addition of TBAPF₆ into the solution of cycHC[8] illustrated the changes in ¹H NMR spectra of cycHC[8] induced by anion association (Figure 30). Downfield shifts were consistently observed for the 2ax, 6ax, and 4ax proton signals, which indicated that the anions were encapsulated within cycHC[8] also in solution, as these hydrogen atoms point into the cavity of cycHC[8] and de-shielding is characteristic of nuclei involved in hydrogen bonding. Upfield shifts were observed for the protons on the external surface of the macrocycle, while the smallest chemical shift changes were seen for the hydrogen atoms 5eq at the portal.

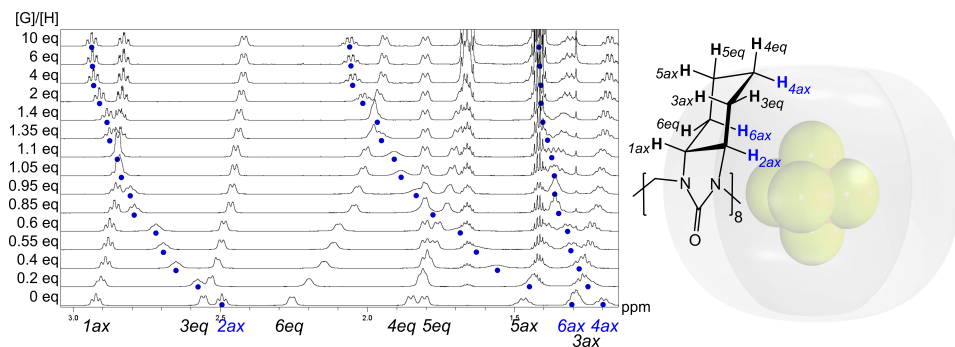


Figure 30. Chemical shift changes of cycHC[8] ¹H NMR signals upon sequential addition of TBAPF₆.

Job's method indicated 1:1 association stoichiometry of the host-guest complexes for all the studied guests in methanol, which was supported by the 1:1 complexation model observed in the crystal structures and by mass spectrometry. The association constants of the host-guest complexes were determined by NMR titration experiments at 288 K. Three cycHC[8] proton signals 1ax, 2ax, and 3eq were followed simultaneously upon the addition of up to 12 equivalents of the guest in small aliquots. Association constants (K_a) obtained by fitting the titration data to 1:1 binding isotherms are compiled in Table 3.

The association of cycHC[8] with large charge-diffuse anions was remarkably strong (K_a up to 250 000 M⁻¹ for SbF₆⁻) in the competitive polar media. This showed that the receptor design approach relying on the construction of a preorganized binding pocket based on 'soft' C–H...anion interactions could be used to selectively target polarizable anions in polar solvents. The selectivity of cycHC[8] appeared to be additionally determined by the dimensions and the shape of its cavity. The large octahedral SbF₆⁻, which, based on the crystal structure formed eight hydrogen bonds with the host ($d(\text{C–H}\cdots\text{F}) = 2.34 \text{ \AA} - 2.65 \text{ \AA}$), had the highest association constant with cycHC[8]. The binding strength of smaller octahedral and tetrahedral anions PF₆⁻, ReO₄⁻, IO₄⁻, ClO₄⁻, and BF₄⁻ decreased exponentially as the size of the guest decreased (Figure 31). Because the tetrahedral anions can form fewer simultaneous hydrogen bonds, lower association constants arise as a result of the diminished stabilization effect of the C–H...anion interactions compared to the larger guests. For example, BF₄⁻, which based on the crystal structure can only form one to three simultaneous close interactions with the host ($d(\text{C–H}\cdots\text{F}) = 2.39\text{--}2.56 \text{ \AA}$) in a given orientation, showed only marginal affinity ($K_a = 48 \text{ M}^{-1}$) towards cycHC[8].

Table 3. Association constants together with the fitting errors for cycHC[8] inclusion complexes with different anions (at 288 K).

Anion	Cation	$V_{\text{anion}} (\text{Å}^3)^{[a]}$	PC ^[b]	$K_a (\text{M}^{-1})$	Solvent
SbF ₆ ⁻	Na ⁺	81.8	0.67	$(2.5 \pm 0.7) \cdot 10^5$	CD ₃ OD
PF ₆ ⁻	TBA ⁺	70.6	0.57	$(2.8 \pm 0.4) \cdot 10^4$	CD ₃ OD
PF ₆ ⁻	TBA ⁺	70.6	0.57	$(2.6 \pm 0.2) \cdot 10^4$	1:1 CD ₃ OD/D ₂ O
PF ₆ ⁻	Na ⁺	70.6	0.57	$(2.0 \pm 0.2) \cdot 10^4$	CD ₃ OD
ReO ₄ ⁻	TBA ⁺	64.8	0.53	$(4.7 \pm 0.4) \cdot 10^3$	CD ₃ OD
IO ₄ ⁻	Na ⁺	64.3	0.52	$(1.8 \pm 0.2) \cdot 10^3$	CD ₃ OD
ClO ₄ ⁻	TBA ⁺	54.7	0.45	$(4.7 \pm 0.2) \cdot 10^2$	CD ₃ OD
BF ₄ ⁻	TBA ⁺	51.6	0.42	$(4.8 \pm 0.4) \cdot 10^1$	CD ₃ OD
CF ₃ SO ₃ ⁻	TBA ⁺	82.3	0.67	$(3.9 \pm 0.5) \cdot 10^1$	CD ₃ OD
CF ₃ CO ₂ ⁻	TBA ⁺	68.7	0.56	< 10	CD ₃ OD

[a] Calculation of the anion volumes used in this work is further described in the Methods and Materials section. [b] The packing coefficient, PC, is defined by Mecozzi and Rebek as the ratio between V_{anion} and $V_{\text{cavity}}(\text{host})$.^[158]

Based on the optimal packing coefficient of 0.55 ± 0.09 ^[158] proposed by Mecozzi and Rebek, which reflects the steric compatibility in host-guest complexes, an optimal fit for the cycHC[8] cavity should follow a statistical distribution around the guest volume of 68 Å^3 . However, despite the better size match to the cavity of cycHC[8], PF₆⁻ (PC = 0.57) was bound weaker with cycHC[8] ($K_a = 28\,000 \text{ M}^{-1}$) than SbF₆⁻ (PC = 0.67). Thus, in the case of strongly interacting host-guest systems, the optimal guest volume could be shifted towards larger guests. This exposes the pitfall of predicting optimal host-guest complexes based on hard-sphere models of atoms in interacting molecules.

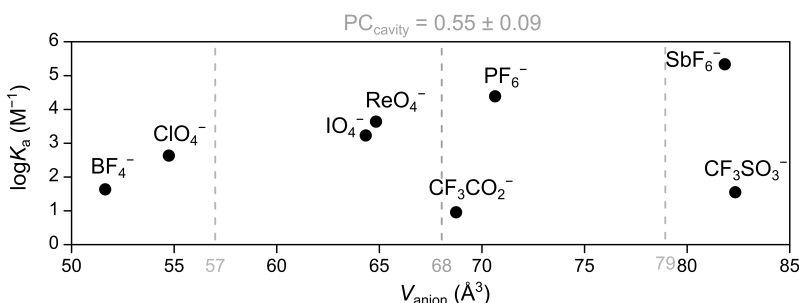


Figure 31. The correlation between the association constant and the anion size, with K_a shown on the logarithmic scale. The optimal packing coefficient (PC) for the cavity, representing the $68 \pm 11 \text{ Å}^3$ anion volume range ($PC = 0.55 \pm 0.09$), is highlighted by grey dashed lines.

Dramatically lower binding constants for CF₃CO₂⁻ ($K_a < 10 \text{ M}^{-1}$) and CF₃SO₃⁻ ($K_a = 39 \text{ M}^{-1}$) provided further proof that the association of cycHC[8] host-guest complexes was not directed only by the steric fit of the host and the guest. CF₃CO₂⁻ is optimally sized (PC = 0.56) for the cycHC[8] cavity and CF₃SO₃⁻ is very close in size to the strongest bound anion SbF₆⁻. Furthermore, CF₃SO₃⁻ was observed to form as many C–H⋯anion interactions ($(d(\text{C–H} \cdots \text{F})) = 2.32\text{--}2.60 \text{ Å}$) as SbF₆⁻ in the crystal structures with cycHC[8], and CF₃CO₂⁻ was previously noted (**Publication 1**) to be an effective template in the synthesis of cycHC[8]. Thus, the selectivity of cycHC[8] against these anions in a methanol solution was initially surprising. Comparison of the surface electrostatic potential of the studied anions (Figure 32) revealed that the inherently symmetric cycHC[8] preferably bound anions with an equally symmetric surface charge distribution. Anions with an

asymmetric charge distribution, such as CF_3CO_2^- and CF_3SO_3^- , with the charge located more on the oxygen atoms compared to the neighboring trifluoromethyl group, have very low affinity towards cycHC[8] in methanol. The templating effect of the CF_3CO_2^- demonstrated in **Publication I** may be induced by the co-solvent acetonitrile used in the synthesis of cycHC[8] providing a more apolar medium compared to methanol, which could affect the anion binding strength.

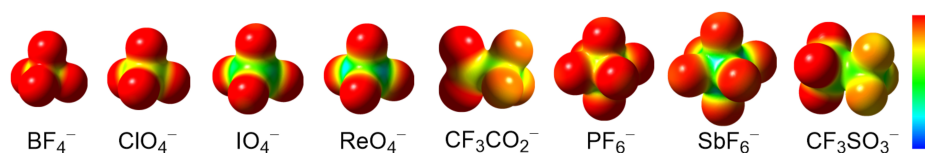


Figure 32. The surface potential of the studied anions calculated using Gaussian 09,^[161] and visualized using GaussView5.^[162] The red to blue surface color range spans from -0.2 to 0.2 . Reprinted, with permission, from **Publication II**.

Notably, the association of anions in methanol was not significantly dependent on the nature of the counter cation, as titrations of cycHC[8] with NaPF_6 and TBAPF_6 yielded similar association constants ($K_a = 20\,000\text{ M}^{-1}$ and $K_a = 28\,000\text{ M}^{-1}$, respectively).

To gain insight into whether the association of the studied anions with cycHC[8] was dependent on the polarity of the environment, a comparative titration of cycHC[8] with TBAPF_6 was performed in an aqueous solution. Experiments in pure water were prevented by the poor solubility of cycHC[8]; however, titration in a 1:1 mixture of $\text{CD}_3\text{OD}/\text{D}_2\text{O}$ demonstrated no significant change in the association strength ($K_a = 26\,000\text{ M}^{-1}$) compared to titration in pure methanol. This indicated that the supramolecular non-covalent interactions in these host-guest complexes were not interrupted by the presence of water.

Titrations of cycHC[8] with NaSbF_6 and NaPF_6 in methanol were also performed using isothermal titration calorimetry (ITC), which produced association constants comparable to those measured by NMR spectroscopy. The binding of anions was found to be exergonic, enthalpically favored, and entropically disfavored (Table 4). The stronger binding of SbF_6^- compared to PF_6^- brought about a larger gain in the enthalpic term, which was in line with the stronger interactions seen in the host-guest crystal structures of SbF_6^- and cycHC[8] compared to structure of the cycHC[8] complex with PF_6^- ($d(\text{C}\cdots\text{F}) = 2.51\text{--}2.93\text{ \AA}$). Binding of SbF_6^- was also accompanied by a larger entropic penalty compared to PF_6^- , which could be explained by the greater decrease in the degrees of freedom of SbF_6^- in the tightly associated host-guest complex. This was also reflected in the higher packing coefficient (PC) and the lower kinetic stability ($\text{CE}^{50\%}$) of the SbF_6^- complex, compared to the complex with PF_6^- .

Table 4. Thermodynamic parameters for the complexation of NaSbF_6 and NaPF_6 with cycHC[8] at 298 K, all energies in kJ mol^{-1} .

Guest	$K_a\ (\text{M}^{-1})$	ITC			NMR ΔG^0	DFT ΔG^0
		ΔH^0	$T\Delta S^0$	ΔG^0		
NaSbF_6	$(1.02 \pm 0.03) \cdot 10^5$	-56.2 ± 0.3	-27.7	-28.5	-30.8	-
NaPF_6	$(1.29 \pm 0.04) \cdot 10^4$	-43.8 ± 0.2	-20.4	-23.4	-24.5	-22

4.2.3 The pathway and kinetics of anion complexation with cycHC[8]

Insight into the kinetics and the reaction pathway of the host-guest complexation of anions with cycHC[8] was gained by variable temperature NMR studies (VT-NMR) and

density functional theory (DFT) calculations. Computations confirmed the preferred inclusion of a single methanol molecule within cycHC[8], as suggested by the SQUEEZE results on the crystal structure in **Publication I**. Modelling the exchange of methanol with PF_6^- in the cavity of cycHC[8] (Figure 33) indicated that the inclusion complex of PF_6^- was 22 kJ mol^{-1} lower in energy than the methanol-solvated cycHC[8] (Table 4). This was in good agreement with the experimental ΔG^0 values from the NMR ($-24.5 \text{ kJ mol}^{-1}$) and ITC ($-23.4 \text{ kJ mol}^{-1}$) titration experiments. However, the existence of a high-energy pre-complex, as suggested by the DFT, was challenged by the first-order association kinetics observed in dilution experiments by NMR. The true reaction pathway of the anion association probably involved more steps, which include the desolvation of the PF_6^- that was not accounted for by the computational three-component model.

The ^1H NMR spectra of cycHC[8] showed an averaged signal for the complexed and non-complexed cycHC[8] at lower than equimolar ratios of the guest in the titration experiments. Thus, the guest exchange was faster than the NMR timescale (few seconds) at the measurement temperatures (288 K) used for the titrations. A slow exchange region was observed below 253 K for SbF_6^- and below 241 K for PF_6^- by variable temperature (VT) NMR, which was also used for the determination of the association rate constants. The complexation rate for PF_6^- (17500 s^{-1}) was an order of magnitude larger than for SbF_6^- (2600 s^{-1}).

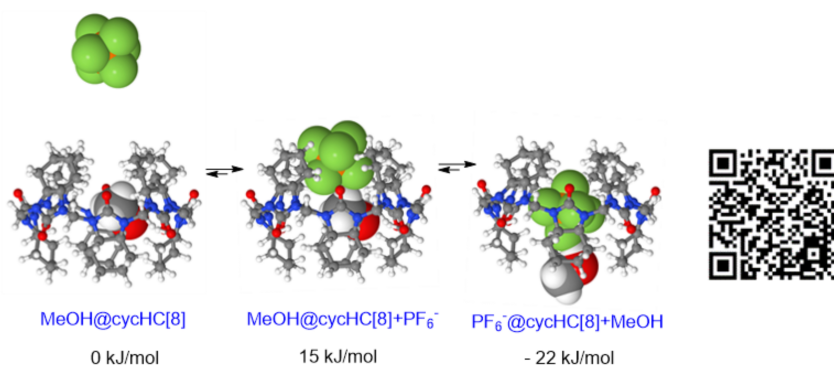


Figure 33. Minimum energy geometries of cycHC[8] complexes with PF_6^- in CH_3OH (reprinted, with permission, from **Publication II**) and the associated relative Gibbs free energy values calculated at BP86-D/TZVPD level of theory. The QR code provides a link to the DFT-based video of the complexation pathway.

In summary, the experimental of this study suggest that the binding of anions with cycHC[8] is a combination of several simultaneous processes. Given the polarizable nature of the bound anions and the increase in affinity according to the Hofmeister bias, the selectivity of these host-guest complexes can be best explained by the chaotropic effect.^[163]

In between directional hydrogen bonding and the non-directional hydrophobic effect in the range of supramolecular forces sits, the chaotropic effect. It has been proposed as the composite of attractive intermolecular forces and the thermodynamic effects of anion (de)solvation. Distinguished from the hydrophobic compounds that have positive free energies of solvation and therefore large positive heat capacity in association with hydrophobic surfaces, the polarizable (chaotropic) anions have negative free energy of solvation. Therefore, chaotropic association has a distinct thermodynamic behavior, dissimilar to the hydrophobic effect.

Host-guest association processes driven by the classical hydrophobic effect are characterized by a strong entropic gain arising from destruction of the solvation shell around the hydrophobic solutes. This occurs as the rotational dynamics of solvent molecules around hydrophobic solutes are restricted.^[163] The thermodynamics of the chaotropic effect, however, display a strong enthalpic gain and an unfavorable entropic term, which are consistent with anion binding to cycHC[8], to biotinurils,^[164] and bambusurils^[10,57,90,165] in polar solvents. Favorable enthalpic contributions in anion encapsulation by cycHC[8] could stem from attractive intermolecular interactions between the host and the anion, as well as the recovery of the hydrogen bonds in the bulk solvent upon desolvation of the weakly solvated anions. A recent study compared the thermodynamics of anion binding with an ethyleneglycol-decorated BU[6] in different solvents.^[57] Sindelar and co-workers proposed that the main driving forces for host-guest complex formation are anion desolvation and the 'non-classical' hydrophobic effect - the expulsion of high-energy solvent from the hydrophobic BU cavity. Since only a single methanol molecule is bound within cycHC[8], as evidenced by crystallographic analysis and computational modelling, it is restricted from forming strong hydrogen bonds. Therefore, it is plausible that the expulsion of this methanol to the bulk solvent could also contribute to the enthalpic term of anion binding in the host-guest complexes.

4.3 Solid-state study of hemicucurbituril hosts (Publication III)

By May 2017, a total of 39 crystal structures of hemicucurbituril (HC) hosts had been published in the Cambridge Structural Database. Studying the guest-binding motifs of these hosts in the solid state and exploring the influence of the size and shape of the guests on the host scaffold therefore became possible. In addition to the eight crystal structures from **Publications I and II**, five crystal structures of the four-membered HCs, 25 structures of six-membered HCs, and the crystal structure of HC[12] were analyzed. Although the solid-state studies provided essentially a frozen view of the host-guest complex, a certain degree of flexibility was observed when comparing the dimensions of a host in a complex with different guests. The following section describes the main conclusions on the modes of guest binding and the potential supramolecular interactions at play in the templated synthesis of HCs.

4.3.1 Anion and guest binding motifs in the crystal structures of hemicucurbiturils

As highlighted earlier, in the absence of halide templates, the synthesis of bambusuril-type (BU[*n*]) hosts led to the formation of four-membered macrocycles. Due to the restricted size of the cavity, no guests were encapsulated within the center of BU[4],^[109] semithio-BU[4],^[105] aza-BU[4],^[106] or allyliminium-BU[4],^[106] which supports the argument that the synthesis of BU[4] does not follow the same templated pathway as the halide-templated six-membered HCs. Based on the crystal structures, the void in the central cavity was not large enough to hold a probe with the dimensions of a hydrogen atom (radius 1.2 Å, grid step 0.2 Å). The eight methine hydrogen atoms point towards the cavity (Figure 34A), due to the stereochemistry of the BU monomers restricting the access to the central cavity of the macrocycle (Figure 34B). The crystal structures, however, revealed that these hydrogen atoms were consistently involved in hydrogen bonds with solvent molecules (Figure 34C), thus suggesting the existence of two alternative binding sites in BU[*n*].

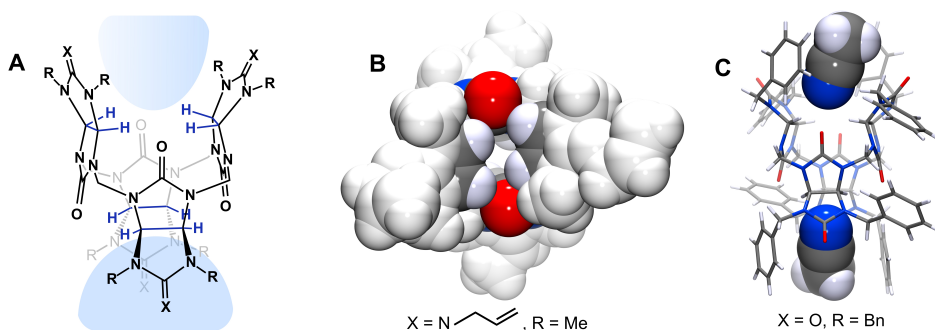


Figure 34. (A) Chemical structure of the BU[4]-type macrocycles, with the methine hydrogens and the binding sites highlighted in blue. (B) Top view of the crystal structure of allylaza-BU[4] (CCDC 1401300), in CPK representation, illustrating the narrow dimensions of the central cavity of BU[4]. The cavity is highlighted in element colors, substituents are drawn in light grey. (C) Crystal structure of BnBU[4] (CCDC 809240) showing the position of CH₃CN in the binding sites. Figures B and C are reprinted, with permission, from **Publication III**.

Such binding motifs were also observed in several crystal structures of six-membered BU-type hosts (Figure 35). While the prevalent host-guest motifs in the latter were those with the halide anion bound to the center of the macrocycle (literature overview, Figure 2), larger guests, such as benzoate, *p*-toluenesulfonate, and diethyl phosphate, were seen to occupy the secondary binding sites and formed 1:2 BU-anion complexes.^[166] As the portals to the central cavity of the BU[6]-type hosts are significantly wider than the four-membered analogues, a guest bound to the center of the macrocycle can generally interact with molecules in the secondary binding sites through hydrogen bonds. A reoccurring motif was observed in which a quaternary host-guest complex was formed with a water molecule trapped in the center of the BU[6] between two anionic guests at the portals (Figure 35B). A positively charged picolyliminium-BU[6] formed triple anion quaternary complexes, with I⁻ at the center and two CF₃SO₃⁻ at the secondary binding sites (Figure 35C).^[106] The secondary binding sites could be blocked by the host *N*-substituents, isolating the centrally bound anion from the surroundings.

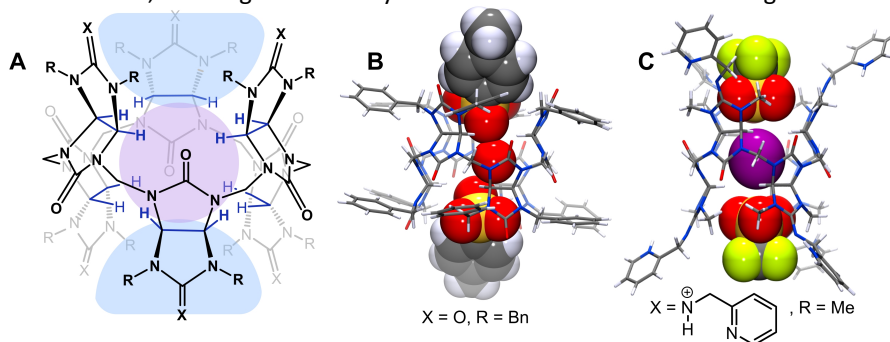


Figure 35. (A) Chemical structure of the BU[6]-type hosts, indicating the central binding site (purple) and the secondary binding sites (blue). (B) Crystal structure of the quaternary complex of BnBU[6] (CCDC 965535), with two *p*-toluenesulfonate anions and a water molecule. (C) Crystal structure of the triple anion quaternary complex of the picolyliminium-BU[6] host (CCDC 1401302), with two CF₃SO₃⁻ at the secondary binding sites and I⁻ at the central binding site. Crystal structure has been refined with all the pyridyl groups protonated (*s.o.f.* set at 0.5), while the chemical structure proposed by the authors suggested protonation at the imine groups, as shown below the figure. Figures B and C are reprinted, with permission, from **Publication III**.

Interestingly, no crystal structures of anion complexes have been reported for the halide-templated achiral (*R,S*)- and chiral (*all-S*)-cycHC[6] hosts.^[12,104] While the (*all-R,S*)-cycHC[6] isomer resembled the bamboo stem shape similar to the bambusuril hosts (Figure 36A), its diastereomeric chiral sibling, the (*all-S*)-cycHC[6], was closer in shape to a barrel (Figure 36B). The published crystal structures of cycHC[6] hosts, obtained from either CH₂Cl₂, CHCl₃, or CCl₄, displayed no encapsulated guests, indicating that the cavities were too small for the encapsulation of the bulky solvent molecules. The solvent-accessible voids in the crystal structure of (*all-S*)-cycHC[6] were analyzed by running the SQUEEZE routine in PLATON (radius 1.2 Å, grid step 0.2 Å) on the data obtained from the authors.^[12] The void in the host cavity was empty, with only three electrons found in the 35 Å³ cavity. This showed that the cavity of (*all-S*)-cycHC[6] did not collapse in the absence of guests in CCl₄ and that the resulting crystal structure contained pores. Void analysis of the (*R,S*)-isomer suggested that the host contained three small pores.^[104] As discussed in the previous section, the larger homologue of the chiral cycHC[6], (*all-R*)-cycHC[8], isolated large charge-diffuse anions selectively within its cavity.

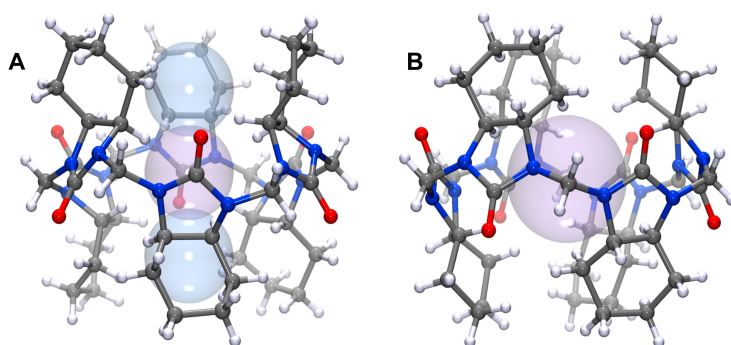


Figure 36. (A) The (*R,S*)-cycHC[6] host (CCDC 716121), with the voids illustrated in purple (central cavity) and blue (secondary binding sites). (B) The (*all-S*)-cycHC[6] host (CCDC 945664), with the empty central cavity (35 Å³) shown in purple.

4.3.2 Guest influence on the shape of the hemicucurbiturils

The crystal structures of the hemicucurbiturils were compared to establish the extent to which the bound guest molecules influenced the shape of the host. This was conducted within groups of hosts sharing the same characteristics (same number of monomers and the same stereoisomers).

A set of parameters was defined for each host type to describe the host shape. These values were then measured over the corresponding crystal structures and correlated to the guest volume (Å³) and shape. No attempt was made to quantitatively compare the cavity sizes of the hosts from different groups. Therefore, the tables in **Publication III** addressed only the flexibility and adaptability of different host in the respective host-guest complexes and do not adequately reflect the guest-accessible physical dimensions of the host cavities (i.e. van der Waals radii of the atoms was not accounted for).

No significant conclusion could be drawn about the guest influence on the four-membered BU-type hosts, due to poor representation in the CSD. Unsubstituted HC[6], BU[6]-type hosts, biotin[6]uril, and the achiral (*all-R,S*)-cycHC[6] in 1:1 inclusion complexes with anions could, however, be compared relative to each other. A weak linear correlation ($R^2 = 54\%$) was observed between the volume of the guest and the calculated V_{cylinder} (Figure 37A). The cylinder approximated the size of the host cavity, defined by the measured parameters, r_{cavity} and h_{cavity} . When comparing the C–H \cdots X⁻

distances to the size of the bound halide in 1:1 host-guest complexes with a single host MeBU[6], Sindelar *et al.* noted that the increasing size of the anion brought about longer C–H...X⁻ distances.^[58] This demonstrated the adaptation of the size of the host to the size of the guest. Weaker correlation among all of the studied six-membered hosts, compared to that with a single macrocyclic host, suggested that the size of the host cavity was also affected by the substituents on the core HC[*n*] structure.

The strongest correlation ($R^2 = 91\%$) to the guest volume was found in the host-guest complexes of cycHC[8] (Figure 37B). However, regardless of the apparent linear correlation between the anion size and the distance from the 2ax hydrogen to the center of the macrocycle, the overall change in the host shape was less than 5%.

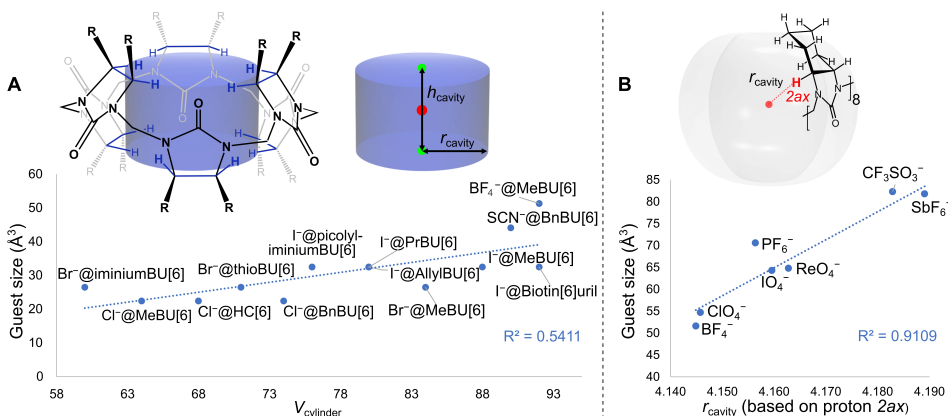


Figure 37. (A) Correlation between the size of the anion and $V_{cylinder}$ in the HC[6], BU[6]-type hosts, biotinuril, and (R,S)-cycHC[6] in 1:1 anion inclusion complexes. (B) Correlation between the size of the anion and the cavity radius of (all-R)-cycHC[8] in the 1:1 anion inclusion complexes. Figures are reprinted, with permission, from **Publication III**.

The relative orientation of the monomers in the largest homologue of the hemicucurbiturils, HC[12], deviated from the alternating orientation seen in the smaller hemicucurbiturils. The unsubstituted ethylene urea monomers are small and the cavity of the 12-membered macrocycle is significantly wider than for example HC[6]. Thus, there is more rotational freedom of the methylene-bridged monomers around the C–N bonds in HC[12], due to lower steric restrictions. The C–N bonded equatorial belt of HC[12] adopted an ellipsoidal shape in the crystal structure of its chloroform solvate, demonstrating that larger homologues of hemicucurbit[*n*]urils could be significantly more flexible.^[89]

The position of the guests and the shortest intermolecular contacts in the crystal structures of the host-guest complexes suggested that the C–H...guest interactions were indeed involved in the association of the guest molecules with all the HC[*n*] hosts. The stereochemistry of the monomeric unit of HC[*n*] significantly affects the shape of the host, such that the BU-type hosts and biotinuril assume a bamboo-stem shape. This created, in addition to the central binding site, two alternative binding sites allowing 2:1 and even 3:1 stoichiometry for binding of anionic guests. Alternatively, the chiral (all-R)-cycHC[8] only formed 1:1 complexes, with the anionic guest isolated from the surroundings within the cavity of the barrel-shaped host.

4.4 Solid-state synthesis of cycHC[n] (Publication IV)

The synthesis of hemicucurbiturils has emerged as an elegant example of thermodynamically controlled anion-templated processes, affording high yields and excellent control over the reaction outcome. In comparison to the kinetically controlled macrocyclization reactions, generally carried out at high-dilution conditions (0.1–1 mM), the thermodynamically controlled reversible macrocyclization reactions of hemicucurbiturils can be performed at relatively high concentrations (4 M). This, together with the scarce but remarkable precedents of covalent macrocyclization reactions by mechanochemistry (Section 1.4.4) and the lack of examples on templated solid-state covalent syntheses, rendered the anion directed synthesis of cycHC[6] and cycHC[8] an excellent model upon which to investigate macrocyclization reactions and templating effects in the solid state.

4.4.1 Mechanochemical synthesis of cycHC[6] by ball milling

Anion-templated synthesis of cycHC[6] was first attempted by ball milling, considering the success of solid state imine condensation reactions (Section 1.4.2), the demonstration of dynamic covalent reactions under mechanochemical conditions (Section 1.4.3), and the efficient use of mechanical grinding for the construction of macrocyclic structures (Section 1.4.4). The liquid-assisted grinding (LAG) approach was chosen, as the reversible formation of acylaminal linkages is acid-catalyzed. The catalytic amount of mineral acid added to the reactants in the milling jar ($\eta = 0.2\text{--}0.25 \mu\text{l mg}^{-1}$) also provides the reaction with the anionic template. All ball milling in these studies used ZrO_2 milling jars (10 ml) and ball bearings (10 mm), as steel jars would be corroded by the acidic conditions. Frequency of milling was 30 Hz.

Halide-templated synthesis of cycHC[6] was explored first, by ball milling the monomer (100 mg) and one equivalent of paraformaldehyde (PFA) in the presence of 30 μl of concentrated aqueous HCl (37%, liquid-to-solids ratio $\eta = 0.25 \mu\text{l mg}^{-1}$) for 60 or 180 minutes (Table 5 entries 1 and 2, Figure 38). The resulting powders were washed with distilled water to quench the reaction by removing the acid additive. Dried products were fully soluble in CH_2Cl_2 and CHCl_3 . ^1H NMR analysis of the quenched reaction products in CDCl_3 revealed the complete disappearance of the starting materials and the appearance of NMR signals indicating the formation of oligomers. However, only a small amount (up to 5%) of the product cycHC[6] was obtained. Identical spectra were obtained if the reaction mixture was immediately dissolved in CDCl_3 , without washing with water. This confirmed that all the water-soluble monomer was consumed during milling, and that the composition of the products was consistent before and after quenching. High-performance liquid chromatography (HPLC) and MS analysis indicated that the products contained linear and cyclic oligomeric products from two to 15 subunits of the monomer.

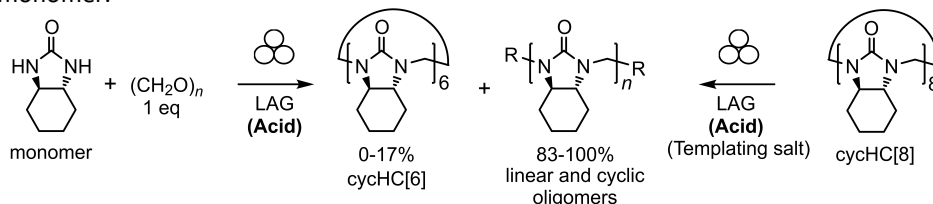


Figure 38. Reaction scheme of cycHC[6] mechanochemical synthesis, starting either from the monomer (left) or the larger homologue cycHC[8] (right). LAG conditions, such as the amount and type of the LAG acid, added templating salts, and milling duration are listed in Table 5.

In a similar re-submission approach to that demonstrated by Atwood *et al.* for the mechanochemical conversion of *p*-benzylcalixarenes (Figure 21A), the synthesis of cycHC[6] was attempted from the larger homologue cycHC[8] by milling in the presence of aqueous HCl (37%). However, re-macrocyclization afforded a similar composition of oligomeric products as when starting from the monomer, with only a small amount (9%) of cycHC[6] obtained (Table 5 entry 3). This indicated that the methylene linkage formation was indeed reversible in the solid-state acid-catalyzed LAG experiments, but also showed that cycHC[6] was not the favored product in mechanochemical conditions. Instead, a mixture of oligomers that resembled the contents of the dynamic covalent library described in **Publication I** were consistently obtained.

The re-macrocyclization was modestly improved by the addition of TMABr to the LAG reactions with aqueous HCl (37%), which resulted in 17% conversion to cycHC[6] after three hours of milling (Table 5 entry 4). However, these conditions did not significantly favor cycHC[6] over cycHC[8], which was persistently obtained in a similar amount to the target product (10%). Larger excess of the chloride template in the form of NH₄Cl or NaCl did not improve the conversion to cycHC[6] (Table 5 entries 5 and 6). Other types of acid, including HBr (aq. 48%), H₂SO₄, or HCO₂H, in combination with the moderately effective TMABr template also did not lead to any improvement in the conversion to cycHC[6] (Table 5 entries 8, 9, and 10 compared to entry 7).

Table 5. Screening the reaction conditions for the synthesis of cycHC[6] by LAG in a ball mill.

Entry	Reactants ^[a]	Acid ^[b]	η ($\mu\text{l mg}^{-1}$)	Additional template	Milling duration (min)	Conversion to cycHC[6] (%) ^[c]
1	monomer + 1 eq PFA	HCl (aq. 37%)	0.25	-	60	5
2	monomer + 1 eq PFA	HCl (aq. 37%)	0.25	-	180	0
3	cycHC[8]	HCl (aq. 37%)	0.3	-	120	9
4	cycHC[8]	HCl (aq. 37%)	0.3	TMABr ^[d]	180	17
5	cycHC[8] ^[e]	HCl (aq. 37%)	0.3	NH ₄ Cl ^[d]	180	6
6	cycHC[8]	HCl (aq. 37%)	0.3	NaCl ^[d]	180	8
7	cycHC[8]	HCl (aq. 37%)	0.3	TMABr ^[d]	60	10
8	cycHC[8]	HBr (aq. 48%)	0.2	TMABr ^[d]	60	9
9	cycHC[8]	H ₂ SO ₄ (>95%)	0.3	TMABr ^[d]	60	7
10	cycHC[8]	HCO ₂ H	0.2	TMABr ^[d]	60	traces ^[f]

[a] 100 mg of the monomer or cycHC[8] was reacted, if not stated otherwise. [b] The volume of the LAG acid provided either 3 eq (HCl), 1.6 eq (HBr), or 4.8 eq (H₂SO₄ and HCO₂H) of the template, compared to the theoretical amount of cycHC[6] formed (0.11 mmol). [c] The conversion to cycHC[6] (%) was determined from the ¹H NMR spectra of the quenched reaction products. [d] Templating salt added an additional 8.5 eq (TMABr), 85 eq (NH₄Cl), or 40 eq (NaCl) of the template to the reaction mixture. [e] 50.3 mg of cycHC[8] was used. [f] 98% of starting cycHC[8] was left.

4.4.2 Combining ball milling with aging for the synthesis of cycHC[6]

Concluding that the solely mechanochemical approach will not allow for the selective formation of cycHC[6], an alternative method was explored, coupling LAG with accelerated aging. 100 mg of the monomer and one equivalent of PFA were milled for 30 or 60 minutes with a small amount HCl (aq. 37%, $\eta = 0.25 \mu\text{l mg}^{-1}$), and the resulting solids were transferred from the milling jar into a glass vial (Figure 39). It is important to note that the performed aging reactions always commenced from freshly milled reaction

mixtures, with limited exposure to air in order to prevent the evaporation of the acid. Retaining the LAG acid in the aging vial has twofold importance - it mediates the interconversion between the members of the dynamic covalent library as the catalyst, and it provides the template which directs the reaction towards the macrocyclic product. To avoid evaporation of the acid from the vial, the vials were always sealed with polytetrafluoroethylene (PTFE) tape between the neck and the cap, and were additionally wrapped with Parafilm.

The reactions were quenched after aging and analyzed by ^1H NMR. The mixture of oligomers obtained by milling converted quantitatively into cycHC[6] in a solid-to-solid process by aging at 45 °C for six days (Table 6, entry 1; Figure 39). The aging step was accelerated at 60 °C, where 68% conversion was reached after one day, and 95% conversion was seen after two days (Table 6, entries 2 and 3, respectively). The isolated yield of cycHC[6] after 30-minute LAG and three days of aging at 60 °C was 90%, reflecting the loss of some of the solid material upon transferring the reaction mixture from the milling jar to the vial for aging, and from the vial to the glass filter for reaction quenching. The isolated yield could, in principle, be improved by aging the solids in the unopened milling jar or by quenching the reaction by evaporating the acid directly from the solids, which was not attempted within this study.

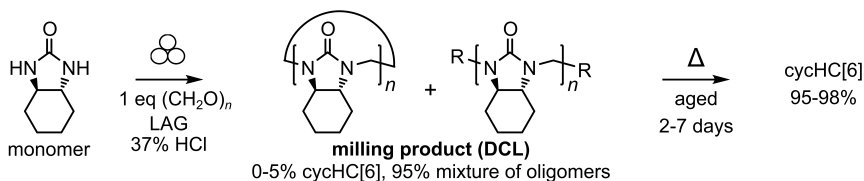


Figure 39. Reaction scheme for the solid-state synthesis of cycHC[6] coupling LAG with accelerated aging. The optimized reaction conditions, such as the amount of LAG acid, milling duration, aging temperature, and duration are listed in Table 6, entries 1, 3-5. The photos in the bottom row show the appearance of the reaction mixture after milling and in the sealed aging vial with the reaction mixture before and after aging at 60 °C.

Equal conversion (95% and 97%) was obtained when aging reactions were commenced either after 30- or 60-minute LAG (Table 6, entries 4 and 5). Reducing the milling duration to five minutes, however, led to a 60% conversion to cycHC[6] upon aging (Table 6, entry 6). While the products from 30- or 60-minute LAG were loose, homogeneous powders (Figure 39), five-minute milling led to waxy, transparent solids (Figure 40A). This could reflect a lower degree of polymerization, as the monomer and the shortest oligomers are soluble in acidic aqueous solution, unlike the longer polymerization products. Manual kneading in a mortar confirmed the existence of a short-lived liquid phase at the start of the condensation reaction (Figure 40B), which solidified into a waxy intermediate similar to that observed after five-minute milling. However, when the manually ground solids were subjected to aging at either 45 or 60 °C, no more than 9% cycHC[6] was obtained (Table 6 entries 7 and 8). Considering that the kneading with a pestle and mortar exposed

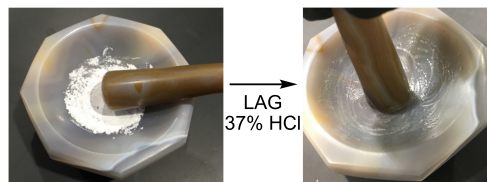
the reaction mixture to air, lower conversion was presumably due to the extensive evaporation of the LAG acid during grinding.

A Table 6, Entry 6:



five minutes of ball milling

B Table 6, Entry 7:



monomer + 1 eq (CH₂O)_n

five minutes of grinding

Figure 40. (A) The waxy transparent solids obtained from the short five-minute ball milling, covering the milling jar walls and the ball. (B) Liquification observed at the start of the grinding reaction using a pestle and mortar.

The presence of both moisture and acid were found to be important for the efficient conversion to cycHC[6], as evidenced by an experiment where the vial was not sealed with PTFE tape and Parafilm, which yielded only 6% conversion even after six weeks of aging (Table 6, entry 9).

Table 6. Screening the reaction conditions for the synthesis of cycHC[6] by coupling LAG and accelerated aging.

Entry	Acid ^[a]	Milling duration (min)	Aging temperature (°C)	Aging duration (days)	Conversion to cycHC[6] (%) ^[b]
1	HCl (aq. 37%)	30	45	6	98
2	HCl (aq. 37%)	30	60	1	68
3	HCl (aq. 37%)	30	60	2	95
4	HCl (aq. 37%)	30	60	3	95
5	HCl (aq. 37%)	60	60	3	97
6	HCl (aq. 37%)	5	60	3	60
7	HCl (aq. 37%)	5 (mortar)	45	7	7
8	HCl (aq. 37%)	5 (mortar)	60	24	9
9	HCl (aq. 37%) ^[c]	30	45	42	6
10	HCl (aq. 10%)	60	45	7	6
11	HCl (aq. 10%)	60	45	15	9
12	HCl (aq. 10%)	60	45	42	11

[a] LAG acid was added in $\eta = 0.25 \mu\text{l mg}^{-1}$ to 100 mg of the monomer and one equivalent of PFA in the milling jar. [b] The conversion to cycHC[6] (%) was determined from the ¹H NMR spectra of the quenched reaction products. [c] Aging was carried out without sealing the vial with PTFE tape and Parafilm.

Similarly, diminished conversion to cycHC[6] was observed when the concentration of the LAG acid was reduced (aq. 10% HCl, $\eta = 0.25 \mu\text{l mg}^{-1}$). ¹H NMR was conducted on the products of reactions aged for seven days, 15 days or 42 days. While the condensation reaction proceeded in reduced acid content, the conversion to cycHC[6] was severely curbed, at only 11% in 42 days (Table 6, entries 10, 11, and 12). When LAG was carried out with concentrated (37%) acid, the cycHC[6] in the aging product was stabilized by three molar equivalents of Cl⁻ during the aging reaction, while the same LAG volume of 10% HCl provided less than an equimolar amount of the template (0.72 eq). This suggests that the sensitivity of these reactions to the evaporation of acid was largely the result of

an insufficient amount of the template in the solids when aging. Estimated maximum water content in the solids was also slightly higher when less concentrated LAG acid was used; 3.2 equivalents of water to the monomer, compared to 2.75 equivalents of water present in the reactions carried out with concentrated HCl. Water molecules can mediate the acid-catalyzed methylene bridge formation and hydrolysis by proton transfer (Figure 13), but may act as competing nucleophiles to the monomer in reacting with the active iminium intermediates, therefore hindering the methylene bridge formation.

4.4.3 Adapting the developed approach to the solid state synthesis of cycHC[8]

On the basis of the developed reaction conditions in **Publication I** for the solution phase synthesis of cycHC[8], trifluoroacetate was first chosen as the template for developing the solid-state synthesis of cycHC[8]. However, when the monomer and PFA were reacted by ball milling in the presence of trifluoroacetic acid ($\eta = 0.08$ or $0.25 \mu\text{l mg}^{-1}$) and aged at either 45 or 60 °C, only a small amount of cycHC[8] was obtained. ^1H NMR analysis of the quenched reaction products revealed that the products mainly consisted of oligomers, containing only up to 7% of cycHC[8] (Table 7 entries 1 and 2). This showed that while the oligomers were produced efficiently, 1.5 or 4.4 equivalents of CF_3CO_2^- could not sufficiently stabilize cycHC[8] during aging.

Considering the results from the anion binding study of cycHC[8] carried out in **Publication II**, the poor templating power of trifluoroacetate was not surprising, as it is bound by cycHC[8] very weakly in polar media ($K_a < 10 \text{ M}^{-1}$). According to the DFT calculations in **Publication I**, formation of a low-energy anion inclusion complex provides the main driving force to push the thermodynamic equilibrium in the acid-induced DCL towards cycHC[8]. Therefore, perchloric acid was chosen next, as ClO_4^- is bound significantly stronger with cycHC[8] ($K_a = 470 \pm 20 \text{ M}^{-1}$) compared to CF_3CO_2^- . Its 70% water solution is stable and safe to handle. HPF_6 and HSbF_6 are incompatible with ZrO_2 milling jars in aqueous conditions (developed by the condensation reaction), as hydrolysis produces HF, which would etch the jars.

Indeed, 98–99% conversion to cycHC[8] was obtained when the monomer was milled for 30 minutes with PFA in the presence of HClO_4 (aq. 70%, $\eta = 0.2 \mu\text{l mg}^{-1}$), and the resulting solid reaction mixture was aged for one day at 45 or 60 °C (Table 7, entries 3 and 4; Figure 41). LAG acid volume was chosen to achieve the three molar equivalents of the template relative to the product cycHC[8], and it was effective for the synthesis of cycHC[6]. The isolated yield of cycHC[8] after 30-minute LAG and one day of aging at 60 °C was 85%, again reflecting the loss of some of the solid material upon transferring the reaction mixture between the milling jar, the vial for aging, and eventually the glass filter where the reaction was quenched. The isolated yield could, in this case, also be improved by aging the solids in an unopened sufficiently sealed milling jar.

Aging of the solid reaction mixture obtained from 30-minute ball milling at room temperature for three days afforded 62% conversion to cycHC[8] (Table 7 entry 5), demonstrating that aging proceeded even without exposing the solids to elevated temperatures.

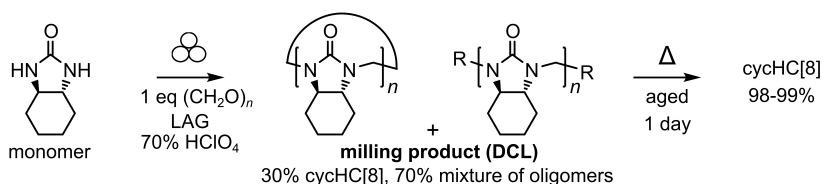


Table 7 entry 4 (aging step):

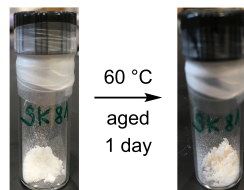


Figure 41. Reaction scheme for the solid-state synthesis of cycHC[8] coupling LAG with accelerated aging. Optimized reaction conditions, such as the amount of LAG acid, milling duration, aging temperature and duration are shown in Table 7, entries 3 and 4. The photos (bottom row) show the appearance of the reaction mixture of Table 7, entry 4 before and after the aging step.

Surprisingly, in contrast to the synthesis of cycHC[6], in which only 5% of cycHC[6] was obtained in the milling step, the perchlorate template afforded 30% of cycHC[8] after 30 minutes of ball milling (Table 7, entry 6). Longer milling afforded even higher conversions (Table 7, entries 7 and 8), which showed that cycHC[8] was amplified by the perchlorate anion under mechanochemical conditions. Milling experiments longer than 180 minutes were not performed.

Table 7. Screening the reaction conditions for the solid-state synthesis of cycHC[8]

Entry	Acid ^[a]	η ($\mu\text{l mg}^{-1}$)	Milling duration (min)	Aging tempera- -ture (°C)	Aging duration (days)	Conversion to cycHC[8] (%) ^[b]
1	CF ₃ CO ₂ H	0.25	60	45	7	7
2	CF ₃ CO ₂ H	0.08	30	60	3	6
3	HClO ₄ (aq. 70%)	0.2	30	45	1	99
4	HClO ₄ (aq. 70%)	0.2	30	60	1	98
5	HClO ₄ (aq. 70%)	0.2	30	20	3	62
6	HClO ₄ (aq. 70%)	0.2	30	-	-	30
7	HClO ₄ (aq. 70%)	0.2	90	-	-	56
8	HClO ₄ (aq. 70%)	0.2	180	-	-	63

[a] LAG acid was added to 100 mg of the monomer and one equivalent of PFA in the milling jar.

[b] The conversion to cycHC[8] (%) was determined from ¹H NMR spectra of the quenched reaction products.

4.4.4 Aging step followed *in situ* by solid-state NMR

To gain insight into the formation of cycHC[6] and cycHC[8] during the aging step, the reaction kinetics were followed *in situ* by solid-state CP-MAS ¹³C NMR spectroscopy. After the 30-minute milling of the monomer and PFA with either HCl (aq. 37%, $\eta = 0.25 \mu\text{l mg}^{-1}$) or HClO₄ (aq. 70%, $\eta = 0.2 \mu\text{l mg}^{-1}$), the resulting solid was transferred to a ZrO₂ NMR rotor, which was closed by Teflon caps and set at 60 °C within the spectrometer. Consecutive ¹³C NMR spectra were recorded at a constant time interval, over a period of one to three days. The linear flexible oligomers had no observable signals in the CP-MAS solid-state NMR measurement conditions; therefore, the formation of the more rigid macrocyclic products could be followed based on the emerging sets of ¹³C signals (Figure 42). Observable cycHC[8] signals in the first spectra of cycHC[8] formation (Figure 42B),

measured directly after milling, confirmed that some of the target product already formed during milling.

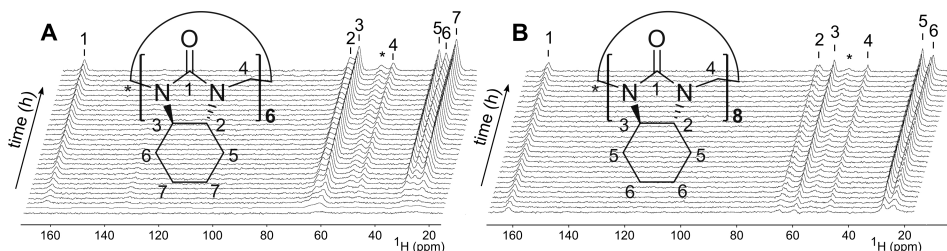


Figure 42. The stacked consecutive ^{13}C NMR spectra of the *in situ* aging reactions, following the formation of (A) cycHC[6] at a time interval of 30 minutes and (B) cycHC[8] at a time interval of three minutes and 45 seconds. ^{13}C NMR signals used for curve fitting are identified and indicated. One of the two symmetry independent methylene bridge ^{13}C signals, denoted by an asterisk, was not used for curve fitting, due to the low signal-to-noise ratio.

The kinetic curves obtained for both cycHC[6] and cycHC[8] are best described by first-order kinetic behavior (Figure 43). First-order reaction rate law was also observed in the solution phase synthesis of cycHC[8] in **Publication I**, which suggests that the reaction pathway in the solid state was not significantly altered from the solution synthesis. The resulting reaction rate constants revealed that the rate of cycHC[8] formation was a magnitude larger than that of cycHC[6] (Figure 43 A and B). The faster rate of cycHC[8] formation, and the observation that it proceeded at a lower temperature (Table 7, entry 5), can be explained by the higher acidity of HClO_4 ($\text{p}K_a -15.7 \pm 2.0^{[167]}$) compared to HCl ($\text{p}K_a -5.9 \pm 0.4^{[167]}$) used in the synthesis of cycHC[6]. Higher acidity promotes faster equilibration between the oligomeric intermediates, which led to faster convergence of the aging reaction.

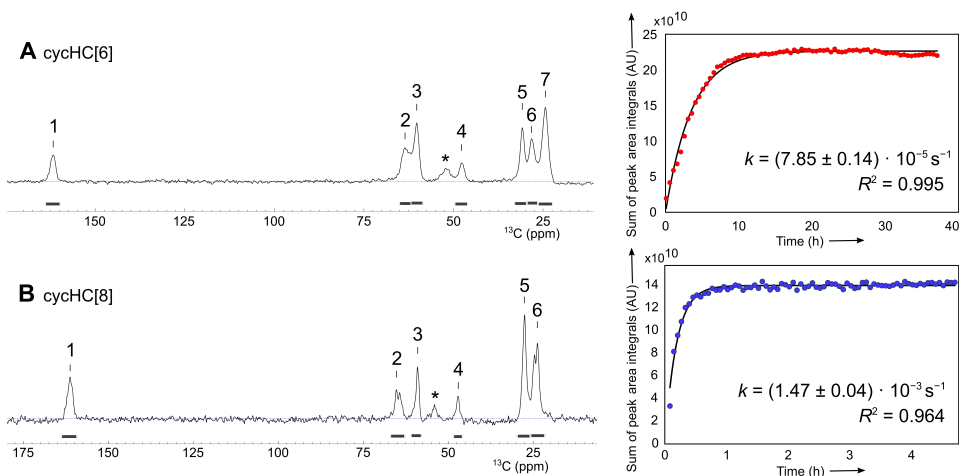


Figure 43. The kinetic curves obtained for the formation of cycHC[6] (red) and cycHC[8] (blue) during respective aging reactions at 60°C , based on the sum of the peak integration areas indicated by black lines below the corresponding ^{13}C NMR spectra of (A) cycHC[6] and (B) cycHC[8].

The reactions followed *in situ* were also quenched by washing with water. Subsequent ^1H NMR analysis in chloroform revealed that both of the reactions converged before full conversion, with 71% of cycHC[6] and 80% of cycHC[8] obtained. Premature convergence

of the reactions was caused either by the slow evaporation of the acid from the NMR rotor at 60 °C, or by the heterogeneous distribution of the solids and the liquid acid catalyst in the rotor during the high-speed spinning (3000 s⁻¹).

4.4.5 Aging followed *ex situ* by PXRD and SEM

The starting mixture and the products of the aging steps were also characterized by powder X-ray diffraction (PXRD) analysis and scanning electron microscopy (SEM). The reactions characterized were performed according to the conditions in Table 6, entry 4 and Table 7, entry 4.

The reaction mixtures obtained from the 30-minute ball milling, which contained mainly oligomers, were amorphous both in the synthesis of cycHC[6] and cycHC[8] (Figure 44A). The reaction products were observed to contain a crystalline phase both in the case of cycHC[6] and cycHC[8] (Figure 44B). The PXRD pattern of the cycHC[6] obtained by the solid-state method matched that of a solution-synthesized product (Figure 44C). Thus, the crystalline phase formed in the solid-state reaction mixture must have formed without the chloride template, or the measured solution-based product was, in fact, an HCl adduct. The powder pattern of the obtained cycHC[8] did not match any of the known crystalline phases of cycHC[8].

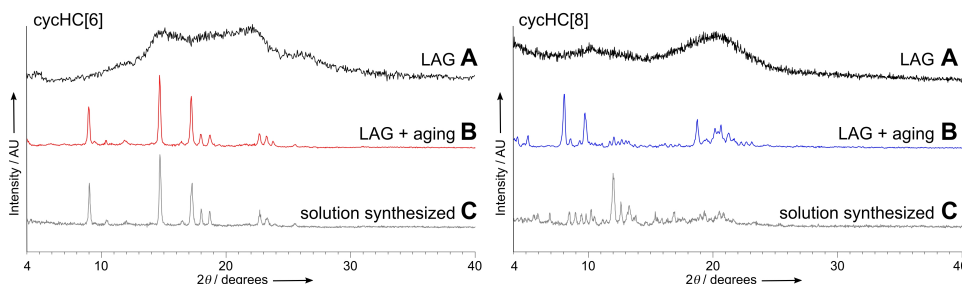


Figure 44. (A) PXRD patterns of the reaction mixtures from the milling jar after LAG. (B) PXRD patterns of the unquenched products from the aging step, containing 96% of cycHC[6] (red) or 98% of cycHC[8] (blue), based on the ¹H NMR analysis of the quenched products. (C) PXRD patterns of the solution-synthesized cycHC[6] and cycHC[8].

SEM micrographs of the samples taken from the freshly milled reaction mixtures (30 minutes) show that the solids at the start of the aging reaction consisted of angular irregular particles, up to 25 μm in diameter (Figure 45, top row). Samples taken from the reaction mixtures after aging revealed that the solids aggregated into larger particles upon aging, consistent with an Ostwald ripening process.^[168] This spontaneous process occurs due to the higher surface energy of the smaller particles, which therefore get deposited onto the surface of larger particles. Round particles of up to 150 μm in diameter, with a seemingly smoother surface were observed after aging in the solid-state synthesis of both cycHC[6] and cycHC[8] (Figure 45, bottom row). Belenguer *et al.* proposed that the crystallite surface solvation free energy could govern the stability order of polymorphs under neat or LAG conditions.^[169] According to this, the aggregation into larger particles in the cycHC[*n*] synthesis could also contribute to the overall free energy of these solid-state reactions.

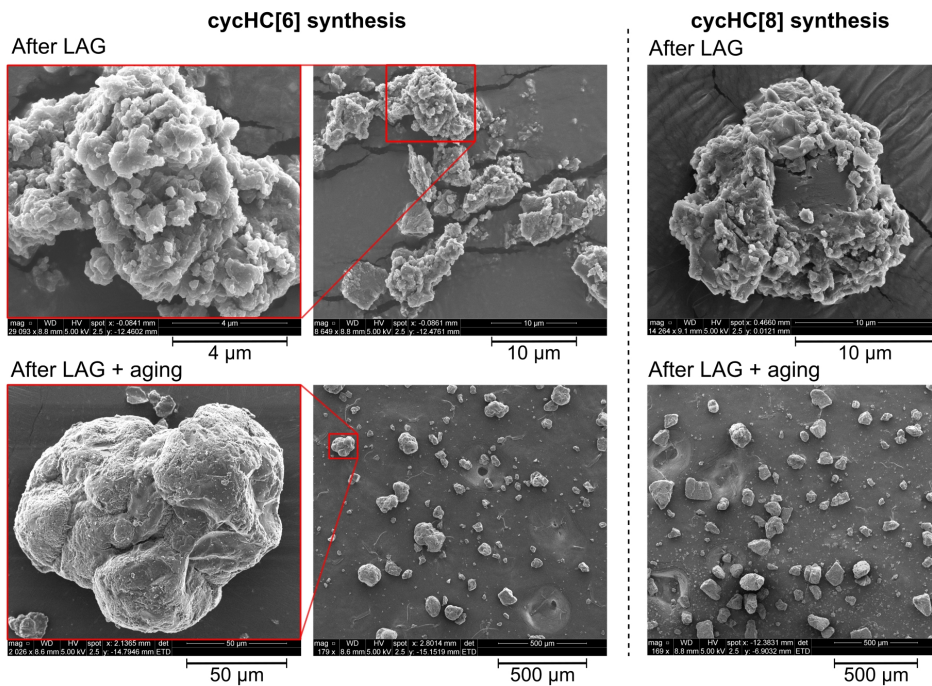


Figure 45. SEM micrographs of the samples taken from the reaction mixtures of cycHC[6] and cycHC[8] solid-state synthesis: from the freshly milled solids (top row) and from unquenched products after the aging step (bottom row).

5 CONCLUSIONS

The solution synthesis of cyclohexanohemicucurbit[8]uril (cycHC[8]) demonstrated that acids, which provide a larger anion ($\text{CF}_3\text{CO}_2\text{H}$, HCO_2H) upon dissociation, allowed for the template-controlled synthesis of the eight-membered macrocycle either from the monomer or by re-macrocyclization from cycHC[6]. Furthermore, using a relatively benign, non-templating acetic acid, conversion between cycHC[6] and cycHC[8] was achieved by directing the dynamic covalent chemistry through the addition of template-containing salts (NaCl for cycHC[6] and NaPF_6 for cycHC[8]). CycHC[8] is the only known octameric macrocycle among the hemicucurbituril hosts.

Single crystal X-ray diffraction analysis was used to determine the structure and dimensions of the novel macrocyclic host. It also revealed that a single disordered methanol molecule was located within the cavity of cycHC[8]. The rapid drying of the crystals observed at room temperature was explained by the presence of continuous solvent-filled channels in the crystal structure of the cycHC[8] methanol solvate.

The crystallographic study of the host-guest complexes of cycHC[8] by single crystal X-ray diffraction unambiguously revealed that the host formed 1:1 inclusion complexes with anions from methanol. Encapsulated anions were completely desolvated and isolated in the center of the cycHC[8] cavity, forming weak $\text{C}-\text{H}\cdots\text{anion}$ hydrogen bonds, as indicated by the Hirshfeld surface and the short contact analysis. The largest guest anions of SbF_6^- , CF_3SO_3^- , and PF_6^- formed several simultaneous hydrogen bonds and appeared to be fixed in the cavity. The smaller tetrahedral anions of ReO_4^- , IO_4^- , ClO_4^- , and BF_4^- appeared disordered between two to four positions, each of which was only involved in a limited number of host-guest interactions. Job's method, NMR titrations, and isothermal titration calorimetry were used to study the anion-binding behavior of cycHC[8] in methanol. Job's method confirmed the 1:1 stoichiometry of the anion inclusion complexes in solution, and NMR titrations revealed the strongest association with SbF_6^- ($K_a = 2.5 \cdot 10^5 \text{ M}^{-1}$), followed by PF_6^- ($K_a = 2.8 \cdot 10^4 \text{ M}^{-1}$), ReO_4^- ($K_a = 4.7 \cdot 10^3 \text{ M}^{-1}$), IO_4^- ($K_a = 1.8 \cdot 10^3 \text{ M}^{-1}$), ClO_4^- ($K_a = 470 \text{ M}^{-1}$), and BF_4^- ($K_a = 48 \text{ M}^{-1}$). The asymmetric charge distribution of the anions resulted in the drastically weaker association of CF_3SO_3^- ($K_a = 39 \text{ M}^{-1}$) and CF_3CO_3^- ($K_a < 10 \text{ M}^{-1}$) with cycHC[8], compared to the similarly sized SbF_6^- and PF_6^- . Therefore, the anions with symmetric charge distribution were preferentially bound with cycHC[8]. ITC revealed that the binding of anions in methanol was enthalpy-driven and entropically disfavored, suggesting that the host-guest complexes were assembled through the chaotropic effect.

The study of the hemicucurbituril ($\text{HC}[n]$) host-guest complexes based on the published crystallographic data highlighted the 1:1, 1:2, and 1:3 host-guest anion binding motifs of the bambusuril-type hosts, in contrast to the exclusively 1:1 binding motif seen with cycHC[8]. Position of the guests in the central binding pocket of $\text{HC}[n]$ and the shallow secondary binding pockets of the BU-type hosts suggested, that $\text{C}-\text{H}\cdots\text{guest}$ interactions were involved in the association of the anions with $\text{HC}[n]$. No crystal structures of anion inclusion complexes with the smallest BU[4]-type hosts have been reported, supporting the observation that these hosts are formed from the BU-monomer in the absence of a suitably sized template. The dimensions of the hemicucurbit[6]uril, bambusurils, biotinuril, and the cycHC[8] hosts in 1:1 complexes with anions were found to adapt to the size of the guest. The strongest linear correlation ($R^2 = 91\%$) was found between the volume of the guest and the radius of the cycHC[8] cavity, however the increase of cavity

radius between the smallest (BF_4^-) and the largest (SbF_6^-) encapsulated guest remained within 5%.

Based on the knowledge gained from the studies of the template-controlled solution-based synthesis of cycHC[n] and the association of anion host-guest complexes with cycHC[8], a novel solid-state anion-templated method was developed for the synthesis of cycHC[6] and cycHC[8]. Ball milling of (*R,R*)-hexahydro-2-benzimidazolinone and paraformaldehyde with a catalytic amount of HCl or HClO_4 provided a solid mixture of oligomeric products, which upon aging at slightly elevated temperatures was found to convert quantitatively into the target macrocyclic product in one to two days. The formation of cycHC[6] or cycHC[8] was dictated by the template in the reaction mixture, Cl^- or ClO_4^- , respectively. The process of solid-to-solid self-organization of the oligomers into the macrocyclic product was studied by powder X-ray diffraction, scanning electron microscopy, and *in situ* solid-state NMR spectroscopy. The aging reactions were best described by first-order kinetic law, with cycHC[8] having an order of magnitude higher formation rate than that of cycHC[6].

REFERENCES

- [1] M. J. Webber, R. Langer, *Chem. Soc. Rev.* **2017**, *46*, 6600–6620.
- [2] D. Wu, A. C. Sedgwick, T. Gunnlaugsson, E. U. Akkaya, J. Yoon, T. D. James, *Chem. Soc. Rev.* **2017**, *46*, 7105–7123.
- [3] J. E. Green, J. Wook Choi, A. Boukai, Y. Bunimovich, E. Johnston-Halperin, E. Deionno, Y. Luo, B. A. Sheriff, K. Xu, Y. Shik Shin, H.-R. Tseng, J. F. Stoddart, J. R. Heath, *Nature* **2007**, *445*, 414–417.
- [4] J. Xie, H.-J. Peng, J.-Q. Huang, W.-T. Xu, X. Chen, Q. Zhang, *Angew. Chemie Int. Ed.* **2017**, *56*, 16223–16227.
- [5] C. Wang, H. Wu, Z. Chen, M. T. Mcdowell, Y. Cui, Z. Bao, *Nat. Chem.* **2013**, *5*, 1042–1048.
- [6] Y. Jin, B. A. Voss, A. Jin, H. Long, R. D. Noble, W. Zhang, *J. Am. Chem. Soc.* **2011**, *133*, 6650–6658.
- [7] B. Li, X. Dong, H. Wang, D. Ma, K. Tan, S. Jensen, B. J. Deibert, J. Butler, J. Cure, Z. Shi, T. Thonhauser, Y. J. Chabal, Y. Han, J. Li, *Nat. Commun.* **2017**, *8*, 485.
- [8] B. P. O’Sullivan, S. D. Freedman, *Lancet* **2009**, *373*, 1891–1904.
- [9] N. N. Andersen, M. Lisbjerg, K. Eriksen, M. Pittelkow, *Isr. J. Chem.* **2018**, *58*, 435–448.
- [10] M. A. Yawer, V. Havel, V. Sindelar, *Angew. Chemie Int. Ed.* **2015**, *54*, 276–279.
- [11] V. Havel, M. A. Yawer, V. Sindelar, *Chem. Commun.* **2015**, *51*, 4666–4669.
- [12] R. Aav, E. Shmatova, I. Reile, M. Borissova, F. Topić, K. Rissanen, *Org. Lett.* **2013**, *15*, 3786–9.
- [13] J. Sokolov, V. Sindelar, *Chem. Eur. J.* **2018**, *24*, 15482–15485.
- [14] M. Lisbjerg, H. Valkenier, B. M. Jessen, H. Al-Kerdi, A. P. Davis, M. Pittelkow, *J. Am. Chem. Soc.* **2015**, *137*, 4948–4951.
- [15] C. Lang, A. Mohite, X. Deng, F. Yang, Z. Dong, J. Xu, J. Liu, E. Keinan, O. Reany, *Chem. Commun.* **2017**, *53*, 7557–7560.
- [16] A. Šlampová, V. Šindelář, P. Kubáň, *Anal. Chim. Acta* **2017**, *950*, 49–56.
- [17] H. Cong, T. Yamato, X. Feng, Z. Tao, *J. Mol. Catal. A Chem.* **2012**, *365*, 181–185.
- [18] H. Cong, T. Yamato, Z. Tao, *J. Mol. Catal. A Chem.* **2013**, *379*, 287–293.
- [19] H. Cong, T. Yamato, Z. Tao, *New J. Chem.* **2013**, *37*, 3778.
- [20] T. Fiala, L. Ludvíková, D. Heger, J. Švec, T. Slanina, L. Vetráková, M. Babiak, M. Nečas, P. Kulhánek, P. Klán, V. Sindelar, *J. Am. Chem. Soc.* **2017**, *139*, 2597–2603.
- [21] J.-L. Do, T. Friščić, *Synlett* **2017**, *28*, 2066–2092.
- [22] N. Stock, S. Biswas, *Chem. Rev.* **2012**, *112*, 933–969.
- [23] J.-L. Do, T. Friščić, *ACS Cent. Sci.* **2017**, *3*, 13–19.
- [24] C. J. Pedersen, *J. Am. Chem. Soc.* **1967**, *89*, 7017–7036.
- [25] C. J. Pedersen, *Angew. Chemie Int. Ed.* **1988**, *27*, 1021–1027.
- [26] J.-M. Lehn, *Angew. Chemie Int. Ed.* **1988**, *27*, 89–112.
- [27] D. J. Cram, *Angew. Chemie Int. Ed.* **1988**, *27*, 1009–1020.
- [28] D. J. Cram, J. M. Cram, *Science (80-.)*. **1974**, *183*, 803–809.
- [29] J. W. Steed, D. R. Turner, K. J. Wallace, *Core Concepts in Supramolecular Chemistry and Nanochemistry*, John Wiley And Sons, Ltd, **2007**.
- [30] G. Cavallo, P. Metrangolo, R. Milani, T. Pilati, A. Priimägi, G. Resnati, G. Terraneo, *Chem. Rev.* **2016**, *116*, 2478–2601.
- [31] F. Biedermann, W. M. Nau, H.-J. Schneider, *Angew. Chemie Int. Ed.* **2014**, *53*, 11158–11171.

- [32] E. P. Kyba, R. C. Helgeson, K. Madan, G. W. Gokel, T. L. Tarnowski, S. S. Moore, D. J. Cram, *J. Am. Chem. Soc.* **1977**, *99*, 2564–2571.
- [33] D. J. Cram, *Angew. Chemie Int. Ed.* **1986**, *25*, 1039–1057.
- [34] J. W. Steed, J. L. Atwood, *Supramolecular Chemistry, 2nd Ed.*, John Wiley And Sons, Ltd, **2009**.
- [35] A. Villiers, *C. R. Hebd. Seances Acad. Sci.* **1891**, *112*, 536–538.
- [36] A. Zinke, E. Ziegler, *Ber. Dtsch. Chem. Ges.* **1944**, *77*, 264.
- [37] R. Behrend, E. Meyer, F. Rusche, *Justus Liebig's Ann. der Chemie* **1905**, *339*, 1–37.
- [38] I. V Kolesnichenko, E. V Anslyn, *Chem. Soc. Rev* **2017**, *46*, 2385.
- [39] J. Zhou, G. Yu, F. Huang, *Chem. Soc. Rev.* **2017**, *46*, 7021–7053.
- [40] B. O. Okesola, D. K. Smith, *Chem. Soc. Rev.* **2016**, *45*, 4226–4251.
- [41] K.-T. Wong, D. M. Bassani, *NPG Asia Mater.* **2014**, *6*, e116.
- [42] C. H. Park, H. E. Simmons, *J. Am. Chem. Soc.* **1968**, *90*, 2431–2432.
- [43] J. L. Sessler, P. A. Gale, W.-S. Cho, *Anion Receptor Chemistry*, The Royal Society Of Chemistry, **2006**.
- [44] J. W. Meisel, S. Negin, M. R. Gokel, G. W. Gokel, in *Compr. Supramol. Chem. 2nd Ed.* (Ed.: J.L. Atwood), Elsevier, **2017**, pp. 495–520.
- [45] N. Busschaert, C. Caltagirone, W. Van Rossom, P. A. Gale, *Chem. Rev.* **2015**, *115*, 8038–8155.
- [46] S. Kubik, in *Synth. Recept. Biomol. Des. Princ. Appl.* (Ed.: B.D. Smith), Royal Society Of Chemistry, **2015**, pp. 129–176.
- [47] Y. Marcus, *J. Chem. Soc. Faraday Trans.* **1991**, *87*, 2995–2999.
- [48] S. Kubik, *Acc. Chem. Res.* **2017**, *50*, 2870–2878.
- [49] F. Hofmeister, *Arch. für Exp. Pathol. und Pharmakologie* **1888**, *24*, 247–260.
- [50] W. Kunz, J. Henle, B. W. Ninham, *Curr. Opin. Colloid Interface Sci.* **2004**, *9*, 19–37.
- [51] F. Hofmeister, *Arch. für Exp. Pathol. und Pharmakologie* **1888**, *25*, 1–30.
- [52] Y. Zhang, P. S. Cremer, *Curr. Opin. Chem. Biol.* **2006**, *10*, 658–663.
- [53] Y. Zhang, P. S. Cremer, *Annu. Rev. Phys. Chem.* **2010**, *61*, 63–83.
- [54] H. I. Okur, J. Hladílková, K. B. Rembert, Y. Cho, J. Heyda, J. Dzubielia, P. S. Cremer, P. Jungwirth, *J. Phys. Chem. B* **2017**, *121*, 1997–2014.
- [55] N. Schwierz, D. Horinek, R. R. Netz, *Langmuir* **2010**, *26*, 7370–7379.
- [56] C. J. Serpell, P. D. Beer, *Anion Sensors*, Elsevier, **2017**.
- [57] T. Fiala, K. Sleziaikova, K. Marsalek, K. Salvadori, V. Sindelar, *J. Org. Chem.* **2018**, *83*, 1903–1912.
- [58] J. Svec, M. Necas, V. Sindelar, *Angew. Chemie Int. Ed.* **2010**, *49*, 2378–2381.
- [59] A. S. Singh, S. S. Sun, *J. Org. Chem.* **2012**, *77*, 1880–1890.
- [60] P. A. Gale, *Acc. Chem. Res.* **2011**, *44*, 216–226.
- [61] A. J. Ayling, M. N. Pérez-Payán, A. P. Davis, *J. Am. Chem. Soc.* **2001**, *123*, 12716–12717.
- [62] A. V. Koulov, T. N. Lambert, R. Shukla, M. Jain, J. M. Boon, B. D. Smith, H. Li, D. N. Sheppard, J.-B. Joos, J. P. Clare, A. P. Davis, *Angew. Chemie Int. Ed.* **2003**, *42*, 4931–4933.
- [63] B. A. McNally, A. V. Koulov, B. D. Smith, J. B. Joos, A. P. Davis, *Chem. Commun.* **2005**, 1087–1089.
- [64] B. A. McNally, A. V. Koulov, T. N. Lambert, B. D. Smith, J. B. Joos, A. L. Sisson, J. P. Clare, V. Sgarlata, L. W. Judd, G. Magro, A. P. Davis, *Chem. Eur. J.* **2008**, *14*, 9599–9606.

- [65] M. Lisbjerg, B. M. Jessen, B. Rasmussen, B. E. Nielsen, A. Madsen, M. Pittelkow, *Chem. Sci.* **2014**, *5*, 2647–2650.
- [66] E. A. Katayev, G. V. Kolesnikov, J. L. Sessler, *Chem. Soc. Rev.* **2009**, *38*, 1572–1586.
- [67] J. A. Gawenis, K. T. Holman, J. L. Atwood, S. S. Jurisson, *Inorg. Chem.* **2002**, *41*, 6028–6031.
- [68] K. Travis Holman, G. William Orr, J. L. Atwood, J. W. Steed, *Chem. Commun.* **1998**, 2109–2110.
- [69] H. Stephan, K. Gloe, W. Kraus, H. Spies, B. Johannsen, K. Wichmann, G. Reck, D. K. Chand, P. K. Bharadwaj, U. Müller, W. M. Müller, F. Vögtle, in *Fundam. Appl. Anion Sep.* (Eds.: B.A. Moyer, R.P. Singh), Kluwer Academic/Plenum Publishers, New York, **2004**, pp. 151–168.
- [70] D. Farrell, K. Gloe, K. Gloe, G. Goretzki, V. McKee, J. Nelson, M. Nieuwenhuyzen, I. Pál, H. Stephan, R. M. Town, K. Wichmann, *Dalt. Trans.* **2003**, 1961–1968.
- [71] Y.-S. Kang, Y. Lu, K. Chen, Y. Zhao, P. Wang, W.-Y. Sun, *Coord. Chem. Rev.* **2019**, *378*, 262–280.
- [72] M. D. Visco, J. Attard, Y. Guan, A. E. Mattson, *Tetrahedron Lett.* **2017**, *58*, 2623–2628.
- [73] M. S. Taylor, E. N. Jacobsen, *J. Am. Chem. Soc.* **2004**, *126*, 10558–10559.
- [74] I. T. Raheem, P. S. Thiara, E. A. Peterson, E. N. Jacobsen, *J. Am. Chem. Soc.* **2007**, *129*, 13404–13405.
- [75] C. R. Kennedy, D. Lehnher, N. S. Rajapaksa, D. D. Ford, Y. Park, E. N. Jacobsen, *J. Am. Chem. Soc.* **2016**, *138*, 13525–13528.
- [76] R. Abbel, C. Grenier, M. J. Pouderoijen, J. W. Stouwdam, P. E. L. G. Leclère, R. P. Sijbesma, E. W. Meijer, A. P. H. J. Schenning, *J. Am. Chem. Soc.* **2009**, *131*, 833–843.
- [77] S. Lee, C. H. Chen, A. H. Flood, *Nat. Chem.* **2013**, *5*, 704–710.
- [78] B. Qiao, G. M. Leverick, W. Zhao, A. H. Flood, J. A. Johnson, Y. Shao-Horn, *J. Am. Chem. Soc.* **2018**, *140*, 10932–10936.
- [79] G. O. Lloyd, J. W. Steed, *Nat. Chem.* **2009**, *1*, 437–442.
- [80] M. Yamanaka, T. Nakamura, T. Nakagawa, H. Itagaki, *Tetrahedron Lett.* **2007**, *48*, 8990–8993.
- [81] R. W. Taylor, T.-C. Lee, O. A. Scherman, R. Esteban, J. Aizpurua, F. M. Huang, J. J. Baumberg, S. Mahajan, *ACS Nano* **2011**, *5*, 3878–3887.
- [82] B. C. Pemberton, R. K. Singh, A. C. Johnson, S. Jockusch, J. P. Da Silva, A. Ugrinov, N. J. Turro, D. K. Srivastava, J. Sivaguru, *Chem. Commun.* **2011**, *47*, 6323–6325.
- [83] S. Walker, R. Oun, F. J. McInnes, N. J. Wheate, *Isr. J. Chem.* **2011**, *51*, 616–624.
- [84] W. A. Freeman, W. L. Mock, N. Y. Shih, *J. Am. Chem. Soc.* **1981**, *103*, 7367–7368.
- [85] K. Kim, N. Selvapalam, Y. H. Ko, K. M. Park, D. Kim, J. Kim, *Chem. Soc. Rev.* **2007**, *36*, 267–279.
- [86] S. J. Barrow, S. Kaser, M. J. Rowland, J. del Barrio, O. A. Scherman, *Chem. Rev.* **2015**, *115*, 12320–12406.
- [87] K. I. Assaf, W. M. Nau, *Chem. Soc. Rev.* **2015**, *44*, 394–418.
- [88] C. A. Burnett, D. Witt, J. C. Fettinger, L. Isaacs, *J. Org. Chem.* **2003**, *68*, 6184–6191.
- [89] Y. Miyahara, K. Goto, M. Oka, T. Inazu, *Angew. Chemie Int. Ed.* **2004**, *43*, 5019–5022.
- [90] T. F. G. G. Cova, S. C. C. Nunes, A. J. M. Valente, T. M. V. D. Pinho e Melo, A. A. C. C. Pais, *J. Mol. Liq.* **2017**, *242*, 640–652.
- [91] M. Sundararajan, R. V. Solomon, S. K. Ghosh, P. Venuvanalingam, *RSC Adv.* **2011**, *1*, 1333–1341.

- [92] M. Öeren, E. Shmatova, T. Tamm, R. Aav, *Phys. Chem. Chem. Phys.* **2014**, *16*, 19198–205.
- [93] S. Kaabel, R. Aav, *Isr. J. Chem.* **2018**, *58*, 296–313.
- [94] I. K. Yoo, Y. K. Kang, *Chem. Phys. Lett.* **2017**, *669*, 110–114.
- [95] M. E. Belowich, J. F. Stoddart, *Chem. Soc. Rev.* **2012**, *41*, 2003.
- [96] X. Su, I. Aprahamian, *Chem. Soc. Rev.* **2014**, *43*, 1963.
- [97] D. K. Kölmel, E. T. Kool, *Chem. Rev.* **2017**, *117*, 10358–10376.
- [98] S. P. Black, J. K. M. Sanders, A. R. Stefankiewicz, *Chem. Soc. Rev.* **2014**, *43*, 1861–1872.
- [99] S. D. Bull, M. G. Davidson, J. M. H. van den Elsen, J. S. Fossey, A. T. A. Jenkins, Y.-B. Jiang, Y. Kubo, F. Marken, K. Sakurai, J. Zhao, T. D. James, *Acc. Chem. Res.* **2013**, *46*, 312–326.
- [100] B. Buchs née Levrand, G. Godin, A. Trachsel, J.-Y. de Saint Laumer, J.-M. Lehn, A. Herrmann, *European J. Org. Chem.* **2011**, *2011*, 681–695.
- [101] L. You, S. R. Long, V. M. Lynch, E. V. Anslyn, *Chem. Eur. J.* **2011**, *17*, 11017–11023.
- [102] E. Prigorchenko, M. Öeren, S. Kaabel, M. Fomitšenko, I. Reile, I. Järving, T. Tamm, F. Topić, K. Rissanen, R. Aav, *Chem. Commun.* **2015**, *51*, 10921–10924.
- [103] M. Fomitšenko, A. Peterson, I. Reile, H. Cong, S. Kaabel, E. Prigorchenko, I. Järving, R. Aav, *New J. Chem.* **2017**, *41*, 2490–2497.
- [104] Y. Li, L. Li, Y. Zhu, X. Meng, A. Wu, *Cryst. Growth Des.* **2009**, *9*, 4255–4257.
- [105] M. Singh, E. Solel, E. Keinan, O. Reany, *Chem. Eur. J.* **2015**, *21*, 536–540.
- [106] M. Singh, E. Solel, E. Keinan, O. Reany, *Chem. Eur. J.* **2016**, *22*, 8848–8854.
- [107] T. Fiala, V. Sindelar, *Synlett* **2013**, *24*, 2443–2445.
- [108] A. Day, A. P. Arnold, R. J. Blanch, B. Snushall, *J. Org. Chem.* **2001**, *66*, 8094–8100.
- [109] V. Havel, J. Svec, M. Wimmerova, M. Dusek, M. Pojarova, V. Sindelar, *Org. Lett.* **2011**, *13*, 4000–4003.
- [110] J. Rivollier, P. Thuéry, M. P. Heck, *Org. Lett.* **2013**, *15*, 480–483.
- [111] V. Martí-Centelles, M. D. Pandey, M. I. Burguete, S. V. Luis, *Chem. Rev.* **2015**, *115*, 8736–8834.
- [112] J. C. Collins, K. James, *Medchemcomm* **2012**, *3*, 1489.
- [113] S. L. James, C. J. Adams, C. Bolm, D. Braga, P. Collier, T. Friščić, F. Grepioni, K. D. M. Harris, G. Hyett, W. Jones, A. Krebs, J. Mack, L. Maini, A. G. Orpen, I. P. Parkin, W. C. Shearouse, J. W. Steed, D. C. Waddell, *Chem. Soc. Rev.* **2012**, *41*, 413–447.
- [114] R. S. Varma, K. P. Naicker, D. Kumar, R. Dahiya, P. J. Liesen, *J. Microw. Power Electromagn. Energy* **1999**, *34*, 43–55.
- [115] L. R. Macgillivray, G. S. Papaefstathiou, T. Friščić, T. D. Hamilton, D. K. Bučar, Q. Chu, D. B. Varshney, I. G. Georgiev, *Acc. Chem. Res.* **2008**, *41*, 280–291.
- [116] K. Tanaka, F. Toda, *Chem. Rev.* **2000**, *100*, 1025–1074.
- [117] J. L. Howard, Q. Cao, D. L. Browne, *Chem. Sci.* **2018**, *9*, 3080–3094.
- [118] D. Tan, T. Friščić, *European J. Org. Chem.* **2018**, *2018*, 18–33.
- [119] T. Friščić, *Chem. Soc. Rev.* **2012**, *41*, 3493.
- [120] I. Halasz, S. A. J. Kimber, P. J. Beldon, A. M. Belenguer, F. Adams, V. Honkimäki, R. C. Nightingale, R. E. Dinnebier, T. Friščić, *Nat. Protoc.* **2013**, *8*, 1718–1729.
- [121] F. Fischer, G. Scholz, S. Benemann, K. Rademann, F. Emmerling, *CrystEngComm* **2014**, *16*, 8272–8278.
- [122] D. Hasa, E. Miniussi, W. Jones, *Cryst. Growth Des.* **2016**, *16*, 4582–4588.
- [123] T. Friščić, A. V. Trask, W. Jones, W. D. S. Motherwell, *Angew. Chemie Int. Ed.* **2006**, *45*, 7546–7550.

- [124] M. Tireli, M. Juribašić Kulcsár, N. Cindro, D. Gracin, N. Biliškov, M. Borovina, M. Ćurić, I. Halasz, K. Užarević, *Chem. Commun.* **2015**, *51*, 8058–8061.
- [125] J. G. Hernández, N. A. J. Macdonald, C. Mottillo, I. S. Butler, T. Friščić, *Green Chem.* **2014**, *16*, 1087–1092.
- [126] T. Friščić, D. G. Reid, I. Halasz, R. S. Stein, R. E. Dinnebier, M. J. Duer, *Angew. Chemie Int. Ed.* **2010**, *49*, 712–715.
- [127] M. J. Cliffe, C. Mottillo, R. S. Stein, D. K. Bučar, T. Friščić, *Chem. Sci.* **2012**, *3*, 2495–2500.
- [128] C. Mottillo, Y. Lu, M.-H. Pham, M. J. Cliffe, T.-O. Do, T. Friščić, *Green Chem.* **2013**, *15*, 2121.
- [129] F. Qi, R. S. Stein, T. Friščić, *Green Chem.* **2014**, *16*, 121–132.
- [130] F. Toda, *Acc. Chem. Res.* **1995**, *28*, 480–486.
- [131] F. Toda, in *Top. Curr. Chem. Vol. 254*, Springer, Berlin, Heidelberg, **2005**, pp. 1–40.
- [132] G. Kaupp, in *Top. Curr. Chem. Vol. 254*, Springer, Berlin, Heidelberg, **2005**, pp. 95–183.
- [133] B. Rodríguez, A. Bruckmann, T. Rantanen, C. Bolm, *Adv. Synth. Catal.* **2007**, *349*, 2213–2233.
- [134] J. G. Hernández, C. Bolm, *J. Org. Chem.* **2017**, *82*, 4007–4019.
- [135] J. Schmeyers, F. Toda, J. Boy, G. Kaupp, *J. Chem. Soc. Perkin Trans. 2* **1998**, *4*, 989–993.
- [136] G. Kaupp, J. Schmeyers, M. R. Naimi-Jamal, H. Zoz, H. Ren, *Chem. Eng. Sci.* **2002**, *57*, 763–765.
- [137] D. Cinčić, I. Brekalo, B. Kaitner, *Chem. Commun.* **2012**, *48*, 11683–11685.
- [138] A. M. Belenguer, T. Friščić, G. M. Day, J. K. M. Sanders, *Chem. Sci.* **2011**, *2*, 696.
- [139] A. M. Belenguer, G. I. Lampronti, D. J. Wales, J. K. M. Sanders, *J. Am. Chem. Soc.* **2014**, *136*, 16156–16166.
- [140] J. B. Ravnsbæk, T. M. Swager, *ACS Macro Lett.* **2014**, *3*, 305–309.
- [141] J. L. Atwood, M. J. Hardie, C. L. Raston, C. A. Sandoval, *Org. Lett.* **1999**, *1*, 164–166.
- [142] N. S. Isaacs, P. J. Nichols, C. L. Raston, C. A. Sandoval, D. J. Young, *Chem. Commun.* **1997**, *1*, 1839–1840.
- [143] F. Weinelt, H. J. Schneider, *J. Org. Chem.* **1991**, *56*, 5527–5535.
- [144] B. A. Roberts, G. W. V. Cave, C. L. Raston, J. L. Scott, *Green Chem.* **2001**, *3*, 280–284.
- [145] J. Antesberger, G. W. V. Cave, M. C. Ferrarelli, M. W. Heaven, C. L. Raston, J. L. Atwood, *Chem. Commun.* **2005**, *0*, 892.
- [146] B. Icli, N. Christinat, J. Tönnemann, C. Schüttler, R. Scopelliti, K. Severin, *J. Am. Chem. Soc.* **2009**, 3154–3155.
- [147] M. Pascu, A. Ruggi, R. Scopelliti, K. Severin, *Chem. Commun.* **2013**, *49*, 45–47.
- [148] Y. Sim, Y. X. Shi, R. Ganguly, Y. Li, F. García, *Chem. Eur. J.* **2017**, *23*, 11279–11285.
- [149] O. V. Dolomanov, L. J. Bourhis, R. J. Gildea, J. A. K. Howard, H. Puschmann, *J. Appl. Crystallogr.* **2009**, *42*, 339–341.
- [150] A. Bondi, *J. Phys. Chem.* **1964**, *68*, 441–451.
- [151] R. S. Rowland, R. Taylor, *J. Phys. Chem.* **1996**, *100*, 7384–7391.
- [152] S. S. Batsanov, *Inorg. Mater.* **2001**, *37*, 871–885.
- [153] M. Fomitšenko, E. Shmatova, M. Öeren, I. Järving, R. Aav, *Supramol. Chem.* **2014**, *26*, 698–703.

- [154] A. L. Spek, *Acta Crystallogr. Sect. C Struct. Chem.* **2015**, *71*, 9–18.
- [155] A. L. Spek, *Acta Crystallogr. Sect. D Biol. Crystallogr.* **2009**, *65*, 148–155.
- [156] W. M. Nau, M. Florea, K. I. Assaf, *Isr. J. Chem.* **2011**, *51*, 559–577.
- [157] C. F. Macrae, I. J. Bruno, J. A. Chisholm, P. R. Edgington, P. McCabe, E. Pidcock, L. Rodriguez-Monge, R. Taylor, J. Van De Streek, P. A. Wood, *J. Appl. Crystallogr.* **2008**, *41*, 466–470.
- [158] S. Mecozzi, J. Rebek, Jr., *Chem. Eur. J.* **1998**, *4*, 1016–1022.
- [159] M. A. Spackman, D. Jayatilaka, *CrystEngComm* **2009**, *11*, 19–32.
- [160] J. J. McKinnon, D. Jayatilaka, M. A. Spackman, *Chem. Commun.* **2007**, 3814–3816.
- [161] *Gaussian 09, Revision C.01*. M. J. Frisch, G. W. Trucks, H. B. Schlegel, G. E. Scuseria, M. A. Robb, J. R. Cheeseman, G. Scalmani, V. Barone, G. A. Petersson, H. Nakatsuji, X. Li, M. Caricato, A. Marenich, J. Bloino, B. G. Janesko, R. Gomperts, B. Mennucci, H. P. Hratchian, J. V. Ortiz, A. F. Izmaylov, J. L. Sonnenberg, D. Williams-Young, F. Ding, F. Lipparini, F. Egidi, J. Goings, B. Peng, A. Petrone, T. Henderson, D. Ranasinghe, V. G. Zakrzewski, J. Gao, N. Rega, G. Zheng, W. Liang, M. Hada, M. Ehara, K. Toyota, R. Fukuda, J. Hasegawa, M. Ishida, T. Nakajima, Y. Honda, O. Kitao, H. Nakai, T. Vreven, K. Throssell, J. A. Montgomery, Jr., J. E. Peralta, F. Ogliaro, M. Bearpark, J. J. Heyd, E. Brothers, K. N. Kudin, V. N. Staroverov, T. Keith, R. Kobayashi, J. Normand, K. Raghavachari, A. Rendell, J. C. Burant, S. S. Iyengar, J. Tomasi, M. Cossi, J. M. Millam, M. Klene, C. Adamo, R. Cammi, J. W. Ochterski, R. L. Martin, K. Morokuma, O. Farkas, J. B. Foresman, and D. J. Fox, Gaussian, Inc., Wallingford CT, **2016**.
- [162] *Gaussview, Version 5*. R. Dennington, T. Keith, J. Millam, Semichem Inc., Shawnee Mission, **2009**.
- [163] W. M. Nau, K. Assaf, *Angew. Chemie Int. Ed.* **2018**, 2–16.
- [164] M. Lisbjerg, B. E. Nielsen, B. O. Milhøj, S. P. A. Sauer, M. Pittelkow, *Org. Biomol. Chem.* **2015**, *13*, 369–373.
- [165] V. Havel, M. Babiak, V. Sindelar, *Chem. Eur. J.* **2017**, *23*, 8963–8968.
- [166] V. Havel, V. Sindelar, M. Necas, A. E. Kaifer, *Chem. Commun.* **2014**, *50*, 1372–1374.
- [167] A. Trummal, L. Lipping, I. Kaljurand, I. A. Koppel, I. Leito, *J. Phys. Chem. A* **2016**, *120*, 3663–3669.
- [168] IUPAC, *Compendium of Chemical Terminology, 2nd Ed. (the “Gold Book”)*, Blackwell Scientific Publications, Oxford, **1997**.
- [169] A. M. Belenguer, G. I. Lampronti, A. J. Cruz-Cabeza, C. A. Hunter, J. K. M. Sanders, *Chem. Sci.* **2016**, *7*, 6617–6627.

ACKNOWLEDGEMENTS

The work presented in this thesis was carried out at Tallinn University of Technology (Estonia), University of Jyväskylä (Finland) and McGill University (Canada). Therefore, I would first like to acknowledge the financial support that made this possible, the ESF Dora Programs, the Ministry of Education and Research (PUT692, IUT19-9) and the ASTRA “TUT Institutional Development Programme 2016-2022” Graduate School of Functional Materials and Technologies (2014-2020.4.01.16-0032). The value of this journey is not only the work, but the people met, and connections made along the way.

I am most grateful to my supervisor, Assoc. Prof. Riina Aav for noticing my interest in crystallography already on the first day I came to the lab as a Bachelor student. Thank you for all the encouraging discussions, trust and unwavering support through all the steps of my education. I would also like to recognize the patience of my first supervisor, Dr. Franz Werner, for taking upon himself the task of introducing me to the field of single crystal X-ray diffraction.

This thesis would not have been possible without the past and present members, and collaborators of the hemicucurbituril research group at TalTech. Elena, Maria, Mario, Kamini and Jasper, know that your friendship and contribution to this thesis is highly regarded. My students, Karin, Oliver, Mari-Liis K. and Jevgenija, I am very grateful for your dedication and hard work. Also, Marina, Lukaš, Anna, Anastassia, Madli, Nele, Mari-Liis L., I am sincerely thankful for the fruitful discussions at the group seminars.

Further, I would like to thank all my colleagues at TalTech for sharing the joy of finding crystals in a vial. A big thank you goes to Priit, for setting up and maintaining the crystallographic unit at TalTech. I am also grateful to Mikk, Anna, Estelle and Lukaš for the great times of plotting strategies to escape the Cylons, conquer new planets, take control of Japan, etc. The board game evenings have made stressful times infinitely easier to bare. Dr. Birgit Maaten and Dr. Heidi Lees are also warmly thanked, with whom we started this journey and have shared its ups and downs.

My heartfelt gratitude goes to my co-supervisor Prof. Kari Rissanen, who offered a starting PhD student and an aspiring crystallographer a chance to be a part of the busy scene of the Rissanen Research group and develop my skillset working alongside professionals in the field. Adj. Prof. Elina Kalenius and Anniina Kiesilä are acknowledged for their help with mass spectrometry. I am also truly grateful for the support and friendship of all the great people I had the pleasure of working with at Jyväskylä.

I would also like to thank Prof. Tomislav Friščić for the support and absolutely contagious enthusiasm during my research work at McGill University. Dr. Robin S. Stein is warmly acknowledged for her expertise and help with solid state NMR. Also, Igor, Zoë, Mihails, Hatem, Louis, Patrick, Dayaker and the rest of the group- thank you for the inspiring discussions and helpful advice, both in and out of the lab.

I am deeply appreciative of my sister Annika, my parents Tiina and Kaido, my aunt Marju, my grandparents, relatives and friends. Without your encouragement and unfaltering support this path would have been impossible.

Finally, I am deeply grateful to you, Filip, for being beside me throughout my studies. You are my constant source of joy and inspiration, my advisor and my fair critic, my best friend and my co-traveler.

ABSTRACT

Anion Recognition and the Templated Solid-State Synthesis of Hemicucurbiturils

This thesis describes the synthesis, structural studies, and anion binding properties of hemicucurbituril-based anion receptors. These electroneutral supramolecular hosts have garnered much attention, due to the strong and selective encapsulation of anionic guests by an ensemble of unconventional C–H···anion hydrogen bonds and the chaotropic effect. The specificity for polarizable anions has been used to achieve selective transmembrane anion transport and as an efficient anion sensor for the analysis of multiple anion mixtures. These and other successful anion host design strategies for the key application as anion receptors are highlighted first within the literature overview of this thesis. This is followed by an introduction to hemicucurbiturils, describing the origin of the anion-binding properties and the role of anionic templates in the synthesis of these macrocyclic hosts. A concise introduction to the field of mechanochemistry is provided next, together with its implementation for the solvent-free covalent synthesis of macrocyclic compounds.

The results of this thesis are divided into four chapters. The first study describes the template-controlled synthesis and crystallographic analysis of the novel cyclohexanohemicucurbit[8]uril (cycHC[8]) macrocyclic host. The novelty of the unique eight-membered hemicucurbituril lies in its larger cavity, offering alternative guest binding selectivity to the predominantly halide-binding six-membered hemicucurbiturils. The second chapter presents the anion-binding behavior of cycHC[8], charted and rationalized using single crystal X-ray diffraction, NMR-spectroscopic and calorimetric methods, mass spectrometry, and computational chemistry. This revealed the formation of strong, size-selective, enthalpy-driven 1:1 host-guest complexes with large, charge-diffuse polarizable anions. The comparison and presentation of the supramolecular anion binding motifs of different types of hemicucurbiturils are then presented in respective host-guest complexes, based on the single crystal X-ray diffraction data published in the Cambridge Structural Database.

The established methods for the solution-based synthesis of cyclohexanohemicucurbit[*n*]urils involve the dissolution of the starting materials in a large excess of acid together with a co-solvent of water or acetonitrile. Additional chromatographic purification methods are generally also necessary after the synthesis. The developed solid-state synthesis described in the final part of this thesis not only reduces the amount of acids used by 100-fold (and eliminates the use of organic solvents), but it also demonstrates that superior selectivity and quantitative yield is achieved by a conceptually novel solid-state approach combining mechanochemistry and aging.

LÜHIKOKKUVÕTE

Hemikukurbituriilid kui anioonide retseptorid ning nende mehhanokeemiline süntees tahkes faasis

Antud doktoritöö keskseks teemaks on supramolekulaarsete retseptorite loomine, täpsemalt hemikukurbituriilide süntees, nende kristallograafiline analüüs ning anioonide sidumisvõime kaardistamine. Hemikukurbituriilid on võõrustaja-molekulid, mis moodustavad anioonidega komplementaarselt paigutatud C–H...anioon vesiniksidemete kaudu tugevaid ja selektiivseid võõrustaja-külaline komplekse. Siiani on hemikukurbituriili-tüüpi anioonide retseptoreid kasutatud näiteks sensorite loomisel, mis on võimelised nii kvalitatiivselt kui kvantitatiivselt määrama anioonide sisaldust segudes. Samuti on loodud sünteetilisi membraani läbivaid anioon-transportereid, mis oleksid võimelised kontrollima ionide tasakaalu rakkudes. Lisaks keskkonnaseireks loodud sensoritele ning rakumembraani muteerunud ionpumpade asendamiseks loodud molekulaarsetele transporteritele tutvustab antud töö kirjanduse ülevaade ka teisi anioonide retseptorite rakendusi. Antakse ülevaade ka kirjanduses avaldatud hemikukurbituriilidest ning anioonide suunavast rollist nende sünteesil. Kirjanduse ülevaate viimane osa tutvustab keskkonnasäästlikku solvendivaba sünteetilist meetodit – mehhanosünteesi, ning koondab kõik seni kirjanduses avaldatud näited makrotsükliliste molekulide mehhanokeemilisest sünteesist.

Neljas teadusartiklis avaldatud doktoritöö tulemused on koondatud vastavalt nelja arutelu peatükki. Esimene neist kirjeldab tsükloheksanohemikukurbit[8]uriili (cycHC[8]) sünteesitingimuste väljatöötamist ning selle uudse võõrustaja-molekuli kristallstruktuuri analüüsi. Kaheksa-ühikulise makrotsükli suurem õõnsus, võrreldes seni loodud kuue-ühikuliste hemikukurbituriilidega, tagab selektiivsuse suurematele külalismolekulidele.

Arutelu teine peatükk kirjeldab cycHC[8] omadusi anioonide retseptorina, mida uuriti kristallograafia, tuumamagnetresonants-spektroskoopia, kalorimeetria, massispektromeetria ning arvutuskeemia meetoditel. Esitletud analüüsi tulemusena selgus, et uus võõrustajamolekul seob eelistatult suuremaid anioone, näiteks SbF_6^- , mis täidab makrotsükli õõnsusest 67%. Sidumise tugevus väheneb eksponentsiaalselt anioonide suuruse kahanemisel: SbF_6^- ($K_a = 250\,000\text{ M}^{-1}$), PF_6^- ($K_a = 28\,000\text{ M}^{-1}$), ReO_4^- ($K_a = 4700\text{ M}^{-1}$), IO_4^- ($K_a = 1800\text{ M}^{-1}$), ClO_4^- ($K_a = 470\text{ M}^{-1}$) ja BF_4^- ($K_a = 48\text{ M}^{-1}$).

Tulemuste kolmandas peatükis analüüsiti Cambridge Structural Database andmebaasis avaldatud kristallstruktuuride põhjal anioonide külaline-võõrustaja komplekse erinevat tüüpi hemikukurbituriilidega. Arutelu kirjeldab molekulidevahelisi interaktsioone ning võõrustaja-molekuli kuju muutust vastavalt külalise suurusele.

Töö viimane peatükk kirjeldab kuue- ja kaheksa-ühikulise tsükloheksanohemikukurbituriili tahke faasi sünteesitingimuste väljatöötamist. Tahkete lähtematerjalide jahvatamisel koos katalüütilise koguse mineraalhappega saadi oligomeeride ja makrotsüklite segu, mis edasisel inkubeerimisel spontaanselt ja kvantitatiivselt iseorganiseerub makrotsükliliseks produktiks. Seejuures määrab produkti selektiivsuse hapest tulenev anioonne mall, nii et Cl^- suunab kuue- ning ClO_4^- kaheksa-ühikulise makrotsükli sünteesi.

Doktoritöö raames kogutud teadmised erinevatest supramolekulaarsetest hemikukurbituriil-anioon kompleksidest võimaldasid luua uudse efektiivse ja solvendivaba sünteesimeetodi hemikukurbituriilide saamiseks. Mallide poolt suunatud iseorganiseerumisel põhinevad sünteesimeetodid võivad muuta ka tööstuses rakendatavate retseptorite valmistamise loodussäästlikumaks.

APPENDIX 1

Publication I

E. Prigorchenko, M. Öeren, **S. Kaabel**, M. Fomitšenko, I. Reile, I. Järving, T. Tamm, F. Topić, K. Rissanen, R. Aav, 'Template-controlled synthesis of chiral cyclohexylhemicucurbit[8]uril,' *Chem. Commun.* **2015**, 51, 10921–10924.

Re-printed with permission from the Royal Society of Chemistry.

Cite this: *Chem. Commun.*, 2015, 51, 10921Received 18th May 2015,
Accepted 3rd June 2015

DOI: 10.1039/c5cc04101e

www.rsc.org/chemcomm

Template-controlled synthesis of chiral cyclohexylhemicucurbit[8]uril†

E. Prigorchenko,^a M. Öeren,^a S. Kaabel,^a M. Fomitšenko,^a I. Reile,^b I. Järving,^a T. Tamm,^a F. Topić,^c K. Rissanen^c and R. Aav*^a

Enantiomerically pure cyclohexylhemicucurbit[8]uril (cycHC[8]), possessing a barrel-shaped cavity, has been prepared in high yield on a gram scale from either (*R,R,N,N'*)-cyclohex-1,2-diyurea and formaldehyde or cycHC[6]. In either case, a dynamic covalent library is first generated from which the desired cycHC can be amplified using a suitable anion template.

Research on new and selective host–guest systems and their applications is currently progressing very quickly.¹ Along with the search for new selective host–guest pairs, new and more efficient synthesis methods for hosts are being developed. Based on the recent success in the field of reversible non-covalent interactions in supramolecular chemistry,² the concept of dynamic covalent chemistry (DCC) has been established.³ Controlling covalent bond formation by non-covalent interactions can serve as an excellent tool for developing efficient adaptive systems, where the formation of the host molecule is based on the structure of the guest.

Cucurbit[*n*]urils⁴ (CB) are non-toxic host molecules⁵ with a wide range of applications.^{1a,d,6} Mechanistic studies have shown that the formation of oligomers and larger CBs proceeds reversibly, indicating that the principles of DCC are applicable in CB chemistry.⁷ Hemicucurbiturils⁸ (HC) are a sub-group of the cucurbituril family (Fig. 1). HCs are known to form complexes with anions⁹ and unsubstituted HCs have been applied as catalysts in organic reactions.¹⁰ It has been shown that biotin[6]uril esters can be applied as transmembrane anion carriers.^{9c} Miyahara *et al.*^{9a} were the first to describe an efficient synthesis of HC[6] and HC[12].

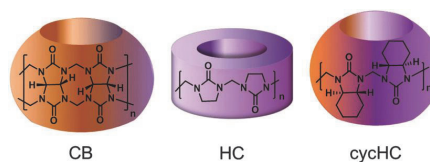


Fig. 1 Generalized shapes of normal CB, HC and chiral cycHC.

High selectivity towards the HC[6] was explained by the template effect of the chloride anion, which was recently confirmed in a biotin[6]uril synthesis.^{9f} The halogen anion is also the necessary template in the synthesis of bambus[6]urils (BU),¹¹ which can be classified as substituted HCs. Presently, besides HC[12], only 6-membered HCs⁸ and 4- and 6-membered BUs¹¹ have been isolated as main products. Until now, there has not been an efficient synthetic method available for the synthesis of 8-membered HCs. The existence of norbornahemicucurbit[8]uril^{8d} has been detected only by mass-spectrometry and (all-*R*)-cyclohexylhemicucurbit[8]uril (cycHC[8]) has only been isolated as a by-product in low yield.^{8c}

Herein we report an efficient synthesis of enantiomerically pure cycHC[8], starting either from its homologue cycHC[6] or (*R,R,N,N'*)-cyclohex-1,2-diyurea **1a** and paraformaldehyde. A mechanism of the transformation of cycHC[6] to cycHC[8] is proposed and proof of complexation with carboxylic acids is presented.

CycHC[6] was synthesized earlier in our group.^{8c} Subsequently, a small amount of its homologue cycHC[8]^{8c} was isolated from the crude product of cycHC[6]. Moreover, we noticed that in the chromatographic sample of cycHC[6] containing formic acid the amount of cycHC[8] gradually increased over time. The screening of reaction conditions for this conversion showed that cycHC[6] was transformed to cycHC[8] in the presence of sulphuric, formic and trifluoroacetic acid, but not acetic acid (S4, ESI†). The conversion of cycHC[6] to cycHC[8] by trifluoroacetic acid catalysis is approximately ten times faster than by formic acid (Table 1, entries 1 and 2). Nevertheless, the isolated yield of cycHC[8] was in both cases 71% in gram scale.

^a Department of Chemistry, Tallinn University of Technology, Akadeemia tee 15, 12618 Tallinn, Estonia. E-mail: riina.aav@ttu.ee

^b National Institute of Chemical Physics and Biophysics, Akadeemia tee 23, 12618 Tallinn, Estonia

^c University of Jyväskylä, Department of Chemistry, Nanoscience Center, P.O. Box 3, FI-40014 Jyväskylä, Finland

† Electronic supplementary information (ESI) available: A detailed description of synthesis, MS, NMR, crystallographic and computational details. CCDC 1053111. For ESI and crystallographic data in CIF or other electronic format see DOI: 10.1039/c5cc04101e

Table 1 Selected reaction conditions and the list of templates for cycHC synthesis

No.	Starting comp.	(Additive)/acid/solvent ^a	Template	Time (h), T	Ratio ^b of cycHC[8] to cycHC[6]	Product	Isolated yield of product (%)
1	cycHC[6]	HCOOH/CH ₃ CN	HCO ₂ ⁻	24, rt	92:8	cycHC[8]	71
2	cycHC[6]	CF ₃ COOH/CH ₃ CN	CF ₃ CO ₂ ⁻	1.5, rt	95:5	cycHC[8]	71
3	cycHC[6]	NaPF ₆ (50 eq.)/CH ₃ COOH/CH ₃ CN	PF ₆ ⁻	24, rt	99:1	cycHC[8]	90
4	1a	HCOOH/CH ₃ CN	HCO ₂ ⁻	24, rt	92:8	cycHC[8]	7
5	1a	NaPF ₆ (50 eq.)/CH ₃ COOH/CH ₃ CN	PF ₆ ⁻	24, rt	95:5	cycHC[8]	55
6	1a	CF ₃ COOH/CH ₃ CN	CF ₃ CO ₂ ⁻	2, rt	96:4	cycHC[8]	73
7 ^c	1a	HCl/H ₂ O	Cl ⁻	24, 70 °C	0:100	cycHC[6] + HCl	85
8	cycHC[8]	HCl/H ₂ O	Cl ⁻	24, 70 °C	5:95	cycHC[6] + HCl	71
9	cycHC[8]	NaCl (50 eq.)/CH ₃ COOH	Cl ⁻	24, 70 °C	40:60	cycHC[6] + HCl	21

^a Generally 300 eq. of organic acid or 4 M HCl were used. ^b Determined by HPLC. ^c Described previously in ref. 8c.

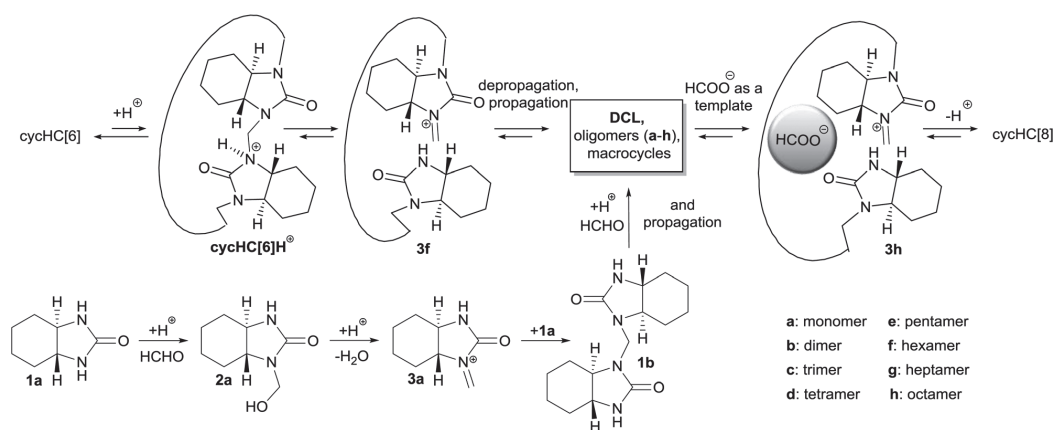
The kinetic data for the conversion of cycHC[6] to cycHC[8] revealed that the overall reaction was pseudo first-order, with a plateau. The fact, that the transformation of cycHC[6] to cycHC[8] proceeds faster in stronger acids (Table 1, compare entries 1 and 2) in combination with the results from DFT computational study of model structures (S29, ESI[†]) allows us to state, that the rate-limiting step of this process is protonation of the macrocycle. Occurrence of side reactions was minimal and no intermediates were detected by NMR (S16, ESI[†]).

Pittelkow *et al.* have shown that dimers are the main intermediates in the formation of biotin[6]uril.^{8f} Also, since cycHC[6] and cycHC[8] differ from each other by a dimer unit, we wanted to examine whether the cycHC[8] formation proceeds *via* dimer addition. We thus introduced ¹³C labels to methylene bridges of cycHC[6]^{8c} and subsequently used a 1:1 mixture of ¹³C-labelled and non-labelled cycHC[6] in cycHC[8] synthesis. The number of ¹³C-labelled methylene groups in isolated cycHC[8] varied from 0 to 8, following a normal distribution, thus confirming that beside dimers, other oligomers or monomers are involved in the reaction (S7, ESI[†]).

HRMS analysis of the reaction mixture showed the presence of cycHC[6–10]¹² and various oligomers (up to an octamer, S14, ESI[†]). The large number of observed intermediates pointed to the presence of a dynamic combinatorial library (DCL).^{3b}

According to DFT-calculated Gibbs' energies of cycHCs it is not the cycle strain, but the inclusion complex with formate anions that induces a preference towards the formation of cycHC[8] (S27, ESI[†]). Based on the experimental observations described above and the energy calculations on a model system (S29, ESI[†]), we propose that the transformation of cycHC[6] to cycHC[8] proceeds through the key steps outlined in Scheme 1. First, a reaction rate-limiting protonation of cycHC[6] occurs, then breakage of the first methylene bridge of cycHC[6]H⁺ takes place, forming the iminium **3f**. The DCL, whose members have been observed by HRMS, is generated through depropagation and propagation reactions. A formate acts as an anionic template and shifts the thermodynamic equilibrium between DCL members towards the formation of cycHC[8].

To verify that an anionic template is necessary to drive the reaction towards the formation of cycHC, we selected an anion that possessed the size and shape suitable for the cavity of cycHC[8], the hexafluorophosphate, in combination with acetic acid. Acetic acid alone was shown not to facilitate the formation of cycHC[8] (S4, ESI[†]). As expected, in the presence of NaPF₆ in acetic acid/acetonitrile, cycHC[6] was efficiently converted to cycHC[8] (Table 1, entry 3). This observation confirmed that even though reaction rate depends on the acid strength, the macrocycle formation is controlled by the anion, acting as a template.

**Scheme 1** Proposed reaction mechanism of the cycHC[8] formation catalysed by formic acid.

And with catalysis of formic and trifluoroacetic acid, their conjugate anions act as templates (Table 1, entries 1 and 2).

Next, based on the proposed mechanism, we envisioned that the DCL members could be generated starting from monomers **1a**. Indeed, using either formic acid, trifluoroacetic acid, or NaPF₆/acetic acid as catalysts afforded cycHC[8] (Table 1, entries 4–6). The lower rate of formation of cycHC[8] from **1a** than from cycHC[6], was due to the additional acid-promoted reactions necessary for building methylene bridges. The best yield and selectivity were achieved with trifluoroacetic acid, giving the cycHC[8] from **1a** on a gram scale in 73% yield. This synthetic method allowed for the preparation of enantiopure chiral macrocycle cycHC[8] very efficiently, in only two steps, starting from commercially available 1,2-cyclohexanediamine.¹³

According to the proposed mechanism, the conversion of cycHC[8] to cycHC[6] in the presence of a halide template, should also be possible. Indeed, using the classic conditions of CB formation (Table 1, entry 8), cycHC[8] was efficiently converted to cycHC[6] with the aid of the chloride anion. Similarly, using NaCl as a templating additive in acetic acid at elevated temperature, cycHC[8] was also converted to cycHC[6] (Table 1, entry 9), again highlighting the role of the templating anion in the reaction.

The crystal structure confirmed the barrel-like shape of cycHC[8] (Fig. 2). According to the crystal structure, the cavity of cycHC[8], similar in size to that of CB[6], is of sufficient size for the encapsulation of a number of organic and inorganic guests (Table 2).

Complexation studies of the cycHC[8] with carboxylic acids were performed by diffusion NMR in CDCl₃. The comparative results of the complexation of cycHC[6] and cycHC[8] are presented in Table 3. The association constants of simple carboxylic acids – acetic, formic and trifluoroacetic acids – follow the order of their acidity (Table 3, entries 1–3) for both hosts.

Analogously to small carboxylic acids, complexation with the more acidic α -methoxy- α -trifluoromethylphenylacetic acid (MTPA) was stronger than with α -methoxyphenylacetic acid (MPA) (Table 3, entries 5 and 6). The opposite preference of complexation of *R*-handed cycHC[6] and cycHC[8] toward MPA enantiomers may suggest different geometries of complexes in these cases. Nevertheless *R*-handed cycHC[8] showed nearly double affinity for *S*-MPA, compared to the *R*-MPA. This result confirms that cycHC[8] forms complexes enantioselectively.

In conclusion, we have presented the first highly efficient synthesis of an 8-membered representative of the cucurbituril family, the (all-*R*)-cyclohexylhemicucurbit[8]uril. We have shown that the reversibility of

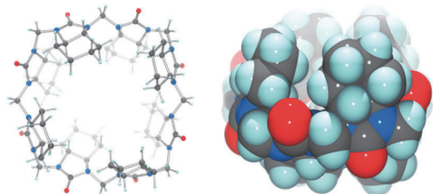


Fig. 2 Crystal structure of cycHC[8]: top view in ball and stick (left) and side view in CPK (right) representations (colour code: C grey, N blue, O red, H turquoise).

Table 2 Dimensions of cycHC[6,8] and CB[6,8]

Parameters ^a	CycHC[6] ^b	CycHC[8]	CB[6] ^c	CB[8] ^c
Opening diameter (Å)	2.2	4.6	3.9	6.9
Cavity diameter (Å)	5.3	8.5	5.8	8.8
Height (Å)	12.1	12.5	9.1	9.1
Cavity volume (Å ³)	35 ^d	123 ^d	119 ± 21	356 ± 16

^a Dimensions account for the van der Waals radii of the various atoms.

^b Opening, cavity and height values are from ref. 14a and cavity volume from ref. 14b.

^c Opening, cavity and height values are from ref. 8c and cavity volume from ref. 14b.

^d Cavity volume of cycHC[6] from ref. 8c and cycHC[8] calculated by analysing the solvent accessible voids in the respective crystal structures using PLATON¹⁵ with a probe radius of 1.2 Å³ and grid steps of 0.2 Å.

Table 3 Association constants K_a (M⁻¹) of carboxylic acids with cycHC[6] and cycHC[8] in 1:1 mixtures in CDCl₃

No.	Guest	CycHC[6] K_a	CycHC[8] K_a
1	CH ₃ COOH	8.0 ± 0.5 ^a	17 ± 2
2	HCOOH	97 ± 1	72.6 ± 0.5
3	CF ₃ COOH	21(±3) × 10 ³	29(±1) × 10 ³
4	<i>R</i> -MPA	27.2 ± 0.8 ^a	27.0 ± 0.5
5	<i>S</i> -MPA	20.1 ± 0.2 ^a	53 ± 3
6	<i>R</i> -MTPA	n.d.	3.3(±0.1) × 10 ²
7	<i>S</i> -MTPA	n.d.	3.0(±0.1) × 10 ²

^a Association constants from ref. 8c; n.d. - not determined.

the methylene bridge formation allows the size of the cycHC macrocycles to be controlled by the anionic templates, with halides driving the equilibrium towards the formation of cycHC[6], while carboxylates and PF₆⁻ promoted the formation of cycHC[8].

Chiral cycHC[8] and cycHC[6] were obtained very efficiently in one step, starting from enantiomerically pure (*R,R,N,N'*)-cyclohex-1,2-diyurea **1a** or either homologue. (all-*R*)-cycHC[8] enantioselectively formed complexes with chiral carboxylic acids, demonstrating chiral discrimination ability. CycHC[8] shows potential for application in host-guest chemistry.^{9g,10,16}

In the present study, DCL members were formed from identical monomeric units. It can be envisioned that by utilizing a mixture of different monomeric ureas and suitable templates, a very efficient yet diverse library of useful hemicucurbituril hosts could become accessible *via* dynamic covalent chemistry.

The authors would like to thank Tiina Aid, Marina Kudrjašova and Jasper Adamson for experimental assistance and Aivar Lõokene, Mart Reimund and Omar Parve for help with the manuscript. This research was supported by the Academy of Finland (KR, grants 263256 and 265328), the Estonian Ministry of Education and Research through Grants IUT19-32, IUT19-9, IUT23-7 and PUT692, TUT grant no. B25, the ESF DoRa, and the EU European Regional Development Fund (3.2.0101.08-0017). Computations were performed on the HPC cluster at TUT, which is part of the ETAIS. FT acknowledges support from NGS-NANO through a PhD fellowship.

Notes and references

- (a) X. Ma and Y. Zhao, *Chem. Rev.*, 2015, DOI: 10.1021/cr500392w; (b) Special Issue: Responsive Host-Guest Systems, *Acc. Chem. Res.*, 2014, 47, 1923; (c) G. Ghale and W. M. Nau, *Acc. Chem. Res.*, 2014, 47, 2150; (d) J. Hu and S. Liu, *Acc. Chem. Res.*, 2014, 47, 2084.

- 2 (a) C. J. Pedersen, *Angew. Chem., Int. Ed. Engl.*, 1988, **27**, 1021; (b) J.-M. Lehn, *Angew. Chem., Int. Ed. Engl.*, 1988, **27**, 89; (c) D. J. Cram, *Angew. Chem., Int. Ed. Engl.*, 1988, **27**, 1009; (d) J.-M. Lehn, *Angew. Chem., Int. Ed.*, 2013, **52**, 2836.
- 3 (a) J.-M. Lehn, *Chem. – Eur. J.*, 1999, **5**, 2455; (b) S. J. Rowan, S. J. Cantrill, G. R. L. Cousins, J. K. M. Sanders and J. F. Stoddart, *Angew. Chem., Int. Ed.*, 2002, **41**, 898; (c) P. T. Corbett, J. Leclaire, L. Vial, K. R. West, J. L. Wietor, J. K. M. Sanders and S. Otto, *Chem. Rev.*, 2006, **106**, 3652; (d) Y. Jin, C. Yu, R. J. Denman and W. Zhang, *Chem. Soc. Rev.*, 2013, **42**, 6634; (e) Y. Jin, Q. Wang, P. Taynton and W. Zhang, *Acc. Chem. Res.*, 2014, **47**, 1575; (f) A. Herrmann, *Chem. Soc. Rev.*, 2014, **43**, 1899; (g) M. Matache, E. Bogdan and N. D. Hádade, *Chem. – Eur. J.*, 2014, **20**, 2106.
- 4 (a) E. Masson, X. Ling, R. Joseph, L. Kyeremeh-Mensah and X. Lu, *RSC Adv.*, 2012, **2**, 1213; (b) K. I. Assaf and W. M. Nau, *Chem. Soc. Rev.*, 2015, **44**, 394.
- 5 (a) R. Oun, R. S. Floriano, L. Isaacs, E. G. Rowan and N. J. Wheate, *Toxicol. Res.*, 2014, **3**, 447; (b) U. Hoffmann, M. Grosse-Sundrup, K. Eikermann-Haerter, S. Zaremba, C. Ayata, B. Zhang, D. Ma, L. Isaacs and M. Eikermann, *Anesthesiology*, 2013, **119**, 317; (c) V. D. Uzunova, C. Cullinane, K. Brix, W. M. Nau and A. I. Day, *Org. Biomol. Chem.*, 2010, **8**, 2037.
- 6 (a) S. Walker, R. Oun, F. J. McInnes and N. J. Wheate, *Isr. J. Chem.*, 2011, **51**, 616; (b) A. I. Day and J. G. Collins, Cucurbituril receptors and drug delivery, in *Supramolecular Chemistry: From Molecules to Nanomaterials*, ed. J. W. Steed and P. A. Gale, John Wiley & Sons, Ltd, 2012, vol. 3, p. 983; (c) L. Peng, A. Feng, M. Huo and J. Yuan, *Chem. Commun.*, 2014, **50**, 13005; (d) V. Mandadapu, A. I. Day and A. Ghanem, *Chirality*, 2014, **26**, 712; (e) A. A. Elbashir and H. Y. Aboul-Enein, *Crit. Rev. Anal. Chem.*, 2015, **45**, 52; (f) S. Gürbüz, M. Idrisa and D. Tuncel, *Org. Biomol. Chem.*, 2015, **13**, 330.
- 7 (a) A. Day, A. P. Arnold, R. J. Blanch and B. Snusball, *J. Org. Chem.*, 2001, **66**, 8094; (b) A. Chakraborty, A. Wu, D. Witt, J. Lagona, J. C. Fettinger and L. Isaacs, *J. Am. Chem. Soc.*, 2002, **124**, 8297; (c) W.-H. Huang, P. Y. Zavalij and L. Isaacs, *J. Am. Chem. Soc.*, 2008, **130**, 8446; (d) L. Isaacs, *Chem. Commun.*, 2009, 619; (e) L. Isaacs, *Isr. J. Chem.*, 2011, **51**, 578; (f) D. Lucas, T. Minami, G. Iannuzzi, L. Cao, J. B. Wittenberg, P. Anzenbacher Jr. and L. Isaacs, *J. Am. Chem. Soc.*, 2011, **133**, 17966.
- 8 (a) Y. Miyahara, K. Goto, M. Oka and T. Inazu, *Angew. Chem., Int. Ed.*, 2004, **43**, 5019; (b) Y. Li, L. Li, Y. Zhu, X. Meng and A. Wu, *Cryst. Growth Des.*, 2009, **9**, 4255; (c) R. Aav, E. Shmatova, I. Reile, M. Borissova, F. Topić and K. Rissanen, *Org. Lett.*, 2013, **15**, 3786; (d) T. Fiala and V. Sindelar, *Synlett*, 2013, 2443; (e) M. Fomitsenko, E. Shmatova, M. Ören, I. Järving and R. Aav, *Supramol. Chem.*, 2014, **26**, 698; (f) M. Lisbjerg, B. M. Jessen, B. Rasmussen, B. Nielsen, A. U. Madsen and M. Pittelkow, *Chem. Sci.*, 2014, **5**, 2647.
- 9 (a) For anion binding of hemicucurbiturils see ref. 8 and H.-J. Buschmann, E. Cleva and E. Schollmeyer, *Inorg. Chem. Commun.*, 2005, **8**, 125; (b) H.-J. Buschmann, A. Zielesny and E. Schollmeyer, *J. Inclusion Phenom. Macrocyclic Chem.*, 2006, **54**, 181; (c) M. Sundararajan, R. V. Solomon, S. K. Ghosh and P. Venunalingam, *RSC Adv.*, 2011, **1**, 1333; (d) H.-J. Buschmann and A. Zielesny, *Comput. Theor. Chem.*, 2013, **1022**, 14; (e) M. Ören, E. Shmatova, T. Tamm and R. Aav, *Phys. Chem. Chem. Phys.*, 2014, **16**, 19198; (f) A. M. Lisbjerg, B. E. Nielsen, B. O. Milhøj, S. P. A. Sauer and N. Pittelkow, *Org. Biomol. Chem.*, 2015, **13**, 369; (g) M. Lisbjerg, H. Valkenier, B. M. Jessen, H. Al-Kerdi, A. P. Davis and M. Pittelkow, *J. Am. Chem. Soc.*, 2015, **137**, 4948.
- 10 (a) H. Cong, T. Yamato and X. Feng, *J. Mol. Catal. A: Chem.*, 2012, **181**; (b) H. Cong, T. Yamato and Z. Tao, *J. Mol. Catal. A: Chem.*, 2013, **287**; (c) H. Cong, T. Yamato and Z. Tao, *New J. Chem.*, 2013, **37**, 3778.
- 11 (a) J. Svec, M. Necas and V. Sindelar, *Angew. Chem., Int. Ed.*, 2010, **49**, 2378; (b) V. Havel, J. Svec, M. Wimmerova, M. Dusek, M. Pojarova and V. Sindelar, *Org. Lett.*, 2011, **13**, 4000; (c) J. Rivollier, P. Thuéry and M.-P. Heck, *Org. Lett.*, 2013, **15**, 480; (d) M. A. Yawer, V. Havel and V. Sindelar, *Angew. Chem., Int. Ed.*, 2015, **54**, 276; (e) M. Singh, E. Solel, E. Keinan and O. Reany, *Chem. – Eur. J.*, 2015, **21**, 536.
- 12 ref. 8e and ESI† for detailed MS data.
- 13 (a) Enantiopure 1,2-cyclohexanediamine can also be isolated from racemic mixture: J. F. Larrow, E. N. Jacobsen, Y. Gao, Y. Hong, X. Nie and C. M. Zepp, *J. Org. Chem.*, 1994, **59**, 1939; (b) J. F. Larrow and E. N. Jacobsen, *Org. Syn., Coll.*, 2004, **10**, 96.
- 14 (a) J. Kim, I.-S. Jung, S.-Y. Kim, E. Lee, J.-K. Kang, S. Sakamoto, K. Yamaguchi and K. Kim, *J. Am. Chem. Soc.*, 2000, **122**, 540; (b) W. M. Nau, M. Florea and K. I. Assaf, *Isr. J. Chem.*, 2011, **51**, 559.
- 15 A. L. Spek, *Acta Crystallogr.*, 2009, **D65**, 148.
- 16 (a) P. A. Gale, *Acc. Chem. Res.*, 2011, **44**, 216; (b) J. Lacour and D. Moraleda, *Chem. Commun.*, 2009, 7073; (c) R. J. Phipps, G. L. Hamilton and F. D. Toste, *Nat. Chem.*, 2012, **4**, 603; (d) K. Wichmann, B. Antonioli, T. Söhnel, M. Wenzel, K. Gloe, K. Gloe, J. R. Price, L. F. Lindoy, A. J. Blake and M. Schröder, *Coord. Chem. Rev.*, 2006, **250**, 2987; (e) T. J. Wenzel, *J. Inclusion Phenom. Macrocyclic Chem.*, 2014, **78**, 1.

Publication II

S. Kaabel, J. Adamson, F. Topić, A. Kiesilä, E. Kalenius, M. Öeren, M. Reimund, E. Prigorchenko, A. Lõokene, H. J. Reich, K. Rissanen, R. Aav, 'Chiral hemicucurbit[8]uril as an anion receptor: selectivity to size, shape and charge distribution,' *Chem. Sci.* **2017**, *8*, 2184–2190.

Re-printed with permission from the Royal Society of Chemistry.

Cite this: *Chem. Sci.*, 2017, 8, 2184

Chiral hemicucurbit[8]uril as an anion receptor: selectivity to size, shape and charge distribution†

Sandra Kaabel,^{ab} Jasper Adamson,^c Filip Topić,^b Anniina Kiesilä,^b Elina Kalenius,^b Mario Öeren,^a Mart Reimund,^a Elena Prigorchenko,^a Aivar Löökene,^a Hans J. Reich,^d Kari Rissanen^{*b} and Riina Aav^{*a}

A novel eight-membered macrocycle of the hemicucurbit[*n*]uril family, chiral (*all-R*)-cyclohexanohemicucurbit[8]uril (**cycHC[8]**)[‡] binds anions in a purely protic solvent with remarkable selectivity. The **cycHC[8]** portals open and close to fully encapsulate anions in a 1 : 1 ratio, resembling a molecular Pac-Man™. Comprehensive gas, solution and solid phase studies prove that the binding is governed by the size, shape and charge distribution of the bound anion. Gas phase studies show an order of $\text{SbF}_6^- \approx \text{PF}_6^- > \text{ReO}_4^- > \text{ClO}_4^- > \text{SCN}^- > \text{BF}_4^- > \text{HSO}_4^- > \text{CF}_3\text{SO}_3^-$ for anion complexation strength. An extensive crystallographic study reveals the preferred orientations of the anions within the octahedral cavity of **cycHC[8]** and highlights the importance of the size- and shape-matching between the anion and the receptor cavity. The solution studies show the strongest binding of the ideally fitting SbF_6^- anion, with an association constant of $2.5 \times 10^5 \text{ M}^{-1}$ in pure methanol. The symmetric, receptor cavity-matching charge distribution of the anions results in drastically stronger binding than in the case of anions with asymmetric charge distribution. Isothermal titration calorimetry (ITC) reveals the complexation to be exothermic and enthalpy-driven. The DFT calculations and VT-NMR studies confirmed that the complexation proceeds through a pre-complex formation while the exchange of methanol solvent with the anion is the rate-limiting step. The octameric **cycHC[8]** offers a unique example of template-controlled design of an electroneutral host for binding large anions in a competitive polar solvent.

Received 16th November 2016
Accepted 29th November 2016

DOI: 10.1039/c6sc05058a

www.rsc.org/chemicalscience

Introduction

The importance of ion recognition and transport in biological systems is well established, bringing about the quest for synthetic receptors capable of binding ions in physiological conditions. The syntheses of crown ethers,¹ cryptands² and cucurbiturils³ among others have contributed to the rich history of cation recognition whereas development of anion receptors effective in protic solvents remains challenging.^{4–7} Anion sensing motifs based on cationic species are usually effective in a narrow range

of pH, plagued by low binding selectivity and counteranion competition for the binding site. Neutral anion receptors relying on hydrogen or halogen bonding are often affected by strong competition from the protic solvent with host-guest interactions having to disrupt the solvation shell of the anion.^{8,9}

Exemplary studies on anion binding by cyclic hexapeptides show that introducing a confined cavity to the structure of the receptor significantly increases the anion binding ability, as abundant 2 : 1 host-guest complexes were observed with halides and SO_4^{2-} where the anion was enclosed in the cavity formed by two cyclopeptide units.^{10,11} This led to the design of sandwich-like bis(cyclopeptide) receptors that reached association constants of up to 10^6 M^{-1} for binding SO_4^{2-} in a water-methanol mixture.^{12,13} Employing a hydrophobic pocket for anion binding in water has been illustrated by the Gibb's octa-acid cavitand,¹⁴ where the binding of partially hydrated anions yielded association constants up to 10^3 M^{-1} at pH 11.5. Likewise, the size-dependent complexation of dodecaborate dianions within the hydrophobic cavity of γ -cyclodextrin was studied by Nau and co-workers, with the strongest association in the case of $\text{B}_{12}\text{Br}_{12}^{2-}$ ($K_a = 9.6 \times 10^5 \text{ M}^{-1}$).¹⁵

Cucurbituril family members have been explored as ion receptors due to their well-defined hydrophobic cavity.^{16,17}

^aDepartment of Chemistry, Tallinn University of Technology, Akadeemia tee 15, 12618 Tallinn, Estonia. E-mail: riina.aav@ttu.ee

^bUniversity of Jyväskylä, Department of Chemistry, Nanoscience Center, P.O. Box. 35, FI-40014 Jyväskylä, Finland. E-mail: kari.rissanen@jyu.fi

^cNational Institute of Chemical Physics and Biophysics, Akadeemia tee 23, 12618 Tallinn, Estonia

^dDepartment of Chemistry, University of Wisconsin, Madison, WI 53706, USA

† Electronic supplementary information (ESI) available: MS, NMR, dynamic NMR and computational details and a DFT-based video of complexation. CCDC 1514736–1514741, 1521388. For ESI and crystallographic data in CIF or other electronic format see DOI: 10.1039/c6sc05058a

‡ The name cyclohexylhemicucurbituril, previously used for these macrocycles, is changed in accordance with the IUPAC nomenclature for fused cycles, as the cyclohexane substituents are fused with the parent hemicucurbituril.

Hemicucurbiturils,¹⁸ cyclohexanohemicucurbit[6]urils,¹⁹ bambus[6]urils²⁰ and biotin[6]urils^{21–23} have been shown to bind anions within their electron-deficient (*i.e.* partially positively charged) hydrophobic cavities. Presently, bambus[6]urils hold the record for the strongest anion binding ($K_a = 5.5 \times 10^7 \text{ M}^{-1}$) by a neutral host in exclusively protic solvent.²⁴ Based on the crystal structures of six-membered hemicucurbiturils, bambus[6]uril^{25–28} and biotin[6]uril²¹ complexes the central cavities readily accommodate halide anions. Larger anions have been shown to prefer the formation of 1 : 2 host : guest complexes with double-cone-shaped bambus[6]urils,^{29,30} with the anions bound away from the centre of the cavity.

We have previously demonstrated the synthesis of the first 8-membered hemicucurbituril, (*all-R*)-cyclohexanohemicucurbit[8]uril (**cycHC[8]**), by an approach using anion-templating.³¹ Given that larger anions such as PF_6^- and CF_3CO_2^- were observed to act as effective templates, we decided to investigate the binding of other larger inorganic anions by **cycHC[8]**. Such anions are for example used in ionic liquids³² (BF_4^- , PF_6^- , SbF_6^- , CF_3SO_3^-) and as oxidizing agents³³ (ClO_4^- , IO_4^-). On the other hand, they are considered as environmental pollutants.^{33,34} Binding of these anions in protic media is important from a biological and environmental point of view.

Results and discussion

The chiral host molecule (*all-R*)-cyclohexanohemicucurbit[8]uril^{34,35} (**cycHC[8]**) fully encapsulates certain anions forming 1 : 1 complexes (Fig. 1) with high selectivity and binding affinities of up to $2.5 \times 10^5 \text{ M}^{-1}$ in methanol.

The scope of anionic guests that form complexes with **cycHC[8]** was determined by mass spectrometry (see ESI†). Only 1 : 1 complexes were observed in ESI-MS spectra and abundant complexes were observed with $\text{SbF}_6^- \approx \text{PF}_6^- > \text{ReO}_4^- > \text{ClO}_4^- > \text{SCN}^- > \text{BF}_4^- > \text{HSO}_4^- > \text{CF}_3\text{SO}_3^-$, ranked by decreasing affinity for **cycHC[8]**. The anions H_2PO_4^- , AcO^- , Br^- , Cl^- , I^- , F^- , NO_3^- and NO_2^- showed only weak complexation, while no complexes were formed with AuBr_4^- , Br_3^- and CN^- . The order of affinity was ascertained through competition experiments, performed on three-component mixtures of the host with two competing anions in 1 : 1 : 1 molar ratio (ESI Fig. S2 and S3†). Halide anions (13 to 35 Å³ in volume³⁶), while readily forming complexes with 6-membered hemicucurbiturils,^{37–41} appear to

have very low affinity towards **cycHC[8]**, presumably due to a mismatch in size with the cavity of **cycHC[8]**. As expected, the affinity towards more heavily solvated anions was found to be lower than for weakly solvated ones. On the other hand, tetrahedral and octahedral anions falling into the volume range of 50 to 80 Å³ form stronger complexes with **cycHC[8]**, presumably due to a better size fit. This is also in good agreement with Rebek's rule suggesting a packing coefficient (PC)⁴² of 0.55 ± 0.09 for optimal fit in the **cycHC[8]** cavity with a volume of 123 Å³.³¹ The MS/MS collision-induced dissociation (CID) experiments (Fig. S4†) on isolated complexes revealed the most efficient dissociation (lowest kinetic stability) for the host–guest complexes with highest PCs (>0.55). This results from the sensitive interplay of the attractive and repulsive forces between the anion and the cavity walls, and the lack of void space. More importantly, it also indicates the full encapsulation of the anions in the complexes in the gas phase. The same phenomenon has been studied in detail with cucurbiturils and azoalkanes,⁴³ but is reported here for the first time with anionic complexes.

The crystal structures of the host–guest complexes, obtained by single crystal X-ray diffraction, demonstrate unambiguously the 1 : 1 stoichiometry of the anion inclusion complexes in the solid state (Fig. 2). Single crystals of the complexes were obtained from solutions of **cycHC[8]** in methanol with the guest added as a tetrabutylammonium (TBA) or tetrabutylphosphonium (TBP) salt. The TBA or TBP cations and a number of solvent molecules fill the space between the capsule-like moieties, affording isostructural crystals regardless of the guest anion used. The guest anions are situated at the center of the **cycHC[8]** cavity, in a manner depending on their size and shape. The octahedral anions SbF_6^- and PF_6^- are locked in a fixed position showing no disorder. Four fluorine atoms of $\text{SbF}_6^-/\text{PF}_6^-$ lying on the equatorial plane of the macrocycle point to the four corners of its square-shaped belt, while the two remaining fluorines point to the opposite portals (Fig. 2a and b). The Hirshfeld surface⁴⁴ plotted for the encapsulated octahedral anion SbF_6^- indicates that the host–guest C–H⋯F interactions are responsible for the fixed orientation of these guests (ESI Fig. S6†). The shortest C–H⋯F distances are found between the four equatorial fluorine atoms and the axial 2*ax* protons in each corner of the macrocyclic cavity (Fig. 3B and Table S3†). In contrast to the octahedral anions, the tetrahedral anions BF_4^- , ClO_4^- , ReO_4^- and IO_4^- have more space inside the cavity (Fig. 2c–f) and show disorder in the crystal. As the host cavity is symmetric and therefore offers a number of equal interaction sites, several orientations of the tetrahedral anions are equally favored. The Hirshfeld surface of encapsulated IO_4^- (Fig. S7†), together with the close contact analysis of other tetrahedral anions (Tables S5–S8†) reveals that these anions can only form a limited number of interactions with the host cavity wall in a given orientation. Smaller anions like BF_4^- and ClO_4^- can form even fewer host–guest interactions simultaneously. The large CF_3SO_3^- anion has two orientations (Fig. 2g and Table S9†). Given that **cycHC[8]** preserves its conformation almost fully regardless of the guest anion encapsulated, its cavity can be considered as an octahedrally shaped void, which

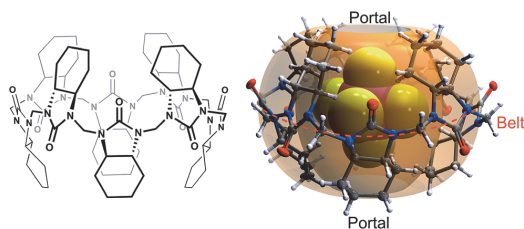


Fig. 1 Molecular structure of (*all-R*)-cyclohexanohemicucurbit[8]uril, **cycHC[8]** (left), and the X-ray structure of an inclusion complex with SbF_6^- (right).

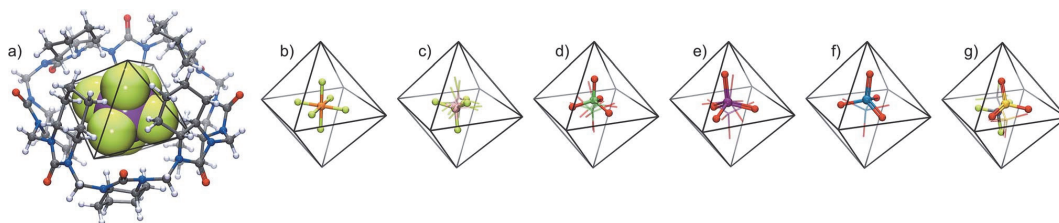


Fig. 2 The crystal structures of 1 : 1 host-guest complexes of (a) SbF_6^- , (b) PF_6^- , (c) BF_4^- , (d) ClO_4^- , (e) IO_4^- , (f) ReO_4^- and (g) CF_3SO_3^- anions in the $\text{cycHC}[8]$ cavity. Minor disorder components are shown as a wireframe model. The host in (b–f) is represented by an octahedron depicting the cavity of $\text{cycHC}[8]$.

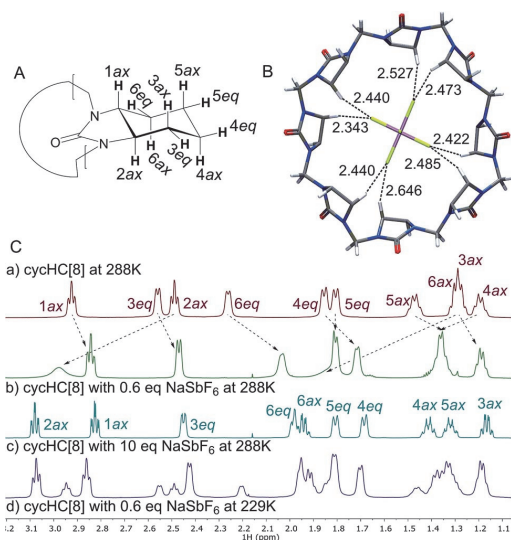


Fig. 3 (A) Labelling of $\text{cycHC}[8]$ protons, (B) C–H...F distances between the host proton $2ax$ and SbF_6^- from the X-ray structure; all $(\text{CH}_2)_4$ groups are omitted for clarity, (C) ^1H NMR in MeOD of (a) free $\text{cycHC}[8]$, (b) $\text{cycHC}[8]$ with 0.6 eq. of NaSbF_6 at 288 K (c) $\text{cycHC}[8]$ with 10 eq. of NaSbF_6 at 288 K; (d) SbF_6^- @ $\text{cycHC}[8]$ and free $\text{cycHC}[8]$ formed from $\text{cycHC}[8]$ with 0.6 eq. of NaSbF_6 at 229 K.

encapsulates guests in a manner depending on their shape, volume and complementarity of the interactions.

Next, we examined anion complexation with $\text{cycHC}[8]$ in solution using ^1H NMR spectroscopy. The complex with SbF_6^- showed the largest complexation-induced chemical shift changes (downfield shifts of 0.52, 0.23 and 0.64 ppm for $2ax$, $4ax$ and $6ax$, respectively). The signals for $2ax$, $4ax$ and $6ax$ in the complex with SbF_6^- also showed significant signal broadening at room temperature, indicating a slow guest exchange rate for SbF_6^- . The guest exchange slows down at low temperature resulting in the signals of SbF_6^- @ $\text{cycHC}[8]$ and excess free $\text{cycHC}[8]$ being separate (Fig. 3C(d)).

The Job plot analysis confirmed 1 : 1 stoichiometry of binding for all studied guests in methanol (ESI^\dagger), as also observed by crystallography in the solid state and by mass

spectrometry in the gas phase. Association constants were determined by NMR titrations (Table 1), simultaneously following three $\text{cycHC}[8]$ proton signals $1ax$, $2ax$ and $3eq$ (Fig. 3A). The association constant for SbF_6^- was, due to the broadening of the $2ax$ signal, determined only from the $1ax$ and $3eq$ proton signals. The range of association constants varied over five orders of magnitude, strongly dependent on the size and shape of the guest. The poor water solubility of $\text{cycHC}[8]$ prevented measurements in pure water, but no significant decrease in binding strength was observed when pure methanol was changed to a 1 : 1 methanol/water mixture (Table 1, rows 2–3).

For tetrahedral and octahedral anions, the affinity to the host grows exponentially with the increasing size of the guest, ranging from 48 M^{-1} for the smallest tested anion BF_4^- to $250\,000 \text{ M}^{-1}$ for the largest tested octahedral anion SbF_6^- (Table 1 and Fig. 4). The anion size dependency for anion binding has also been discussed by Sindelar and co-workers for a bambus[6]juril host in chloroform,²⁴ with the highest selectivity towards ClO_4^- . Given the double-cone shape of the dodecabenzylbambus[6]juril host and the restricted diameter of

Table 1 Association constants K_a for $\text{cycHC}[8]$ inclusion complexes with anions, measured in MeOD at 288 K by ^1H NMR titration experiments. Volumes of the anions (V_{anion}) and their packing coefficients (PC)^a

Anion	Cation	$V_{\text{anion}} (\text{\AA}^3)$	PC	$K_a (\text{M}^{-1})$
SbF_6^-	Na^+	81.8	0.67	$(2.5 \pm 0.7) \times 10^5$
PF_6^-	Bu_4N^+	70.6	0.57	$(2.8 \pm 0.4) \times 10^4$
PF_6^- ^b	Bu_4N^+	70.6	0.57	$(2.6 \pm 0.2) \times 10^4$
PF_6^-	Na^+	70.6	0.57	$(2.0 \pm 0.2) \times 10^3$
ReO_4^-	Bu_4N^+	64.8	0.53	$(4.7 \pm 0.4) \times 10^3$
IO_4^-	Na^+	64.3	0.52	$(1.8 \pm 0.2) \times 10^3$
ClO_4^-	Bu_4N^+	54.7	0.45	$(4.7 \pm 0.2) \times 10^2$
BF_4^-	Bu_4N^+	51.6	0.42	$(4.8 \pm 0.4) \times 10$
CF_3SO_3^-	Bu_4N^+	82.3	0.67	$(3.9 \pm 0.5) \times 10$
CF_3CO_2^-	Bu_4N^+	68.7	0.56	<10

^a Anion volume is based on optimized anion geometries (BP86-D/def2-TZVPD) and calculated using a triangulated sphere model (based on CSD default atomic radii) through the Olex2 program package.⁴³ PC is defined as the ratio between the V_{anion} to $V_{\text{cavity(host)}}$.⁴² $V_{\text{cavity(cycHC}[8])} = 123.0 \text{ \AA}^3$ is measured from the crystal structure of $\text{cycHC}[8]$.³¹
^b ^1H NMR in 1 : 1 MeOD/ D_2O .

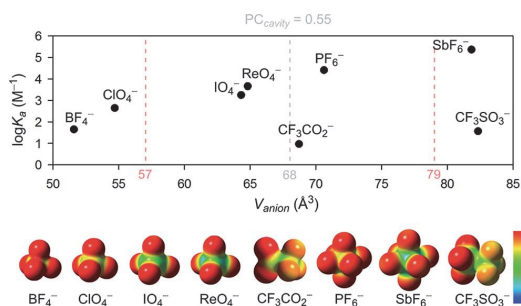


Fig. 4 The association constant dependency on the anion size and the electrostatic surface potential of the studied anions. Surface potential calculated using Gaussian 09,⁴⁶ visualized using GaussView5,⁴⁷ red to blue surface color range spans from -0.2 to 0.2 . Pale red dashed lines represent the $68 \pm 11 \text{\AA}^3$ anion volume range ($\text{PC} = 0.55 \pm 0.09$).

the central cavity of 6-membered hemicucurbiturils, it seems that anions larger than perchlorate are bound away from the center of the bambus[6]juril macrocycle, inside the cone-shaped pockets formed by the extending substituents.^{25,30} With **cycHC[8]**, a single binding site is suggested by the crystal structures, with the anion in each case fully encapsulated in the center of the cavity. The selectivity of this 8-membered host is therefore determined by the parameters of its central cavity. Based on the crystal structures, the correlation between the binding strength and the size of the anion can arguably be ascribed to the number of host-guest interactions an anion can form simultaneously. Thus smaller anions BF_4^- and ClO_4^- , which are able to form only one or two $\text{C}\cdots\text{H}\cdots\text{anion}$ interactions in a given orientation, are bound with considerably lower affinities.

Surprisingly, however, the association constant for the binding of roughly octahedral CF_3SO_3^- is dramatically lower compared to the similarly sized octahedral guest SbF_6^- , regardless of the several interactions between the host and the encapsulated CF_3SO_3^- apparent in the crystal structure (Table S9†). Given the inherent symmetry of **cycHC[8]**, one can argue that the binding might be stronger with anions having the charge equally distributed over the surface. To assess whether the low binding affinity of CF_3SO_3^- is caused by the asymmetric charge distribution, a control experiment was conducted with CF_3CO_2^- , similar in volume to PF_6^- , but with a charge distribution resembling that in CF_3SO_3^- . The fact that CF_3CO_2^- , which effectively templates the synthesis of **cycHC[8]** (in acetonitrile) and has been shown by diffusion NMR to bind to **cycHC[8]** in chloroform,³¹ does not bind to **cycHC[8]** in methanol ($K_a < 10$), indicates that the binding of anions to **cycHC[8]** in methanol is sensitive to charge distribution around the anion.

According to the range of optimal packing coefficients, 0.55 ± 0.09 , the association constants within the tested group of tetrahedral and octahedral anions with roughly spherical charge distribution should follow a statistical distribution around the optimal guest fit at $\text{PC} = 0.55$. For **cycHC[8]**, with a cavity volume 123.0\AA^3 , the optimal guest volume should

therefore centre in the range of $68 \pm 11 \text{\AA}^3$ (Fig. 4). However, the strongest association was in fact observed for SbF_6^- ($V_{\text{anion}} = 81.8 \text{\AA}^3$), suggesting a shift from the optimal PC to higher values which might be due to the stabilizing effect of host-guest interactions with tighter-fitting guests like SbF_6^- or the conformational flexibility of the macrocycle itself.

Next, isothermal titration calorimetry (ITC) was used to determine thermodynamic parameters for the complexes of **cycHC[8]** with SbF_6^- and PF_6^- in methanol. The raw thermogram and the binding isotherm for SbF_6^- are presented in Fig. 5 with the calculated parameters given in Table 2. The K_a values obtained by ITC were comparable with those obtained by NMR spectroscopy. Similarly to NMR, ITC showed higher affinity of **cycHC[8]** for SbF_6^- than PF_6^- , with binding being exothermic, enthalpy driven and entropically disfavored for both. Comparing the two anions revealed that the binding of SbF_6^- was accompanied by a greater change in both enthalpy and entropy. This is in line with tighter binding of the larger SbF_6^- anion, giving rise to a stronger host-guest interaction (enthalpic term) but also a greater loss in degrees of freedom (entropic term). Generally, the thermodynamic profile of **cycHC[8]** binding resembles the behavior of other hemicucurbiturils.³⁷

The complexation kinetics of normal cucurbiturils has been thoroughly^{48–56} studied and the exchange of neutral guests has been shown to proceed through a single step,^{55,56} while the complexation of cationic guests proceeds through a number of intermediates.^{50–54} To the best of our knowledge, the kinetics of anion binding by hemicucurbiturils has not been previously studied. A particularly interesting aspect of the **cycHC[8]** behavior is the conformational dynamics of guest encapsulation. Given the bulkiness of the encapsulated guests (Fig. 1), the conformation of the host clearly has to change considerably for the guest to pass through the narrow portals of **cycHC[8]**. The

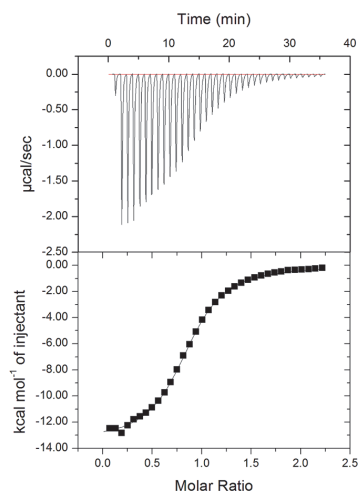


Fig. 5 Raw thermogram (above) for SbF_6^- titration with **cycHC[8]** and the binding isotherm (below) from the integrated thermogram fit using the one-site model.

Table 2 Thermodynamic and kinetic parameters for the complexation with cycHC[8] at 298 K, all energies given in kJ mol⁻¹

Guest	ITC titration			ΔG°			VT-NMR			Association rate constant ^a $k \times 10^3 \text{ s}^{-1}$
	$K_a \text{ (M}^{-1}\text{)}$	ΔH°	$T\Delta S^\circ$	ITC titration	NMR titration	DFT calc.	Activation parameters for complex formation			
							ΔH^\ddagger	$T\Delta S^\ddagger$	ΔG^\ddagger	
NaSbF ₆	$(1.02 \pm 0.03) \times 10^5$	-56.2 ± 0.3	-27.7	-28.5	-30.8	—	38.6	-13.4	51.9	2.6
NaPF ₆	$(1.29 \pm 0.04) \times 10^4$	-43.8 ± 0.2	-20.4	-23.4	-24.5	-22	42.1	-5.5	47.5	17.5

^a Determined at 291 K.

flexibility of the host is seemingly crucial to the encapsulation and, likewise, to the ejection of the guests, and the reaction pathway of host-guest complex formation was therefore studied computationally. Density functional theory (DFT) calculations were used to model the complexation of cycHC[8] with PF₆⁻ utilizing COSMO solvation model for methanol.^{57,58}

By positioning up to four methanol molecules inside the cavity of cycHC[8] we found that, at temperatures above 100 K, a single molecule of methanol is preferably accommodated within the cavity, close to its center. As the association constants derived from NMR titration with sodium and tetrabutylammonium PF₆⁻ salts were very similar, cation influence was assumed to be negligible and was not studied. Modelling the exchange of methanol in MeOH@cycHC[8] with PF₆⁻ showed the initial formation of a pre-complex with PF₆⁻ at the portal of cycHC[8] (MeOH@cycHC[8] + PF₆⁻; Fig. 6). Next, through a transition state involving the dissociation of a hydrogen bond between methanol and cycHC[8], the inclusion complex PF₆⁻@cycHC[8] is formed (the complexation reaction pathway is visualized in a video, ESI[†]). The DFT-derived Gibbs free energy difference indicates that the methanol-solvated cycHC[8] is 22 kJ mol⁻¹ higher in energy compared to its inclusion complex with PF₆⁻, which is in good agreement with the experimental ΔG values calculated from equilibrium constants obtained by NMR and ITC analyses (Table 2).

Additional experimental insight into the kinetics of the complexation and the reaction pathway was gained by variable temperature NMR (VT-NMR) studies of SbF₆⁻ and PF₆⁻, using a 2 : 1 host-to-guest ratio (Fig. 7). The complexation reaction

order was determined by dilution experiments near the coalescence temperature (241 K and 253 K for SbF₆⁻ and PF₆⁻, respectively).

Reaction rates remained constant upon dilution, indicating that the complexation process follows first order kinetics, characteristic for a unimolecular reaction. This suggests that the overall complexation reaction occurs *via* a low-energy pre-complex. Moreover, the complexation reaction rate constants for both SbF₆⁻ and PF₆⁻ (Table 2) were determined, allowing us to derive the activation parameters (Table 2) using the Eyring equation (for details, see ESI[†]). As expected, the complexation rate constant was an order of magnitude higher for PF₆⁻ than for the larger SbF₆⁻, also in good agreement with our initial solution studies by NMR. The entropy of activation of the complexation is negative for both anions, as expected for the host and guest forming one host-guest complex. Other entropic contributions that play a role in the host-guest formation reaction are the entropic penalty of orientation of the guest within the macrocycle and the desolvation of the cavity of the host and the collapse of the methanol cluster around the chaotropic guests.

Both the computational and kinetic studies propose the existence of pre-complexes, although the computations suggest them to be higher in energy than the precursors, whereas the VT-NMR results require this pre-complex to be more stable than

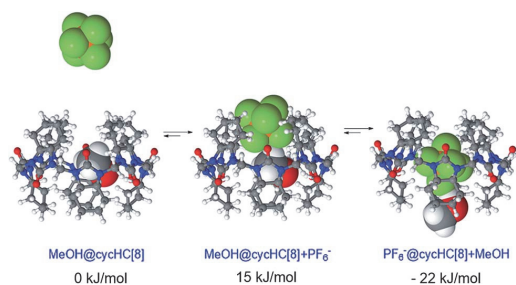


Fig. 6 Minimum energy geometries of cycHC[8] complexes with PF₆⁻ in MeOH and the associated relative Gibbs free energy values.

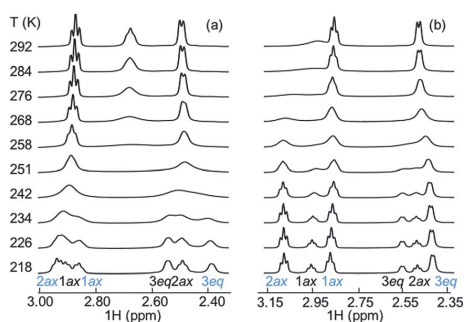


Fig. 7 Evolution of proton resonances in the variable temperature NMR study (a) for PF₆⁻ and (b) for SbF₆⁻. The cycHC[8] and guest concentrations were 2.6 mM and 1.5 mM in MeOD solution, respectively. At 218 K, the hydrogen signals labelled with blue arise from the host-guest complex and black ones from the free host.

the starting components. This reflects a complicated complexation reaction pathway that includes several steps. We propose that either the anion pre-complex formation or the reorganization of the methanol solvation shell around anions and the macrocycle play an important role, which merits further investigation.

Conclusions

The inherently chiral (*all-R*)-cyclohexanohemicucurbit[8]uril, **cycHC[8]**, is the first example of an octameric macrocycle of the hemicucurbituril family acting as a neutral host that fully encapsulates anions as 1 : 1 complexes in gas, solution and solid state. The binding affinity strongly depends on the size, shape and charge distribution of the anion. Crystallographic studies show the importance of the shape fit between the **cycHC[8]** cavity and the anion guest, with the octahedral guests bound in a perfectly ordered manner, while the tetrahedral guests exhibited various degrees of disorder. Moreover, due to the unique size and shape of **cycHC[8]**, the large, octahedrally shaped SbF_6^- was found to be the most tightly bound guest, closely followed by PF_6^- . On the other hand, binding of the similarly sized CF_3SO_3^- and CF_3CO_2^- was around four orders of magnitude weaker, which could be ascribed to their asymmetric charge distribution limiting the number of hydrogen bonds that can be formed simultaneously. The complexation was found to proceed through the formation of a pre-complex, accompanied by the ejection of a solvent molecule from the **cycHC[8]** cavity and involving a large movement of the portals during the encapsulation.

This work, besides being the first comprehensive anion-binding study on an eight-membered hemicucurbituril-type macrocycle, also demonstrates the unique anion binding properties of a macrocyclic host easily accessible through a simple templated synthetic protocol.³¹ Moreover, it proposes a pathway to and encourages the preparation of new hemicucurbiturils for anion binding and transport, catalysis in confined space and other supramolecular applications.

Author contribution

The manuscript was written through contributions of all authors.

Acknowledgements

This research was supported by the Academy of Finland (KR: grants 263256, 265328 and 292746, EK: grants 284562 and 278743), the Estonian Ministry of Education and Research through Grants IUT19-32, IUT19-9, IUT23-7 and PUT692, TUT grant No. B25, the ESF DoRa, and the EU European Regional Development Fund through the Center of Excellence in Molecular Cell Engineering projects 3.2.0101.08-0017 and TK134. Computations were performed on the HPC cluster at TUT, which is part of the ETAIS project. FT acknowledges the support from NGS-NANO through a Ph.D. fellowship. The authors would like to thank Marina Kudrjašova and Mari-Liis Kasemets for

assistance with NMR, Ly Pärnaste with ITC, Toomas Kaevand with computations and Lauri Kivijärvi with MS experiments.

Notes and references

- 1 C. J. Pedersen, *Angew. Chem.*, 1988, **100**, 1053; *Angew. Chem., Int. Ed. Engl.*, 1988, **27**, 1021.
- 2 J.-M. Lehn, *Angew. Chem.*, 1988, **100**, 91; *Angew. Chem., Int. Ed. Engl.*, 1988, **27**, 89.
- 3 W. A. Freeman, W. L. Mock and N. Y. Shih, *J. Am. Chem. Soc.*, 1981, **103**, 7367.
- 4 M. J. Langton, C. J. Serpell and P. D. Beer, *Angew. Chem., Int. Ed.*, 2016, **55**, 1974.
- 5 P. A. Gale and C. Caltagirone, *Chem. Soc. Rev.*, 2015, **44**, 4212.
- 6 N. H. Evans and P. D. Beer, *Angew. Chem., Int. Ed.*, 2014, **53**, 11716.
- 7 J. L. Sessler, P. A. Gale and W.-S. Cho, *Anion Receptor Chemistry*, ed. J. F. Stoddart, Royal Society of Chemistry, Cambridge, 2006.
- 8 P. A. Gale, E. N. W. Howe and X. Wu, *Chem*, 2016, **1**, 351.
- 9 S. Kubik, *Chem. Soc. Rev.*, 2010, **39**, 3648.
- 10 S. Kubik, R. Goddard, R. Kirchner, D. Nolting and J. Seidel, *Angew. Chem., Int. Ed.*, 2001, **40**, 2648.
- 11 S. Kubik and R. Goddard, *Proc. Natl. Acad. Sci. U. S. A.*, 2002, **99**, 5127.
- 12 S. Kubik, R. Kirchner, D. Nolting and J. Seidel, *J. Am. Chem. Soc.*, 2002, **124**, 12752.
- 13 F. Sommer and S. Kubik, *Org. Biomol. Chem.*, 2014, **12**, 8851.
- 14 P. Sokkalingam, J. Shraberg, S. W. Rick and B. C. Gibb, *J. Am. Chem. Soc.*, 2016, **138**, 48.
- 15 K. I. Assaf, M. S. Ural, F. Pan, T. Georgiev, S. Simova, K. Rissanen, D. Gabel and W. M. Nau, *Angew. Chem., Int. Ed.*, 2015, **54**, 6852.
- 16 E. Masson, X. Ling, R. Joseph, L. Kyeremeh-Mensah and X. Lu, *RSC Adv.*, 2012, **2**, 1213.
- 17 S. J. Barrow, S. Kasera, M. J. Rowland, J. Del Barrio and O. A. Scherman, *Chem. Rev.*, 2015, **115**, 12320.
- 18 Y. Miyahara, K. Goto, M. Oka and T. Inazu, *Angew. Chem., Int. Ed.*, 2004, **43**, 5019.
- 19 R. Aav, E. Shmatova, I. Reile, M. Borissova, F. Topić and K. Rissanen, *Org. Lett.*, 2013, **15**, 3786.
- 20 J. Svec, M. Necas and V. Sindelar, *Angew. Chem., Int. Ed.*, 2010, **49**, 2378.
- 21 M. Lisbjerg, B. M. Jessen, B. Rasmussen, B. Nielsen, A. Ø. Madsen and M. Pittelkow, *Chem. Sci.*, 2014, **5**, 2647.
- 22 M. Lisbjerg, B. E. Nielsen, B. O. Milhøj, S. P. A. Sauer and M. Pittelkow, *Org. Biomol. Chem.*, 2015, **13**, 369.
- 23 M. Lisbjerg, H. Valkenier, B. M. Jessen, H. Al-Kerdi, A. P. Davis and M. Pittelkow, *J. Am. Chem. Soc.*, 2015, **137**, 4948.
- 24 M. A. Yawer, V. Havel and V. Sindelar, *Angew. Chem., Int. Ed.*, 2015, **54**, 276.
- 25 V. Havel, J. Svec, M. Wimmerova, M. Dusek, M. Pojarova and V. Sindelar, *Org. Lett.*, 2011, **13**, 4000.
- 26 J. Svec, M. Dusek, K. Fejfarova, P. Stacko, P. Klan, A. E. Kaifer, W. Li, E. Hudeckova and V. Sindelar, *Chem.-Eur. J.*, 2011, **17**, 5605.

- 27 J. Rivollier, P. Thuéry and M.-P. Heck, *Org. Lett.*, 2013, **15**, 480.
- 28 M. Singh, E. Solel, E. Keinan and O. Reany, *Chem.–Eur. J.*, 2015, **21**, 536.
- 29 T. Fiala and V. Sindelar, *Supramol. Chem.*, 2016, **28**, 810.
- 30 V. Havel, V. Sindelar, M. Necas and A. E. Kaifer, *Chem. Commun.*, 2014, **50**, 1372.
- 31 E. Prigorchenko, M. Öeren, S. Kaabel, M. Fomitšenko, I. Reile, I. Järving, T. Tamm, F. Topić, K. Rissanen and R. Aav, *Chem. Commun.*, 2015, **51**, 10921.
- 32 H. Olivier-Bourbigou, L. Magna and D. Morvan, *Appl. Catal., A*, 2010, **373**, 1.
- 33 E. T. Urbansky, *Biorem. J.*, 1998, **2**, 81.
- 34 R. F. M. Frade and C. A. M. Afonso, *Hum. Exp. Toxicol.*, 2010, **29**, 1038.
- 35 M. Fomitšenko, E. Shmatova, M. Öeren, I. Järving and R. Aav, *Supramol. Chem.*, 2014, **26**, 698.
- 36 Anion volumes in this report are calculated using a triangulated sphere model (based on CSD default atomic radii) through Olex2 program package. Ref. 42.
- 37 H.-J. Buschmann, E. Cleva and E. Schollmeyer, *Inorg. Chem. Commun.*, 2005, **8**, 125.
- 38 H.-J. Buschmann, A. Zielesny and E. J. Schollmeyer, *J. Inclusion Phenom. Macrocyclic Chem.*, 2006, **54**, 181.
- 39 M. Sundararajan, R. V. Solomon, S. K. Ghosh and P. Venuvanalingam, *RSC Adv.*, 2011, **1**, 1333.
- 40 H.-J. Buschmann and A. Zielesny, *Comput. Theor. Chem.*, 2013, **1022**, 14.
- 41 M. Öeren, E. Shmatova, T. Tamm and R. Aav, *Phys. Chem. Chem. Phys.*, 2014, **16**, 19198.
- 42 S. Mecozzi and J. Rebek, *Chem.–Eur. J.*, 1998, **4**, 1016.
- 43 T.-C. Lee, E. Kalenius, A. I. Lazar, K. I. Assaf, N. Kuhnert, C. H. Grün, J. Jänis, O. A. Scherman and W. M. Nau, *Nat. Chem.*, 2013, **5**, 376.
- 44 M. A. Spackman and D. Jayatilaka, *CrystEngComm*, 2009, **11**, 19.
- 45 O. V. Dolomanov, L. J. Bourhis, R. J. Gildea, J. A. K. Howard and H.-J. Puschmann, *J. Appl. Crystallogr.*, 2009, **42**, 339.
- 46 M. J. Frisch, G. W. Trucks, H. B. Schlegel, G. E. Scuseria, M. A. Robb, J. R. Cheeseman, G. Scalmani, V. Barone, B. Mennucci, G. A. Petersson, H. Nakatsuji, M. Caricato, X. Li, H. P. Hratchian, A. F. Izmaylov, J. Bloino, G. Zheng, J. L. Sonnenberg, M. Hada, M. Ehara, K. Toyota, R. Fukuda, J. Hasegawa, M. Ishida, T. Nakajima, Y. Honda, O. Kitao, H. Nakai, T. Vreven, J. A. Montgomery Jr, J. E. Peralta, F. Ogliaro, M. Bearpark, J. J. Heyd, E. Brothers, K. N. Kudin, V. N. Staroverov, R. Kobayashi, J. Normand, K. Raghavachari, A. Rendell, J. C. Burant, S. S. Iyengar, J. Tomasi, M. Cossi, N. Rega, J. M. Millam, M. Klene, J. E. Knox, J. B. Cross, V. Bakken, C. Adamo, J. Jaramillo, R. Gomperts, R. E. Stratmann, O. Yazyev, A. J. Austin, R. Cammi, C. Pomelli, J. W. Ochterski, R. L. Martin, K. Morokuma, V. G. Zakrzewski, G. A. Voth, P. Salvador, J. J. Dannenberg, S. Dapprich, A. D. Daniels, Ö. Farkas, J. B. Foresman, J. V. Ortiz, J. Cioslowski and D. J. Fox, *Gaussian 09, Revision E.01*, Gaussian, Inc., Wallingford CT, 2009.
- 47 R. Dennington, T. Keith and J. Millam, *GaussView, Version 5*, Semichem Inc., Shawnee Mission, KS, 2009.
- 48 W. L. Mock and N.-Y. Shih, *J. Org. Chem.*, 1986, **51**, 4440.
- 49 W. L. Mock and N.-Y. Shih, *J. Am. Chem. Soc.*, 1989, **111**, 2697.
- 50 R. Hoffmann, W. Knoche, C. Fenn and H.-J. Buschmann, *J. Chem. Soc., Faraday Trans.*, 1994, **90**, 1507.
- 51 C. Márquez and W. M. Nau, *Angew. Chem., Int. Ed.*, 2001, **40**, 3155.
- 52 C. Márquez, R. R. Hudgins and W. M. Nau, *J. Am. Chem. Soc.*, 2004, **126**, 5806.
- 53 X. Ling, E. L. Samuel, D. L. Patchell and E. Masson, *Org. Lett.*, 2010, **12**, 2730.
- 54 H. Tang, D. Fuentealba, Y. H. Ko, N. Selvapalam, K. Kim and C. Bohne, *J. Am. Chem. Soc.*, 2011, **133**, 20623.
- 55 J.-S. Yu, F.-G. Wu, L.-F. Tao, J.-J. Luo and Z.-W. Yu, *Phys. Chem. Chem. Phys.*, 2011, **13**, 3638.
- 56 Z. Miskolczy and L. Biczók, *J. Phys. Chem. B*, 2014, **118**, 2499.
- 57 TURBOMOLE V6.5 2013, a development of University of Karlsruhe and Forschungszentrum Karlsruhe GmbH, 1989-2007, TURBOMOLE GmbH, since 2007, available from <http://www.turbomole.com>.
- 58 A. Klamt and G. Schüürmann, *J. Chem. Soc., Perkin Trans. 2*, 1993, 799.

Publication III

S. Kaabel, R. Aav, 'Templating Effects in the Dynamic Chemistry of Cucurbiturils and Hemicucurbiturils,' *Isr. J. Chem.* **2018**, *58*, 296–313.

Re-printed with permission. Copyright © 2017, John Wiley and Sons.

Templating Effects in the Dynamic Chemistry of Cucurbiturils and Hemicucurbiturils

Sandra Kaabel^[a] and Riina Aav^{*[a]}

Abstract: This review concentrates on the remarkable macrocyclisation chemistry of cucurbituril family members. During a single step in the condensation reaction of cucurbit[6]uril or hemicucurbit[12]uril 24 new C–N bonds are formed. In the case of hemicucurbit[12]uril this leads to the highly efficient formation of a covalently bound chain of 48 atoms. This phenomenon is possible because all cucurbiturils are built up of dynamic covalent acylaminal linkers.

Moreover, the reversibility of acylaminal linkages makes the formation of macrocycles susceptible to external stimuli. Influence of the chain-growth and chain-cycle equilibrium and the effect of different templates in CB chemistry is discussed. As anions have a pronounced effect on formation of hemicucurbiturils, a comprehensive overview on their role in modifying the solid-state structures of hemicucurbiturils is given.

Keywords: cucurbituril · dynamic covalent chemistry · template · crystal structure · inclusion complexes

1. Introduction

The family of cucurbiturils has grown exponentially in the number of homologues, analogues and derivatives.^[1,2] The structure of the first 6-membered cucurbituril (CB[6]) was reported by Freeman and Mock^[3] in 1981 (Scheme 1, upper) and it remained the only cucurbituril homologue for a decade.^[4] The first paper published on hemicucurbiturils (HC) by Miyahara^[5] in 2004, however already reported tuneable high yielding synthesis of two homologues from the same starting materials (Scheme 1, lower), highlighting the potential of direct quantitative polymerisation reaction toward differently sized macrocycles.

It is remarkable that during the formation of CB[6] or HC[12] in a single step 24 new C–N bonds and in case of HC[12] a covalently bound chain of 48 atoms is formed. Macrocycle formation reactions are known to be challenging. Learning how to build macrocyclic molecules with controlled topology and function has been recognised with Nobel Prizes in 1987 and 2016.^[6] Macrocyclisation usually requires preorganization of the acyclic intermediate.^[7] Therefore in most cases macrocycles are made in several steps from preoriented linear molecules. Dynamic covalent chemistry^[8–11] (DCC) could circumvent the necessity for a multistep procedure to form a preorganized oligomer. DCC can grant control over the formation of highly complex products in a single step. In addition to the example of the formation of the unsubstituted HCs shown on Scheme 1, also 4- and 6-membered bambusurils^[12–14] (BU) and 6- and 8-membered cyclohexanohemicucurbiturils^[15] (cycHC) are made from their respective starting monomers using DCC. In principle, all cucurbituril family members are formed through the same acid catalysed polymerisation reaction between cyclic urea and formaldehyde, creating the acylaminal linkers between monomers. Current review will focus on this macrocyclisation reaction, with the

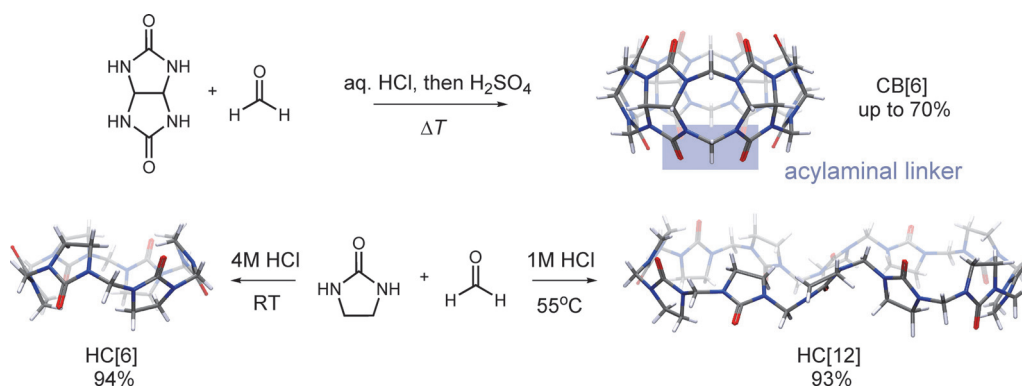
aim of demonstrating the potential of templating in the formation of cucurbiturils. A comprehensive analysis of the crystal structures of hemicucurbiturils is presented in this review, aimed to ascertain the extent of the role templating guests play in modifying the solid-state structure of these macrocyclic hosts.

2. Dynamic Covalent Bonds

Condensation between aldehydes and amines is one of most widely utilized reactions in organic chemistry. Due to reversible nature of this reaction it is most actively used in catalysis, but has also found application in reactions using dynamic covalent chemistry. The latter are based on the formation of reversible covalent bonds between the components of a reaction mixture, that equilibrate until the products with the lowest energy are formed. In this approach dynamic combinatorial libraries (DCL) of intermediates are generated, which may allow for the deliberate amplification of a particular species by an external stimulus. Although many reversible reactions exist, not all of them are useful as dynamic linkers. Rapid equilibration between library members under controlled conditions is necessary, making imines,^[16] hydrazones^[17] (Scheme 2, A,B), disulphides^[18] and boronates^[19] currently the most applied linkers.^[20] Moreover, also amins^[21,22] and hemiaminals^[23–25] have been successfully applied in dynamic combinatorial chemistry (Scheme 2, C).

[a] S. Kaabel, R. Aav

Department of Chemistry and Biotechnology, School of Science, Tallinn University of Technology, Akadeemia tee 15, 12618, Tallinn, Estonia
E-mail: riina.aav@ttu.ee



Scheme 1. The first synthesized CB^[6] (upper) and HC^{s[6]} (lower).

Formation of the methylene bridges of CBs proceeds through aminal formation. As outlined below, (Scheme 2, D) two C–N bonds are formed during one methylene bridge formation. The first step is an acid catalysed water elimination and iminium formation. Iminiums are high energy intermediates and react fast with available nucleophiles in the media. Lifetime of intermediate iminium ions in aqueous solution is in the range of picoseconds^[26–28]. The presence of iminiums in the synthesis of substituted HCs (cycHCs) was demonstrated by MS, by quenching the reaction with the addition of different nucleophiles, and by DFT study on the methylene bridge formation pathway.^[15] A computational study on the pathway of acyliminium intermediate formation from ethyleneurea and formaldehyde was recently published by Yoo and Kang,^[29] which shows the involvement of urea carbonyl group during iminium formation (Scheme 3, A).

Importance of C=O group during formation of bambusurils has been experimentally observed by Reany and Keinan,^[14] as the condensation of formaldehyde with thio-analogue of ethyleneurea (Scheme 3, B) does not result in formation of thioacylaminal linker. At the same time mono-thioglycoluril can be condensed to thiobambusurils (thioBU[*n*]), if methylene bridges are formed between ethyleneurea part of

the monomer and alkylthiourea is carried along as substituent of the resulting HC (Scheme 3, C). These observations revealed the sensitivity of this structural system. The formed iminium intermediate (Scheme 2, D) reacts further with a nitrogen of the nucleophile and affords the ammonium intermediate, which after deprotonation results in the formation of the neutral aminal linkage. According to theoretical study in presence of water, the formation of the second C–N bond and deprotonation is mediated by water and the urea C=O group (Scheme 3, A).^[29] In general aminals and hemiaminals are labile compounds and hydrolyse easily back to aldehydes and amines. Therefore this dynamic multicomponent chemistry (Scheme 2 C) has been utilized in chiral sensing.^[30–32] Non-enolizable aromatic aldehydes are preferred in these applications, as enamine formation is avoided. The preferred formation of either aminal or hemiaminal was shown to depend on the geometry of the amine.^[30] In CBs the aminal is formed adjacent to the acyl groups. As the latter have electron accepting properties and delocalize the nucleophilicity of nitrogen, these aminal linkages are less susceptible to hydrolysis compared to alkyl-aminals. In acidic conditions however, the protonation of either the carbonyl group or the nitrogens of acylaminals can eventually lead to the regener-



Sandra Kaabel received her B.Sc (2012) and M. Sc. (2014) degrees in Chemistry from Tallinn University of Technology, Estonia. She is currently pursuing her doctoral studies in the group of Assoc. Prof. Riina Aav in the field of supramolecular chemistry, under the co-supervision of Dr. Riina Aav and Acad. Prof. Kari Rissanen from University of Jyväskylä. Her research focuses on the structural analysis of complex host-guest systems and on the development of new synthetic receptors.



Riina Aav is an Assoc. Prof. at Tallinn University of Technology, Department of Chemistry and Biotechnology. She obtained her Eng, MSc, and PhD (2005) degrees from TTU. She has worked with Prof. Alexandre Alexakis at the University of Geneva, Switzerland and Prof. Scott Eric Denmark at University of Illinois at Urbana-Champaign, USA. Her group research interests are the synthesis and characterisation of asymmetric organic compounds, container molecules, their formation, structure, chiroptical and supramolecular properties as well as their applications.

Review

that the protonation site may depend on proton carrier and media. According to our knowledge the experimental kinetic data on formation and cleavage of single acylaminal linker have not been published. Though the kinetic studies by Anslyn et al.^[23] of mechanism of Zn-mediated hemiaminal formation involving secondary amine, aromatic aldehyde and secondary alcohol showed that the rate limiting step of the dynamic equilibrium was not acid-promoted water elimination, but rather the decomplexation of Zn(II) from the assembly. Which leads to suggestion that control over the formation of products, connected through aminal-hemiaminal dynamic covalent bonds, proceeds through external stimuli from reaction media and templates. The overall process for macrocycle formation involves several important steps, including chain-growth equilibrium, chain-cycle equilibrium and product stabilisation equilibrium, either through solubility or through complex formation (Scheme 4).

3. Chain Growth Equilibrium

Day et al.^[36] studied the controlling factors of CB formation and demonstrated that the chain growth step depends on the acidity of the media and the concentration of urea. The reaction is faster in presence of stronger acids, most probably due to facilitated iminium formation and longer lifetime of cationic intermediates. Formation of larger CB homologues is observed at higher urea concentrations. By performing the CB synthesis in concentrated HCl and varying the glycoluril concentration from 0.1 to 200 mg/ml, the CB[5] formation decreased from 58% to 17% and the fraction of higher homologues increased.

Also, for example, CB[8] was not detected in a diluted reaction mixture, but raising glycoluril concentration from 0.1 to 2000 mg/ml the yield of CB[8] was increased to 12%.^[36]

This observation is fully consistent with Jacobson-Stockmayer theory for equilibrium polymerisation, as at higher concentrations the rate of intermolecular reactions increases, therefore longer oligomers are formed preferably.^[8,37,38]

Isaacs et al.^[39] uncovered the inverted-CBs, studied their formation and concluded that thermodynamically unstable intermediates can be isolated if during synthesis lower temperature and deficiency of formaldehyde is used. In these conditions Isaacs et al.^[40] were also able to isolate linear

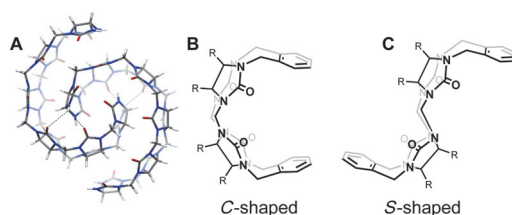
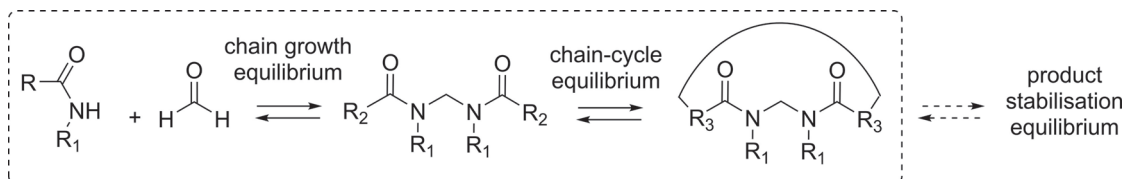


Figure 2. A) Crystal structure of C-shaped 6-membered glycoluril oligomer^[40] (CCDC 701740); B) C-shaped dimer of glycoluril with aromatic terminal groups; S-shaped dimer of glycoluril with aromatic terminal groups.^[41]

oligomers containing 2–6 monomers and determine their crystal structures (Figure 2, A).

The glycoluril monomers are all oriented with the urea carbonyl groups and *endo* faces of the glycolurils pointing toward each other. Day called this all-*endo* and Isaacs C-shaped oligomer (Figure 2, A,B). Formation of C-shaped oligomers is key for preorganisation of linear chain for cyclisation. Additionally to that, there are diastereomeric combinations, where *exo*- and *endo*-faces of monomers will alternate. Such oligomers may take the shape of the letter S (Figure 2, C). Semiempirical computational studies^[36,41] proved the S-shaped oligomers to be higher in energy compared to the C-shaped oligomers. This was also confirmed experimentally by Isaacs, who demonstrated that C-shaped substituted glycoluril dimers are thermodynamically more stable by 1.55–3.25 kcal mol⁻¹ compared to the S-shaped diastereomers^[41] (Figure 2, B,C). As a result, double bridged oligomers are preorganized suitably for macrocyclisation. The fascinating crystal structure of the double bridged 6-membered oligomer (Figure 2, A) revealed that the oligomer encloses a compartment potentially able to bind guests. For selective isolation of 6-membered C-shaped oligomers^[42] in 10% yield and their further conversion to functionalized-CBs^[43–48] Isaacs utilized a carefully chosen guest, the *p*-xylylenediammonium which prevented through negative templating the macrocyclisation and assisted precipitation of the hexamer.

Single bridged HCs, including BUs and biotinuril have the same acylaminal dynamic linker between monomers as all CB family members. Currently no crystal structures have been reported from any oligomers of these compounds. Though,



Scheme 4. General scheme of dynamic formation of CB macrocycles.

along with analysis of intermediates of biotin[6]uril, Pittelkow et al.^[49] was able to isolate in 11% a single enantiomer of biotin dimer, as the most abundant oligomer. During the study on the (*R,R*)-cycHC[*n*] formation, Aav et al. observed oligomers of different lengths and noticed that their length depended on reaction conditions. No single most prevalent oligomer has been observed during synthesis of chiral cycHCs.^[15,50] Also, surprisingly, a very large discrepancy in the UV absorbance between linear and macrocyclic congeners of cycHCs was observed (Table 1).^[50] We speculate that it is due to higher conformational flexibility of these compounds compared to their cyclic analogues.

Table 1. UV absorption of linear oligomer and macrocycles formed from cyclohexanediyurea.^[50]

Compound	ϵ_{210} ($M^{-1} \text{ cm}^{-1}$)
6-membered oligomer	$(2 \pm 1) \cdot 10^3$
(<i>R,S</i>)-cycHC[6]	$(18.4 \pm 0.2) \cdot 10^3$
(<i>R,R</i>)-cycHC[6]	$(17 \pm 2) \cdot 10^3$

Computational study performed by Yoo and Kang^[29] on the formation mechanism of unsubstituted HCs concluded that the formation of *anti*-oriented dimers is more favourable. *Anti*-oriented dimers are formed through a lower energy transition state compared to their *syn*-conformers, which contributes to explaining the alternate orientation of urea groups in HCs. In the same study geometries of oligomers with up to 6-membered chain (Figure 3) were calculated. It is clear, that single bridged ethyleneurea oligomers can adapt a conformation suitable for macrocyclisation, though without conformational analysis it cannot be concluded that these geometries are the most abundant in reaction media.

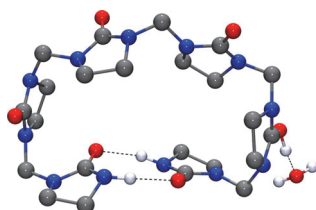


Figure 3. Geometry of ethyleneurea hexamer with H_2O .^[29]

4. Chain Cycle Equilibrium

Next step after the formation of oligomers is macrocyclisation, and its efficiency is determined by chain-cycle equilibrium (Scheme 5). This equilibrium is dependent on difference between inter- and intra-molecular reaction rates. Intermolecular reaction will lead to growth of oligomers and intra-molecular will terminate it by macrocycle formation. In high

dilution conditions intermolecular reaction rate is suppressed compared to intramolecular reaction,^[51] which is why this strategy is the most prevalent in macrocycle chemistry. But high dilution might not be applicable, if the target is to form long chain oligomers for larger macrocycles. Therefore, templating would be the most attractive way to control chain-cycle equilibrium. There are different ways of action of templates.^[6,7,52,53] In broader sense templates can have either kinetic or thermodynamic effect, this classification was introduced by Thomson and Bush^[52] and later greatly expanded by S. and H. Anderson and Sanders.^[53] If a template selectively complexes with one particular linear oligomer from the dynamic covalent library, and promotes its macrocyclisation by changing the rate of its formation – then it is called the kinetic template effect (Scheme 5, route A).^[8]

If a template complexes with the macrocycle and thus improves its thermodynamic stability, equilibrium between oligomers and macrocycles changes and thermodynamically most favourable product is amplified. (Scheme 5, route B). Thermodynamic equilibrium may also be shifted by selective complexation of the template with one particular component in the dynamic mixture, which causes a change in its solubility. In that case the template will affect the solubility equilibrium and through that also equilibrium within the DCL. (Scheme 5, route C). In the latter case amplification of thermodynamically unfavourable macrocycles may happen, as the removal of one component from the dynamic mixture is controlled by the solubility equilibrium.

It should be noted that it is experimentally challenging to distinguish between presented pathways. Changes in transition state need to be assessed to recognize kinetic templating. On the other hand, as many of the cucurbituril macrocyclisation reactions proceed in heterogenous systems, it is not trivial to determine whether the template stabilizes the product or just removes it from the equilibrium. Nevertheless, rough analysis based on the available literature is attempted with the goal to encourage discussion and additional experimental studies, leading to better understanding of the templating effects in CB chemistry.

The complexation ability of uril macrocycles depends on their electronic structure. Map of electronic potential of CB[7] and the methylsubstituted bambus[6]uril (MeBU[6]) is shown on Figure 4.^[54]

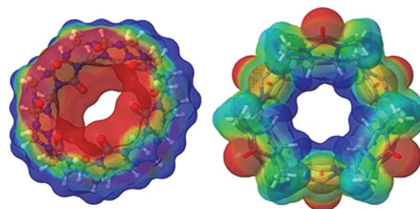
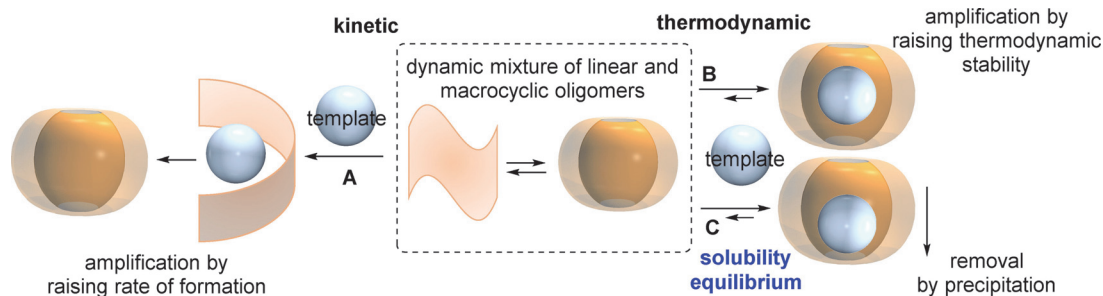


Figure 4. A) Map of electronic potential of CB[7] and MeBU[6]. Reprinted with permission from ref. [54]



Scheme 5. Templates effecting the dynamic formation of macrocycles.

Electron rich oxygens of urea monomers surround the opening of the CB cavity, through which electron poor cationic species bind to CBs. The binding properties of CBs have been extensively studied,^[55] as many of the CB applications are based on it. Urea carbonyl groups of single bridged hemicucurbiturils are not aligned and their cavities are electron poor, preferably binding anions. The interaction properties the CBs and HCs also play a role in their templated reactions.

Formation of CB[6] and substituted CB[5]s, such as MeCB[5] (Figure 5), are thermodynamically most favourable compared to their homologues.^[56] It has been shown by modelling that oxonium acts as a template and stabilises smaller macrocycles,^[56] affecting macrocyclisation by thermodynamic template effect (Scheme 5, route B).

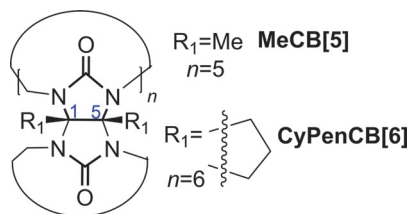


Figure 5. Structures of substituted CBs MeCB[5] and CyPenCB[6].

The first experimental study on influence of acids^[36] and salts^[57] on the ratio of the formed CB products was done by Day et al., which found that the addition of KCl (60 mol% based on monomer) to the mixture of oligomers heated in concentrated HCl, shifted the reaction toward the formation of the 5-membered homologue (Table 2, line 1). CB[5] was isolated in a 28–32% yield, which is much higher than the 8% collected from the reaction without this additive. The ability of the potassium ion to shift equilibrium toward smaller macrocycles has also been seen by Isaacs.^[43] Namely in presence of KI, the ratio of 6 to 7 membered CBs was 2.3 whereas in the absence of this salt prevalence of CB[6]

decreased to 1.5. Day^[57] proposed that metal cations bind to the oligomers and induce macrocyclisation through kinetic template effect outlined on Scheme 5 as route A. It should be noted that none of the cations, Li^+ , Na^+ , K^+ , Rb^+ , Cs^+ and NH_4^+ , that were studied, were able to show exclusive selectivity toward the formation of one single homologue. Intriguingly, CB[5] itself has also served as a template in the formation of CB[5]@CB[10] (Table 2, line 5).^[36,58] Isolation of CB[10] from CB[5] was succeeded by guest exchange.^[59,60] Inspired by CB[5] acting as a neutral template, also *o*-carborane was tested as a template for CB[7]. In presence of 20 mol% (based on monomer) of *o*-carborane no significant influence on the ratio of the formed homologues was observed.^[61]

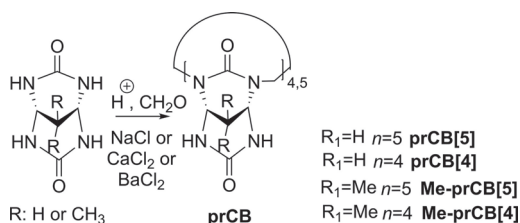
Presence of NH_4Cl lowers the solubility of MeCB[5]^[62] and it was therefore used as an additive in the synthesis of MeCB[5]. The macrocycle was isolated as an ammonium salt in higher 36% yield, versus 14% without extra added NH_4Cl (Table 2, lines 2). Notably Miyahara^[62] confirmed, that solubility equilibrium of $\text{MeCB}[5] \cdot \text{NH}_4^+$ complex did not affect the formation of 5-membered macrocycle, but increased product isolation efficiency. Formation of substituted CBs can be directed by addition of Li_2CO_3 and CsCl ,^[63] as these templates increase fraction of CyPenCB[6] and CyPenCB[7] on expense of the 5-membered homologue (Table 2, lines 3 and 4). As the change in ratio of homologues was determined from the crude mixture, template effects by either route A or B (Scheme 5) can be attributed to this reaction.

Pressocucurbiturils (prCB) are CB derivatives, where instead of glycoluril, the propanediurea is used as the monomer (Scheme 6).^[64–67] The isolation of first prCB, the Me-prCB[5] was reported simultaneously by Sindelar^[64] and Wang.^[65] Very recently it was demonstrated that presence of CaCl_2 induces the formation of the first 4-membered double bridged CB, the Me-prCB[4] (Table 2, line 6).^[66] The templated synthesis of prCB[4] and prCB[5] was demonstrated in the presence of Ca^{2+} in 23% yield and Ba^{2+} in 20% yield, respectively (Table 2, lines 7 and 8).^[67] Without the BaCl_2 additive and in presence of NaCl, 5-membered prCB[5] was also formed, but could not be isolated in pure form.^[64] The presence of Ca^{2+} and Ba^{2+} salts induced the precipitation of

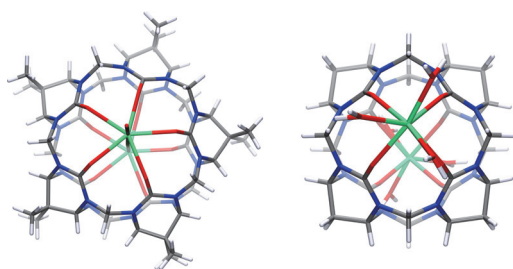
Table 2. Templates that supported the formation of double bridged CBs and tentative mode of templating.

No	Double bridged CB	Isolated yield	Template	Route in Scheme 5	Year	Ref
1.	CB[5]	28–32%	KCl	A	2002	57
2.	MeCB[5]	36%	NH ₄ Cl	A and/or C for isolation	2002	62
3.	CyPenCB[6]	39%	Li ₂ CO ₃	A or B	2012	63
4.	CyPenCB[7]	9%	Li ₂ CO ₃	A or B	2012	63
5.	CB[5]@CB[10]	5–8%	CB[5]	B and/or C ^a	2002	36
6.	Me-prCB[4]	5%	CaCl ₂	C	2017	65
7.	prCB[4]	23%	CaCl ₂	C	2017	66
8.	prCB[5]	20%	BaCl ₂	C	2017	66

^a In heterogeneous reaction conditions solubility equilibrium through pathway C is marked effective, where it cannot be unequivocally concluded whether the product solubility only influences its isolation or also the product formation.

**Scheme 6.** Formation of pressocucurbiturils (prCB) from propane-dureas.^[64–67]

macrocycles from the reaction mixture in a 1:2 complex, with metals bound to prCBs at the portals (Figure 6). This reflects the importance of the solubility equilibrium of the macrocycle complexes, and determines that the template effect by route C on Scheme 5 is most likely effective in this case. Although on the basis of published data no conclusions can be made, whether Ca²⁺ and Ba²⁺ salts also increased fraction of formed macrocycles in the reaction mixture.

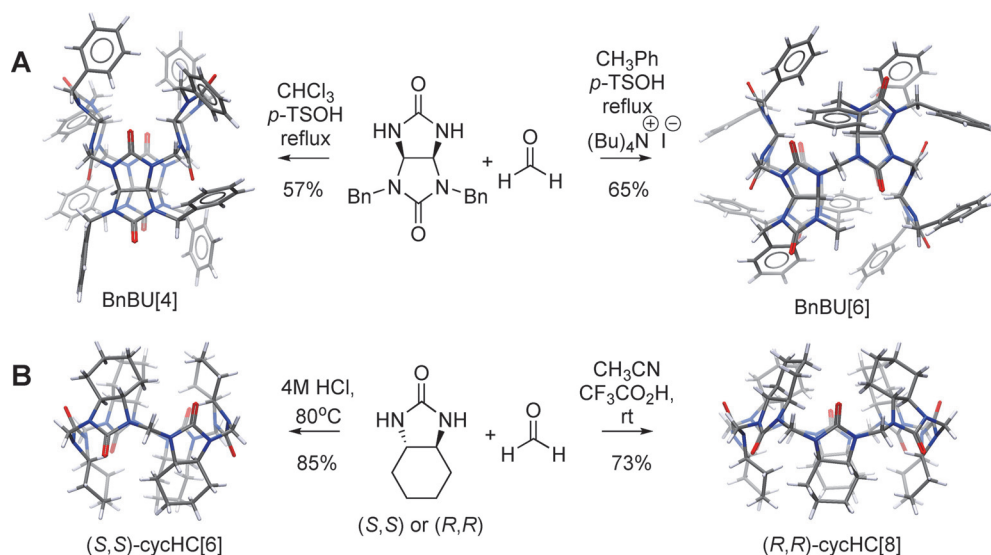
**Figure 6.** Crystal structures of Me-prCB[5]^[65] (CCDC 1036915) and prCB[4]^[67] (CCDC 1548029) as Ca²⁺ complexes. Colour codes: C grey, H white, N blue, O red, Ca²⁺ turquoise, Cl⁻ (at the centre of Me-prCB[5]) green

As noted earlier, size of single bridged HCs can be controlled in much greater extent compared to the double bridged cucurbiturils. The unsubstituted HCs (Scheme 1) are

not the only kind of HCs which can be directed toward different homologues. The first bambusuril was introduced by Sindelar^[68] and soon after they noticed^[12] that without the presence of a halide anion in the condensation of cyclic alkylurea and formaldehyde, the 4-membered homologue would be formed. In presence of halides prevalent formation of 6-membered bambusurils was observed (Scheme 7, A). After that finding a whole family of BUs has been prepared, including several 4-membered and 6-membered BUs.^[13,14,68–70]

In non-templated conditions chain-cycle equilibrium is shifted toward macrocycle formation and as soon as 4-membered oligomer is formed it closes to a macrocycle. All six-membered HCs form complexes with halides and it has been shown that Cl⁻, Br⁻, I⁻ and ClO₄⁻ are suitable templates for 6-membered BU (Table 3, lines 4–7, 11, 12). Representative structures of HCs discussed in this paper are shown on Figure 8. There is no report on the binding of oligomers to anions, therefore the most likely templating effect taking place is by route B shown on Scheme 5. Reactions performed in aqueous solution are often heterogeneous, therefore effects through solubility equilibrium is likely to contribute as well (Scheme 5, route C). Beside BUs 6-membered HCs have also been prepared from cyclohexa-1,2-diylurea (Table 3, lines 3, 8),^[71,72] norbornene (Table 3, line 9)^[73] and biotin (Table 3, line 10).^[49] In these examples also halide anions were used to control the size of 6-membered macrocycles.

Deeper understanding of the dynamic character of HCs was achieved from a study on the formation of 8-membered (*R,R*)-cycHC.^[15] Anion size was found to control the formation of either 6- or 8-membered cycHCs (Scheme 7, B). It was shown that starting either from monomers or other (*R,R*)-cycHC[*n*] homologues dynamic covalent library could be directed toward the formation of a specific macrocycle. The PF₆⁻, HCO₂⁻ and CF₃CO₂⁻ acted as templates for the formation of 8-membered (*R,R*)-cycHC (Table 3, lines 13, 14) and halides directed the formation of 6-membered (*R,R*)-cycHC (Table 3, line 8). Contrary to the mechanism proposed for formation of biotinuril,^[49] ¹³C isotope labelling experiment confirmed that formation of (*R,R*)-cycHC[8] from cycHC[6] does not go through dimer addition, as carbon-isotopes were randomly distributed in the product. This confirms that HCs depolymerise in the presence of acid to form a dynamic



Scheme 7. Non-templated formation of 4-membered and the template directed formation of 6- and 8-membered single bridged CBs. A) bambusurils [12] (BU); B) cyclohexanohemicuributurils (cycHCs).^[15] BU figures are based on the crystal structures CCDC 809240 and 809242 from ref. [12], cycHC figures are based on the crystal structures CCDC 945664 from ref. [72] and CCDC 1053111 from ref. [15].

Table 3. Templates that supported formation of single bridged HCs and tentative mode of templating.

No	Single bridged CB	Isolated yield	Template	Route in Scheme 5	Year	Ref
1.	HC[6]	94 %	Cl ⁻	B and/or C ^a	2004	5
2.	HC[12]	93 %	Cl ⁻	B and/or C	2004	5
3.	(<i>R,S</i>)-cycHC[6]	78 %	Cl ⁻	B and/or C	2009	71
4.	MeBU[6]	30 %	Cl ⁻	B and/or C	2010	68
5.	BnBU[6]	65 %	I ⁻	B	2011	12
6.	PrBU[6]	15 %	Cl ⁻	B and/or C	2011	12
7.	AllylBU[6]	60 %	I ⁻	B	2013	13
8.	(<i>S,S</i>)-cycHC[6]	85 %; 64 %	Cl ⁻ ; Br ⁻	B and/or C	2013	72
9.	norbornaHC[6]	9 %	Cl ⁻	B and/or C	2013	73
10.	Biotin[6]uril	48 %; 63 %	Cl ⁻ ; Br ⁻	B and/or C	2014	49
11.	p(MeOCO)BnBU[6]	42 %	Br ⁻	B	2015	69
12.	thioBU[6]	82 %	Cl ⁻ ; Br ⁻ ; I ⁻ ; ClO ₄ ⁻	B	2015	14
13.	(<i>R,R</i>)-cycHC[8] from (<i>R,R</i>)-cycHC[6]	71 %; 71 %; 90 %	HCO ₂ ⁻ ; PF ₆ ⁻ ; CF ₃ CO ₂ ⁻	B	2015	15
14.	(<i>R,R</i>)-cycHC[8] from monomers	7 %; 55 %; 73 %	HCO ₂ ⁻ ; PF ₆ ⁻ ; CF ₃ CO ₂ ⁻	B	2015	15

^a In heterogeneous reaction conditions solubility equilibrium through pathway C is marked effective, where it cannot be unequivocally concluded whether the product solubility only influences its isolation or also the product formation.

covalent library, in which the equilibrium is driven, as a response to the added template, towards the recombination of the thermodynamically most favourable product. According to DFT-calculated Gibbs' energies of (*R,R*)-cycHC[6] and (*R,R*-

cycHC[8] and their formate anion inclusion complexes, it is not the cycle strain of (*R,R*)-cycHCs, but the inclusion complex with HCO₂⁻, which induces a preference towards the formation of (*R,R*)-cycHC[8].^[15] (*S,S*)-CycHC[6] is shown to

form inclusion complexes with halides^[35] and (*R,R*)-cycHC[8] to form anion inclusion complexes size selectively with larger anions.^[74] Therefore, formation of chiral cycHCs proceeds according to the route B, whereas water solubility equilibrium of route C on Scheme 5 can also be effective in reactions conducted in water (Table 3, lines 3, 8, 13, 14).

The selective formation of either 6- or 12-membered HCs in presence of a Cl^- anion (Scheme 1)^[5] can be explained by the joint impact of both the acid and the template. Higher concentration of HCl accelerates the condensation reaction and concurrently the higher abundance of Cl^- enhances the thermodynamic stability of HC[6] through complexation, suggesting that templating effect through the route B (Scheme 5) takes place (Table 3, line 1). Thermodynamic parameters for the binding of anions with substituted HCs^[74,75] have proven that anion binding in protonic media is entropically disfavoured, which is why at elevated temperatures the binding of anions is suppressed. This might explain why at lower Cl^- concentration and at higher temperature, binding of Cl^- to HC[6] is weaker and HC[6] is apparently thermodynamically less stabilized. In such conditions the chain growth process is not terminated by the formation of HC[6], so it proceeds towards the formation of longer oligomers necessary for formation of HC[12].^[5] Furthermore, Buschmann et al.^[76] have shown by a computational study that HC[12] can also be stabilized by Cl^- anions, as HC[12] can take a conformation with two compartments suitable for accommodation of Cl^- anions (Figure 7). Therefore it is plausible that formation of both HC[6] and HC[12] are templated by Cl^- according to thermodynamic control and as products HC[6] and HC[12] both precipitate out of the reaction media routes B and C are operative, Scheme 5 (Table 3, lines 1,2). Anion templated mechanism is operating for all HCs, and Sindelar et al. have proposed that anion binding may play role also in normal CB formation.^[77]

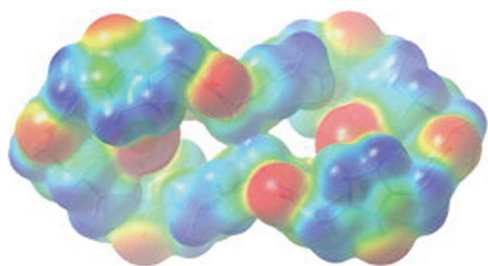


Figure 7. Map of electronic potential of $2\text{Cl}^-@$ HC[12]. Reprinted with permission from reference [76]

Control over the formation of double bridged CBs is challenging, mainly templates that allow selective isolation of a member of the dynamic equilibrium have been utilized. Nevertheless, the influence of metal cations on distribution of

macrocyclic homologues is observed and therefore search for more effective templates is encouraged. The dynamic character of acylaminal linkers is more pronounced in singlebridged HCs. In non-templated conditions 4-membered HCs are selectively synthesised, while templates direct the formation of larger macrocycles. Small anions like halides give mainly 6-membered HCs, while also 8- and 12-membered homologues of this family have been prepared with high efficiency.

Structural interplay of hosts with their guests gives an insight to the possible interactions with templates, therefore the crystal structures of single bridged HCs are analysed in next section. Structures of double bridged CB family members in solid state are not discussed, as they have been reviewed previously.^[78]

5. Hemicucurbiturils in Solid State

The dimensions of the hemicucurbiturils (HC[*n*]) were measured based on their respective single crystal X-ray data published in the Cambridge Structural Database (entries up to May 2017). We were particularly interested in comparing the cavity dimensions of different HCs and investigating short host-guest interactions, to probe the extent to which the overall shape of the host is affected by the size and position of the guest molecule within the cavity. The common property of all HCs with an even number of ethyleneurea is the alternate orientation of the monomers, which creates a partially positively charged cavity that attracts anions. The precise shape and size of the cavity depends on the stereochemistry of the HC and the number of monomers, ranging from inaccessible narrow cavity of 4-membered HCs to larger open cylindrical or isolated spherical cavities in 6- and 8-membered HCs, to a loosely shaped elongated cavity of HC[12]. Although crystal structures essentially provide a frozen view on the arrangement of molecules, a measure for the flexibility of the hosts could also be gained, when comparing the cavity dimensions of a single host in a complex with several different guests.

The following analysis of the dimensions and host-guest interactions of HCs is divided into sections to compare similar hosts in higher detail. HC[*n*] are grouped based on the number of monomers, with HC[6] further divided into (*R,S*)-isomers and (*R,R*)- or (*S,S*)-isomers based on stereochemistry of the ethyleneurea stereocenters.

Bambusurils,^[12] thiobambusurils^[14] and azabambusurils^[70] syntheses have afforded the isolation of four-membered macrocyclic molecules, for which five crystal structures in total have been published. The small central cavity of these tetrameric molecules is bordered from sides by flat urea groups and rimmed on the portals by the tightly sitting ethylene hydrogens (Figure 9, A and B). These two hydrogens on each substituted ethyleneurea monomer face towards the cavity, and create very narrow oblong passages to the central cavity (Figure 9, C). The portal and cavity dimensions of the tetrameric BU[*n*] are presented in Table 4. No guest molecules

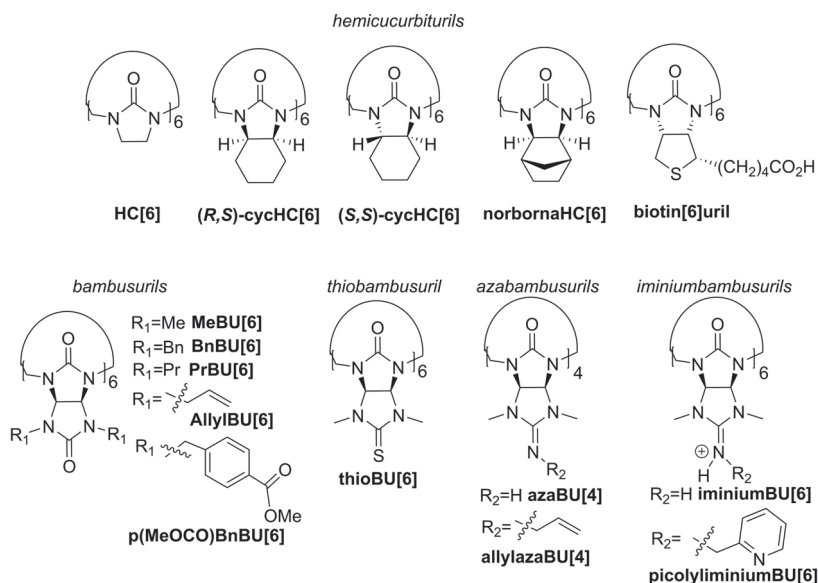


Figure 8. Representative structures with abbreviated names of substituted HCs discussed in this paper.

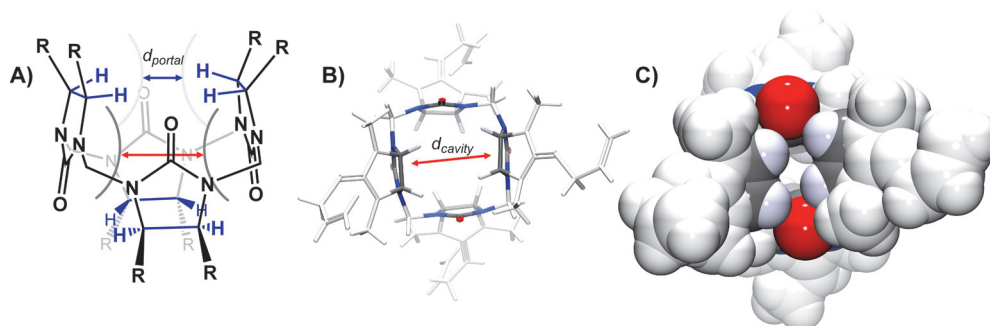


Figure 9. A) The chemical structure of BU[4]s, with the ethylene hydrogens on the portal highlighted in blue. The portal diameter is indicated with a blue arrow, the cavity diameter with a red arrow. B) top view on a crystal structure of allylazaBU[4] (CCDC 1401300 from ref. [70]) with the cavity highlighted in element colours (C grey, N blue, O red and H white) and the substituents in light grey. C) the CPK representation of the crystal structure.

are included to the centre of the cavity of BU[4], due to its restricted size, but various guests can be seen to interact with the portal hydrogens through weak hydrogen bonds from a secondary binding site (Figure 10). Notably, in the crystal structure of BnBU[4],^[12] two of the benzyl substituents on each portal create a deep binding pocket for the acetonitrile through additional favourable π - π stacking interactions (Figure 10, A). The DMSO molecules in the fascinating crystal structure of a linear thioBU[4]·HgCl₂ coordination polymer^[14] are also situated close to the bambusuril portals, fixed by two moderately strong C-H...O hydrogen bonds (Figure 10, B).

The corresponding binding sites in the crystal structures of azaBU_s^[70] are sandwiched between stacked azaBU_s by the pincer-like *N*-allyl groups (Figure 10, C). These 171 Å³ voids (in CCDC 1401300) are reported to contain disordered solvent molecules.

Of all the hemicucurbituril homologues, the 6-membered are the most synthetically diverse. This is represented also by the largest number of crystal structures in the CSD, affording a sample of 25 structures to compare, the results of which are compiled into Table 5. Due to a significant difference in the shape of (*S,S*)-cycHC[6] (Table 5, line 25)^[72] and the 6-

Table 4. Comparison of the tetrameric bambus[4]uril derivatives.

Line no.	BU[<i>n</i>]	CCDC	CSD	<i>n</i>	guest (centre)	guest (portal)	$d_{portal}^{[a]}$	$d_{cavity}^{[b]}$	Ref.
1	BnBU[4]	809240	IYONI	4	none	MeCN	2.63	5.58, 5.59	12
2	thioBU[4]	1005159	LOWGAH	4	none	MeCN, BU[4] ^[c]	2.58	5.27, 5.72	14
3	thioBU[4]	1005161	LOWGIP	4	none	DMSO	2.81	5.62, 5.51	14
4	allyliminiumBU[4]	1401299	ATUFAY	4	none	Void ^[d]	2.96	5.12, 5.49	70
5	allylazaBU[4]	1401300	ATUFEC	4	none	Void ^[e]	2.87	5.49, 5.43	70

^[a] The distance between the hydrogen atoms across the portal of the BU[4]*s* at its narrowest point. ^[b] The distance between carbonyl carbon atoms across the cavity of BU[4]*s*. ^[c] A sulphur atom of a neighbouring thioBU[4] is inserted to the secondary binding site. ^[d] Void contains disordered methanol molecules and traces of chloroform, that are omitted from the structure using the Squeeze technique (Platon, Speck, 2009). ^[e] Void (171 Å³) contains disordered methanol and chloroform molecules, that are omitted from the structure using the Squeeze technique (Platon, Speck, 2009).

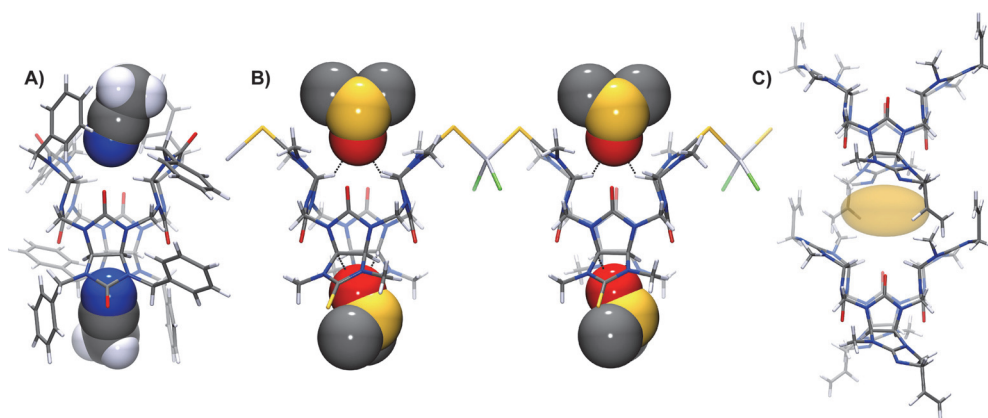


Figure 10. A) Position of guest MeCN molecules in the secondary binding sites of BnBU[4] (CCDC 809240 from ref. [12]). B) Fragment of the coordination polymer thioBU[4]·HgCl₂ (CCDC 1005161, from ref. [14]) showing the hydrogen bonded DMSO molecules on each portal ($d(D\cdots A)$ 3.077 Å and 3.069 Å). The hydrogen atoms on the methyl groups of DMSO are not modelled in the crystal structure. C) allylazaBU[4], stacked along the crystallographic *b*-axis (CCDC 1401299, from ref. [70]), with the sandwiched void illustrated by a yellow oblate spheroid.

membered (*R,S*)-isomers, these diastereomeric hosts are discussed separately.

The central cavity of the unsubstituted HC[6] and (*R,S*)-isomers of substituted HC[6] is represented by a cylindrical space between two coplanar layers of inwards facing ethyleneurea hydrogens that rim the narrowest parts of the cavity (Figure 11, A). These hydrogens are common in all of the substituted (*R,S*)-stereoisomers and unsubstituted HCs. In order to ascertain, whether the size of the guest is reflected in the size and shape of the host, the radius from the portal centroids to these hydrogens (r_{cavity}) and height of the cavity (h_{cavity}) was measured (Figure 11, A), from which the volume of the cylindrical space was calculated ($V_{cylinder}$). Additionally, the radius from the cavity centroid to the carbonyl oxygen (r_O) was measured (Figure 11, B), to follow changes in the angle of the monomer respective to the central axis of the macrocycle. Changes in the angle of the monomers is indicated by a simultaneous contraction of r_O and expansion of r_{cavity} or vice versa, which signifies a degree of flexibility of the HC[*n*].

The central cavity of HC[6] is sufficiently large for the complexation of a variety of anionic or neutral guest molecules. Most prevalent of such are the 1 : 1 complexes with halide anions, where the anion is bound within the centre of the partially positively charged HC[6] cavity, held in place by multiple C–H \cdots X[−] hydrogen bonds to the ethylene hydrogens. Sindelar et al. observed that the C–H \cdots X[−] distances in MeBU[6] crystal structures with either Cl[−], Br[−] or I[−], increase with increasing radius of the halide bound, indicating that the macrocycle adapts to the larger size of the guest.^[68] Following the dimensions of the unsubstituted hemicucurbit[6]uril,^[5] biotin[6]uril,^[49] bambus[6]uril^[68,79] and its derivatives,^[13,70,80] the same trend is seen within all host types in their respective 1 : 1 host-guest anion inclusion complexes. The overall correlation between the cavity size ($V_{cylinder}$) of the macrocycles and the size of the guest anion is weak (Figure 12), indicating that the cavity size is not determined solely by the encapsulated guest, but is also affected by the substituents on the core HC[*n*] structure.

Table 5. Comparison of the hexameric hemicucurbit[6]uril derivatives, ordered smallest to largest according to $V_{cylinder}^{[a]}$

Line no.	HC[<i>n</i>]	CCDC	CSD	<i>n</i>	guest	r_{cavity}	r_o	h_{cavity}	$V_{cylinder}$	Ref.
1	MeBU[6]	761932	GVVLEP	6	Cl ⁻	2.55	5.25	3.36	68	68
2	iminiumBU[6]	1401301	ATUFIG	6	Br ⁻	2.57, 3.01 ^[b]	5.23	3.39	70	70
3	HC[6]	235284	WAFHER	6	Cl ⁻	2.63	5.25	3.33	72	5
4	(<i>R,S</i>)-cycHC[6], CHCl ₃	716122	OGUQIR	6	none	2.65	5.18	3.29	73	71
5	thioBU[6]	1005160	LOWGEL	6	Br ⁻	2.6	5.21	3.44	73	14
6	(<i>R,S</i>)-cycHC[6], CH ₂ Cl ₂	716121	OGUQEN	6	none	2.7	5.18	3.32	76	71
7	BnBU[6]	999880	WUPWUB	6	Cl ⁻	2.66	5.16	3.44	76	80
8	picolyliminiumBU[6]	1401302	ATUFOM	6	I ⁻	2.67	5.17	3.44	77	70
9	Biotin[6]uril	988132	JOBZUX	6	I ⁻	2.68, 2.52	4.98	3.64	77	49
10	(<i>R,S</i>)-cycHC[6], 2:1 CHCl ₃	716124	OGUQUD	6	none	2.71	5.1	3.37	78	71
11	(<i>R,S</i>)-cycHC[6], 2:1 CCl ₄	716123	OGUQOX	6	none	2.71	5.1	3.38	78	71
12	BnBU[6]	965535	SISCOO	6	H ₂ O & tosylates	2.69	5.15	3.49	80	82
13	AllylBU[6]	901486	LETGEY	6	I ⁻	2.7	5.14	3.50	80	13
14	PrBU[6] ^[c]	811118	IYONUG	6	I ⁻	2.78	5.23	3.44	83	12
15	Biotin[6]uril	994261	JOCBAG	6	EtOH	2.70, 3.01	4.95	3.69	85	49
16	BnBU[6]	953267	SISCI	6	H ₂ O & benzoates	2.23, 3.14	5.08	3.52	85	82
17	Biotin[6]uril	1029718	ZOXNOR	6	H ₂ O	2.97, 2.54	5.03	3.56	85	75
18	MeBU[6]	805141	IWEMED	6	Br ⁻	2.77	5.12	3.52	85	79
19	BnBU[6]	809242	IYONOA	6	H ₂ O & 2 Cl ⁻	2.77	5.07	3.58	86	12
20	HC[6]	235286	WAFHIV	6	propargyl alcohol	2.81	5.09	3.48	86	5
21	BnBU[6]	1419473	WUPXAI	6	SCN ⁻	2.75, 2.80	5.05	3.61	87	80
22	MeBU[6]	805140	IWEMAZ	6	I ⁻	2.82	5.1	3.52	88	79
23	MeBU[6]	1439451	YAKNUW	6	diethyl phosphate	2.83	4.95	3.64	91	83
24	MeBU[6]	805142	IWEMIH	6	BF ₄ ⁻	2.86	5.07	3.56	92	79
25	(<i>S,S</i>)-cycHC[6] ^[d]	945664	FIDVEV	6	none	2.96 (6ax) 3.23 (2ax)	5.03	8.15 ^[e]	N/A	72

^[a] The volume of the cavity was approximated to the volume of the cylindrical space ($V_{cylinder}$) between the two circular planes of the portal ethylene hydrogens. ^[b] Two values are given for the HC[6], where the two portals are significantly different in size. ^[c] One of the ethyleneurea hydrogens is missing from the crystal structure. ^[d] The radius of the ball-shaped cavity is measured as the average distance between the cavity centroid and the inwards facing 2ax and 6ax protons. ^[e] The cavity height is calculated between the two portal centroids of cycHC[6].

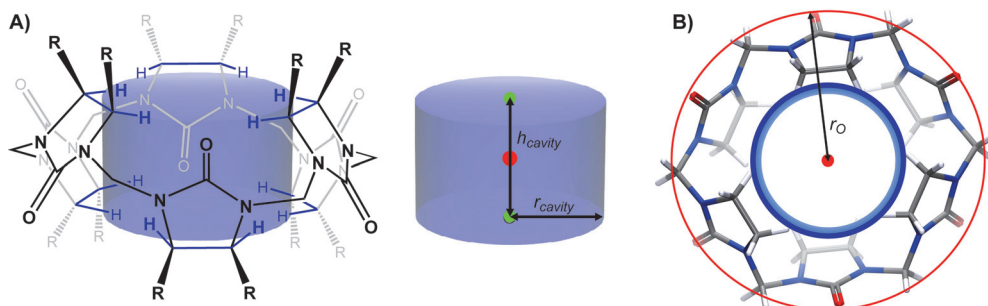


Figure 11. A) The chemical diagram of 6-membered substituted ((*R,S*)-isomer) or unsubstituted HCs, with the cylindrical cavity and the rimming ethylene hydrogens highlighted in blue. Centroids used in the measurements are represented by red (cavity centroid) and green dots (portal centroid). B) The crystal structure of HC[6] (CCDC 235284, from ref. [5]) showing the top view of the cylindrical cavity.

Neutral molecules such as water, ethanol or propargyl alcohol can also be bound inside hemicucurbit[6]urils.^[5,49,75] The portals to the central cavity are, in majority of the crystal structures, wide enough to allow the encapsulated anionic or neutral guest to interact with molecules outside the central cavity, thus forming quaternary complexes through additional binding sites at the portals of the HC[6]. Fascinating

exceptions to this are the crystal structures of I⁻@AllylBU[6], Cl⁻@BnBU[6] and SCN⁻@BnBU[6] complexes, where the *N*-allyl or *N*-benzyl substituents shield the portals on the core bambus[6]uril, thus fully isolating the guest anions from the surroundings (Figure 13).^[13,80]

A number of examples of quaternary complexes root from the complexation of anions too large to fit into the central

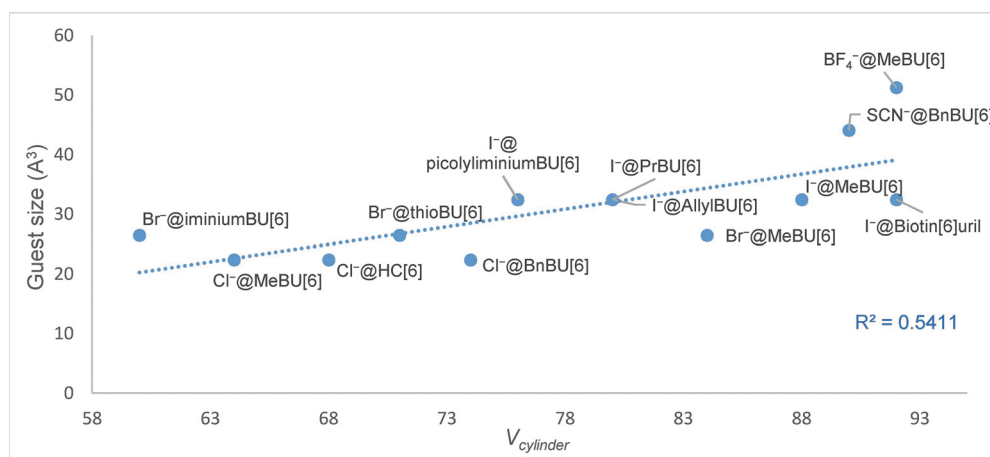


Figure 12. Correlation of the volume of the cavity of $\text{HC}[n]$ to the guest size. Anion volume is calculated using a triangulated sphere model (based corresponding crystal structure) through the Olex2 program package.^[81]

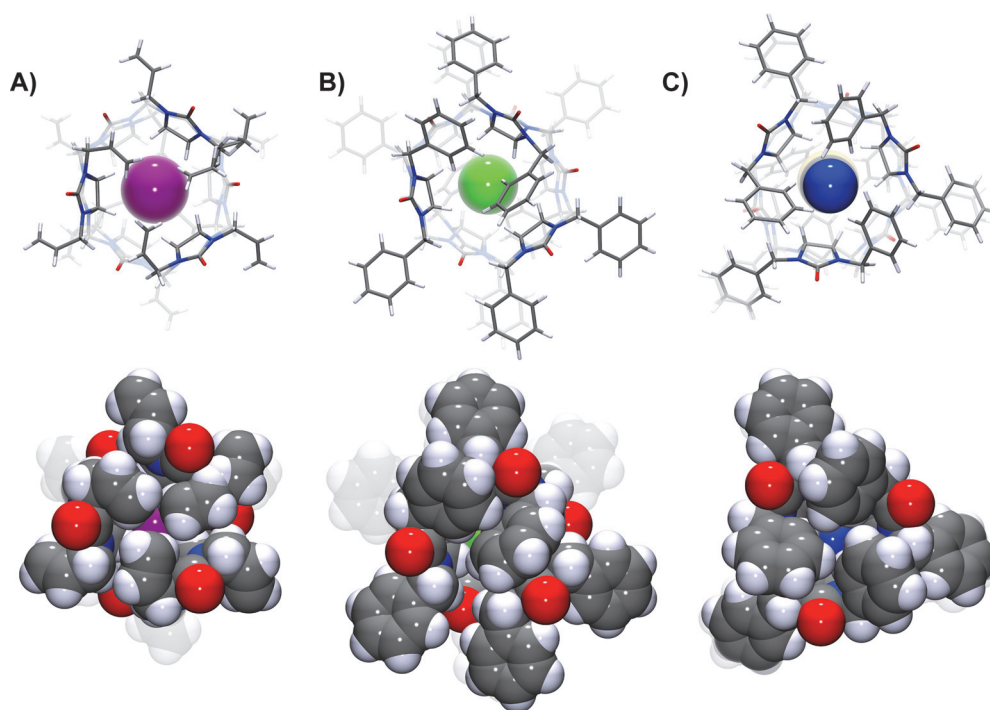


Figure 13. Top view of the stick and CPK representations of the crystal structures of A) $\text{AllyIBU}[6]$ iodide complex (CCDC 901486, from ref. [13]); B) $\text{BnBU}[6]$ chloride complex (CCDC 999880, from ref. [80]) and C) $\text{BnBU}[6]$ thiocyanate complex (CCDC 1419473, from ref. [79])

cavity of MeBU[6]s and BnBU[6]s. Benzoate, tosylate and diethyl phosphate occupy the binding sites close to the portals of the cavity, with a single trapped water molecule bridging the width of the cavity between the two anions (Figure 14, A, B and C).^[82,83] The water molecule in these structures is disordered between two positions. The resulting tertiary or quaternary complexes are further stabilized by hydrogen bonds between the guests and the portal hydrogens. Surprisingly, chloride anions are also able to form such quaternary complexes, upon crystallization of BnBU[6] and tetrabutylammonium chloride from chloroform in the presence of trace amounts of water (Figure 14, D).^[12]

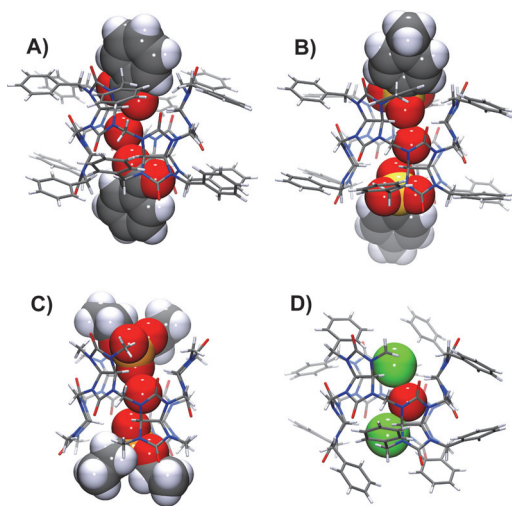


Figure 14. Water-mediated quaternary complexes of BnBU[6] with A) benzoate (CCDC 953267, from ref. [82]), B) tosylate (CCDC 965535, from ref. [82]) and D) chloride (CCDC 809242, from ref. [12]), and a similar MeBU[6] complex C) with diethylphosphate (CCDC 1439451, from ref. [83])

The guests in the two shallow binding pockets on the portals of the bambusuril, are inserted between the portal ethylene hydrogens. The dimensions of the cavity can therefore be affected by steric repulsion from bulky guests or by strong portal-to-guest interactions. BnBU[6], for example adopts a pronounced ellipsoidal shape in complex with benzoates,^[82] reflecting the flat shape of the guests.

Exceptional triple anion quaternary complexes are described for the positively charged picolyliumBU[6] host, where additionally to the iodide or bromide at the center of the cavity, two trifluoromethanesulfonate anions are located at the portal binding pockets.^[70]

The reported structures of (*R,S*)-cycHC[6] contain no resolved guest molecules within the cavity of the macrocycle.^[71] The dominating interactions involve hydrogen bond-

ing between the carbonyl groups and surrounding solvent molecules, or between neighbouring macrocycles, which in some solvent combinations leads to the formation of supramolecular cages potentially capable of accommodating large guest molecules.

The diastereomers of the latter, the (*S,S*)- or (*R,R*)-cycHC[*n*]^[15,72,74,84] are ball shaped hosts, contrasting to the cylindrical or bamboo stem shapes of the (*R,S*)-isomers. The cyclohexano groups on each side of the cycHC[*n*] lean together, creating a round cavity bordered by narrow portals. The cavity dimensions of (*S,S*)-cycHC[6] (Figure 15, A) and (*R,R*)-cycHC[8] (Figure 15, C) were measured as illustrated on Figure 15, B. The radius of the portal (r_{portal}) was measured as the average distance from the portal centroid to the portal-rimming hydrogens *4ax* and *5eq*; the cavity radius (r_{cavity}) was measured as the average distance from the cavity centroid to both the *2ax* and *6ax* hydrogens, as these extend furthest into the cavity of the cycHC[*n*] and cavity height (h_{cavity}) was measured as the distance between the centroids of opposite portals.

The crystal structure of (*S,S*)-cycHC[6] contains small isolated voids within the cavities of the macrocycles.^[72] Based on the lack of electron density in these voids,^[85] no guest molecules are encapsulated. The larger 8-membered homologue (*R,R*)-cycHC[8] on the other hand holds a cavity sufficiently large to encapsulate a variety of guest molecules (Figure 16).^[15,74] The guest anions are fixed within (*R,R*)-cycHC[8] through multiple C–H...anion host-guest interactions. Large octahedral anion SbF_6^- that ideally fits the size and shape of the (*R,R*)-cycHC[8] cavity is able to form sixteen simultaneous C–H...F hydrogen bonds.^[74] Smaller tetrahedral anions form fewer simultaneous hydrogen bonds to the host and are therefore disordered in the crystal structure.^[74]

Comparing the dimensions of (*R,R*)-cycHC[8] in all of its reported anion inclusion complexes, it transpires that the cavity size of (*R,R*)-cycHC[8] changes very little between the complexes with different anions (Table 6). Cavity radius r_{cavity} changes within the range of 0.047 Å (at *2ax* hydrogens) and 0.113 Å (at *6ax* hydrogens) and the portal radii r_{portal} varies in the range of 0.154 Å.

Regardless of the narrow flexibility window of r_{cavity} and r_{portal} these parameters appear to be correlated to the size of the bound anion, indicating that (*R,R*)-cycHC[8] does adapt to a small extent to the bound guest molecule (Figure 17). This effect is in the range of 5%, which is less prominent compared to the bambus[6]uril halide complexes, where the r_{cavity} of BU[6] changes from 2.55 Å in a Cl^- complex, to 2.77 Å in Br^- and 2.82 Å in I^- , corresponding to a 9.5% change

Whether the isostructurality of the anion inclusion complexes of (*R,R*)-cycHC[8] is caused by these insignificant changes in the shape of the host, or whether the isostructural packing of molecules causes the apparent rigidity of the host is a topic for further discussions.

The largest hemicucurbituril macrocycle synthesized and crystallized is the unique hemicucurbit[12]uril.^[15] The monomers of HC[12] seem to deviate from the alternate orientation in the crystal structure as there is less restrictions to the angle

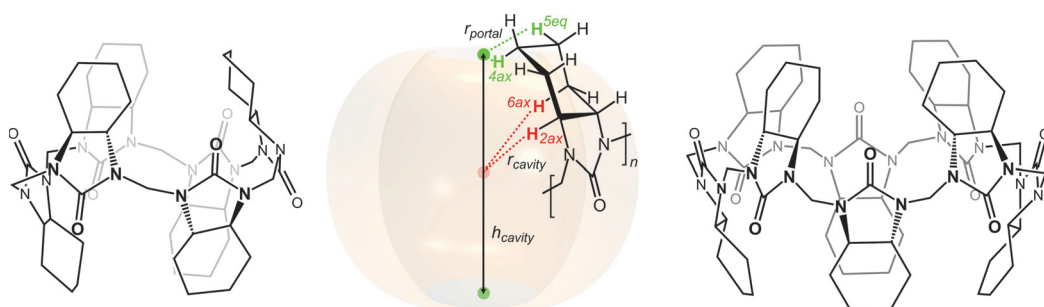


Figure 15. The structure of (*S,S*)-cycHC[6] (on the left) and (*R,R*)-cycHC[8] (on the right). Centroids used in the measurements are drawn as red (cavity centroid) and green dots (portal centroid) on a graphic representation of the ball-like cycHC[*n*] (center). A monomer of cycHC[*n*] is drawn on the graphic, to highlight the hydrogens *5eq* and *4ax* that rim the portals (green) and the hydrogens *2ax* and *6ax* that are located on the inside wall of the cavity.

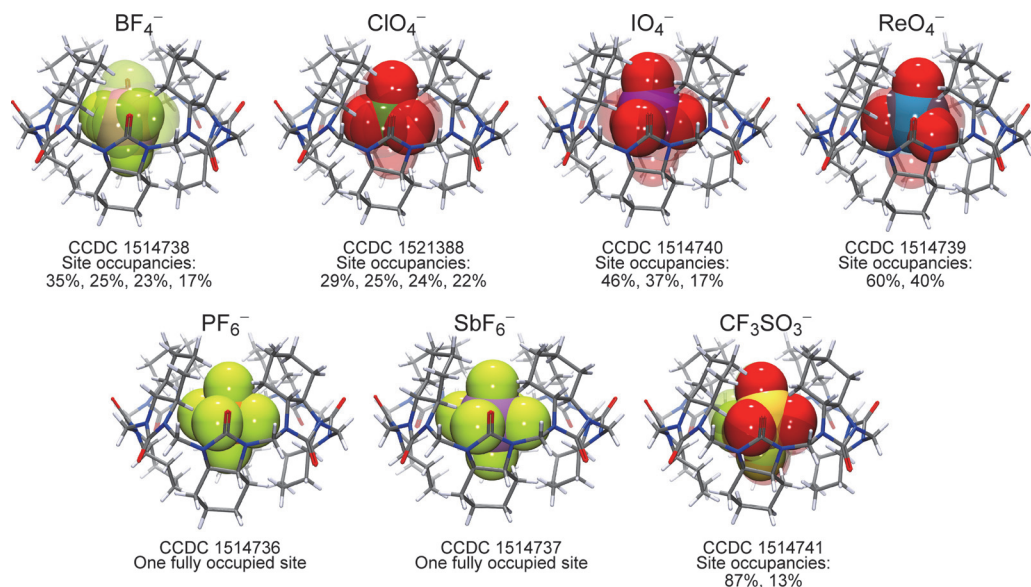


Figure 16. The position of anions in the host-guest complexes of (*R,R*)-cycHC[8] in the respective crystal structures [74]

at which the monomer can be tilted respective to the central axis of the macrocycle. HC[12] adopts an ellipsoidal form in the crystal structure of the chloroform clathrate, with two carbonyl groups of the closest monomers pointed into the central cavity (Figure 18).

6. Summary

The dynamic character of CBs is rooted in the reversible formation of its acylaminal linkers, which can be controlled

by external stimuli. Both the kinetic and thermodynamic template effects may influence the formation of the acylaminals, and it is evident that solubility equilibrium plays an important role in the chemistry of CBs. Thermodynamically favourable *C*-shape of oligomers preorganise the linear oligomers, which often leads to non-templated macrocyclisation. Nevertheless, in one-pot polymerisation reaction some CB family members can be prepared selectively and effectively through formation of 12 to 24 C–N bonds. According to our knowledge the experimental kinetic data on formation and cleavage of single acylaminal linker have not been explored.

Table 6. Comparison of the dimensions of cyclohexanohemicucurbit[8]uril in complex with different guest molecules.

Line no.	HC[8]	CCDC	CSD	<i>n</i>	guest	r_{cavity}	r_o	h_{cavity}	r_{portal}	Ref
1	(<i>R,R</i>)-cycHC[8]	1053111	QUMNIX	8	disordered MeOH ^[a]	3.669 (6ax), 4.316 (2ax)	6.615	7.619	3.271	15
2	(<i>R,R</i>)-cycHC[8]	1514736	ECADIY	8	PF ₆ ⁻	3.591 (6ax), 4.156 (2ax)	6.729	7.334	3.066	74
3	(<i>R,R</i>)-cycHC[8]	1514737	ECADOE	8	SbF ₆ ⁻	3.636 (6ax), 4.189 (2ax)	6.709	7.440	3.071	74
4	(<i>R,R</i>)-cycHC[8]	1514738	ECADUK	8	BF ₄ ⁻	3.566 (6ax), 4.145 (2ax)	6.733	7.287	2.985	74
5	(<i>R,R</i>)-cycHC[8]	1514739	ECAFAS	8	ReO ₄ ⁻	3.631 (6ax), 4.163 (2ax)	6.717	7.398	3.047	74
6	(<i>R,R</i>)-cycHC[8]	1514740	ECAFEE	8	IO ₄ ⁻	3.591 (6ax), 4.160 (2ax)	6.724	7.403	3.042	74
7	(<i>R,R</i>)-cycHC[8]	1514741	ECAFIA	8	CF ₃ SO ₃ ⁻	3.633 (6ax), 4.183 (2ax)	6.710	7.378	3.062	74
8	(<i>R,R</i>)-cycHC[8]	1521388	UBIBOZ	8	ClO ₄ ⁻	3.576 (6ax), 4.146 (2ax)	6.735	7.297	2.988	74

^[a] Void (123 Å³) at the cavity centre contains a diffuse methanol molecule, which is omitted from the structure using the Squeeze technique (Platon, [86]).

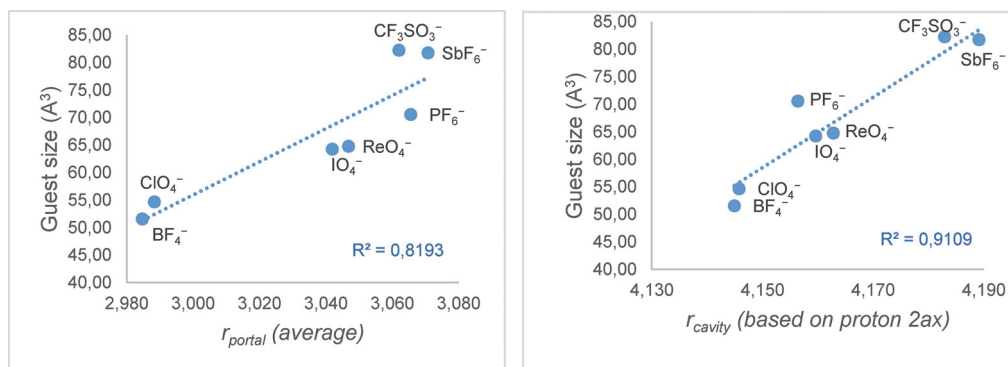


Figure 17. Correlation of the average portal radius (r_{portal}) of (*R,R*)-cycHC[8] to the guest size (left) and the correlation of the (*R,R*)-cycHC[8] cavity radius measured at the 2ax hydrogen (r_{cavity}) to the guest size (right). Anion volume is calculated using a triangulated sphere model (based corresponding crystal structure) through the Olex2 program package. [81]

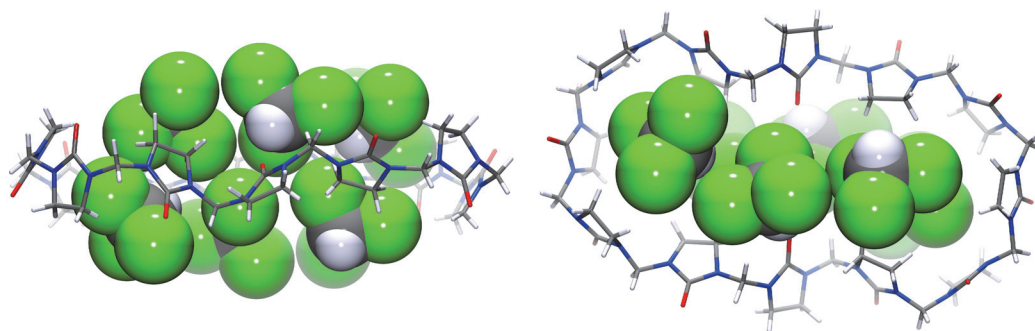


Figure 18. Side and top view of the HC[12] as seen in the crystal structure (CCDC 235287, from ref. [5])

Therefore further investigations may lead to improvement on understanding and eventually new outcomes in CB chemistry. The crystallographic analysis of hemicucurbiturils maps out the potential interactions of these macrocycles with templating compounds. The size of the encapsulated guest molecule is observed to have an effect on the cavity size of the HC[*n*]

host, indicating that HC[*n*]s are able to adapt to the size of the guest. Templates can affect distribution between formed double bridged CBs and moreover formation of singlebridged HCs can be controlled by a template with exceptional selectivity. Based on that one can envision further develop-

ment toward adaptable hosts, utilizing acylaminal linkage as a new tool.

Acknowledgement

Writing of this paper was supported the Estonian Ministry of Education and Research through Grant PUT692.

References

- [1] E. Masson, X. Ling, R. Joseph, L. Kyeremeh-Mensah, X. Lu, *RSC Adv.* **2012**, *2*, 1213–1247.
- [2] R. Aav, S. Kaabel, M. Fomitšenko, Cucurbiturils: Synthesis, Structures, Formation Mechanisms, and Nomenclature. In *Comprehensive Supramolecular Chemistry II* (Ed. J. L. Atwood), Elsevier, Oxford, **2017**, pp. 203–220.
- [3] W. Freeman, W. L. Mock, N.-Y. Y. Shih, *J. Am. Chem. Soc.* **1981**, *103*, 7367–7368.
- [4] A. Flinn, G. C. Hough, F. Stoddart, D. J. Williams, *Angew. Chem.* **1992**, *104*, 1550–1551.
- [5] Y. Miyahara, K. Goto, M. Oka, T. Inazu, *Angew. Chem. Int. Ed.* **2004**, *43*, 5019–5022.
- [6] The Nobel Prize in Chemistry 1987, awarded to Donald J. Cram, Jean-Marie Lehn and Charles J. Pedersen. The Nobel Prize in Chemistry 2016, awarded to Jean-Pierre Sauvage, Sir J. Fraser Stoddart and Bernard L. Feringa.
- [7] V. Martí-Centelles, M. D. Pandey, M. I. Burguete, S. V. Luis, *Chem. Rev.* **2015**, *115*, 8736–8834.
- [8] S. J. Rowan, S. J. Cantrill, G. R. L. Cousins, J. K. M. Sanders, J. F. Stoddart, *Angew. Chem., Int. Ed.* **2002**, *41*, 898–952.
- [9] P. T. Corbett, J. Leclaire, L. Vial, K. R. West, J. L. Wietor, J. K. M. Sanders, S. Otto, *Chem. Rev.* **2006**, *106*, 3652–3711.
- [10] Y. Jin, Q. Wang, P. Taynton, W. Zhang, *Acc. Chem. Res.* **2014**, *47*, 1575–1586.
- [11] A. Herrmann, *Chem. Soc. Rev.* **2014**, *43*, 1899–1933.
- [12] V. Havel, J. Svec, M. Wimmerova, M. Dusek, M. Pojarova, V. Sindelar, *Org. Lett.* **2011**, *13*, 4000–4003.
- [13] J. Rivollier, P. Thuéry, M. P. Heck, *Org. Lett.* **2013**, *15*, 480–483.
- [14] M. Singh, E. Solel, E. Keinan, O. Reany, *Chem. Eur. J.* **2015**, *21*, 536–540.
- [15] E. Prigorchenko, M. Öeren, S. Kaabel, M. Fomitšenko, I. Reile, I. Järving, T. Tamm, F. Topić, K. Rissanen, R. Aav, *Chem. Commun.* **2015**, *51*, 10921–10924.
- [16] M. E. Beliwich, J. F. Stoddart, *Chem. Soc. Rev.* **2012**, *41*, 2003–2024.
- [17] X. Su, I. Aprahamian, *Chem. Soc. Rev.* **2014**, *43*, 1963–1981; D. K. Kölmel, E. T. Koolm, *Chem. Rev.* **2017**, *117*, 10358–10376.
- [18] S. P. Black, J. K. M. Sanders, A. R. Stefankiewicz, *Chem. Soc. Rev.* **2014**, *43*, 1861–1872.
- [19] S. D. Bull, M. G. Davidson, J. M. H. van den Elsen, J. S. Fossey, A. T. A. Jenkins, Y.-B. Jiang, Y. Kubo, F. Marken, K. Sakurai, J. Zhao, T. D. James, *Acc. Chem. Res.* **2012**, *46*, 312–326.
- [20] M. Matache, E. Bogdan, N. D. Hädade, *Chem. Eur. J.* **2014**, *20*, 2106–2131.
- [21] G. Godin, B. Levrant, A. Trachsel, J.-M. Lehn, A. Herrmann, *Chem. Commun.* **2010**, *46*, 3125–3127.
- [22] B. Buchs, G. Godin, A. Trachsel, J.-Y. de Saint Laumer, J.-M. Lehn, A. Herrmann, *Eur. J. Org. Chem.* **2011**, 681–695.
- [23] H. H. Jo, R. Edupuganti, L. You, K. N. Dalby, E. V. Anslyn, *Chem. Sci.* **2015**, *6*, 158–164.
- [24] Y. Zhou, Y. Yuan, L. You, E. V. Anslyn, *Chem. Eur. J.* **2015**, *21*, 8207–8213.
- [25] L. You, S. R. Long, V. M. Lynch, E. V. Anslyn, *Chem. Eur. J.* **2011**, *17*, 11017–11023.
- [26] K. N. Dalby, W. P. Jencks, *J. Am. Chem. Soc.* **1997**, *119*, 7271–7280.
- [27] S. Eldin, J. A. Digits, S.-T. Huang, W. P. Jencks *J. Am. Chem. Soc.* **1995**, *117*, 6631–6632.
- [28] S. Eldin, W. P. Jencks *J. Am. Chem. Soc.* **1995**, *117*, 4851–4857.
- [29] I. K. Yoo, Y. K. Kang, *Chem. Phys. Lett.* **2017**, *669*, 92–98.
- [30] Y. Zhou, H. Ye, L. You, *J. Org. Chem.* **2015**, *80*, 2627–2633.
- [31] L. You, G. Pescitelli, E. V. Anslyn, L. Di Bari, *J. Am. Chem. Soc.* **2012**, *134*, 7117–7125.
- [32] L. You, J. S. Berman, E. V. Anslyn, *Nat. Chem.* **2011**, *3*, 943–948.
- [33] A. E. Rowan, J. A. A. W. Elemans, R. J. M. Nolte, *Acc. Chem. Res.* **1999**, *32*, 995–1006.
- [34] R. J. Jansen, R. de Gelder, A. E. Rowan, H. W. Scheeren, R. J. M. Nolte, *J. Org. Chem.* **2001**, *66*, 2643–2653.
- [35] M. Öeren, E. Shmatova, T. Tamm, R. Aav, *Phys. Chem. Chem. Phys.* **2014**, *16*, 19198–19205.
- [36] A. Day, A. P. Arnold, R. J. Blanch, B. Snushall, *J. Org. Chem.* **2001**, *66*, 8094–8100.
- [37] H. Jacobson, W. H. J. Stockmayer, *Chem. Phys.* **1950**, *18*, 1600–1606.
- [38] G. Ercolani, L. Mandolini, P. Mencarelli, S. Roelens, *J. Am. Chem. Soc.* **1993**, *115*, 3901–3908.
- [39] L. Isaacs, S.-K. Park, S. Liu, Y. H. Ko, N. Selvapalam, Y. Kim, H. Kim, P. Y. Zavalij, G.-H. Kim, H.-S. Lee, K. Kim, *J. Am. Chem. Soc.* **2005**, *8*, 18000–18001.
- [40] W.-H. Huang, P. Y. Zavalij, L. Isaacs, *J. Am. Chem. Soc.* **2008**, *130*, 8446–8454.
- [41] A. Chakraborty, A. Wu, D. Witt, J. Lagona, J. C. Fettinger, L. Isaacs, *J. Am. Chem. Soc.* **2002**, *124*, 8297–8306.
- [42] D. Lucas, T. Minami, G. Iannuzzi, L. Cao, J. B. Wittenberg, P. Anzenbacher, L. Isaacs, *J. Am. Chem. Soc.* **2011**, *133*, 17966–17976.
- [43] B. Vinciguerra, L. Cao, J. R. Cannon, P. Y. Zavalij, C. Fenselau, L. Isaacs, *J. Am. Chem. Soc.* **2012**, *134*, 13133–13140.
- [44] L. Cao, G. Hettiarachchi, V. Briken, L. Isaacs, *Angew. Chem. Int. Ed.* **2013**, *52*, 12033–12037.
- [45] Y. Yu, J. Li, M. Zhang, L. Cao, L. Isaacs, *Chem. Commun.* **2015**, *51*, 3762–3765.
- [46] J. B. Wittenberg, P. Y. Zavalij, L. Isaacs, *Angew. Chem. Int. Ed.* **2013**, *52*, 3690–3694.
- [47] L. Gilberg, M. S. Khan, M. Enderesova, V. Sindelar, *Org. Lett.* **2014**, *16*, 2446–2449.
- [48] B. Vinciguerra, P. Y. Zavalij, L. Isaacs, *Org. Lett.* **2015**, *17*, 5068–5071.
- [49] M. Lisbjerg, B. M. Jessen, B. Rasmussen, B. E. Nielsen, A. Ø. Madsen, M. Pittelkow, *Chem. Sci.* **2014**, *5*, 2591–2908.
- [50] M. Fomitšenko, A. Peterson, I. Reile, H. Cong, S. Kaabel, E. Prigorchenko, I. Järving, R. Aav, *New J. Chem.* **2017**, *41*, 2490–2497.
- [51] P. Ruggli, *Liebigs Ann. Chem.* **1912**, *392*, 92–100.
- [52] M. C. Thompson, D. H. Busch, *J. Am. Chem. Soc.* **1964**, *86*, 213–217.
- [53] S. Anderson, H. L. Anderson, J. K. M. Sanders, *Acc. Chem. Res.* **1993**, *26*, 469–475.
- [54] T. F. G. G. Cova, S. C. C. Nunes, A. J. M. Valente, T. M. V. D. Pinho e Melo, A. A. C. C. Pais, *J. Mol. Liq.* **2017**, *242*, 640–652.

- [55] S. J. Barrow, S. Kaser, M. J. Rowland, J. Del Barrio, O. A. Scherman, *Chem. Rev.* **2015**, *115*, 12320–12406.
- [56] K. S. Oh, J. Yoon, K. S. Kim, *J. Phys. Chem. B.* **2001**, *105*, 9726–9731.
- [57] A. I. Day, R. J. Blanch, A. Coe, A. P. J. Arnold, *Incl. Phenom. Macrocycl. Chem.* **2002**, *43*, 247–250.
- [58] A. I. Day, R. J. Blanch, A. P. Arnold, S. Lorenzo, G. R. Lewis, I. Dance, *Angew. Chem. Int. Ed.* **2002**, *41*, 275–277.
- [59] S. Liu, P. Y. Zavalij, L. Isaacs, *J. Am. Chem. Soc.* **2005**, *127*, 16798–16799.
- [60] Y.-Q. Yao, Q. Liu, Y. Huang, Q.-J. Zhu, Y.-Q. Zhang, X. Xiao, Z. Tao, G. Wei, *Aust. J. Chem.* **2017**, *70*, 637–641.
- [61] R. J. Blanch, A. J. Sleeman, T. J. White, A. P. Arnold, A. I. Day, *Nano Lett.* **2002**, *2*, 147–149.
- [62] Y. Miyahara, K. Abe, T. Inazu, *Angew. Chem. Int. Ed.* **2002**, *41*, 3020–3023.
- [63] F. Wu, L.-H. Wu, X. Xiao, Y.-Q. Zhang, S. F. Xue, Z. Tao, A. I. Day, *J. Org. Chem.* **2012**, *77*, 606–611.
- [64] L. Ustrnul, P. Kulhanek, T. Lizal, V. Sindelar, *Org. Lett.* **2015**, *17*, 1022–1025.
- [65] X. Jiang, X. Yao, X. Huang, Q. Wang, H. Tian, *Chem. Commun.* **2015**, *51*, 2890–2892.
- [66] Y. Wu, L. Xu, Y. Shen, Y. Wang, L. Zou, Q. Wang, X. Jiang, J. Liu, H. Tian *Chem. Commun.* **2017**, *53*, 4070–4072.
- [67] Y. Shen, L. Zou, Q. Wang, *New J. Chem.* **2017**, *41*, 7857–7860.
- [68] J. Svec, M. Necas, V. Sindelar, *Angew. Chem., Int. Ed.* **2010**, *49*, pp 2378–2381.
- [69] M. A. Yawer, V. Havel, V. Sindelar, *Angew. Chem. Int. Ed.* **2015**, *54*, 276–279.
- [70] M. Singh, E. Solel, E. Keinan, O. Reany, *Chem. Eur. J.* **2016**, *22*, 8848–8854.
- [71] Y. Li, L. Li, Y. Zhu, X. Meng, A. Wu, *Cryst. Growth Des.* **2009**, *9*, 4255–4257.
- [72] R. Aav, E. Shmatova, I. Reile, M. Borissova, F. Topić, K. Rissanen, *Org. Lett.* **2013**, *15*, 3786–3789.
- [73] T. Fiala, V. Sindelar, *Synlett.* **2013**, *24*, 2443–2445.
- [74] S. Kaabel, J. Adamson, F. Topić, A. Kiesilä, E. Kalenius, M. Öeren, M. Reimund, E. Prigorchenko, A. Löökene, H. J. Reich, K. Rissanen, R. Aav, *Chem. Sci.*, **2017**, *8*, 2184–2190.
- [75] M. Lisbjerg, B. E. Nielsen, B. O. Milhøj, S. P. A. Sauer, M. Pittelkow, *Org. Biomol. Chem.* **2015**, *13*, 369–373.
- [76] H.-J. Buschmann, A. Zielesny, *Comput. Theor. Chem.* **2013**, *1022*, 14–22.
- [77] T. Lizal, L. Ustrnul, M. Necas, V. Sindelar *J. Org. Chem.* **2016**, *81*, 8906–8910.
- [78] X.-L. Ni, X. Xiao, H. Cong, L.-L. Liang, K. Cheng, X.-J. Cheng, N.-N. Ji, Q.-J. Zhu, S.-F. Xue, Z. Tao, *Chem. Soc. Rev.* **2013**, *42*, 9480–9508.
- [79] J. Svec, M. Dusek, K. Fejfarova, P. Stacko, P. Klan, A. E. Kaifer, W. Li, E. Hudeckova, V. Sindelar. *Chem. Eur. J.* **2011**, *17*, 5605–5612.
- [80] V. Havel, V. Sindelar, *ChemPlusChem.* **2015**, *80*, 1601–1606.
- [81] O. V. Dolomanov, L. J. Bourhis, R. J. Gildea, J. A. K. Howard, H.-J. Puschmann, *J. Appl. Crystallogr.* **2009**, *42*, 339–341.
- [82] V. Havel, V. Sindelar, M. Necas, A. E. Kaifer, *Chem. Commun.* **2014**, *50*, 1372–1374
- [83] T. Fiala, V. Sindelar, *Supramol. Chem.* **2016**, *28*, 810–816.
- [84] M. Fomitsenko, E. Shmatova, M. Öeren, I. Järving, R. Aav, *Supramol. Chem.* **2014**, *26*, 698–703.
- [85] The electron density in the voids was determined by running the PLATON (A. L. Spek, *Acta Cryst.* **2009**, *D56*, 148–155) void calculation algorithm on the CIF file of the crystal structure of the cycHC[6] (CCDC 945664, from ref. 72)
- [86] A. L. Spek, *Acta Cryst.* **2015**, *C71*, 9–18.

Received: September 15, 2017

Accepted: November 18, 2017

Published online on December 12, 2017

Publication IV

S. Kabel, R. S. Stein, M. Fomitšenko, I. Järving, T. Friščić, R. Aav, 'Size-control by anion templating in mechanochemical synthesis of hemicucurbiturils in the solid state,' **2018**, *submitted to a peer-reviewed journal, manuscript available from ChemRxiv doi: 10.26434/chemrxiv.7376489.v1.*

APPENDIX 2

Optimized geometries of the anions

SbF_6^-

7			
Sb	-0.4401731	0.0054092	-0.0000003
F	-1.3120043	1.0687484	1.3533347
F	0.4316657	-1.0579331	-1.3533339
F	-1.3203380	1.0327580	-1.3754023
F	0.4399993	-1.0219381	1.3754032
F	1.0423274	1.2394840	-0.0204354
F	-1.9226662	-1.2286684	0.0204341

PF_6^-

7			
P	-0.4401702	0.0054086	0.0000000
F	-1.1827590	0.9137292	1.1544302
F	0.3024197	-0.9029115	-1.1544300
F	-1.1897347	0.8830807	-1.1732524
F	0.3093949	-0.8722638	1.1732520
F	0.8229787	1.0600731	-0.0175498
F	-1.7033186	-1.0492562	0.0175500

ReO_4^-

5			
Re	-0.9075448	-0.0287095	0.2737279
O	-1.4558000	1.1176228	1.4819247
O	-0.6893959	0.7942371	-1.2591058
O	0.6163402	-0.7315202	0.7829310
O	-2.1048082	-1.2956902	0.0877219

IO_4^-

5			
I	-0.0001446	-0.0003511	0.0004845
O	0.5566575	1.2992939	1.0248908
O	0.3383899	0.3881185	-1.6677479
O	0.8257720	-1.4770700	0.4313868
O	-1.7206826	-0.2099946	0.2109895

ClO_4^-

5			
Cl	-0.9080835	-0.0288068	0.2735734
O	-1.3690348	0.9370914	1.2911480
O	-0.7235469	0.6648033	-1.0170977
O	0.3753925	-0.6205793	0.7023818
O	-1.9159361	-1.0965685	0.1171940

BF_4^-

5			
B	-0.9082447	-0.0288106	0.2734406
F	-1.3419092	0.8808757	1.2312203
F	-0.7341527	0.6247624	-0.9412476

F	0.2997884	-0.5861813	0.6771005
F	-1.8566906	-1.0347062	0.1266858

CF_3SO_3^-

8			
C	-2.5755426	0.5538750	-0.2519256
F	-3.0043967	1.5921206	-1.0273491
F	-3.4296568	0.4774810	0.8100455
F	-2.7556671	-0.5842197	-0.9839070
S	-0.7724660	0.7731359	0.2961695
O	-0.8361708	2.0099953	1.0860408
O	-0.0694021	0.8747281	-0.9897391
O	-0.5271040	-0.4571276	1.0606750

CF_3CO_2^-

7			
C	-2.4860785	0.6382439	-0.2652717
F	-3.1110498	1.5911564	-1.0471799
F	-3.2816165	0.4909716	0.8437609
F	-2.6037945	-0.5423536	-0.9557057
C	-0.9783923	1.0646826	0.0567829
O	-0.8645475	1.7476550	1.0979349
O	-0.1576370	0.6782224	-0.8045012

CH_3CO_2^-

7			
O	8.79460	4.99453	-1.18371
O	7.84141	4.97473	0.79911
C	7.77997	5.00610	-0.45453
C	6.44191	5.06470	-1.13433
H	6.56794	5.08315	-2.09897
H	5.91917	4.28079	-0.89048
H	5.97066	5.86822	-0.85326

HCO_2^-

4			
C	0.00000	2.72285	1.75600
O	1.11360	2.16601	1.75600
H	0.00000	3.68726	1.75600
O	-1.11383	2.16590	1.75600

SO_4^{2-}

5			
S	6.78101	3.29083	9.67115
O	7.53583	2.06888	9.34991
O	6.38942	3.28196	11.08389
O	7.60424	4.47820	9.42143
O	5.56767	3.35630	8.84076

APPENDIX 3

Crystallographic data for the unpublished crystal structures

Single crystal X-ray diffraction data was collected on Agilent SuperNova Dual diffractometer, equipped with an Atlas detector and an Oxford Cryostream cooling system, using mirror-monochromatized Cu- $K\alpha$ radiation (1.54178 Å). *CrysAlisPro*^[A1] was used for data collection, processing and for applying numerical absorption correction.^[A2] Structures were solved using *SHELXT*.^[A3] The structures were refined by full matrix least-squares method against F^2 with *SHELXL-2016*^[A4] through *WinGX*^[A5] and *OLEX2*^[A6] program packages. All non-hydrogen atoms were refined with anisotropic atomic displacement parameters, hydrogen atoms were calculated to their optimal positions and treated as riding on their parent carbon and oxygen atoms, with $U_{\text{iso}}(\text{H}) = 1.2U_{\text{iso}}(\text{C})$ for CH and CH₂. Appropriate restraints were applied to the geometry and atomic displacement parameters of the atoms throughout the structures. Namely, SIMU restrains on the anisotropic displacement parameters of the two components of the cyclohexano-group disorder in K(PF₆@cycHC[8]), and SADI restraints on the bond distances of these disorder components were applied. RIGU restraints were applied to the anisotropic displacement parameters throughout the structure. The figures were drawn using the programs Mercury^[A7] and POV-Ray.^[A8]

Refinement details for K(PF₆@cycHC[8])

The position of two potassium ions was located from the electron density map, based on the highest residual electron density peaks (4.8 e⁻ Å⁻³ and 3.96 e⁻ Å⁻³) and refined with *s.o.f.* 0.5 each (Figure A1). Attempts to refine the position of the solvent molecules and the remaining potassium ion disorder components (sum of *s.o.f.* 1) were unsuccessful. The highest residual electron density at peaks 2.7 – 2.8 Å from the carbonyl groups (Table A3) reflect the positional disorder between hydrogen bonded methanol molecules and potassium ions, which could not be modelled accurately. One of the cyclohexano-groups of cycHC[8] was modelled in two disorder components (*s.o.f.* 0.612(17)/0.388(12)).

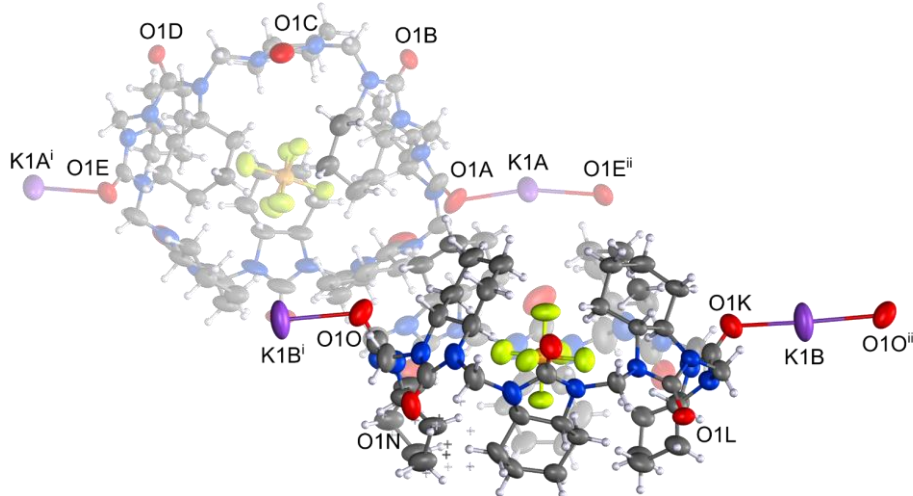


Figure A1. The asymmetric unit in the crystal structure of K(PF₆@cycHC[8]), showing the position of the encapsulated PF₆⁻ anions and the potassium ions between the filled molecular capsules. The anisotropic displacement ellipsoids are drawn at a 50% probability level. Symmetry codes: i) $x, 1 + y, z$; ii) $x, -1 + y, z$.

Table A1. Crystallographic data for the inclusion complex of $K(\text{PF}_6@ \text{cycHC}[8])$. Data for the model (Figure A1) both before and after running the SQUEEZE procedure is presented. The solvent accessible voids determined by SQUEEZE are listed in Table A2. Highest residual electron density peaks in the dataset before the SQUEEZE procedure (left) are compiled in Table A3.

K(PF₆@cycHC[8])		
Empirical formula	C ₁₂₈ H ₁₉₂ F ₁₂ K ₁ N ₃₂ O ₁₆ P ₂	
Formula weight	2783.71	
Temperature/K	123.00(10)	
Crystal system	monoclinic	
Space group	C2	
<i>a</i> /Å	49.6606(8)	
<i>b</i> /Å	18.8972(2)	
<i>c</i> /Å	22.1724(3)	
α /°	90	
β /°	124.956(2)	
γ /°	90	
Volume/Å ³	17053.7(6)	
<i>Z</i>	4	
<i>D</i> _{calc} /g cm ⁻³	1.084	
μ /mm ⁻¹	1.170	
Crystal size/mm ³	0.4615 × 0.3297 × 0.1408	
Shape and colour of cryst.	colourless, block	
Crystalliz. solvent	methanol	
Radiation	Cu <i>K</i> α (λ = 1.54184)	
2 θ range for data collection/°	6.176 to 149.238	
Index ranges	-61 ≤ <i>h</i> ≤ 54, -23 ≤ <i>k</i> ≤ 23, -27 ≤ <i>l</i> ≤ 27	
Reflections collected	77808	
Independent reflections	33120 [<i>R</i> _{int} = 0.0188, <i>R</i> _{sigma} = 0.0213]	
Dataset:	Before SQUEEZE	After SQUEEZE
Data/restraints/parameters	33120/1851/1769	33120/1855/1769
Goodness-of-fit on <i>F</i> ²	2.249	1.367
Final <i>R</i> indexes [<i>I</i> ≥ 2 σ (<i>I</i>)]	<i>R</i> ₁ = 0.1738, <i>wR</i> ₂ = 0.4401	<i>R</i> ₁ = 0.0925, <i>wR</i> ₂ = 0.2784
Final <i>R</i> indexes [all data]	<i>R</i> ₁ = 0.1770, <i>wR</i> ₂ = 0.4490	<i>R</i> ₁ = 0.0952, <i>wR</i> ₂ = 0.2879
Largest diff. peak/hole / e Å ⁻³	3.83/-0.64	2.63/-0.47
Flack parameter <i>x</i>	0.095(6)	0.057(5)

Table A2. Solvent accessible voids (probe radius 1.2 Å, grid step 0.2 Å) determined by SQUEEZE procedure, containing the disordered solvent (methanol) molecules and the remaining unresolved *K* disorder components. The coordinates of the voids are given as an average over the extent of the void.

Void no.	<i>x</i>	<i>y</i>	<i>z</i>	Void volume (Å ³)	e ⁻ count
1	0.000	-0.217	0.500	219	55
2	0.000	-0.203	0.000	1596	499
3	0.500	0.297	1.000	1596	499
4	0.500	0.283	0.500	219	55

Table A3. The highest residual electron density peaks in the dataset before running the SQUEEZE procedure, which reflect the position of disordered hydrogen bonded methanol molecules and potassium ions.

Q peak	$e^- \text{ \AA}^{-3}$	Closest to	Distance to the closest atom (\AA)
1	3.83	O1B	2.74
2	3.14	O1I	2.76 (1.83 from K1A)
3	3.07	O1M	2.71 (2.64 from K1A)
4	3.00	O1G	2.72
5	2.71	O1N	2.74
6	2.52	O1L	2.68
7	2.41	O1H	2.66
8	2.40	H1A	2.64
9	2.34	O1P	2.84
10	2.20	K1A	2.59

Refinement details for Na(SbF₆@cycHC[8])

The position of the sodium ions was modelled over four positions, located based on the highest residual electron density peaks (4.8, 4.14, 3.69 and 3.02 $e^- \text{ \AA}^{-3}$) and refined with fixed *s.o.f.* 0.5 (Figure A2). The highest remaining residual electron density at peaks 2.7 – 2.8 \AA from the carbonyl groups (Table A2) reflect the disordered hydrogen bonded methanol molecules, which could not be modelled accurately.

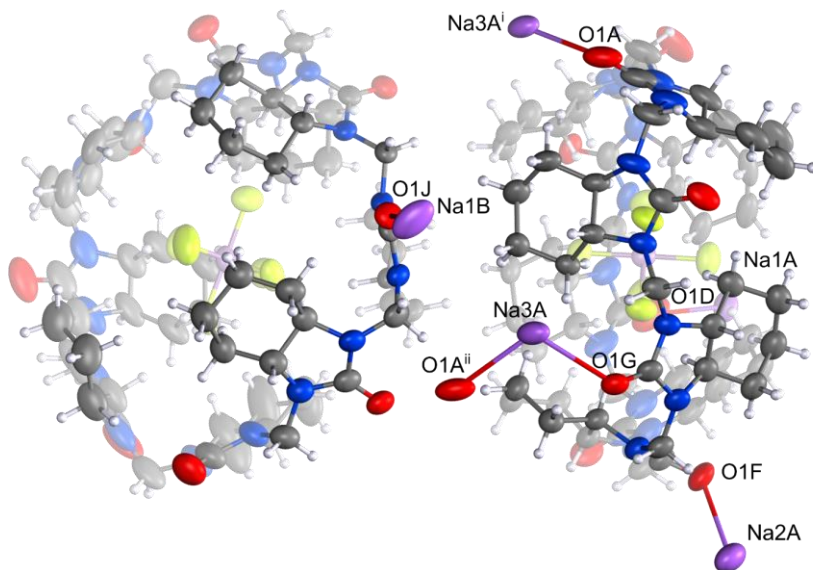


Figure A2. The asymmetric unit in the crystal structure of Na(SbF₆@cycHC[8]), showing the position of the encapsulated SbF₆⁻ anions and the sodium ions (*s.o.f.* 0.5 each) between the filled molecular capsules. The anisotropic displacement ellipsoids are drawn at a 50% probability level. Symmetry codes: i) 1.5 - x, 0.5 + y, 1.5 - z; ii) 1.5 - x, -0.5 + y, 1.5 - z.

Table A2. Crystallographic data for the inclusion complex of Na(SbF₆@cycHC[8]). Data for the model (Figure A2) both before and after running the SQUEEZE procedure is presented. The solvent accessible voids determined by SQUEEZE are listed in Table A5. Highest residual electron density peaks in the dataset before the SQUEEZE procedure (left) are compiled in Table A6.

Na(SbF₆@cycHC[8])		
Empirical formula	C ₆₄ H ₉₆ F ₆ N ₁₆ NaO ₈ Sb	
Formula weight	1476.30	
Temperature/K	123.01(10)	
Crystal system	monoclinic	
Space group	I2	
a/Å	22.29786(17)	
b/Å	18.91742(17)	
c/Å	41.3649(3)	
α/°	90	
β/°	98.8036(8)	
γ/°	90	
Volume/Å ³	17242.9(2)	
Z	8	
D _{calc} /g cm ⁻³	1.137	
μ/mm ⁻¹	3.138	
Crystal size/mm ³	0.2198 × 0.1848 × 0.1133	
Shape and colour of cryst.	colourless, block	
Crystalliz. solvent	methanol	
Radiation	Cu Kα (λ = 1.54184)	
2θ range for data collection/°	6.158 to 147.014	
Index ranges	-26 ≤ h ≤ 27, -23 ≤ k ≤ 22, -49 ≤ l ≤ 51	
Reflections collected	79079	
Independent reflections	33117 [R _{int} = 0.0245, R _{sigma} = 0.0285]	
Dataset:	Before SQUEEZE	After SQUEEZE
Data/restraints/parameters	33117/1699/1747	33117/1699/1747
Goodness-of-fit on F ²	1.303	1.035
Final R indexes [I ≥ 2σ (I)]	R ₁ = 0.0911, wR ₂ = 0.2637	R ₁ = 0.0452, wR ₂ = 0.1303
Final R indexes [all data]	R ₁ = 0.0945, wR ₂ = 0.2741	R ₁ = 0.0483, wR ₂ = 0.1351
Largest diff. peak/hole / e Å ⁻³	2.73/-0.92	1.95/-0.72
Flack parameter x	-0.001(2)	-0.0075(16)

Table A5. Solvent accessible voids (probe radius 1.2 Å, grid step 0.2 Å) in the unit cell of Na(SbF₆@cycHC[8]) determined by SQUEEZE procedure, containing the disordered solvent (methanol) molecules. The coordinates of the voids are given as an average over the extent of the void.

Void no.	x	y	z	Void volume (Å ³)	e ⁻ count
1	0.000	-0.128	0.000	1922	597
2	0.998	0.372	0.500	1922	597

Table A6. The highest residual electron density peaks in the dataset before running the SQUEEZE procedure, which mainly reflect the position of disordered hydrogen bonded methanol molecules.

Q peak	$e^- \text{ \AA}^{-3}$	Closest to	Distance to the closest atom (\AA)
1	2.73	O1K	2.72
2	2.63	O1I	2.75
3	2.59	Na1A	1.97
4	2.53	O1B	2.81
5	2.49	O1C	2.74
6	2.48	O1B	2.70
7	2.42	O1O	2.77
8	2.15	O1E	2.63
9	2.09	O1H	2.78
10	2.08	Na1A	2.78

Appendix 3 References

- A1 *CrysAlisPro*, **2014**, Agilent Technologies. Version 1.171.38.41
- A2 R. C. Clark, J. S. Reid, *Acta Crystallogr.* **1995**, *A51*, 887–897.
- A3 G. M. Sheldrick, *Acta Crystallogr.* **2015**, *A71*, 3–8.
- A4 G. M. Sheldrick, *Acta Crystallogr.* **2008**, *D64*, 112–122.
- A5 L. J. Farrugia, *J. Appl. Cryst.* **2012**, *45*, 849–854.
- A6 O. V. Dolomanov, L. J. Bourhis, R. J. Gildea, J. A. K. Howard, H.-J. Puschmann, *J. Appl. Crystallogr.* **2009**, *42*, 339–341.
- A7 C. F. Macrae, P. R. Edgington, P. McCabe, E. Pidcock, G. P. Shields, R. Taylor, M. Towler, J. van de Streek, *J. Appl. Crystallogr.* **2006**, *39*, 453–457.
- A8 *Persistence of Vision (TM) Raytracer*; Persistence of Vision Pty. Ltd.: Williamstown, Victoria, Australia, **2004**.

AUTHOR'S CONFERENCE PRESENTATIONS

Oral presentations

1. 'Template-driven self-assembly of hemicucurbit[n]uril macrocycles in the solid state.' *The 5th Crystal Engineering and Emerging Materials Workshop of Ontario and Quebec (CEMWOQ-5), Montreal, Canada, 16.–19.08.2018.*
2. 'Template-driven assembly of hemicucurbit[n]uril macrocycles in the solid state.' *The German-Polish-Baltic Conference on Organic Chemistry, Hamburg, Germany, 15.–19.04.2018.*
3. 'Cyclohexylhemicucurbit[8]uril: a chiral macrocyclic host for anionic guests.' *The 29th European Crystallographic Meeting (ECM29), Young Crystallographers' Satellite Meeting, Rovinj, Croatia, 23.08.2015.*

Poster presentations

1. 'Templated assembly of hemicucurbit[n]uril macrocycles in the solid state.' *International Symposium on Macrocyclic and Supramolecular Chemistry (ISMSC 2018), Quebec City, Canada, 8.–13.08.2018.*
2. 'Template-driven assembly of hemicucurbit[n]uril macrocycles in the solid state.' *Gordon Research Conference on Crystal Engineering (GRC), Newry, Maine, USA, 24.–29.06.2018.*
3. 'Binding of anionic and neutral guests by different homologues and stereoisomers of cyclohexanohemicucurbiturils.' *International Symposium on Macrocyclic and Supramolecular Chemistry (ISMSC 2017), Cambridge, United Kingdom, 2.–6.08.2017.*
4. 'Complexation of Anionic and Neutral Guests to Cyclohexanohemicucurbit[8]uril.' *The 5th International Conference on Cucurbiturils (ICCB 2017), Brno, Czech Republic, 27.–30.06.2017.*
5. 'Host-Guest Complexes with a Chiral Hemicucurbit[8]uril.' *23rd International Conference on the Chemistry of the Organic Solid State (ICCOSS-XXIII), Stellenbosch, South Africa, 2.–7.04.2017.*
6. 'Host-Guest Complexes with a Chiral Hemicucurbit[8]uril.' *Scientific Conference of the Functional Materials and Technologies graduate school, Tartu, Estonia, 7.–8.03.2017.*
7. 'Crystallographic study of cyclohexanohemicucurbit[n]urils and their complexes.' *3rd European Crystallography School (ECS3), Bol, Croatia, 25.09.–2.10.2016.*
8. 'Cyclohexanohemicucurbit[8]uril – a Neutral Host for Anionic Guests.' *11th International Symposium on Macrocyclic and Supramolecular Chemistry (ISMSC 2016), Seoul, Korea, 11.–14.08.2016.*
9. 'Cyclohexanohemicucurbit[8]uril – a neutral host for anionic guest.' *Balticum Organicum Syntheticum (BOS 2016), Riga, Latvia, 3.–6.08.2016.*
10. 'Cyclohexylhemicucurbit[8]uril: a chiral macrocyclic host for anionic guests' *The 29th European Crystallographic Meeting (ECM29), Rovinj, Croatia, 23.–28.08.2015. Acta Cryst., 2015, A71, s474.*

CURRICULUM VITAE

Personal data

Name: Sandra Kaabel
Date of birth: 03.12.1989
Place of birth: Tallinn, Estonia
Citizenship: Estonian

Contact data

E-mail: sandra.kaabel@taltech.ee

Education and degrees awarded

2014 – ... **Ph.D.**, Tallinn University of Technology, Department of Chemistry and Biotechnology
2012 – 2014 **M.Sc. (*cum laude*)**, Tallinn University of Technology, Department of Chemistry
2009 – 2012 **B.Sc.**, Tallinn University of Technology, Department of Chemistry
1997 – 2009 Viimsi Keskkool

International research experience

Aug 2017 – Mar 2018 Visiting Ph.D. student in Prof. Tomislav Friščić's group, Department of Chemistry, McGill University, Canada
Nov 2014 – Apr 2015 Visiting Ph.D. student in Prof. Kari Rissanen's group, Department of Chemistry, University of Jyväskylä, Finland

International studies

Sept 2012 – May 2013 Study exchange, Chalmers University of Technology, Sweden

Language competence

Estonian Native
English Fluent
Finnish Beginner

Professional employment

2017 – ... Tallinn University of Technology, Department of Chemistry and Biotechnology, Ph.D. Student and Early Stage Researcher

Professional associations

2014 – ... European Crystallographic Association, Individual Member
2017 – ... Royal Society of Chemistry, Associate Member

Honors and awards

2018, Poster Prize, GRC on Crystal Engineering, Newry, Maine, USA
2018, Synthesis Best Paper Award 2017 - Kriis, *et al.*, *Synthesis* **2017**, 49, 604–614.
2016, Tallinn University of Technology Research Article of the Year 2016 in natural, exact and health sciences - Kaabel *et al.*, *Chem. Sci.* **2017**, 8, 2184–2190.
2016, *Organic & Biomolecular Chemistry* Poster Prize, BOS, Riga, Latvia
2016, *Synfacts* Poster Prize, BOS, Riga, Latvia
2016, *Organic Chemistry Frontiers* Poster Prize, ISMSC 2016, Seoul, South Korea

Travel awards and scholarships

2018, *Dora Pluss Short-term Mobility Grant*, ISMSC 2018, Quebec City, Canada
2018, *International Union of Crystallography (IUCr) Young Scientist Travel Award* and *Travel grant* from the Graduate School of Functional Materials, GRC on Crystal Engineering, Newry, Maine, USA
2017, *Dora Pluss Mobility Grant* for a research visit to McGill University, Canada
2017, *Dora Pluss Short-term Mobility Grant*, ISMSC 2017, Cambridge, United Kingdom
2017, *Travel award* from the organizing committee of ICCB 2017, Brno, Czech Republic
2017, *Travel award* from the organizing committee and *Travel grant* from the Graduate School of Functional Materials, ICCOSS-XXIII, Stellenbosch, South Africa
2016, *Travel award* from the organizing committee and *Dora Pluss Short-term Mobility Grant*, ISMSC 2016, Seoul, South Korea
2016, *IUCr Young Scientist Award*, ECS3, Bol, Croatia
2015, *IUCr Young Scientist Award*, ECM29, Rovinj, Croatia
2015, Kristjan Jaagu travel fellowship, ECM29, Rovinj, Croatia
2014, *Dora Mobility Grant* for a research visit to the University of Jyväskylä, Finland

Supervised theses

Jevgenija Martõnova, **B.Sc.**, 2018

'X-ray diffraction analysis of porous metal-organic frameworks and the stability of their crystalline structures after solvent exchange,' Tallinn University of Technology, Department of Chemistry and Biotechnology

Mari-Liis Kasemets, **M.Sc.**, 2016

'Cyclohexanohemicucurbit[8]uril Anion Complexes in Methanol,' Tallinn University of Technology, Department of Chemistry (co-supervised with Prof. Riina Aav)

Karin Kreekman, **B.Sc.**, 2016

'Synthesis and Analysis of Cyclohexanohemicucurbituril Homologues,' Tallinn University of Technology, Department of Chemistry (co-supervised with Prof. Riina Aav)

Teaching experience

Autumn 2015, Exercise tutorials of Organic Chemistry I

Spring 2016, Exercise tutorials of Organic Chemistry II

ELULOOKIRJELDUS

Isikuandmed

Nimi: Sandra Kaabel
Sünniaeg: 03.12.1989
Sünnikoht: Tallinn, Eesti
Kodakondsus: Eesti

Kontaktandmed

E-post: sandra.kaabel@taltech.ee

Hariduskäik

2014 – ... **Ph.D.**, Tallinna Tehnikaülikool, Keemia ja biotehnoloogia instituut
2012 – 2014 **M.Sc. (cum laude)**, Tallinna Tehnikaülikool, Keemia ja biotehnoloogia instituut
2009 – 2012 **B.Sc.**, Tallinna Tehnikaülikool, Keemiasstituut
1997 – 2009 Keskkool Viimsi Keskkool

Rahvusvaheline teadustöö

aug 2017 – märts 2018 Külalisdoktorant, Prof. Tomislav Friščići uurimisrühm, McGill Ülikool, Kanada
nov 2014 – apr 2015 Külalisdoktorant, Prof. Kari Rissaneni uurimisrühm, Jyväskylä Ülikool, Soome

Rahvusvaheline õppetöö

sept 2012 – mai 2013 Vahetusüliõpilane, Chalmers Tehnikaülikool, Rootsi

Keelteoskus

Eesti keel emakeel
Inglise keel kõrgtase
Soome keel algtase

Teenistuskäik

2017 – ... Tallinna Tehnikaülikool, Keemia ja biotehnoloogia instituut, doktorant-nooremteadur

Kuuluvus erialaühingutesse

2014 – ... European Crystallographic Association, *Individual Member*
2017 – ... Royal Society of Chemistry, *Associate Member*

Teaduspreemiad ja tunnustused

2018, Posterettekande auhind, GRC, Newry, Maine, Ameerika Ühendriigid.
2018, *Synthesis Best Paper Award 2017* - Kriis, et al., *Synthesis* **2017**, 49, 604–614.
2016, Tallinna Tehnikaülikooli loodusteaduste valdkonna aasta parim teadusartikkel - Kaabel et al., *Chem. Sci.* **2017**, 8, 2184–2190.
2016, *Organic & Biomolecular Chemistry* posterettekande auhind, BOS, Riia, Läti
2016, *Synfacts* posterettekande auhind, BOS, Riia, Läti
2016, *Organic Chemistry Frontiers* posterettekande auhind, ISMSC 2016, Seoul, Lõuna-Korea

Stipendiumid

2018, *Dora Pluss* lühiajalise õpirände stipendium, ISMSC 2018, Quebec City, Kanada
2018, *IUCr Young Scientist Travel Award* ning Funktsionaalsete materjalide ja tehnoloogiate doktorikooli stipendium, GRC on Crystal Engineering, Newry, Maine, USA
2017, *Dora Pluss* stipendium McGill Ülikoolis uurimisprojekti teostamiseks
2017, *Dora Pluss* lühiajalise õpirände stipendium, ISMSC 2017, Cambridge, Suurbritannia
2017, Konverentsi korraldajate stipendium (*Travel award*), ICCB 2017, Brno, Tšehhi Vabariik
2017, Konverentsi korraldajate stipendium (*Travel award*) ja Funktsionaalsete materjalide ja tehnoloogiate doktorikooli stipendium, ICCOSS-XXIII, Stellenbosch, Lõuna-Aafrika Vabariik
2016, Konverentsi korraldajate stipendium (*Travel award*) ja *Dora Pluss* lühiajalise õpirände stipendium, ISMSC 2016, Seoul, Lõuna-Korea
2016, *IUCr Young Scientist Award*, ECS3, Bol, Horvaatia
2015, *IUCr Young Scientist Award*, ECM29, Rovinj, Horvaatia
2015, Kristjan Jaagu välissõidu stipendium, ECM29, Rovinj, Horvaatia
2014, *Dora T6* stipendium Jyväskylä Ülikoolis uurimisprojekti teostamiseks

Juhendatud väitekirjad

Jevgenija Martõnova, **B.Sc.**, 2018

'Poorsete metall-orgaaniliste võrgustike monokristallide röntgendifraktsioonanalüüs ning kristallstruktuuride püsivuse uurimine solvendivahetusel,' Tallinna Tehnikaülikool, Keemia ja biotehnoloogia instituut

Mari-Liis Kasemets, **M.Sc.**, 2016

'Tsükloheksanopoolkukurbit[8]juriili kompleksid anioonidega metanoolis,' Tallinna Tehnikaülikool, Keemiainstituut (kaasjuhendaja dotsent Riina Aav)

Karin Kreekman, **B.Sc.**, 2016

'Tsükloheksanopoolkukurbituriili homoloogide süntees ja analüüs,' Tallinna Tehnikaülikool, Keemiainstituut (kaasjuhendaja dotsent Riina Aav)

Õpetamiskogemus

Sügis 2015, Orgaaniline keemia I harjutustunnid

Kevad 2016, Orgaaniline keemia II harjutustunnid